In Vivo Cofactor Biosynthesis and Maintenance in the Class Ia Ribonucleotide Reductase Small Subunit of *Escherichia coli*

by

Chia-Hung Wu

B.S. Chemistry
National Taiwan University, 1999

Submitted to the Department of Chemistry
in Partial Fulfillment of the Requirements for the Degree of

Doctor of Philosophy in Biological Chemistry

at the
MASSACHUSETTS INSTITUTE OF TECHNOLOGY

January 2009

Signature of Author:_____
Department of Chemistry
January 19, 2009

Certified by: _____
JoAnne Stubbe
Novartis Professor of Chemistry and Professor of Biology
Thesis Supervisor

Accepted by:_____
Robert W. Field
Haslam and Dewey Professor of Chemistry
Chairman, Departmental Committee on Graduate Students

This Doctoral Thesis has been examined by a committee of the Department of Chemistry as follows:

Catherine L. Drennan
Professor of Chemistry and Professor of Biology
Investigator and Professor, Howard Hughes Medical Institute
Chair

JoAnne Stubbe
Novartis Professor of Chemistry and Professor of Biology
Thesis Supervisor

Graham C. Walker
American Cancer Society Research Professor of Biology

TO MY PARENTS

ACKNOWLEDGMENTS

I would like to thank everyone.

I am especially grateful to my advisor, JoAnne, without whom this thesis may never have existed. Her unique, unparalleled enthusiasm and dedication to scientific research are the greatest inspiration not only to those around her but also to the broader scientific community. Were it not for her passion, my life in MIT would not be so rich and fulfilling. It was a precious privilege to have had the opportunity to learn under JoAnne. I feel really proud to be one of her students.

I am indebted to my thesis committee, Prof. Cathy Drennan and Prof. Graham Walker who have given me suggestions on my projects, taken the time to read and critique my thesis, and allowed me to defend on Martin Luther King Day.

Many thanks to my collaborators Prof. Carsten Krebs and his graduate student, Wei Jiang in Penn State University for their Mössbauer experiments on YfaE and whole cell samples, as well as for their insightful data analysis and discussions.

There are many wonderful Chemistry professors who have been great tutors and mentors in my grad school journey: Alex Klibanov, Sarah O'Connor, Stuart Licht, Alice Ting, Barbara Imperiali, and John Essigmann, who not only infused their scientific expertise to enrich my knowledge but also generously provided their wisdom on dealing with non-scientific issues.

What closer relationship can one have other than his labmates in grad school? I would like to thank former senior grad students in the lab who helped me in numerous ways: Michelle Chang, Cyril Yee and Erin Artin (Jelena Antonic) for their help with experiments and advice when I first joined the lab; Jesse (Jingyang) Chen, Aaron Hoskins, Greg Lohman, Deborah Perlstein and Jiamin Tian who were such great lab-siblings and who never hesitated to assist me whenever I had any question; Mohammad Seyedsayamdost for his peculiar life style and quick wits as well as his great sense of humor and kindness. I also want to thank former postdocs whom I had many memorable interactions with: Allison Ortigosa, John Robblee, Pinghua Liu, Aimin He, Dapeng Sun, Yongting Wang, Lana Saleh, Natalie Artzi, Bryan Greehagen, Tom Haller and Deborah Stoner-Ma. Special thanks to Daniela Hristova who was not only a great coworker but also a great social activity partner that eased so much stress in the lab. Thanks to

Luke Thompson whose broad knowledge and abilities to learn new things are a great inspiration to me.

Even though I tried to mentor newcomers as much as I could, I am the one who actually benefited the most from interactions with junior members in the lab. I am greatly thankful to Jun Wang for her persistence and unintentional jokes that made everyone laugh, Clemment Chan for his free food radar, Joey Cotruvo for his instincts and approaches in research, Ellen Minnihan for her never-give-up strength, Mimi Cho for her joyful personalities, Rachael Buckley for her role as a social ambassador. Thanks to current postdocs and lab affiliates who helped to keep the lab running and participated in all sorts of lab activities: Ping Li, Quamrul Hassan, Sumit Chakraborty, Kenichi Yokoyama, Laurie Grove, Yan Zhang, Danny Lutterman, Richard Kelley, Charles Budde and Chris Brigham. Special thanks to Crystal Shih who took time to proof-read my thesis and helped me with experiments at the last minute making my process of leaving the lab much smoother. Her positive attitude really helped me to get through the difficulties during my thesis-writing period. Thanks to visiting students and UROPs who help the lab in many different ways: Veronica Mugnaini, Grace Kenney, Judith Zaugg, Tomislav Argirevic, Gustavo Afanador, Matt Winston, Kapil Amarnath, Lars Plate, Rebecca Hirsch, Thomas Martinez, and Holger Armbruster. Thanks to Kendra Leith for her kind words and good suggestions in picking gifts. Thanks to indispensable administrative assistants Shannon McElhiney, Lenore Rainey, Betty-Lou McClanahan and Elizabeth Fong. Special thanks to Susan Brighton for her advice on grad school life.

I would also like to thank people outside the lab who helped me in many different ways: Viviana Izzo, Daniel Jarosz, Yun Wang, Leslie Murray, Rachel Behan and Patricia Brennecke.

I am also grateful to my classmates who helped me turn into a more social person than I was before I came to the US: Galen Loving, Mary and Jeff Farbman, Rebecca Somers, Jennifer Schefiliti, JieJin Chen, Leah Blasiak, Elvedin Lukovic, Langdon Martin, Mathew Tantama, Beth McCoy, Tammy Lam, Cintyu Wong, Ka-Lo Yeh, Hao Huang, Luke Firmansjah, Matt Hill, Chiao-Lun Cheng, Emily Nytko, Elizabeth Young, Xiao Yin Mak, Liane Klingensmith, Satoko Hirai, Allison Ondrus and Mike Schmidt.

Many thanks to friends from Taiwan: Chi-Wang Lin, Sharon Lin, Wan-Chen Lin, Yu-Ju Lin, Scott Chen, Cheng-Hsun Wu, Yen-Jie Lee, Tzu-ling Chang, Wen-yi Huang, Chia-Hui Kao and Lifen Huang.

Many thanks to other chemistry people who were always cheerful whenever I bumped into them: Susan Lyndon, Jackie Chan, Christian Gonzalez, Mariya Barch, Sarah Slavoff, Christine Tingberg, Alisha Weight, Nancy Yerkes, Galia Debelouchina, Samuel Lipoff, Woon Ju Song, Simone Friedle, Hee-Sun Han, Jess Vey, Laura Jennings, Sarah Barkow, Katherine Lovejoy, Irwin Chen, Marta Fernandez Suarez, Melva James, Ganpan Gao and Xiao-an Zhang.

Thanks to my dearest neighbors, the Imperiali lab members, who were always friendly and willing to give suggestions on experimental designs, provide chemicals or invite me to their social activities: Melissa Shults, Deborah Rothman, Beth Vogel, Mary O'Reilly, Eranthie Weerapana, Mark Chen, Wendy Iskenderian, Brenda Goguen, Angelyn Larkin, Meredith Hartley, Marcie Jaffee, Katja Barthelmes, Eugenio Vazquez, Jebrell Glover, Goufeng Zhang, Dora Carrico-Moniz, Seungjib Choi, Bianca Sculimbrene, Nelson Olivier, Anne Reynolds, Matthieu Sainlos, Jerry Troutman, Juan Antonio Gonzalez-Vera and Melanie Bonnekessel.

I also thank Deborah Pheasant in the Biophysical Instrumentation Facility for her help with isothermal calorimetry (ITC) experiments.

It was a real privilege to live in the best graduate community in MIT, Sidney Pacific, in which all sorts of social activities broaden my international scope. Many thanks to the house masters: Roger and Dottie Mark, Annette Kim, Roland Tang for their assistance and advice in general grad school life. Thanks to my student officer bosses Jane Kim and Michelle Sander who supported me when I was a hall councilor and a controller, respectively. Thanks to my roommates, Richard Ott, David Harris, Roger Aronow, Yue (Nina) Chen, Kehan Tian, Haegyu Lee, Jeremy Bigness, Andrea Vascellari and William Uspal. Thanks my fellow officers and SP neighbors whom I learned so much from and spent great time with: Leslie Rogers, Sophie Cariou, Robert Wang, Ben Mares, Monika Schleier-Smith, Nanako Takahashi, Viara Nedeva, Natalija Jovanovic, Matt Walker, Daniel Weller, Hila Hashami, Adrienne Li, Lynne Waldman, Carol Xia Hua, Nan Gu, Ardavan Oskooi, Vivienne Sze, Swati Mohan, Jessica Edmonds, Christiana Athanasiou, Eric Lam, Rosaria Chiang, Monica Martinez-Bravo, David Uniman, Hoda Eydgahi, Alex Lewis, Joseph Laracy, Matthew Eddy, Alison Kremer, Allan Fong, Zhunping Zhang, Mihir Mehta, Lynne Salameh, Joseph Thomer, Heejim Kim, Takayo Kotani, Lucy Wang, Jennifer Fang, Miso Kim, Amber Jain, Daryush Mehta, Pavithra Harsha, Sabrina Spencer, Johnna Powell, Mary Lee, Katarzyna Puchala, Jose Alberto Ortega, Timothy Chan, Sriram Krishnan, David Oertel, Jane Diecker, Shelly-Levy Tzedek, Tom Ouyang, Zahra Khan,

Ju Jin An, Elizabeth Godoy, Noashin Haque, Murat Acar, Fang Zao, George Aoude, Fang Xia, Yong Li, Jason Hatzakis, Sabrina Chang, Elisabeth Megally, Esmeralda Megally, Patta Yoda, Mengjin Tian, Thibault Prevost, Akane Matsuo, Annie Gai, Chris Mandy, James Lee, Ana Luisa Santos, Martin Cuyegkeng and Nadia Cheng.

Special thanks to my host family: Debbie Levey, Crispin Weinberg, Ariel Weinberg, Jasper Weinberg, Miranda Weinberg and Anahita Maghami. Debbie was always there to provide insightful advice and support to help me deal with all sorts of ordeals unpreventable in grad school life. Numerous dinners and conversations in her house helped me to learn more about the US and also a variety of cultural aspects.

I would like to thank friends outside of MIT who broaden my cultural and spiritual horizon: Tenzin Namdag, Duncan Lorien. Gabriel Solomon, Kale Laverentz, Anya Obizhaeva and Rays Jiang.

I would like to express my deepest appreciation of my other gurus in my grad life: my advisors in Taiwan, I-Jy Chang and Steve Roffler; my violin teachers, Alexey Shabalin and Sarita Uranovosky; and my spiritual guru, Tenzin Priyadarshi Shukla. Their constant and unconditional support enriched my life so much; they are the very sources of inspiration and motivation for my wanting to become a better person.

Finally and most importantly, I would like to thank my family. My deepest gratitude to my Mom and Dad, my sister Meng-Ting, my brother Chia-Chen and sister-in-law Wen-Shi. They are always there to help me. Without their support, it would have been impossible for me to take the chance to study abroad in a totally foreign environment. I will always feel grateful and indebted to them. I would like to dedicate this thesis to my family.

I want to thank all those I have not named but who have helped me in many different ways.
Without any of you, I would not be who I am. Thank you all!

In Vivo Cofactor Biosynthesis and Maintenance in the Class Ia Ribonucleotide Reductase Small Subunit of *Escherichia coli*

by

Chia-Hung Wu

Submitted to the Department of Chemistry
on January 2009 in Partial Fulfillment of the
Requirements for the Degree of Doctor of Philosophy in
Biological Chemistry

Abstract

The small subunit (β_2) of *Escherichia coli* class Ia ribonucleotide reductases (RNRs) contains a diferric tyrosyl radical (Y•) cofactor essential for the conversion of nucleotides to deoxynucleotides that are needed for DNA synthesis and repair. The mechanism and factors involved in the biosynthesis, maintenance and regulation of this cluster remains unclear. To understand these pathways, the genes contiguous to *nrdB* (gene encoding β) in 181 bacterial genomes were analyzed which revealed a highly conserved [2Fe2S]-ferredoxin, YfaE in *E. coli*. YfaE has been cloned, expressed, reconstituted, and characterized by UV-visible, EPR and Mössbauer spectroscopies. Titration of met-β_2 (an inactive diferric-β_2 with Y• reduced) with $[2Fe2S]^{1+}$-YfaE results in formation of diferrous-β_2 with one Fe reduced/YfaE oxidized. At the end point of titration, exposure of the reduced cluster to O_2 in the absence of an additional reducing equivalent yields the diferric-Y• with 2 Fe/Y• generated, suggesting that the reducing equivalent required for cluster assembly is supplied by β_2, likely by W48. The k_{obs} for the reaction between met-β_2 and $[2Fe2S]^{1+}$-YfaE determined by anaerobic stopped flow spectroscopy is ~1-5 s^{-1}. Studies of conserved Lys to Ala mutations of β_2 indicate electrostatic interactions may play an important role for interaction with YfaE. Quantitative Western blots of the whole cells suggest that YfaE acts catalytically in reactivating met-β_2 in vivo. Titration experiments establish that met-β_2 can be reduced by catalytic amounts of YfaE, Fre (a flavin reductase) and flavin with consumption of NADPH. In the presence of a Y• scavenger, hydroxyurea, *ΔyfaE* shows slower growth rates than the isogenic wt strain and Western blots analysis shows up-regulation of YfaE expression, supporting YfaE's role in the reactivation of diferric-β_2 in vivo. To investigate the iron sources for diferric-Y• assembly, changes in Fe pools inside the cell subsequent to expression of β_2 was monitored by whole cell Mössbauer spectroscopy. The results show that both Fe^{2+} and Fe^{3+} pools can provide the iron for cluster assembly, suggesting a reduction mechanism(s) for Fe^{3+} to allow it function in this capacity. A potential role of YfaE as an iron chaperone for iron delivery to β_2 has also been investigated.

Thesis Supervisor: JoAnne Stubbe
Title: Novartis Professor of Chemistry and Professor of Biology

Table of Contents

List of Figures

List of Tables

Abbreviations

α	Ribonucleotide reductase large subunit
Abs	antibodies
ADP	Adenosine−5'−diphosphate
Amp	Ampicillin
Apo-β_2	Iron-free form of β_2
Ara	L−Arabinose
ATP	Adenosine−5'−triphosphate
β	Ribonucleotide reductase small subunit
Buffer A	100 mM Tris, 150 mM NaCl, 5% glycerol, pH 7.6
CAP	Calf−intestine alkaline phosphatase
CDP	Cytidine−5'−diphosphate
Cm	Chloramphenicol
CS-β_2	C-terminal StrepII tagged β_2
CV	Column volume
dATP	2'−Deoxyadenosine−5'−triphosphate
dC	2'−Deoxycytidine
dCDP	2'−Deoxycytidine−5'−diphosphate
Δ9D	Delta-9 desaturase
DFT	Density functional theory
dGTP	2'−Deoxyguanosine−5'−triphosphate
DTT	Dithiothreitol
EDTA	Ethylenediaminetetraacetic acid
ENDOR	Electron-nulear double resonance
EPR	Electron paramagnetic resonance
ESI	Electrospray ionization
ET	Electron transfer
EXAFS	Extended X-ray absorption fine structure
FAD	Flavin adenine dinucleotide

$FADH_2$	Flavin adenine dinucleotide, reduced form
FMN	Flavin mononucleotdie
$FMNH_2$	Flavin mononucleotdie, reduced form
Fdx	Ferredoxin
Fre	NAD(P)H:flavin oxidoreductase
GEMMA	Gas-phase electrophoretic mobility macromolecule analysis
GDP	Guanosine−5'−diphosphate
Hepes	4−(2−Hydroxyethyl)piperazine−1−ethanesulfonic acid
HU	Hydroxyurea
IPTG	Isopropyl−β−D−thiogalactopyranoside
Kan	Kanamycin
LC	Liquid chromatography
LB	Luria Bertani
MCD	Magentic circular dichrorism
Met-β_2	Tyrosyl radical reduced β_2
MeV	Methyl viologen
MMO	Methane monooxygenase
MMOR	Methane monooxygenase reductase
MS	Mass spectrometry
NADH	β−Nicotinamide adenine dinucleotide, reduced form
NAD^+	β−Nicotinamide adenine dinucleotide, oxidized form
NADPH	β−Nicotinamide adenine dinucleotide phosphate, reduced form
$NADP^+$	β−Nicotinamide adenine dinucleotide phosphate, oxidized form
NMR	Nuclear magnetic resonance
NS-β_2	N-terminal StrepII tagged β_2
PCET	Proton−coupled electron transfer
PLP	Pyridoxal−5'−phosphate
RFQ	Rapid freeze quench
RNR	Ribonucleotide reductase
SEC	Size exclusion chromatography
SDS-PAGE	Sodium dodecylsulfate polyacrylamide gel electrophoresis
SF	Stopped flow

SOD	Superoxide dismutase
$WH^{+\bullet}$	Tryptophan cation radical
Tris	Tris(hydroxymethyl)aminomethane
TTP	Thymidine−5'−triphosphate
UDP	Uridine−5'−diphosphate
wt	Wild type
$Y^{\bullet}$	Tyrosyl radical
YfaE	2Fe2S ferredoxin

Chapter 1

Introduction to Ribonucleotide Reductase Small Subunit

General introduction

Ribonucleotide reductases (RNRs) are essential proteins in all organisms and catalyze the conversion of purine and pyrimidine nucleotides to deoxynucleotides, supplying the monomeric precursors (dNTPs) for DNA replication and repair (**Figure 1-1**) (*7, 9-13*). Their central role in nucleic acids metabolism has made them a successful drug target for anti-tumor therapies (*14-20*). There are three classes of RNRs characterized by the metallo-cofactors used for initiating the nucleotide reduction process (**Figure 1-2**) (*2*). The class Ia and Ib RNRs, found in eubacteria and eukaryotes, contain a diferric-tyrosyl radical (Y•) cofactor. The class Ic RNR, recently identified in *Chlamydia trachomatis*, a human intracellular parasite, employs a Mn^{IV}-Fe^{III} cofactor. The class II RNRs use adenosylcobanamin (AdoCbl) as a cofactor and are found in bacteria, archaera and eukaryotes. The class III RNRs require an Fe-S cluster and *S*-adenosylmethionine (SAM) to generate a stable glycyl radical (G•) cofactor. The class III RNRs are found only in facultative and obligate anaerobes (*16-20*).

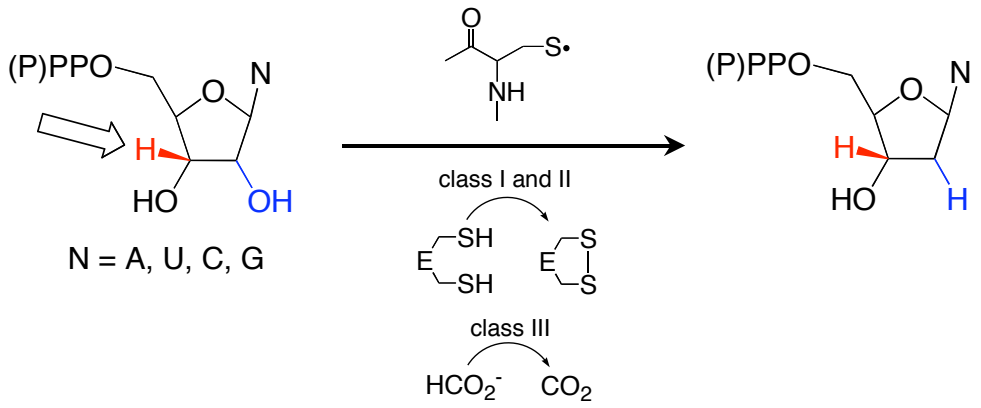

Figure 1-1. Reaction catalyzed by RNR. The arrow indicates the 3′ hydrogen (red) abstracted by the thiyl radical in the active site. The electron source for the reduction of the 2′ hydroxyl (blue) is supplied via formation of a disulfide (class I and II) or via oxidation of formate (class III).

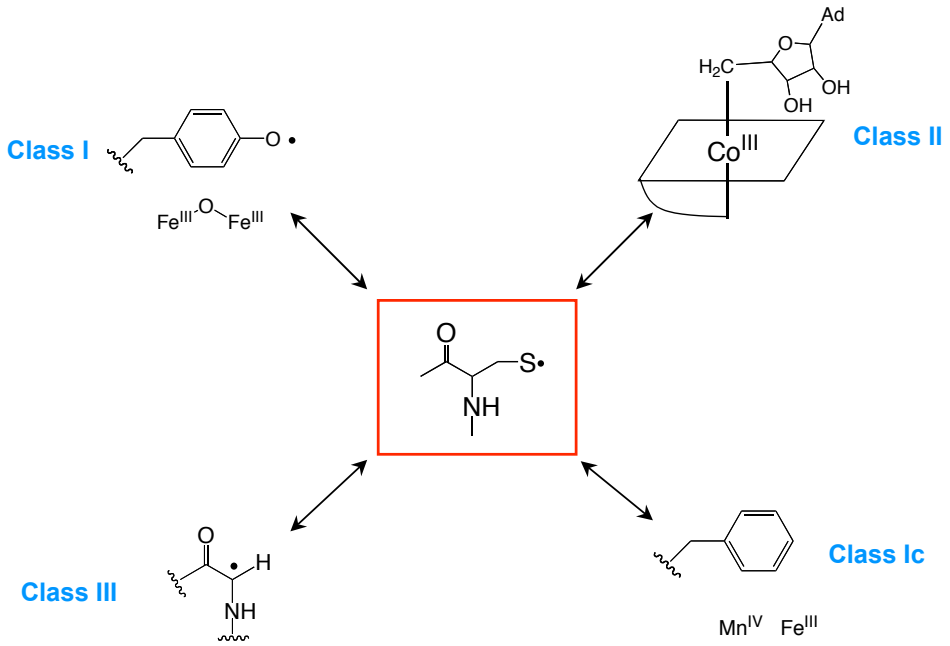

Figure 1-2. Three classes of RNRs. The class I RNRs have a diferric-Y• cofactor, the class II RNRs use adenosylcobalamin, the class III RNRs contain a glycyl radical and the class Ic RNRs harbor a Mn^{IV}-Fe^{III} cluster. All these cofactors are used to generate the thiyl radical

The function of the metallo-cofactors in all classes of RNR is to generate a transient thiyl radical for initiation of the radical dependent nucleotide reduction by abstracting the 3′-hydrogen atom of the nucleotides (**a, Figure 1-3**) (*21, 22*). The 3′-nucleotide radical (**b, Figure 1-3**) formed after the 3′-hydrogen abstraction undergoes protonation of the 2′-hydroxyl group and elimination and generates 3′-keto-2′-deoxynucleotide radical (**c, Figure 1-3**) which then accepts a hydrogen atom from an adjacent active site cysteine, forming a 3′-keto-2′-deoxynucleotide and a disulfide radical anion (**d, Figure 1-3**). The 3′-keto-2′-deoxynucleotide is reduced by the disulfide radical anion concomitant with protonation by the active site E441 and becomes a 2′-deoxy-3′-nucleotide radical with the formation of a disulfide bond (**e, Figure 1-3**). This 2′-

deoxy-3′-nucleotide radical then re-abstracts a hydrogen atom from the active site cysteine and becomes a 2′-deoxynucleotide with the regeneration of the thiyl radical (**f, Figure 1-3**). In the class I and II RNRs, the electron source for the nucleotide reduction is provided by the formation of the disulfide bond between conserved cysteines in the active site. This disulfide can then be reduced by the cysteines located in the C-terminus of the subunit possessing the active site. These cysteines, located in the disordered C-terminal tail are re-reduced by thioredoxin and thioredoxin reductase (or glutaredoxin and glutaredoxin reductase) using NADPH as the electron source. In the class III RNRs, formate provides the reducing equivalent and is converted to CO_2 (**Figure 1-1**) (*12*).

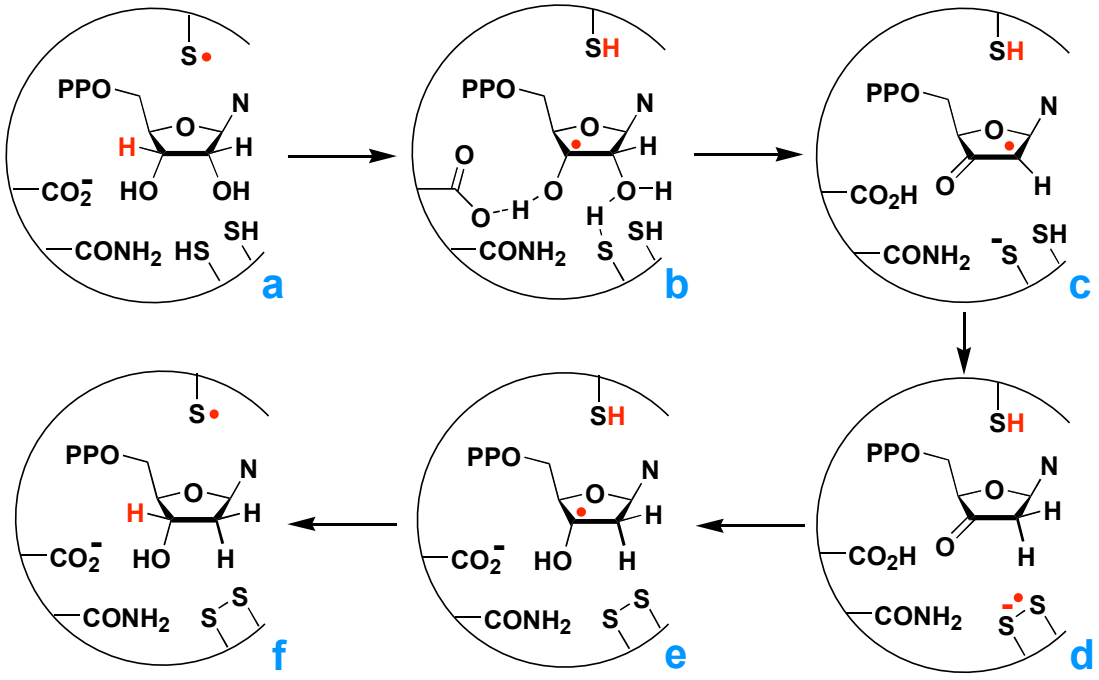

Figure 1-3. Mechanism for nucleotide reduction. The mechanism is proposed to be common for class I and II of RNRs. See text for descriptions of each step.

The class Ia RNR

The class I RNRs are composed of two subunits, the large subunit α_n harbors the transient thiyl radical (C•) and the small subunit β_2 contains the diferric-Y• cofactor essential for the generation of the C•. In *E. coli*, α exists as a homodimer whereas in mouse, α has been shown to form different oligomeric states (α_2, α_4 or α_6), depending on the concentration of ATP and dNTPs (*23-26*). Besides the site for nucleotide reduction, α also contains different allosteric effector binding sites. The specificity site (S-site) binds ATP, dATP, TTP and dGTP that determines which substrate (CDP, GDP, UDP and ADP) is preferred for reduction (*27-29*). The class Ia RNRs are distinct from the class Ib RNRs in that the class Ia RNRs contain a second allosteric site called activity site (A-site). Under low dATP concentrations and in the presence of ATP, the overall rate of nucleotide reduction increases whereas under high dATP concentrations, the activity of RNR is inhibited by dATP's binding to this activity site (*27*). A third allosteric regulation site (H-site), which binds ATP weakly, has been proposed to play an important role in the oligomeric states in mouse RNR (*25, 30*).

The class Ia RNR from *E. coli* will be the focus of this thesis. The large (α) and small (β) subunit of *E. coli* class Ia RNR is encoded by *nrdA* and *nrdB*, respectively. The large subunit can form a homodimer (α_2) of 172 kDa and the small subunit forms a homodimer (β_2) with a molecular mass of 87 kDa. As in other organisms, in *E. coli*, α_2 contains the site of nucleotide reduction and the specificity and activity sites (**Figure 1-4**) (*4*). β_2 contains the essential diferric-Y• cofactor (**Figure 1-5**) (*8, 31*). The two subunits form a 1:1 complex with a K_d of 0.2 μM or less in the presence of substrates and effectors (*32*). Sucrose gradient ultracentrifugation studies by Brown and Reichard suggest that dATP causes α to form higher molecular weight aggregates (*33*). Recently an inactive $\alpha_4\beta_4$ complex (*E. coli*) formed in the presence of dATP was observed

by a method called gas-phase electrophoretic mobility macromolecule analysis (GEMMA) (*34*). However this result is inconsistent with SEC from our own lab in which dATP generates an $\alpha_2\beta_2$ complex (Hassan, unpublished results).

So far only the individual structure of α_2 (co-crystalized with a 21-mer peptide identical to the C-terminal tail of β_2) and β_2 but not a structure of $\alpha_2\beta_2$ complex have been solved. However, Uhlin and Eklund have generated a docking model from individual α_2 and β_2 structures based on shape complementarity (**Figure 1-6**) (*4, 8, 31*). The most intriguing feature from this docking model is that the Y122 (Y• in β_2) is > 35 Å away from C439 (C• in α_2), suggesting the generation of the thiyl radical C439• by Y122• requires an unprecedented long range radical propagation step thought to involve redox active amino acids and proton coupled electron transfer (PCET) (**Figure 1-7**) (*1*).

Based on this docking model, a radical transfer pathway composed of absolutely conserved amino acid residues was proposed (β: Y122 → W48 → Y356) → (α: Y731 → Y730 → C439) (**Figure 1-7**) (*4*). Site-directed mutants (SDM) of these conserved residues indicated their importance (*35-38*). However, loss of catalytic activity precluded analysis of function. Recent methods (native protein ligation and evolution of suppressor tRNA/aminoacyl-tRNA synthetase pairs specific for an unnatural amino acid have allowed investigation of the proposed pathway by substitution of the conserved Ys in the pathway (Y356-β; Y731 and Y730 in α) with unnatural amino acids. Fluorotyrosines (2,3-F_2Y, 3.5-F_2Y, 2,3,5-F_3Y, 2,3,6-F_3Y and F_4Y), 3-nitrotyrosine, 3-hydroxyltyrosine and 3-aminotyrosine allow modulation of the protonation state and reduction potential, key for analysis of PCET (*39-43*). This elegant approach has provided the first direct evidence for the residues involved in the radical transfer pathway (Y356 in β; Y731 and Y730 in α). These studies confirmed pre-steady state experiments that substrate and

effector binding in α triggers the rate limiting conformational change, which leads to initiation of the radial transfer and formation of the active transient C439• required for catalysis. These substitutions have made the study of the radical propagation mechanism possible and unprecedented reaction in biology and a target of a currently used anti-tumor agent (*39-43*).

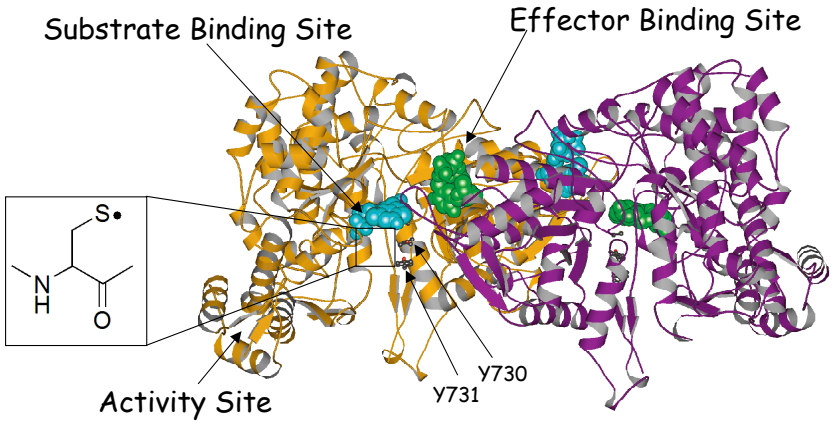

Figure 1-4. Crystal structure of *E. coli* class Ia RNR large subunit α_2 (*4-6*). The arrows indicate the active site where nucleotide reduction occurs, the allosteric specificity site that controls which nucleotide is reduced, the activity site which controls overall rate of nucleotide reduction and the two Ys (730, 731) which involve in the generation of the C•. The substrate GDP (blue CPK) in the active site and effector TTP (green CPK) at the allosteric sites are shown. The blow up shows the C• in the active site essential for catalysis.

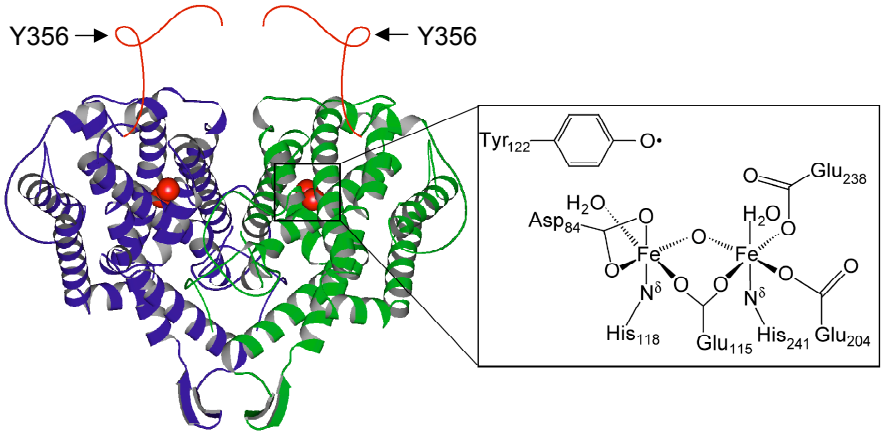

Figure 1-5. Crystal structure of *E. coli* class Ia RNR small subunit β_2 (*3, 4, 7, 8*). The C-terminal end of β_2 (residues 345-375) is thermally disordered (red). The blow up shows the diferric-Y• cluster required to generate the thiyl radical in α_2 for nucleotide reduction. The iron atoms of the diferric cluster are shown in red spheres. The arrow shows the Y356 involved in radical propagation between the two subunits.

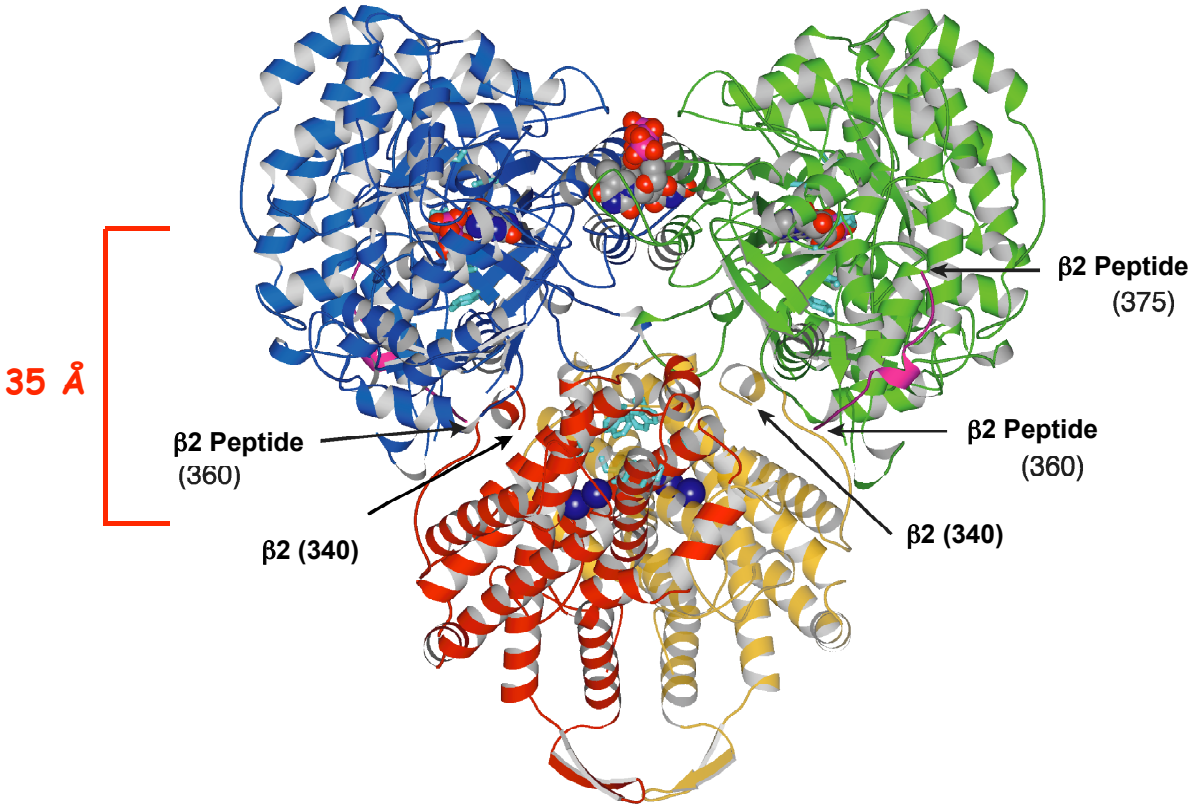

Figure 1-6. Docking model for *E. coli* class Ia RNR $\alpha_2\beta_2$ complex (*4-7*). The α_2 subunit is in blue and green and the β_2 subunit is in red and orange. A C-terminal peptide from β_2 (355-375) was used to obtain crystals of α_2 in which only residues from 360-375 are visible in the structure. Residues 341-359 in β_2 and residues 733-761 in α_2 are not visible in this structure. The Y• in β_2 required to generate the C• in α_2 for catalysis are > 35 Å removed.

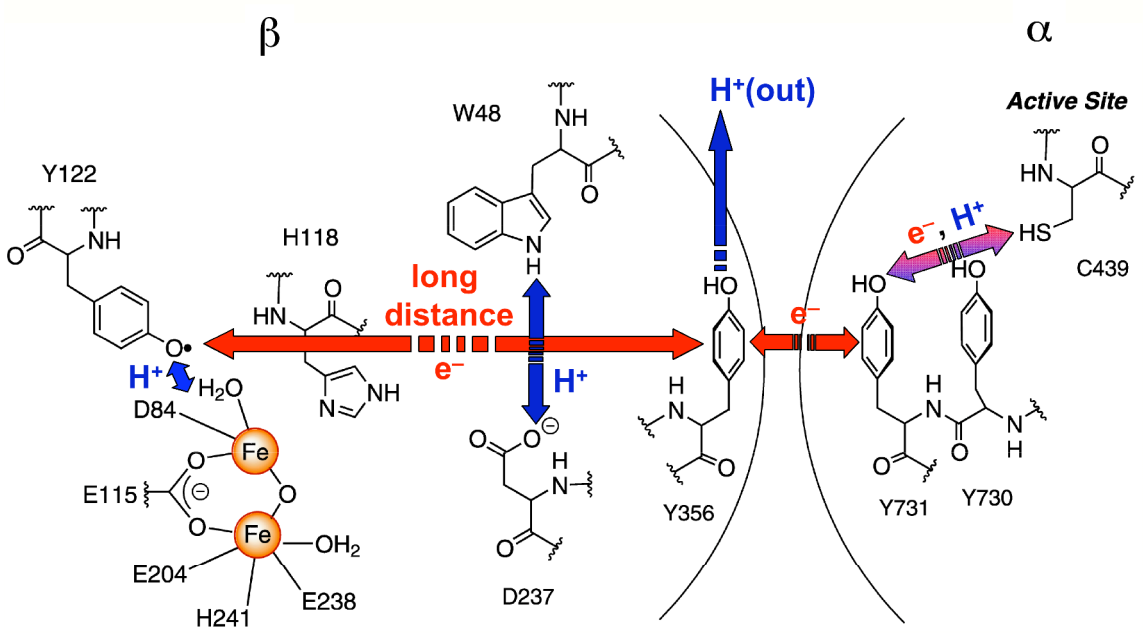

Figure 1-7. The proposed PCET pathway of *E. coli* class Ia RNR (*1*). The radical propagation pathway composed of conserved amino acids: (β: Y122 → W48 → Y356) → (α: Y731 → Y730 → C439) are shown (red line). Y356 locates in the disordered C-terminus of β_2 and its position is unknown.

The diferric-Y• cluster of E. coli class Ia RNR

In addition to research on the mechanisms of nucleotide reduction by the active site C• and on the radical transfer pathways from the Y• to generate the C•, the mechanism of formation of the essential diferric-Y• cluster in vitro has also been extensively investigated. Early studies by Atkin et al showed that the β_2 diferric-Y• cofactor can be self-assembled from apo-β_2 in the presence of Fe^{2+}, O_2 and reductant (*44*). The stoichiometry of this assembly requires oxidation of two ferrous irons and Y122 and requires an additional reducing equivalent to provide the four electrons needed for reduction of O_2 to H_2O (**Figure 1-8**). Optimized reconstitution conditions now give 1.2 Y• and 3.2-3.6 Fe per β_2. Theoretically one β_2 can have 2 Y• and 4 Fe. The main reason for the substoichiometric amounts of Y• and Fe per β_2 is due to the inability to control the iron delivery and the additional reducing equivalent which could be supplied by Fe^{2+} from the reconstitution. This substoichiometry complicates the interpretations of spectroscopic studies on the intermediates formed during the cluster assembly, and leads us to investigate that how the delivery of iron and the reducing equivalent is controlled for the assembly of the diferric-Y• cofactor of β_2 inside the cell.

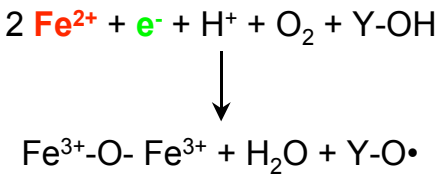

Figure 1-8. Stoichiometry of the diferric-Y• cluster formation. Two ferrous iron, one electron and one tyrosine provide the four electrons needed to reduce one O_2 and generate one diferric-Y• cofactor and one water molecule. However, so far only substoichiometric amounts of Y• (< 1 Y•/β) have been obtained from experiments in vitro. The in vivo source of iron (red) and the reducing equivalent (green) are unknown.

There are several challenges in studying the biosynthesis of diferric-Y• cofactor of β_2. First, apo-β_2 can self-assemble, which can complicate the determination of successful cofactor assembly by biosynthetic means. Second, Fe^{2+} is weakly bound which makes it difficult to find "factors" that deliver iron as it dissociates. Third, Fe^{2+} is easily oxidized at pH 7. Fourth, there is often redundancy in important pathways. Although efficiency may vary, cells still are able to survive if one single pathway is deleted, which makes it difficult to identify the function of a specific pathway.

To address these issues, our approach is heavily based on our knowledge on the in vitro cluster assembly, the iron homeostasis pathways in *E. coli*, and the biosynthesis of FeS proteins. Studies on the diferric-Y• cofactor assembly in vitro provide the basis for us to formulate the mechanism of iron delivery (Chapter 4 and 5) and source of reducing equivalents (Chapter 2 and 3). Current understanding of the iron homeostasis in *E. coli* provides the basis for us to design experiments to investigate iron delivery pathways for β_2 (Chapter 4). Studies on the biosynthesis of FeS proteins provide the basis for our experimental design to look for biosynthetic machineries (Chapter 2) and investigate potential iron chaperones (Chapter 3 and 5).

The diferric-Y• cofactor assembly in vitro

The mechanism of diferric-Y• cluster assembly in vitro has been studied in great detail with wt and mutant β_2s (**Figure 1-9**) (*3, 5-7*). The assembly starts with a conformational change in apo-β_2 followed by sequential loading of two ferrous irons to specific sites (*7, 45*). An alternative model has been proposed by Hendrich and coworkers based on studies using EPR spectroscopy and Fe^{2+} and Mn^{2+} loading in apo-β_2. The model suggests that binding of one Fe^{2+} in a β subunit lowers the affinity for the second metal in the same subunit and prohibits iron-binding of the other subunit. The binding of the second metal in the same subunit is triggered by exposure to O_2 or in high glycerol buffers (*46*).

Reaction of Fe^{2+}-loaded β_2 with O_2 yields a transient diferric-peroxide intermediate observed in β_2 mutants in *E. coli* and wt-β_2 in mouse (*13, 47*). In addition a transient intermediate in the *E. coli* wt-β_2 formed and disappeared within 10 ms was also observed by Tong et al and is likely the peroxide intermediate (*7*). This diferric-peroxide intermediate is proposed to be reduced by W48 (the same W in the PCET pathway, **Figure 1-7**) to form a tryptophan cation radical ($WH^{+\bullet}$) and an Fe^{IV}-Fe^{III} intermediate (X) with a rate constant of 60-80 s^{-1} when the apo-β_2 is preloaded with Fe^{2+} (**Figure 1-9**) (*48*). When the reaction starts with apo-β_2 without preloaded Fe^{2+}, the rate of formation of X is masked by a conformational change of apo-β_2 (k_{obs}~5-10 s^{-1}) (**Figure 1-9**).

There is agreement in the field that X is kinetically competent in generating the diferric-Y• cluster and that it has a Fe^{IV}-Fe^{III} core structure. EXAFS (extended X-ray absorption fine structure) studies revealed a short Fe-Fe distance (2.5 Å) (*49*). In conjunction with studies of $^{17}O_2$, $H_2{}^{17}O$, and ^2H_2O ENDOR (electron-nulear double resonance), EPR and Mössbauer spectroscopies using rapid freeze quench (RFQ) technique, a structure of X composed of a

terminal hydroxyl on Fe^{III} and an oxo bridge in addition to bridges from carboxylate oxygen(s) from E115 and E238 between Fe^{III} and Fe^{IV} was proposed [$(HO)Fe^{III}(\mu\text{-}O)Fe^{IV}$] (*50-52*). Alternate structures of X were also proposed based on studies by MCD (magnetic circular dichrorism) [$Fe^{III}(\mu\text{-}O)(\mu\text{-}OH)Fe^{IV}$] (*48*) or DFT (density functional theory) [$(H_2O)Fe^{III}(\mu\text{-}O)(\mu\text{-}O)Fe^{IV}$] (*53, 54*). Determining a structural model of X that is in agreement with all spectral studies is complicated by heterogeneity of the sample (only substoichiometric amount of Y• per diferric center was formed in the cofactor assembly in vitro) and variation in sample preparation.

After the formation of the X-$WH^{+\bullet}$ intermediate, in the presence of reducing equivalent such as excess Fe^{2+}, DTT, or ascorbate, the $WH^{+\bullet}$ near the surface is rapidly reduced to W at a rate > 20 s^{-1} (**Figure 1-9, a**) and then intermediate X is reduced to a diferric center concomitant with oxidation of Y122 to Y• at a rate constant of ~1 s^{-1} (**Figure 1-9, c**) (*6*). When no reductant is ready available, Y122 is oxidized by $WH^{+\bullet}$ at a rate > 3 s^{-1} (**Figure 1-9, b**), followed by a slow reduction of the intermediate X to form the diferric cluster (**Figure 1-9, c**). The electron source for this step has not been identified (*5*).

Lessons learned from in vitro studies in controlling delivery of iron (addressed in Chapter 4 and 5) and the reducing equivalent (addressed in Chapter 2 and 3) are likely to play an important role in vivo. Whether β_2 assembly in vivo similarly proceeds through "X" and $WH^{+\bullet}$ intermediates as observed in vitro is important to establish.

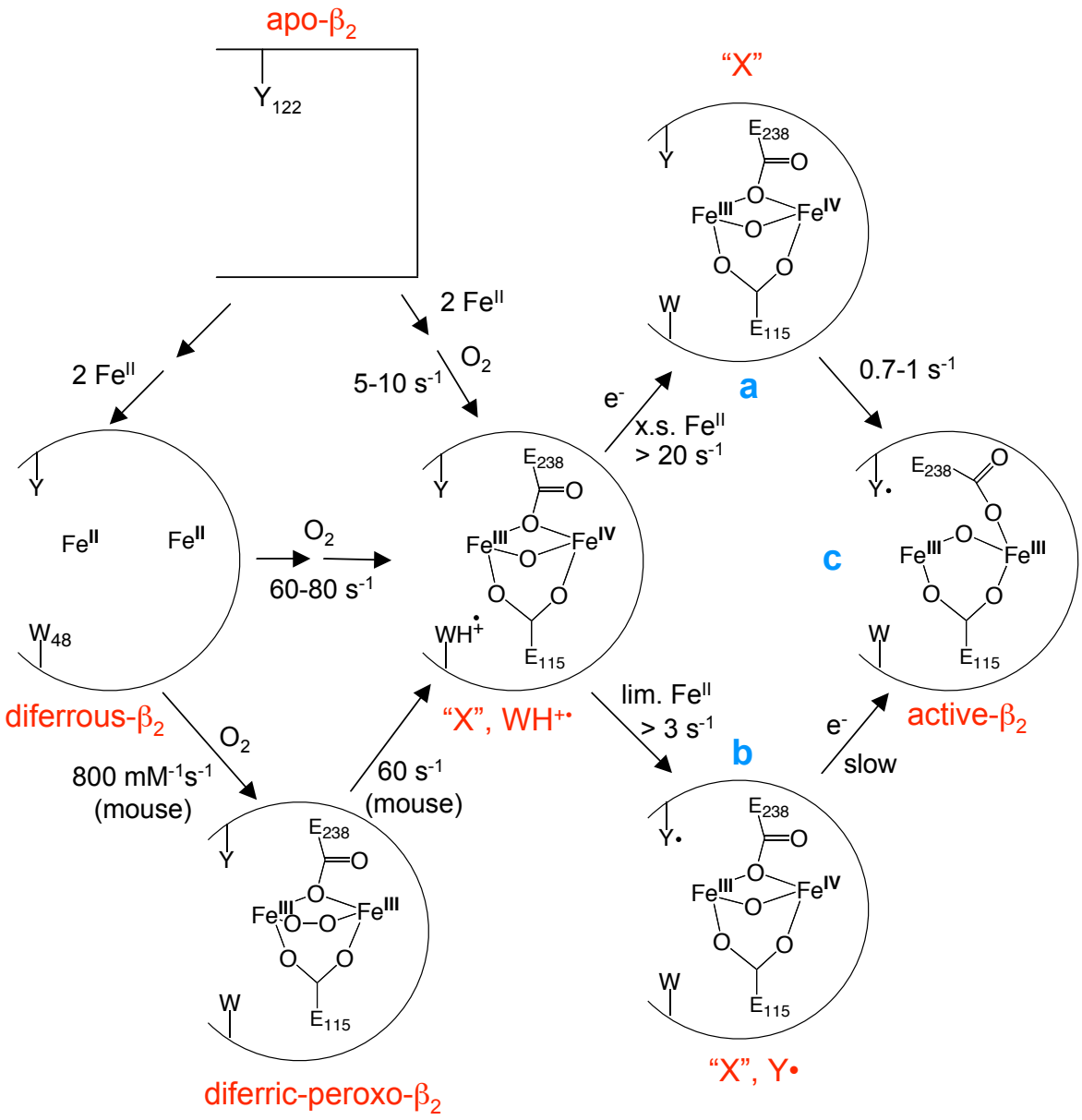

Figure 1-9. Working model for in vitro cluster assembly in β_2 (*3*). The exact structures and ligand coordinations of the intermediates are still under investigation. See text for descriptions of each step.

Brief overview of *E. coli* iron homeostasis and possible mechanisms of sources of Fe for β_2

To look for iron delivery pathways for β_2, an understanding of the iron homeostasis in *E. coli* may help us identify possible sources of iron for the diferric-Y• cofactor of β_2. In nature, most of the iron is in +3 oxidation state. Due to its extremely low solubility (~10^{-18} M at pH 7.0), iron uptake in bacteria is very challenge and creative solution of secretion of high affinity Fe^{3+} chelating agents, siderophores (K_d~10^{-30} M) that are then taken up by a number of outer membrane transporters powered by protein complex TonB-ExbB-ExbD using transmembrane potential (**Figure 1-10**) (*55*). The ferric-siderophores bind to specific periplasmic binding proteins that deliver them to specific ATP-binding cassette (ABC) transporter complexes which allow their transport to cross the plasma membrane. The iron from the internalized ferric-siderophores can then dissociate from the complex subsequent to reduction to lower affinity Fe^{2+} or in the case of very tight binders such as enterobactin, degradation occurs with esterases. Bacteria also use other strategies to uptake iron, for example, transporting host iron-binding proteins like transferrin, lactoferrin, or hemoglobin through specific receptors; lowering the pH of the environment to increase the solubility of ferric iron; reducing ferric irons to ferrous form by outer membrane reductases and diffusion through outer membrane porins or ferrous and divalent cation transporters (*55, 56*).

By examining the iron homeostasis network, two possible direct iron sources for apo-β_2: one is the membrane transporters, the other is iron storage proteins. In *E. coli*, there are three outer membrane ferric-siderophore transport systems and three known permeases in the plasma membrane that transport ferrous iron (*55-58*). The major ferric-siderophore uptake system is ferric-enterobactin (or enterochelin, a catecholate-type siderophore), which involves 7 transport genes (*fepA-G*) and 6 genes involved in its biosynthesis (*entA-F*). The second is the ferric-citrate

transport system, which contains 5 transport genes (*fecA-E*). The source of citrate is the TCA cycle. The third is the ferric-hydroxamate (ferrichrome) transport system, which also has 5 transport genes (*fhuA-E*). In contrast with the enterobactin and citrate transport systems, the ferrichrome system contain two outer membrane transporters, FhuA and FhuE, and no biosynthetic machinery. The source of hydroxamate may be fungi or other bacteria. The transports of these three ferric-siderophores through the outer membrane are all TonB dependent (**Figure 1-10**).

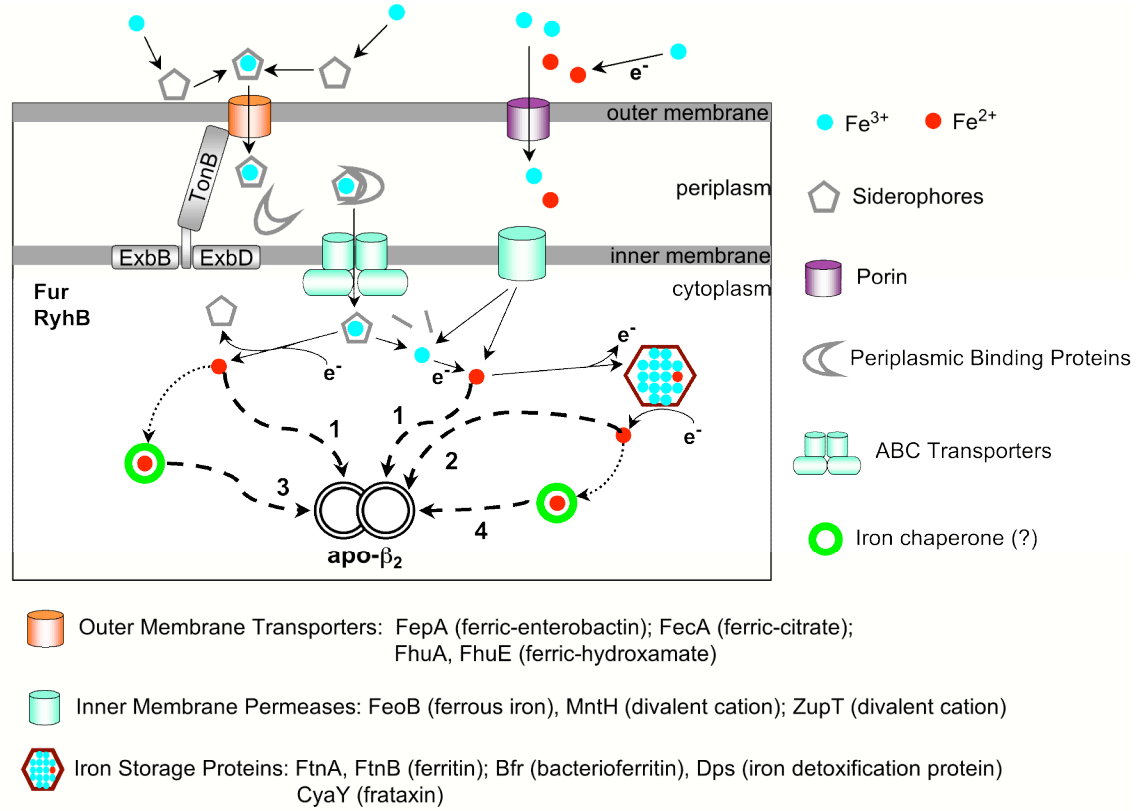

Figure 1-10. Iron homeostasis in *E. coli*: a working model for how apo-β_2 obtains iron. Path 1: from membrane transporters, path 2: from iron storage proteins or labile iron pools, path 3: iron chaperone mediated delivery using Fe^{2+} from membrane transporters, path 4: iron chaperone mediated delivery using Fe^{2+} from iron storage proteins.

Transport of ferrous iron are through porins in the outer membrane and then by at least three different permeases in the plasma membrane. The major ferrous iron uptake mechanism involves the Feo system, which is composed of 3 genes (*feoABC*). *FeoB* encodes a ~85 kDa cytoplasmic membrane permease with a K_m for Fe^{2+} ~0.5 μM (*59*). Ferrous iron from the periplasm can also be transported into the cytosol by two non-specific divalent cation permeases: the manganese transporter (MntH) and the zinc transporter (ZupT) (*60, 61*).

The other possible iron source is iron storage proteins. There are three common iron storage proteins in *E. coli*: ferritin, bacterioferritin (Bfr), and iron detoxification protein (Dps) (*62*). The larger (~500 kDa) ferritin and bacterioferritin can accommodate at least 2000 Fe^{3+} atoms as ferrihydrate per 24-mer, while the smaller (~250 kDa) Dps can store about 500 iron atoms per 12-mer. The in vivo release of stored iron from ferritins or Dps remains elusive but must occur by a reductive mechanism. For bacterioferritin, it is proposed that a ferredoxin, Bfd (Bfr-associated ferredoxin) interacts with Bfr to mediate the release of stored iron by reducing ferric irons to soluble ferrous form. The *E. coli* Bfd is induced under iron limiting condition. Recently a newly discovered protein CyaY, a human frataxin homologue, has been proposed to function as an iron storage protein (*63*). Details of CyaY will be discussed in the upcoming secsion.

Regulations of expression of iron transporters and iron storage proteins are mainly through the bacteria global iron regulator, Fur (ferric uptake regulator). Fur is a homodimer, composed of 15-17 kDa subunits. It binds ferrous iron via its C-terminal, histidine-rich domain and represses the transcription of target genes by DNA binding via its N-terminal domain (*55, 64*). The DNA binding affinity of Fur increases ~1000 fold when loaded with ferrous iron. Interestingly, the affinity of Fur for ferrous iron is about 10 μM, which is similar to the estimated

concentration of the labile iron pool inside the cells (*64, 65*). Therefore, Fur may be designed to respond to physiological fluctuations of the labile iron pool inside the cells. Under iron-replete conditions, Fe^{2+}-Fur represses the expression of proteins related to Fe uptake such as iron membrane transporters or iron-chelating siderophore biosynthesis.

Fe^{2+}-Fur also represses the transcription of a small non-coding RNA, RyhB. RyhB is proposed to act as an antisense RNA, which binds to and facilitates the degradation of target mRNAs that encode Fe-containing proteins such as ferritins or bacterioferritins (*66-68*). Therefore, Fe^{2+}-Fur enhances the expression of Fe-storage proteins indirectly by repressing RyhB. Interestingly, when Fur is deleted in *E. coli*, they are iron deficient (~70% decrease) due to low expression of iron storage proteins and other Fe-binding proteins (*69*).

The source of iron will be dependent on growth conditions and ultimately the iron delivered to apo-β_2 needs to be in the ferrous form. However, the reactivity of Fe^{2+} with O_2 and H_2O_2 require that Fe^{2+} is sequestered inside the cell to prevent the formation of hydroxyl radicals (HO•) via the Fenton reaction (*70*). Based on the iron homeostasis network, several pathways by which apo-β_2 can obtain ferrous iron are postulated (**Figure 1-10**): the first one is directly from a membrane transporter (path 1); the second pathway is from iron storage proteins or labile iron pools which supplies loosely bound ferrous ions (path 2) (*64, 65*); a third pathway is based on our understanding of copper deliver via "chaperone" proteins. Interestingly in the systems thus far characterized, the chaperone proteins are structurally homologous to the proteins to which they are delivering the metal (*71*). Thus a third possibility is from an iron chaperone which obtains ferrous iron from membrane transporters; and a fourth possibility is from iron storage proteins but mediated by an iron chaperone (path 4) (**Figure 1-10**).

The knowledge of the iron delivery pathways in *E. coli* have provided the basis for our experimental design of applying whole cell EPR and Mössbauer spectroscopies to investigate the role of these pathways in the biosynthesis of the diferric-Y• cofactor of β_2 (Chapter 4). In addition to studies on Fe homeostasis, studies on the biosynthesis of other Fe-containing proteins could serve a great paradigm for us to formulate possible mechanisms for the biosynthesis of the diferric-Y• cluster.

Biosynthesis of FeS clusters

FeS centers are the "oldest" type of cluster and likely play an essential role in iron homeostasis in all organisms. The biosynthesis of a diverse range of clusters, which also can self-assemble, have been most extensively studied. Thus lessons learned from these studies may provide insights into design of experiments with cluster assembly in β_2.

FeS proteins play important roles in various cellular functions, including electron transfer (ferredoxin), coupling proton and electron transfer (Rieske protein, nitrogenase), substrate binding and activation (dehydratases, acetyl-CoA synthase, radical SAM enzymes, sulfite reductase), regulation of enzyme activity (glutamine PRPP amidotransferase, ferrochelatase), regulation of gene expression (IscR, SoxR, FNR, IRP), Fe storage (ferredoxins, polyferredoxins), disulfide reduction (thioredoxin reductase) and sulfur donation (biotin synthase) (*72-75*).

In prokaryotes, machineries essential for FeS cluster biosynthesis are encoded in operons such as *nif* (nitrogen fixation), *isc* (iron sulfur cluster) and *suf* (sulfur utilization factors) operons. These machineries are conserved in eukaryotes and archaea. Earlier studies on nitrogenase in *A. vinelandii* by Dean and coworkers revealed two key proteins, NifS and NifU that are involved in the cluster maturation of the nitrogenase (*76*). The fact that deletions of either *nifS* or *nifU* did not abolish nitrogenase activity led to the identification of *isc* operon in *A. vinelandii* (*77*). An example of redundancy, that is observed frequently for important metabolic components. In *E. coli*, two FeS biosynthetic operons, *isc* (containing *iscRSUA-hscBA-fdx* genes) and *suf* (containing *sufABCDSE* genes) have been identified. The *isc* operon contains the housekeeping genes in *E. coli*. Deletion of genes in this operon is lethal or causes a severe growth defect. On the other hand deletion of genes in the *suf* operon shows a prominent phenotype only when cells

are grown under oxidative stress or iron starvation conditions (*78-80*). The house keeping *isc* operon in *E. coli* will be the focus of the following sections.

Proposed biosynthetic pathway for FeS cluster assembly

A biosynthetic pathway for the FeS cluster assembly is shown in **Figure 1-11**. Details of each step will be discussed in the following sections. The sulfur source is from L-cysteine, which is converted to L-alanine by cysteine desulfurase (IscS, NifS, SufS/SufE or CsdA/CsdE) and then transferred directly or through an intermediate protein to scaffold proteins (IscU, NifU, IscA, SufA, ISU). The iron, which ultimately comes from iron transporters and/or iron storage proteins, may be delivered by iron chaperone(s) (CyaY, IscA) to scaffold proteins. In vitro, either [2Fe2S] or [4Fe4S] clusters can be assembled on the scaffold proteins which can then be transferred into the target apo-proteins (*81-83*). Accessory proteins such as ferredoxin, protein folding ATPase chaperones, HscA/HscB or SufBCD complex have been shown to facilitate the cluster transfer to target apo-proteins at the expense of ATP (*82, 84-86*).

Cysteine desulfurases

Cysteine desulfurases catalyze the conversion of L-cysteine to L-alanine and persulfide using pyridoxal-phosphate (PLP) as a cofactor (*87, 88*). IscS or NifS form homodimers required for desulfurase activity (*89, 90*). In the Suf system, desulfurase SufS forms a complex with SufE, which facilitates sulfide transfer to scaffold protein SufA (*91*). In the Isc system, it has been shown that IscS forms a complex with Fdx, but the function of Fdx, reductive liberation of S^{2-} for delivery to scaffold proteins remains to be established (*92*). Recently, studies by Fontecave and coworkers showed that IscS co-purifies with CyaY and that Fe^{3+}-CyaY can be reduced to Fe^{2+}-CyaY by cysteines. Therefore, a model in which FeS cluster is assembled on

IscS followed by delivery of the cluster into IscU has also been proposed (*93*). The K_d between IscS and IscU determined by ITC is ~2 μM, which is much lower than their estimated cellular concentrations ([IscS] ~ 45 μM, [IscU] ~ 40 μM), suggesting that in vivo IscS and IscU might be present in the form of a complex (*84, 94*).

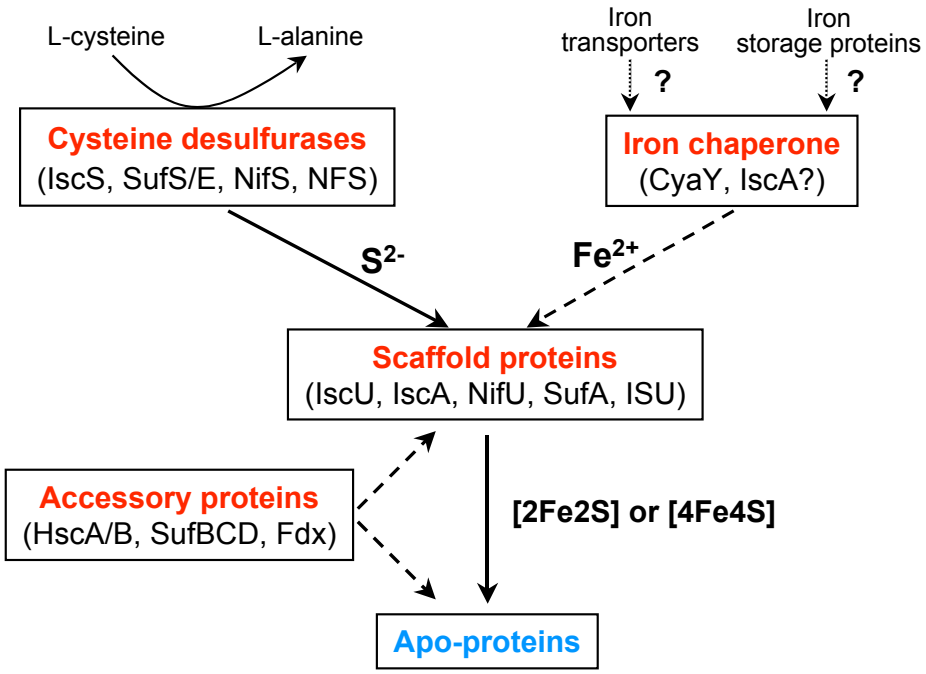

Figure 1-11. A working model for FeS cluster assembly. Cysteine desulfurases convert cysteine to alanine to provide sulfide for assembling FeS clusters in scaffold proteins. The iron could come from iron chaperone frataxin/CyaY or IscA. The [2Fe2S] or [4Fe4S] clusters assembled in the scaffold proteins are delivered to recipient apo-proteins with assists from accessory proteins.

Scaffold protein-IscU

In the U-type scaffold protein typified by IscU, one $[2Fe2S]^{2+}$ per IscU dimer can be reconstituted in vitro by Fe^{2+} and S^{2-}. The $[2Fe2S]^{2+}$-$IscU_2$ can transfer its cluster in vitro to [2Fe2S]-requiring apo-proteins such as apo-Fdx at a turnover rate of 0.21 min^{-1} (*95, 96*). The rate of [2Fe2S] transfer can be facilitated by molecular chaperones HscA and HscB (**Figure 1-12**). It has been shown by ITC that apo-IscU binds to HscA and HscB with K_d of 1.6 and ~13 μM, respectively (*84, 97*). The cellular concentrations of IscU, HscA, and HscB are ~40, ~20, and ~10 μM, respectively, determined by Western blots (*84, 98*). Therefore, fair amounts of the IscU-HscA or IscU-HscB complex can be formed in vivo and play a significant role in the FeS cluster assembly.

HscB interacts with both HscA and IscU, increases the ATPase activity of HscA (~4 fold) and enhances the K_m between HscA and IscU by ~17-fold. In the presence of both HscB and IscU, the ATPase activity of HscA was enhanced by ~400-fold (*84, 85, 99*). Furthermore, recent studies have shown that the rate of cluster transfer from $[2Fe2S]^{2+}$-$IscU_2$ to apo-Fdx increases ~20 fold in the presence of DTT, excess ATP, and stoichiometric amounts of HscA and HscB, indicating a physiological role of HscA/HscB molecular chaperones in facilitating efficient FeS cluster transfer from scaffold proteins to apo-proteins (*85, 96*).

Besides $[2Fe2S]^{2+}$-$IscU_2$, other forms of FeS cluster can be assembled on IscU. In vitro, it has been demonstrated that after prolonged incubation (~6.5-14 h) with Fe^{3+}, IscS, L-cysteine and β-mercaptoethanol, two $[2Fe2S]^{2+}$ per IscU dimer can be reconstituted (**Figure 1-12**) (*82*). Furthermore, a slow reductive coupling (~7.5-12.5 h) between the two $[2Fe2S]^{2+}$ clusters to form one $[4Fe4S]^{2+}$ triggered by dithionite or reduced IscFdx has been shown by UV-vis and Mössbauer spectroscopies (*82*). This conversion can be reversed in the presence of O_2 (**Figure 1-12**). Also, it has been shown by Mössbauer spectroscopy that only the $[4Fe4S]^{2+}$, but not the

$[2Fe2S]^{2+}$ cluster in IscU can be transferred in vitro to [4Fe4S]-requiring apo-aconitase at a turnover number of 0.074 min^{-1} (*83*). The presence of HscA/HscB has no effect on the rate of [4Fe4S] cluster transfer. In vivo, the two cluster forms of IscU could be an equilibrium maintained by IscFdx and oxygen (or reactive oxygen species formed under oxidative stress).

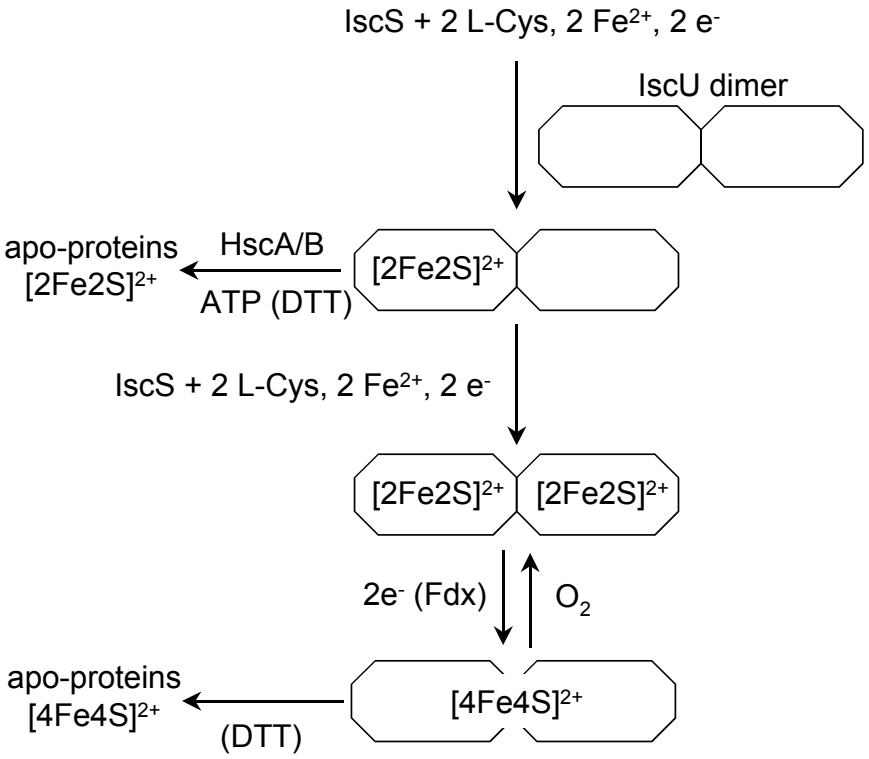

Figure 1-12. Formation of FeS clusters in scaffold protein IscU. Apo-IscU can be loaded with one [2Fe2S] cluster at the interface between its two monomers. A second [2Fe2S] cluster can be assembled on [2Fe2S]-IscU and through reductive coupling by ferredoxin (Fdx) or dithionite can form a [4Fe4S]-IscU. This two [2Fe2S] cluster to one [4Fe4S] cluster conversion is reversible by O_2 oxidation. The [2Fe2S]- and [4Fe4S]-IscU can deliver its cluster to [2Fe2S]- and [4Fe4S]-type apo-proteins, respectively.

Recent studies by Dean and coworkers have shown that endogenous IscU with an affinity tag purified from *A. vinelandii* contains one $[2Fe2S]^{2+}$ cluster per dimer (*100*). This [2Fe2S] cluster is oxygen sensitive, similar to the $[2Fe2S]^{2+}$-$IscU_2$ assembled in vitro (*81*). No [4Fe4S] cluster was observed from endogenously purified IscU, probably because the cluster is too labile for purification or the in vivo concentration is too low to detect.

One major problem with the in vitro studies described above is that the rate of FeS cluster transfer (<1 min^{-1}) and the rate of the interconversion between [4Fe4S] and [2Fe2S] (several hours) are very slow, too slow to be physiologically relevant. Inside the cell the rate of reaction must be enhanced to be of physiological relevant. The mechanism of this enhancement remains to be established.

Scaffold protein-IscA

In vivo, the exact function of the scaffold protein IscA is still under debate. Because of the high affinity for ferric iron ($K_d = 3 \times 10^{19}$ M^{-1}) observed in *E. coli* IscA in the presence of DTT or NADPH and catalytic amounts of thioredoxin (TrxA) and thioredoxin reductase (TrxB) (*101, 102*), it has been proposed that IscA acts as an iron chaperone for IscU (*103, 104*). It is worth noting that despite the high affinity for Fe^{3+} measured in vitro, only ~10% of IscA as isolated is iron-loaded.

Both [2Fe2S] and [4Fe4S] clusters can form on IscA by in vitro reconstitution in the presence of Fe^{2+} and S^{2-} or Fe^{2+} and L-cysteine with IscS (*105-107*). Heterologous expression of *A. ferrooxidans* IscA in *E. coli* contains one intact [4Fe4S] cluster per monomer subsequent to its purification (*108*). The reconstituted $[2Fe2S]^{2+}$-$IscA_2$ in vitro (one cluster per dimer) from a cyanobacterium is capable of transferring its FeS cluster to a [2Fe2S]-requiring apo-Fdx or a [4Fe4S]-requiring apo-adenosine 5'-phosphosulfate reductase (APR). In the former case, after

$[2Fe2S]^{2+}$-$IscA_2$ was mixed with apo-Fdx (1:1 ratio) under anaerobic condition in the presence of DTT, ~50% of the cluster was transferred into apo-Fdx in 10 min and the reaction reached ~80% completion after ~1 h. In the latter case, [4Fe4S]-APR, the rate of cluster transfer was not determined and it is unclear whether the formation of the [4Fe4S] cluster occurs in IscA (similar to IscU) or in the target proteins (*109*).

Despite similar functions proposed for IscU and IscA, kinetic analyses in *E. coli* IscU and IscA showed a tighter apparent K_m between $[2Fe2S]^{2+}$-$IscU_2$ and apo-Fdx (~27 μM) than between $[2Fe2S]^{2+}$-$IscA_2$ and apo-Fdx (~210 μM). In addition, the turnover number of delivery of [2Fe2S] clusters into apo-Fdx is ~7 fold higher from $[2Fe2S]^{2+}$-$IscU_2$ (0.21 min^{-1}) compared to that from $[2Fe2S]^{2+}$-$IscA_2$ (0.029 min^{-1}) (*95*). Even though so far only the in vivo [IscU] has been determined (~40 μM), given the low concentration of Fdx in vivo (~5 μM), $[2Fe2S]^{2+}$-$IscA_2$ is unlikely to be the physiological FeS cluster donor for apo-Fdx (*84, 110*). This suggests that IscU and IscA likely have distinct substrates in vivo. The observation that IscA can accept an FeS cluster from IscU but not the other way around implies that IscA might be an intermediate FeS scaffold protein between IscU and apo-proteins (*107*).

Iron chaperone: frataxin?

The source of sulfide for the FeS cluster assembly on scaffold proteins is provided by Cys and cysteine desulfurases, whereas the source of iron has been postulated to come from frataxin. Frataxin, a ~13 kDa protein, was first recognized in an inherited autosomal recessive syndrome, Friedreich ataxia, characterized by ataxia, cardiomyopathy and high incidence of diabetes (*111*). Disruption of the frataxin gene in yeast (*yfh1*) causes iron accumulation in mitochondria, loss of respiratory function, mitochondrial DNA depletion and increased sensitivity to oxidative stress (*112*). Although in eukaryotes, the mature form of frataxin is

targeted to and functions in mitochondria, an artificially generated cytosolic frataxin can rescue the survival of mitochondrial frataxin-deficient cells, suggesting the extramitochondrial frataxin is able to replace the mitochondrial frataxin (*113*).

An eukaryotic frataxin homologue in *E. coli*, CyaY, which shares ~25% sequence identity with frataxin has been characterized (*114*). Anaerobic isothermal calorimetry (ITC) studies demonstrated that at least two ferrous iron can bind to one CyaY monomer with a $K_d \sim 4$ μM and up to 26 ferric iron can bind to one CyaY monomer (*63*). Analytical ultracentrifugation experiments showed that CyaY tetramers are formed in the presence of ferrous iron under anaerobic conditions but upon exposure to O_2, higher molecular weight aggregates of CyaY are formed (*63*). Whether there is any physiological role for the oligomerization of CyaY is unknown.

For yeast frataxin (Yfh1), studies using size-exclusion chromatography (SEC) and inductively coupled plasma mass spectroscopy (ICP-MS) suggest that Yfh1 is in a monomeric state and anaerobic ITC experiments demonstrated that Yfh1 binds two ferrous iron per monomer with an affinity of 2~3 μM (*115*). Physical analysis using dynamic light scattering, gel filtration, and analytical ultracentrifugation indicate that upon addition of ferrous iron aerobically, Yfh1 forms a stable multimer of 840 kDa, corresponding to 48 protein monomers which contain ~50 Fe per monomer (*116, 117*). The conserved acidic residues on the surface of frataxin have been shown to be the iron binding ligands. Mutations on the conserved acidic residues seem to have no effect on the formation of aggregation (*118*). Because of the ferroxidase activity of frataxin and its ability to bind a large amount of iron, it has been proposed that frataxin can serve as an iron storage protein and prevent oxidative stress caused by redox-active iron (*119, 120*). However, in human cells, deletion of frataxin does not appear to affect

the iron pools in mitochondria (*121*). In addition, it has been demonstrated by using a mutant of Yfh1 which is unable to form multimer forms, that the iron-induced oligomerization does not play a critical role for Yfh1's function in vivo, suggesting that the major role of frataxin in vivo may not be as an iron storage protein (*122*).

The exact physiological function of frataxin is still controversial. It has been proposed that frataxin can function as an iron chaperone for the FeS biosynthesis. For yeast frataxin, mutagenesis and solution NMR structural studies suggest the conserved acidic residues in Yfh1 are responsible for iron binding and are essential for interaction with Isu1 (IscU-like scaffold protein in yeast) or ferrochelatase (The protein that delivers iron to heme dependent proteins) (*115, 123, 124*). Studies on human enzymes also showed that frataxin can provide iron for ferrochelatase (*125*). Surface plasma resonance reveals that the binding affinity between human frataxin and human ferrochelatase is about 40 nM (*126*). In yeast, frataxin (Yfh1) and mitochondrial iron tranport proteins (Mrs3p and Mrs4p) can cooperate to provide iron for heme biosynthesis in mitochondria (*127*). Frataxin can also interact with aconitase and in the presence of DTT and citrate, convert inactive $[3Fe4S]^{1+}$-aconitase into active $[4Fe4S]^{2+}$ enzyme (*128*). These studies suggest that frataxin may be a general iron donor for different Fe-containing proteins.

Even though deleterious effects in the frataxin-deficient strains have been demonstrated in yeast and human cells, a deletion of *cyaY* does not show obvious difference in bacterial growth, iron content, and survival rate upon exposed to H_2O_2 compared to wild type, suggesting CyaY may have different functions from its eukaryotic homologues (*129*).

Because of the central role of FeS biosynthesis in iron homeostasis, studies on how frataxin and CyaY deliver iron into scaffold proteins could serve a great paradigm in thinking

about the possible mechanism of iron delivery into apo-β_2 and experimental designs to examine proposed mechanisms.

The first example demonstrates the involvement of frataxin in the FeS cluster assembly in vitro was carried out using human proteins (*130*). Holo-frataxin was reconstituted by aerobic incubation with excess $FeCl_3$ at room temperature for 5 h, followed by passage through a Sephadex G-25 column to remove unbound Fe^{3+}. The reconstituted holo-frataxin contained 6 Fe^{3+} per monomer. The transfer of Fe^{3+} from holo-frataxin to apo-ISU (IscU equivalent) was monitored at A_{456nm}, indicative of the formation of $[2Fe2S]^{2+}$ clusters in ISU. The reaction was carried out under anaerobic conditions in the presence of 4.3 mM DTT and 2.4 mM Na_2S, in addition to 100 μM apo-ISU and 40 μM holo-frataxin. The observed rate constant for the formation of $[2Fe2S]^{2+}$-ISU was ~0.075 min^{-1}. Furthermore, in the absence of apo-ISU, ferric iron was not released from holo-frataxin. When the holo-frataxin was replaced by "free iron" (It is unclear whether Fe^{2+} or Fe^{3+} was used), the rate of cluster formation was negligible. These results support that iron is directly transferred from holo-frataxin into apo-ISU.

The second example involves *E. coli* CyaY (*93*). Fe^{3+}-loaded CyaY was reconstituted by incubation aerobically with 15-fold molar excess $FeCl_3$ for 2 h at 4 ºC, followed by passage through a NAP10 desalting column. The Fe^{3+}-loaded CyaY was further purified by a Superdex 200 gel filtration column and the soluble oligomers (dimers to pentamers), which contained ~20 Fe^{3+}/CyaY, were isolated. To examine whether the Fe^{3+}-CyaY could deliver Fe^{3+} to apo-IscU under anaerobic conditions, 50 μM apo-IscU was incubated with 5 mM DTT for 30 min followed by passage through a spin column to remove DTT. Fe^{3+}-CyaY (containing 150 μM Fe^{3+}), 1 μM IscS and 2 mM L-cysteine were then added into the DTT-treated apo-IscU and the formation of $[2Fe2S]^{2+}$-IscU was monitored at A_{456nm}. An k_{obs} of 0.127 min^{-1} was obtained and

~90% of IscU dimer contained a $[2Fe2S]^{2+}$ cluster 2 h after addition of Fe^{3+}-CyaY. Because no DTT was present, the authors further demonstrated that L-cysteine is likely the reductant for the reduction of the Fe^{3+} in CyaY and proposed a model in which FeS clusters were pre-assembled in IscS and then transferred into IscU.

The third example is from studies on *Drosophila* frataxin (Dfh) (*131*). ITC studies established that Dfh binds one Fe^{2+} per monomer with a K_d of ~6 μM and the Fe^{2+} loaded holo-Dfh monomer binds to one ISU monomer with an affinity of ~0.2 μM. The holo-Dfh was prepared by incubation of apo-Dfh with 1:1 ratio of Fe^{2+} for 20 min at 30 ºC under anaerobic conditions and used without further purification. The holo-Dfh mediated FeS assembly in apo-ISU was demonstrated by addition with 100 μM holo-Dfh into 100 μM ISU under anaerobic condition in the presence of 4.3 mM DTT and 2.4 mM Na_2S and the formation of $[2Fe2S]^{2+}$-ISU was monitored at A_{426nm}. The observed rate constant for the $[2Fe2S]^{2+}$ formation is 0.096 min^{-1}. A control experiment in which holo-Dfh was replaced by Fe^{2+} showed negligible $[2Fe2S]^{2+}$-ISU formation, supporting the FeS cluster assembly in apo-ISU is frataxin mediated.

Even though these experiments strongly suggest iron-loaded frataxin/CyaY can deliver its iron for FeS cluster assembly in ISU/IscU, the rate of the cluster formation in ISU/IscU is very slow (0.075-0.127 min^{-1}), too slow to be of physiologically relevant. In the case of CyaY, the rate of CyaY mediated cluster formation is even slower than the rate of cluster transfer from $[2Fe2S]^{2+}$-$IscU_2$ to apo-Fdx (0.21 min^{-1}) (*95*). These results suggest that certain components inside the cell that can facilitate the iron delivery are required to make the role of frataxin as an iron chaperone physiologically important. Because in vivo the Fe^{3+}-frataxin rather than the Fe^{2+}-frataxin is likely to be more physiologically relevant, the DTT and L-cysteine used in the in vitro studies as reductants for reduction of the Fe^{3+}-frataxin maybe a reason for the slow turnovers.

Whether the more physiologically relevant reductants such as ferredoxins could enhance the reduction and transfer of the Fe^{3+} in frataxin remains to be established.

Studies on class Ia RNR cofactor maintenance in vivo

In addition to biosynthetic pathways for metallo-cofactors, there exist maintenance pathways that can repair the cofactors that are damaged during catalysis or oxidative stress (*132, 133*). The evolutionary advantage for a maintenance pathway is that the active metallo-proteins can be regenerated without biosynthesis of the protein which might be more time- and resource-consuming.

Hydroxyurea (HU) is known to reduce the Y• of β_2, generating inactive met-β_2 (a form of β_2 in which the diferric center is intact but the Y• is reduced), resulting inactivation of RNR, which can lead to cell death (*27, 134*). In early 1980s Reichard and coworkers discovered that Y• can be regenerated in vivo from HU-treated cells after removal of the HU (*135*). To look for components in crude cell lysate of *E. coli* that are responsible for the reintroduction of the Y• of β_2, a superoxide dismutase (SOD), an NAD(P)H:flavin oxidoreductsse (Fre), and an ill-defined "Fraction B", were isolated. The function of Fre was initially proposed to generate reduced flavins, which reduce the iron center of met-β_2 to diferrous-β_2, from which the active cofactor is regenerated in the presence of O_2. The reduction requires NAD(P)H, a flavin, DTT and Fraction B. It was found that Fraction B can be substituted with ferrous iron (*136, 137*). The postulated role of SOD is to detoxify reactive O_2 species generated from reactions between reduced flavins and O_2.

The use of flavins as a substrate rather than a cofactor in Fre is rather unusual. The K_m for the flavins are between 0.6 to 2.2 μM (*136, 138*) and for NADH and NADPH is about 8-25 and 32-50 μM, respectively (*136, 139*). A combination of riboflavin and NADPH shows the highest rate of oxidation of NAD(P)H (k_{cat} = 52 s^{-1} , k_{cat}/K_m = 21 $\mu M^{-1}s^{-1}$) (*138*). Reasons for the requirement of Fraction B for reduction of met-β_2 by reduced flavins generated by Fre are not well understood. Despite heroic efforts, purification of a specific component from Fraction B

that is responsible for its activity was not successful. From subsequent studies it was proposed that the role of Fraction B is to provide soluble aqueous ferrous iron for reduction of met-β_2 in the presence of the Fre system (*137*).

In addition to in vitro studies, the role of Fre in vivo was investigated by comparing the growth rate in the presence of HU between wt *E. coli* K-12 and its isogenic *fre* deletion strain, LS1312. When cells were grown in M9 minimal medium, 14 and 38 mM HU were required to cause 50% growth inhibition in LS1312 and K-12 wt, respectively, supporting the role of Fre in the regeneration of the Y• in vivo (*140*).

Despite these studies, the role of Fre in the maintenance of the Y• was called into question because of the slow turnover number ($< 0.001\ s^{-1}$) in reduction of met-β_2. Furthermore, even though Fre is homologous to the C-terminal domain of MMOR, the fully functional MMOR contains two domains: an FAD and NADH binding C-terminal domain and a [2Fe2S] binding N-terminal domain that is homologous to ferredoxin. The ferredoxin-like domain of MMOR is the direct electron donor for MMO instead of the FAD-domain (*141*), which implies that Reichard's pathway utilizing Fre, while promising, was incomplete. Therefore, while early workers realized a maintenance pathway existed, they were unable to shed light on any details.

Models for cofactor biosynthesis, maintenance, and regulation in vivo

Based on the studies on the cofactor assembly in vitro which requires the controlled delivery of Fe^{2+}, O_2, and a reducing equivalent, and the cofactor maintenance which requires reduction of met-β_2 followed by delivery of O_2 and a reducing equivalent, a working model for in vivo biosynthesis (Pathway A), maintenance (Pathway B) and regulation (Pathway C) of the diferric-Y• cofactor has been proposed (**Figure 1-13**) (*142, 143*). In the biosynthetic pathway, apo-β_2 is first loaded with Fe^{2+} to generate diferrous-β_2. The source of iron and the control of delivery of the two ferrous irons per active site of β_2 monomer without the generation of destructive metabolites of O_2 are currently unknown. Once the diferrous-β_2 is formed, the active cofactor can be assembled by addition of O_2 and a reducing equivalent.

The Y• in the active cofactor is inherently unstable (half-life of the *E. coli* β_2 Y• is several days (*44*) while that of mouse β_2 is 10 min (*144*)) and is also susceptible to one electron reduction by small molecules such as hydroxyurea (HU) (*44*) or proteins inside the cell, resulting an inactive met-β_2 (*135, 145*). Once this met-β_2 is formed, there exists a maintenance pathway (*135*) (**Figure 1-13**) in which the activity of β_2 can be regenerated by reduction of the diferric cluster to a diferrous cluster and this cluster is assembled to the active diferric-Y• cluster by the biosynthetic pathway.

Finally a regulatory pathway (**Figure 1-13**) could have evolved to control the level of the Y• as a mechanism for modulating RNR activity. In this pathway the reduction of the Y• and its regeneration might be carefully coordinated. For example outside the S phase of the cell cycle when DNA is not being replicated, RNR activity might be turned off by Y• reduction, and during the S phase the Y• could instead be regenerated. The regulatory mechanism may or may not overlap with the maintenance pathway.

In this model, there are three key elements that power these pathways in vivo. The first is the source of iron, which is the major unsolved problem in metallo-protein biosynthesis. The iron could come from membrane iron transporters, iron storage proteins, iron chaperones or iron-chelating small molecules. The second is the electron source required for the biosynthetic and maintenance pathways. The reducing equivalents may or may not be the same in these two pathways. The third element is the small molecules or proteins that reduce the Y• in vivo in the regulatory pathway (**Figure 1-13**). Looking for the first two elements will be the focus of this thesis.

Our approach is heavily based on our knowledge on the in vitro cluster assembly, the iron homeostasis pathways in *E. coli*, and the biosynthesis of FeS proteins. Studies on the diferric-Y• cofactor assembly in vitro provide the basis for us to formulate the mechanism of iron delivery (Chapter 4 and 5) and source of reducing equivalents (Chapter 2 and 3). Current understanding of the iron homeostasis in *E. coli* provides the basis for us to design experiments to investigate iron delivery pathways for β_2 (Chapter 4). Studies on the biosynthesis of FeS proteins provide the basis for our experimental design to look for biosynthetic machineries (Chapter 2) and investigate potential iron chaperones (Chapter 3 and 5).

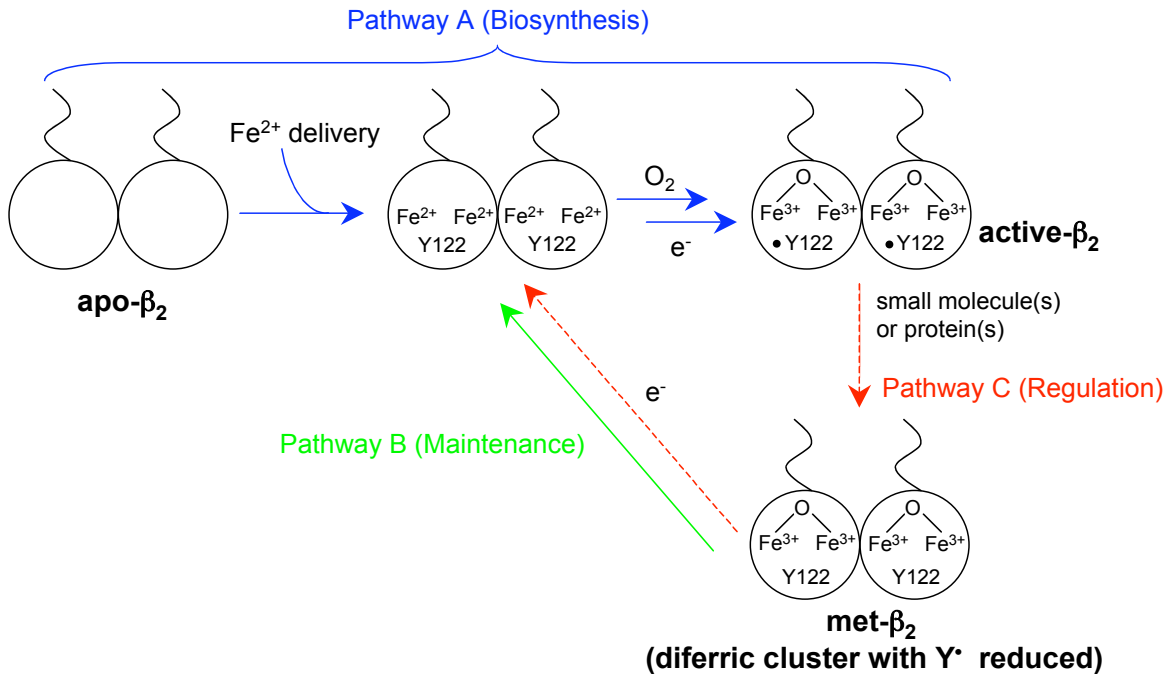

Figure 1-13. A working model for biosynthesis, maintenance, and regulation of the diferric-Y• cofactor of β_2 in vivo. In the biosynthetic pathway A (blue), apo-β_2 forms active β_2 in the presence of ferrous iron, a reducing equivalent and O_2. The Y• of the active diferric-Y• cofactor can be reduced and forms inactive met-β_2. Met-β_2 can be reactivated by reduction of the ferric iron in the cluster to diferrous-β_2 (maintenance pathway B, green) which can then form active-β_2 through biosynthetic pathway. The activity of RNR may be modulated in vivo via a regulatory pathway (red) where proteins or small molecules mediate Y• reduction. The met-β_2 can be converted to the active diferric-Y• cofactor via the maintenance and biosynthetic pathway (= regulatory pathway). The reducing equivalent may or may not be the same as the ones in the maintenance pathway.

Chapter preview

At the beginning of this work, nothing was known about the biosynthesis of the diferric-Y• cofactor of RNR. Previous studies on the maintenance of the diferric-Y• cofactor left several unanswered questions. Multiple approaches have been applied to reveal machineries for biosynthesis and maintenance of the diferric-Y• cluster in β_2. In **Chapter 2**, we report the discovery of an open reading frame annotated [2Fe2S] ferredoxin (YfaE in *E. coli*) through genome comparisons. YfaE has been cloned, expressed, resolubilized, reconstituted anaerobically with Fe^{2+}, Fe^{3+}, and S^{2-}, and characterized by mass spectrometry, size-exclusion chromatography as well as by Mössbauer, EPR, and UV-visible spectroscopies. Characterization has established that YfaE is a monomer and contains a redox active $[2Fe2S]^{1+/2+}$ cluster.

We then investigate the role of YfaE in the maintenance of the diferric-Y• cofactor by titration of met-β_2 with $[2Fe2S]^{1+}$-YfaE anaerobically. The results indicate formations of an equilibrium mixture of diferrous-β_2 and $[2Fe2S]^{2+}$-YfaE with one Fe reduced per YfaE oxidized. At the end point of the titration, O_2 was added to the mixture and the diferric-Y• was formed with a stoichiometry of 2 Fe/Y• and a specific activity correlated with the amount of Y•. Because no excess reductant was present, the reducing equivalent required for diferric-Y• formation is supplied by β_2. Under anaerobic conditions, stopped flow kinetics have been used to monitor the reduction of the diferric-cluster and formation of $[2Fe2S]^{2+}$-YfaE. The titrations and kinetic studies provide the first evidence for a protein involved in the maintenance pathway and likely the biosynthetic pathway.

In **Chapter 3**, we further investigate the binding affinity and the nature of interaction between YfaE and β_2. Different methodologies have been examined to determine the K_d between YfaE and β_2. We first attempt to derive the K_d by stopped flow kinetic analyses.

However, it was found that the interaction between $[2Fe2S]^{1+}$-YfaE and met-β_2 does not follow a rapid binding equilibrium condition required for deriving the K_d by kinetic analysis. We also test applying isothermal titration calorimetry (ITC) and anaerobic ultrafiltration to determine the K_d between $[2Fe2S]^{1+}$-YfaE and apo-β_2 but these experiment were unsuccessful.

We next investigate the nature of binding between YfaE and β_2. Based on the studies on the binding interface between Δ^9-desaturase (Δ9D) (a structural and functional homologue of β_2) and a plant ferredoxin (*146*), we hypothesize that electrostatic interaction could play an important role for binding between YfaE and β_2. Different mutants of YfaE and met-β_2 in which the conserved charged residues on the surface potentially responsible for binding were mutated into alanine and the rate of redox reaction between the two proteins was determined by stopped flow (SF) spectroscopy. The observed rate constants decrease ~250-fold in the reactions between $[2Fe2S]^{1+}$-YfaE and met-β_2-K38A/K42A/K229A mutant compared to wt met-β_2, implying that these conserved lysines in β_2 may play a role for interacting with YfaE.

Our interests then turn to the study of the role of YfaE in vivo. To gain insight into whether YfaE acts catalytically or stoichiometrically in reducing met-β_2 in vivo, quantitative Western blots on *E. coli* whole cells were carried out. The [YfaE] was found to be at least 10 fold less than [met-β_2], therefore YfaE is likely to act catalytically in vivo. We then examine potential candidates that can reduce $[2Fe2S]^{2+}$-YfaE. We first focus on the flavin reductase, Fre, due to its association with Y• maintenance. The results show that Fre is able to reduce YfaE. Furthermore, we show that met-β_2 can be reduced by consumption of NADPH in the presence of catalytic amounts of YfaE, Fre and riboflavin, suggesting that YfaE and Fre could act together in regenerating the Y• in vivo. The role of YfaE in vivo is further supported by the growth of *ΔyfaE* in the presence of hydroxyurea. The results reveal a much slower rate of growth of *ΔyfaE*

than the wild type. Furthermore, Western blots analysis of HU treated cells reveals an up-regulation of YfaE expression, supporting the role of YfaE in the maintenance of the Y• in vivo.

In **Chapter 4**, we focus on investigation of how iron is delivered into apo-β_2 in vivo. We first examine whether CyaY can be an iron chaperone for apo-β_2. CyaY was overexpressed, purified and reconstituted with Fe^{2+} under anaerobic conditions. However, no Fe^{2+} loaded CyaY was isolated. We next developed a sensitive colorimetric assay to determine components in fractionated crude cell lysate that are responsible for iron incorporation into apo-β_2. We use apo-β_2-W48F/F208Y, which forms Fe-catechol clusters in the presence of Fe^{2+} and O_2 for the colorimetric assay. The formation of Fe-catechol complex can be monitored at A_{660nm}, which is away from background absorption of crude cell lysate. However, in the presence of crude cell lyaste and Fe^{2+}, no Fe-catechol formation was observed in apo-β_2-W48F/F208Y mutant, implying that there might be molecules in the cell lysate that chelate the exogenous Fe^{2+} and the availability of the ferrous iron pool inside the cells are tightly controlled.

We then searched for the existence of iron chaperones for β_2 by protein co-purification. We inserted a 6xHis or a StrepII affinity tag at different positions in β_2 and compared the elution patterns between wild type β_2 and β_2-E115A, a mutant that remains in the apo-form. No difference between the elution patterns was observed. Furthermore, in vivo cross-linking by formaldehyde generates the same elution patterns between wt and E115A mutant, suggesting that the nature of the interaction may be too weak or too transient, or the amount of the iron chaperone, if any, is too low to detect by this method.

Based on ourstudies which determined the concentration of Y• and β_2 in vivo, we turned to apply the whole cell EPR to investigate iron delivery pathways for apo-β_2. In this approach, β_2 is overexpressed in knockouts of Fe^{3+} or Fe^{2+} membrane transporters and the Y•

signal in the whole cells is determined by EPR spectroscopy. If the delivery of iron into apo-β_2 relies on one or two major iron trafficking pathways, the deletion of that pathway may result in less efficient iron delivery and a phenotype of lower Y• signal from the whole cells may be observed. The results suggest that a ferrous plasma membrane transporter (FeoB) might play a major role in supplying the iron required for diferric-Y• cofactor assembly.

Last we apply Mössbauer spectroscopy to monitor the iron migration inside the cells in the early stage of β_2 expression. By analyzing the iron species in the whole cells at different time points after induction of β_2, we were able to observe a decrease of Fe^{2+} species concomitantly with an increase of the diferric cluster of β_2, indicating that a Fe^{2+} pool(s) is the immediate iron source for β_2 biosynthesis. This is the first direct observation of the source of iron for the biosynthesis of β_2 in vivo. This result is also consistent with the observation that the Fe^{2+} transporter, FeoB, plays a major role in the iron delivery to apo-β_2.

In **Chapter 5**, we investigate the possibility of YfaE as an iron chaperone for β_2. A serendipitous observation was made when $[2Fe2S]^{1+}$-YfaE was mixed with apo-β_2 followed by exposure to O_2, small amounts of the Y• was formed. Because no other iron source was available, the iron must be coming from YfaE. Mössbauer experiments using apo-β_2 and $[2^{57}Fe2S]^{1+}$-YfaE demonstrate that the iron in the diferric cluster comes from YfaE after the sample was exposed to O_2. The amount of the Y• form reached ~1 Y•/β_2 after $[2Fe2S]^{1+}$-YfaE was mixed with apo-β_2 and incubated aerobically at 37 ºC for ~4 h. The formation of the Y• can be facilitated by DTT. Results from size-exclusion chromatography indicate the formation of YfaE-dimer in the presence of DTT. A model of how YfaE could function as an iron chaperone for apo-β_2 was proposed.

References

(1) Stubbe, J., Nocera, D. G., Yee, C. S., and Chang, M. C. Y. (2003) Radical initiation in the class I ribonucleotide reductase: Long-range proton-coupled electron transfer? *Chem Rev 103*, 2167-2201.

(2) Stubbe, J., and van der Donk, W. A. (1998) Protein radicals in enzyme catalysis. *Chem Rev 98*, 705-762.

(3) Ravi, N., Bollinger, J. M., Huynh, B. H., Edmondson, D. E., and Stubbe, J. (1994) Mechanism of assembly of the tyrosyl radical-diiron(III) cofactor of *Escherichia coli* ribonucleotide reductase. 1. Mössbauer characterization of the diferric radical precursor. *J Am Chem Soc 116*, 8007-8014.

(4) Uhlin, U., and Eklund, H. (1994) Structure of ribonucleotide reductase protein R1. *Nature 370*, 533-539.

(5) Bollinger, J. M., Tong, W. H., Ravi, N., Huynh, B. H., Edmondson, D. E., and Stubbe, J. (1994) Mechanism of assembly of the tyrosyl radical-Diiron(III) cofactor of *Escherichia coli* ribonucleotide reductase. 3. Kinetics of the limiting Fe^{2+} reaction by optical, EPR, and Mössbauer spectroscopies. *J Am Chem Soc 116*, 8024-8032.

(6) Bollinger, J. M., Tong, W. H., Ravi, N., Huynh, B. H., Edmondson, D. E., and Stubbe, J. (1994) Mechanism of assembly of the tyrosyl radical-diiron(III) cofactor of *Escherichia coli* ribonucleotide reductase. 2. Kinetics of the excess Fe^{2+} reaction by optical, EPR, and Mössbauer spectroscopies. *J Am Chem Soc 116*, 8015-8023.

(7) Tong, W. H., Chen, S., Lloyd, S. G., Edmondson, D. E., Huynh, B. H., and Stubbe, J. (1996) Mechanism of assembly of the diferric cluster-tyrosyl radical cofactor of *Escherichia coli* ribonucleotide reductase from the diferrous form of the R2 subunit. *J Am Chem Soc 118*, 2107-2108.

(8) Nordlund, P., Sjöberg, B. M., and Eklund, H. (1990) Three-dimensional structure of the free radical protein of ribonucleotide reductase. *Nature 345*, 593-8.

(9) Nordlund, P., and Reichard, P. (2006) Ribonucleotide reductases. *Annu Rev Biochem 75*, 681-706.

(10) Jordan, A., and Reichard, P. (1998) Ribonucleotide reductases. *Annu Rev Biochem 67*, 71-98.

(11) Kolberg, M., Strand, K. R., Graff, P., and Andersson, K. K. (2004) Structure, function, and mechanism of ribonucleotide reductases. *Biochim Biophys Acta 1699*, 1-34.

(12) Licht, S., and Stubbe, J. (1999) Mechanistic investigations of ribonucleotide reductases, in *Comprehensive Natural Products Chemistry* (Poulter, C. D., Ed.) pp 163-203, Elsevier Science, New York.

(13) Yun, D., Garcia-Serres, R., Chicalese, B. M., An, Y. H., Huynh, B. H., and Bollinger, J. M., Jr. (2007) (μ-1,2-peroxo)diiron(III/III) complex as a precursor to the diiron(III/IV) intermediate X in the assembly of the iron-radical cofactor of ribonucleotide reductase from mouse. *Biochemistry 46*, 1925-32.

(14) Rosell, R., Crino, L., Danenberg, K., Scagliotti, G., Bepler, G., Taron, M., Alberola, V., Provencio, M., Camps, C., De Marinis, F., Sanchez, J. J., and Penas, R. (2003) Targeted therapy in combination with gemcitabine in non-small cell lung cancer. *Semin Oncol 30*, 19-25.

(15) Davidson, J. D., Ma, L. D., Flagella, M., Geeganage, S., Gelbert, L. M., and Slapak, C. A. (2004) An increase in the expression of ribonucleotide reductase large subunit 1 is associated with gemcitabine resistance in non-small cell lung cancer cell lines. *Cancer Res 64*, 3761-3766.

(16) Stubbe, J., Ge, J., and Yee, C. S. (2001) The evolution of ribonucleotide reduction revisited. *Trends Biochem Sci 26*, 93-99.

(17) Sintchak, M. D., Arjara, G., Kellogg, B. A., Stubbe, J., and Drennan, C. L. (2002) The crystal structure of class II ribonucleotide reductase reveals how an allosterically regulated monomer mimics a dimer. *Nat Struct Biol 9*, 293-300.

(18) Licht, S., Gerfen, G. J., and Stubbe, J. (1996) Thiyl radicals in ribonucleotide reductases. *Science 271*, 477-81.

(19) Logan, D. T., Su, X. D., Aberg, A., Regnstrom, K., Hajdu, J., Eklund, H., and Nordlund, P. (1996) Crystal structure of reduced protein R2 of ribonucleotide reductase: The structural basis for oxygen activation at a dinuclear iron site. *Structure 4*, 1053-1064.

(20) Jiang, W., Yun, D., Saleh, L., Barr, E. W., Xing, G., Hoffart, L. M., Maslak, M. A., Krebs, C., and Bollinger, J. M., Jr. (2007) A manganese(IV)/iron(III) cofactor in *Chlamydia trachomatis* ribonucleotide reductase. *Science 316*, 1188-91.

(21) Stubbe, J., and Ackles, D. (1980) On the mechanism of ribonucleoside diphosphate reductase from *Escherichia coli*. Evidence for 3'-C--H bond cleavage. *J Biol Chem 255*, 8027-30.

(22) Stubbe, J., Ator, M., and Krenitsky, T. (1983) Mechanism of ribonucleoside diphosphate reductase from *Escherichia coli*. Evidence for 3'-C--H bond cleavage. *J Biol Chem 258*, 1625-31.

(23) Wang, J., Lohman, G. J., and Stubbe, J. (2007) Enhanced subunit interactions with gemcitabine-5'-diphosphate inhibit ribonucleotide reductases. *Proc Natl Acad Sci U S A 104*, 14324-9.

(24) Kashlan, O. B., and Cooperman, B. S. (2003) Comprehensive model for allosteric regulation of mammalian ribonucleotide reductase: refinements and consequences. *Biochemistry 42*, 1696-1706.

(25) Kashlan, O. B., Scott, C. P., Lear, J. D., and Cooperman, B. S. (2002) A comprehensive model for the allosteric regulation of mammalian ribonucleotide reductase. Functional consequences of ATP- and dATP-induced oligomerization of the large subunit. *Biochemistry 41*, 462-474.

(26) Rofougaran, R., Vodnala, M., and Hofer, A. (2006) Enzymatically active mammalian ribonucleotide reductase exists primarily as an $\alpha_6\beta_2$ octamer. *J Biol Chem 281*, 27705-27711.

(27) Brown, N. C., Eliasson, R., Reichard, P., and Thelander, L. (1969) Spectrum and iron content of protein B2 from ribonucleoside diphosphate reductase. *Eur. J. Biochem. 9*, 512-8.

(28) von Dobeln, U., and Reichard, P. (1976) Binding of substrates to *Escherichia coli* ribonucleotide reductase. *J Biol Chem 251*, 3616-22.

(29) Uppsten, M., Farnegardh, M., Jordan, A., Eliasson, R., Eklund, H., and Uhlin, U. (2003) Structure of the large subunit of class Ib ribonucleotide reductase from *Salmonella typhimurium* and its complexes with allosteric effectors. *J Mol Biol 330*, 87-97.

(30) Scott, C. P., Kashlan, O. B., Lear, J. D., and Cooperman, B. S. (2001) A quantitative model for allosteric control of purine reduction by murine ribonucleotide reductase. *Biochemistry 40*, 1651-1661.

(31) Eriksson, M., Uhlin, U., Ramaswamy, S., Ekberg, M., Regnstrom, K., Sjoberg, B. M., and Eklund, H. (1997) Binding of allosteric effectors to ribonucleotide reductase protein R1: reduction of active-site cysteines promotes substrate binding. *Structure 5*, 1077-92.

(32) Kasrayan, A., Birgander, P. L., Pappalardo, L., Regnstrom, K., Westman, M., Slaby, A., Gordon, E., and Sjöberg, B. M. (2004) Enhancement by effectors and substrate nucleotides of R1-R2 interactions in *Escherichia coli* class Ia ribonucleotide reductase. *J Biol Chem 279*, 31050-7.

(33) Brown, N. C., Larsson, A., and Reichard, P. (1967) On the subunit structure of ribonucleoside diphosphate reductase. *J Biol Chem 242*, 4272-3.

(34) Rofougaran, R., Crona, M., Vodnala, M., Sjoberg, B. M., and Hofer, A. (2008) Oligomerization status directs overall activity regulation of the *Escherichia coli* class Ia ribonucleotide reductase. *J Biol Chem 283*, 35310-8.

(35) Ekberg, M., Sahlin, M., Eriksson, M., and Sjöberg, B. M. (1996) Two conserved tyrosine residues in protein R1 participate in an intermolecular electron transfer in ribonucleotide reductase. *J Biol Chem 271*, 20655-20659.

(36) Rova, U., Adrait, A., Potsch, S., Gräslund, A., and Thelander, L. (1999) Evidence by mutagenesis that Tyr(370) of the mouse ribonucleotide reductase R2 protein is the connecting link in the intersubunit radical transfer pathway. *J Biol Chem 274*, 23746-23751.

(37) Rova, U., Goodtzova, K., Ingemarson, R., Behravan, G., Gräslund, A., and Thelander, L. (1995) Evidence by site-directed mutagenesis supports long-range electron transfer in mouse ribonucleotide reductase. *Biochemistry 34*, 4267-4275.

(38) Climent, I., Sjöberg, B. M., and Huang, C. Y. (1992) Site-directed mutagenesis and deletion of the carboxyl terminus of *Escherichia coli* ribonucleotide reductase protein R2 - Effects on catalytic activity and subunit interaction. *Biochemistry 31*, 4801-4807.

(39) Seyedsayamdost, M. R., Reece, S. Y., Nocera, D. G., and Stubbe, J. (2006) Mono-, di-, tri-, and tetra-substituted fluorotyrosines: new probes for enzymes that use tyrosyl radicals in catalysis. *J Am Chem Soc 128*, 1569-79.

(40) Seyedsayamdost, M. R., and Stubbe, J. (2006) Site-specific replacement of Y356 with 3,4-dihydroxyphenylalanine in the beta2 subunit of *E. coli* ribonucleotide reductase. *J Am Chem Soc 128*, 2522-3.

(41) Seyedsayamdost, M. R., and Stubbe, J. (2007) Forward and reverse electron transfer with the Y356DOPA-beta2 heterodimer of *E. coli* ribonucleotide reductase. *J Am Chem Soc 129*, 2226-7.

(42) Seyedsayamdost, M. R., Xie, J., Chan, C. T., Schultz, P. G., and Stubbe, J. (2007) Site-specific insertion of 3-aminotyrosine into subunit alpha2 of *E. coli* ribonucleotide reductase: direct evidence for involvement of Y730 and Y731 in radical propagation. *J Am Chem Soc 129*, 15060-71.

(43) Seyedsayamdost, M. R., Yee, C. S., Reece, S. Y., Nocera, D. G., and Stubbe, J. (2006) pH Rate profiles of FnY356-R2s (n = 2, 3, 4) in *Escherichia coli* ribonucleotide reductase: evidence that Y356 is a redox-active amino acid along the radical propagation pathway. *J Am Chem Soc 128*, 1562-8.

(44) Atkin, C. L., Thelander, L., Reichard, P., and Lang, G. (1973) Iron and free-radical in ribonucleotide reductase - exchange of iron and Mössbauer-spectroscopy of protein-B2 subunit of *Escherichia coli* enzyme. *J Biol Chem 248*, 7464-7472.

(45) Bollinger, J. M., Chen, S. X., Parkin, S. E., Mangravite, L. M., Ley, B. A., Edmondson, D. E., and Huynh, B. H. (1997) Differential iron(II) affinity of the sites of the diiron cluster in protein R2 of *Escherichia coli* ribonucleotide reductase: Tracking the individual sites through the O_2 activation sequence. *Journal of the American Chemical Society 119*, 5976-5977.

(46) Pierce, B. S., and Hendrich, M. P. (2005) Local and global effects of metal binding within the small subunit of ribonucleotide reductase. *J Am Chem Soc 127*, 3613-3623.

(47) Bollinger, J. M., Krebs, C., Vicol, A., Chen, S. X., Ley, B. A., Edmondson, D. E., and Huynh, B. H. (1998) Engineering the diiron site of Escherichia coli ribonucleotide reductase protein R2 to accumulate an intermediate similar to H-peroxo, the putative peroxodiiron(III) complex from the methane monooxygenase catalytic cycle. *J Am Chem Soc 120*, 1094-1095.

(48) Mitic, N., Clay, M. D., Saleh, L., Bollinger, J. M., and Solomon, E. I. (2007) Spectroscopic and electronic structure studies of intermediate X in ribonucleotide reductase R2 and two variants: A description of the Fe(IV)-oxo bond in the Fe(III)-O-Fe(IV) dimer. *J Am Chem Soc 129*, 9049-9065.

(49) Riggs-Gelasco, P. J., Shu, L. J., Chen, S. X., Burdi, D., Huynh, B. H., Que, L., and Stubbe, J. (1998) EXAFS characterization of the intermediate X generated during the assembly of the *Escherichia coli* ribonucleotide reductase R2 diferric tyrosyl radical cofactor. *J Am Chem Soc 120*, 849-860.

(50) Burdi, D., Sturgeon, B. E., Tong, W. H., Stubbe, J. A., and Hoffman, B. M. (1996) Rapid freeze-quench ENDOR of the radical X intermediate of *Escherichia coli* ribonucleotide reductase using $^{17}O_2$, $H_2{}^{17}O$, and ^2H_2O. *J Am Chem Soc 118*, 281-282.

(51) Burdi, D., Willems, J. P., Riggs-Gelasco, P., Antholine, W. E., Stubbe, J., and Hoffman, B. M. (1998) The core structure of X generated in the assembly of the diiron cluster of ribonucleotide reductase: $^{17}O_2$ and $H_2{}^{17}O$ ENDOR. *J Am Chem Soc 120*, 12910-12919.

(52) Willems, J. P., Lee, H. I., Burdi, D., Doan, P. E., Stubbe, J., and Hoffman, B. M. (1997) Identification of the protonated oxygenic ligands of ribonucleotide reductase intermediate X by Q-band ^1H, ^2H CW and pulsed ENDOR. *J Am Chem Soc 119*, 9816-9824.

(53) Han, W. G., Liu, T., Lovell, T., and Noodleman, L. (2005) Active site structure of class I ribonucleotide reductase intermediate X: a density functional theory analysis of structure, energetics, and spectroscopy. *J Am Chem Soc 127*, 15778-90.

(54) Han, W. G., Liu, T., Lovell, T., and Noodleman, L. (2006) Seven clues to the origin and structure of class-I ribonucleotide reductase intermediate X. *J Inorg Biochem 100*, 771-9.

(55) Andrews, S. C., Robinson, A. K., and Rodriguez-Quinones, F. (2003) Bacterial iron homeostasis. *FEMS Microbiol Rev 27*, 215-37.

(56) Guerinot, M. L. (1994) Microbial iron transport. *Annu Rev Microbiol 48*, 743-72.

(57) Braun, V., Hantke, K., and Koster, W. (1998) Bacterial iron transport: mechanisms, genetics, and regulation. *Met Ions Biol Syst 35*, 67-145.

(58) Wandersman, C., and Delepelaire, P. (2004) Bacterial iron sources: from siderophores to hemophores. *Annu Rev Microbiol 58*, 611-47.

(59) Cartron, M. L., Maddocks, S., Gillingham, P., Craven, C. J., and Andrews, S. C. (2006) Feo--transport of ferrous iron into bacteria. *Biometals 19*, 143-57.

(60) Makui, H., Roig, E., Cole, S. T., Helmann, J. D., Gros, P., and Cellier, M. F. (2000) Identification of the *Escherichia coli* K-12 Nramp orthologue (MntH) as a selective divalent metal ion transporter. *Mol Microbiol 35*, 1065-78.

(61) Grass, G., Franke, S., Taudte, N., Nies, D. H., Kucharski, L. M., Maguire, M. E., and Rensing, C. (2005) The metal permease ZupT from *Escherichia coli* is a transporter with a broad substrate spectrum. *J Bacteriol 187*, 1604-11.

(62) Andrews, S. C. (1998) Iron storage in bacteria. *Adv Microb Physiol 40*, 281-351.

(63) Bou-Abdallah, F., Adinolfi, S., Pastore, A., Laue, T. M., and Dennis Chasteen, N. (2004) Iron binding and oxidation kinetics in frataxin CyaY of *Escherichia coli*. *J Mol Biol 341*, 605-15.

(64) Bagg, A., and Neilands, J. B. (1987) Ferric uptake regulation protein acts as a repressor, employing iron (II) as a cofactor to bind the operator of an iron transport operon in *Escherichia coli*. *Biochemistry 26*, 5471-7.

(65) Keyer, K., and Imlay, J. A. (1996) Superoxide accelerates DNA damage by elevating free-iron levels. *Proc Natl Acad Sci U S A 93*, 13635-40.

(66) Masse, E., Escorcia, F. E., and Gottesman, S. (2003) Coupled degradation of a small regulatory RNA and its mRNA targets in *Escherichia coli*. *Genes Dev 17*, 2374-83.

(67) Masse, E., and Gottesman, S. (2002) A small RNA regulates the expression of genes involved in iron metabolism in *Escherichia coli*. *Proc Natl Acad Sci U S A 99*, 4620-5.

(68) Masse, E., Vanderpool, C. K., and Gottesman, S. (2005) Effect of RyhB small RNA on global iron use in *Escherichia coli*. *J Bacteriol 187*, 6962-71.

(69) Abdul-Tehrani, H., Hudson, A. J., Chang, Y. S., Timms, A. R., Hawkins, C., Williams, J. M., Harrison, P. M., Guest, J. R., and Andrews, S. C. (1999) Ferritin mutants of *Escherichia coli* are iron deficient and growth impaired, and fur mutants are iron deficient. *J Bacteriol 181*, 1415-28.

(70) Pierre, J. L., and Fontecave, M. (1999) Iron and activated oxygen species in biology: the basic chemistry. *Biometals 12*, 195-9.

(71) Huffman, D. L., and O'Halloran, T. V. (2001) Function, structure, and mechanism of intracellular copper trafficking proteins. *Annu Rev Biochem 70*, 677-701.

(72) Beinert, H., Holm, R. H., and Munck, E. (1997) Iron-sulfur clusters: nature's modular, multipurpose structures. *Science 277*, 653-9.

(73) Johnson, D. C., Dean, D. R., Smith, A. D., and Johnson, M. K. (2005) Structure, function, and formation of biological iron-sulfur clusters. *Annu Rev Biochem 74*, 247-81.

(74) Fontecave, M., and Ollagnier-de-Choudens, S. (2008) Iron-sulfur cluster biosynthesis in bacteria: Mechanisms of cluster assembly and transfer. *Arch Biochem Biophys 474*, 226-37.

(75) Ayala-Castro, C., Saini, A., and Outten, F. W. (2008) Fe-S cluster assembly pathways in bacteria. *Microbiol Mol Biol Rev 72*, 110-25, table of contents.

(76) Jacobson, M. R., Brigle, K. E., Bennett, L. T., Setterquist, R. A., Wilson, M. S., Cash, V. L., Beynon, J., Newton, W. E., and Dean, D. R. (1989) Physical and genetic map of the major nif gene cluster from Azotobacter vinelandii. *J Bacteriol 171*, 1017-27.

(77) Zheng, L., Cash, V. L., Flint, D. H., and Dean, D. R. (1998) Assembly of iron-sulfur clusters. Identification of an iscSUA-hscBA-fdx gene cluster from *Azotobacter vinelandii*. *J Biol Chem 273*, 13264-72.

(78) Takahashi, Y., and Tokumoto, U. (2002) A third bacterial system for the assembly of iron-sulfur clusters with homologs in archaea and plastids. *J Biol Chem 277*, 28380-3.

(79) Outten, F. W., Djaman, O., and Storz, G. (2004) A suf operon requirement for Fe-S cluster assembly during iron starvation in Escherichia coli. *Mol Microbiol 52*, 861-72.

(80) Nachin, L., Loiseau, L., Expert, D., and Barras, F. (2003) SufC: an unorthodox cytoplasmic ABC/ATPase required for [Fe-S] biogenesis under oxidative stress. *Embo J 22*, 427-37.

(81) Agar, J. N., Krebs, C., Frazzon, J., Huynh, B. H., Dean, D. R., and Johnson, M. K. (2000) IscU as a scaffold for iron-sulfur cluster biosynthesis: sequential assembly of [2Fe-2S] and [4Fe-4S] clusters in IscU. *Biochemistry 39*, 7856-62.

(82) Chandramouli, K., Unciuleac, M. C., Naik, S., Dean, D. R., Huynh, B. H., and Johnson, M. K. (2007) Formation and properties of [4Fe-4S] clusters on the IscU scaffold protein. *Biochemistry 46*, 6804-11.

(83) Unciuleac, M. C., Chandramouli, K., Naik, S., Mayer, S., Huynh, B. H., Johnson, M. K., and Dean, D. R. (2007) In vitro activation of apo-aconitase using a [4Fe-4S] cluster-loaded form of the IscU [Fe-S] cluster scaffolding protein. *Biochemistry 46*, 6812-21.

(84) Hoff, K. G., Silberg, J. J., and Vickery, L. E. (2000) Interaction of the iron-sulfur cluster assembly protein IscU with the Hsc66/Hsc20 molecular chaperone system of *Escherichia coli*. *Proc Natl Acad Sci U S A 97*, 7790-5.

(85) Bonomi, F., Iametti, S., Morleo, A., Ta, D., and Vickery, L. E. (2008) Studies on the mechanism of catalysis of iron-sulfur cluster transfer from IscU[2Fe2S] by HscA/HscB chaperones. *Biochemistry*.

(86) Eccleston, J. F., Petrovic, A., Davis, C. T., Rangachari, K., and Wilson, R. J. (2006) The kinetic mechanism of the SufC ATPase: the cleavage step is accelerated by SufB. *J Biol Chem 281*, 8371-8.

(87) Zheng, L., White, R. H., Cash, V. L., Jack, R. F., and Dean, D. R. (1993) Cysteine desulfurase activity indicates a role for NIFS in metallocluster biosynthesis. *Proc Natl Acad Sci U S A 90*, 2754-8.

(88) Mihara, H., and Esaki, N. (2002) Bacterial cysteine desulfurases: their function and mechanisms. *Appl Microbiol Biotechnol 60*, 12-23.

(89) Kaiser, J. T., Clausen, T., Bourenkow, G. P., Bartunik, H. D., Steinbacher, S., and Huber, R. (2000) Crystal structure of a NifS-like protein from *Thermotoga maritima*: implications for iron sulphur cluster assembly. *J Mol Biol 297*, 451-64.

(90) Cupp-Vickery, J. R., Urbina, H., and Vickery, L. E. (2003) Crystal structure of IscS, a cysteine desulfurase from *Escherichia coli*. *J Mol Biol 330*, 1049-59.

(91) Loiseau, L., Ollagnier-de-Choudens, S., Nachin, L., Fontecave, M., and Barras, F. (2003) Biogenesis of Fe-S cluster by the bacterial Suf system: SufS and SufE form a new type of cysteine desulfurase. *J Biol Chem 278*, 38352-9.

(92) Tokumoto, U., Nomura, S., Minami, Y., Mihara, H., Kato, S., Kurihara, T., Esaki, N., Kanazawa, H., Matsubara, H., and Takahashi, Y. (2002) Network of protein-protein interactions among iron-sulfur cluster assembly proteins in *Escherichia coli*. *J Biochem 131*, 713-9.

(93) Layer, G., Ollagnier-de Choudens, S., Sanakis, Y., and Fontecave, M. (2006) Iron-sulfur cluster biosynthesis: characterization of *Escherichia coli* CyaY as an iron donor for the assembly of [2Fe-2S] clusters in the scaffold IscU. *J Biol Chem 281*, 16256-63.

(94) Urbina, H. D., Silberg, J. J., Hoff, K. G., and Vickery, L. E. (2001) Transfer of sulfur from IscS to IscU during Fe/S cluster assembly. *J Biol Chem 276*, 44521-6.

(95) Bonomi, F., Iametti, S., Ta, D., and Vickery, L. E. (2005) Multiple turnover transfer of [2Fe2S] clusters by the iron-sulfur cluster assembly scaffold proteins IscU and IscA. *J Biol Chem 280*, 29513-8.

(96) Chandramouli, K., and Johnson, M. K. (2006) HscA and HscB stimulate [2Fe-2S] cluster transfer from IscU to apoferredoxin in an ATP-dependent reaction. *Biochemistry 45*, 11087-95.

(97) Silberg, J. J., Hoff, K. G., Tapley, T. L., and Vickery, L. E. (2001) The Fe/S assembly protein IscU behaves as a substrate for the molecular chaperone Hsc66 from Escherichia coli. *J Biol Chem 276*, 1696-700.

(98) Vickery, L. E., Silberg, J. J., and Ta, D. T. (1997) Hsc66 and Hsc20, a new heat shock cognate molecular chaperone system from *Escherichia coli*. *Protein Sci 6*, 1047-56.

(99) Dutkiewicz, R., Schilke, B., Knieszner, H., Walter, W., Craig, E. A., and Marszalek, J. (2003) Ssq1, a mitochondrial Hsp70 involved in iron-sulfur (Fe/S) center biogenesis. Similarities to and differences from its bacterial counterpart. *J Biol Chem 278*, 29719-27.

(100) Raulfs, E. C., O'Carroll, I. P., Dos Santos, P. C., Unciuleac, M. C., and Dean, D. R. (2008) In vivo iron-sulfur cluster formation. *Proc Natl Acad Sci U S A 105*, 8591-6.

(101) Ding, H., and Clark, R. J. (2004) Characterization of iron binding in IscA, an ancient iron-sulphur cluster assembly protein. *Biochem J 379*, 433-40.

(102) Ding, H., Harrison, K., and Lu, J. (2005) Thioredoxin reductase system mediates iron binding in IscA and iron delivery for the iron-sulfur cluster assembly in IscU. *J Biol Chem 280*, 30432-7.

(103) Ding, H., Clark, R. J., and Ding, B. (2004) IscA mediates iron delivery for assembly of iron-sulfur clusters in IscU under the limited accessible free iron conditions. *J Biol Chem 279*, 37499-504.

(104) Ding, B., Smith, E. S., and Ding, H. (2005) Mobilization of the iron centre in IscA for the iron-sulphur cluster assembly in IscU. *Biochem J 389*, 797-802.

(105) Krebs, C., Agar, J. N., Smith, A. D., Frazzon, J., Dean, D. R., Huynh, B. H., and Johnson, M. K. (2001) IscA, an alternate scaffold for Fe-S cluster biosynthesis. *Biochemistry 40*, 14069-80.

(106) Ollagnier-de Choudens, S., Nachin, L., Sanakis, Y., Loiseau, L., Barras, F., and Fontecave, M. (2003) SufA from *Erwinia chrysanthemi*. Characterization of a scaffold protein required for iron-sulfur cluster assembly. *J Biol Chem 278*, 17993-8001.

(107) Ollagnier-de-Choudens, S., Sanakis, Y., and Fontecave, M. (2004) SufA/IscA: reactivity studies of a class of scaffold proteins involved in [Fe-S] cluster assembly. *J Biol Inorg Chem 9*, 828-38.

(108) Zeng, J., Geng, M., Jiang, H., Liu, Y., Liu, J., and Qiu, G. (2007) The IscA from *Acidithiobacillus* ferrooxidans is an iron-sulfur protein which assemble the [Fe4S4] cluster with intracellular iron and sulfur. *Arch Biochem Biophys 463*, 237-44.

(109) Wollenberg, M., Berndt, C., Bill, E., Schwenn, J. D., and Seidler, A. (2003) A dimer of the FeS cluster biosynthesis protein IscA from cyanobacteria binds a [2Fe2S] cluster between two protomers and transfers it to [2Fe2S] and [4Fe4S] apo proteins. *Eur J Biochem 270*, 1662-71.

(110) Ta, D. T., and Vickery, L. E. (1992) Cloning, sequencing, and overexpression of a [2Fe-2S] ferredoxin gene from Escherichia coli. *J Biol Chem 267*, 11120-5.

(111) Campuzano, V., Montermini, L., Molto, M. D., Pianese, L., Cossee, M., Cavalcanti, F., Monros, E., Rodius, F., Duclos, F., Monticelli, A., Zara, F., Canizares, J., Koutnikova, H., Bidichandani, S. I., Gellera, C., Brice, A., Trouillas, P., De Michele, G., Filla, A., De Frutos, R., Palau, F., Patel, P. I., Di Donato, S., Mandel, J. L., Cocozza, S., Koenig, M., and Pandolfo, M. (1996) Friedreich's ataxia: autosomal recessive disease caused by an intronic GAA triplet repeat expansion. *Science 271*, 1423-7.

(112) Babcock, M., de Silva, D., Oaks, R., Davis-Kaplan, S., Jiralerspong, S., Montermini, L., Pandolfo, M., and Kaplan, J. (1997) Regulation of mitochondrial iron accumulation by Yfh1p, a putative homolog of frataxin. *Science 276*, 1709-12.

(113) Condo, I., Ventura, N., Malisan, F., Tomassini, B., and Testi, R. (2006) A pool of extramitochondrial frataxin that promotes cell survival. *J Biol Chem 281*, 16750-6.

(114) Cho, S. J., Lee, M. G., Yang, J. K., Lee, J. Y., Song, H. K., and Suh, S. W. (2000) Crystal structure of Escherichia coli CyaY protein reveals a previously unidentified fold for the evolutionarily conserved frataxin family. *Proc Natl Acad Sci U S A 97*, 8932-7.

(115) Cook, J. D., Bencze, K. Z., Jankovic, A. D., Crater, A. K., Busch, C. N., Bradley, P. B., Stemmler, A. J., Spaller, M. R., and Stemmler, T. L. (2006) Monomeric yeast frataxin is an iron-binding protein. *Biochemistry 45*, 7767-77.

(116) Adamec, J., Rusnak, F., Owen, W. G., Naylor, S., Benson, L. M., Gacy, A. M., and Isaya, G. (2000) Iron-dependent self-assembly of recombinant yeast frataxin: implications for Friedreich ataxia. *Am J Hum Genet 67*, 549-62.

(117) Gakh, O., Adamec, J., Gacy, A. M., Twesten, R. D., Owen, W. G., and Isaya, G. (2002) Physical evidence that yeast frataxin is an iron storage protein. *Biochemistry 41*, 6798-804.

(118) Adinolfi, S., Trifuoggi, M., Politou, A. S., Martin, S., and Pastore, A. (2002) A structural approach to understanding the iron-binding properties of phylogenetically different frataxins. *Hum Mol Genet 11*, 1865-77.

(119) Park, S., Gakh, O., Mooney, S. M., and Isaya, G. (2002) The ferroxidase activity of yeast frataxin. *J Biol Chem 277*, 38589-95.

(120) O'Neill, H. A., Gakh, O., Park, S., Cui, J., Mooney, S. M., Sampson, M., Ferreira, G. C., and Isaya, G. (2005) Assembly of human frataxin is a mechanism for detoxifying redox-active iron. *Biochemistry 44*, 537-45.

(121) Sturm, B., Bistrich, U., Schranzhofer, M., Sarsero, J. P., Rauen, U., Scheiber-Mojdehkar, B., de Groot, H., Ioannou, P., and Petrat, F. (2005) Friedreich's ataxia, no changes in mitochondrial labile iron in human lymphoblasts and fibroblasts: a decrease in antioxidative capacity? *J Biol Chem 280*, 6701-8.

(122) Aloria, K., Schilke, B., Andrew, A., and Craig, E. A. (2004) Iron-induced oligomerization of yeast frataxin homologue Yfh1 is dispensable in vivo. *EMBO Rep 5*, 1096-101.

(123) He, Y., Alam, S. L., Proteasa, S. V., Zhang, Y., Lesuisse, E., Dancis, A., and Stemmler, T. L. (2004) Yeast frataxin solution structure, iron binding, and ferrochelatase interaction. *Biochemistry 43*, 16254-62.

(124) Foury, F., Pastore, A., and Trincal, M. (2007) Acidic residues of yeast frataxin have an essential role in Fe-S cluster assembly. *EMBO Rep 8*, 194-9.

(125) Yoon, T., and Cowan, J. A. (2004) Frataxin-mediated iron delivery to ferrochelatase in the final step of heme biosynthesis. *J Biol Chem 279*, 25943-6.

(126) Lesuisse, E., Santos, R., Matzanke, B. F., Knight, S. A., Camadro, J. M., and Dancis, A. (2003) Iron use for heme synthesis is under control of the yeast frataxin homologue (Yfh1). *Hum Mol Genet 12*, 879-89.

(127) Zhang, Y., Lyver, E. R., Knight, S. A., Lesuisse, E., and Dancis, A. (2005) Frataxin and mitochondrial carrier proteins, Mrs3p and Mrs4p, cooperate in providing iron for heme synthesis. *J Biol Chem 280*, 19794-807.

(128) Bulteau, A. L., O'Neill, H. A., Kennedy, M. C., Ikeda-Saito, M., Isaya, G., and Szweda, L. I. (2004) Frataxin acts as an iron chaperone protein to modulate mitochondrial aconitase activity. *Science 305*, 242-5.

(129) Li, D. S., Ohshima, K., Jiralerspong, S., Bojanowski, M. W., and Pandolfo, M. (1999) Knock-out of the *cyaY* gene in *Escherichia coli* does not affect cellular iron content and sensitivity to oxidants. *FEBS Lett 456*, 13-6.

(130) Yoon, T., and Cowan, J. A. (2003) Iron-sulfur cluster biosynthesis. Characterization of frataxin as an iron donor for assembly of [2Fe-2S] clusters in ISU-type proteins. *J Am Chem Soc 125*, 6078-84.

(131) Kondapalli, K. C., Kok, N. M., Dancis, A., and Stemmler, T. L. (2008) *Drosophila* frataxin: an iron chaperone during cellular Fe-S cluster bioassembly. *Biochemistry 47*, 6917-27.

(132) Djaman, O., Outten, F. W., and Imlay, J. A. (2004) Repair of oxidized iron-sulfur clusters in *Escherichia coli*. *J Biol Chem 279*, 44590-9.

(133) Toraya, T. (2000) Radical catalysis of B12 enzymes: structure, mechanism, inactivation, and reactivation of diol and glycerol dehydratases. *Cell Mol Life Sci 57*, 106-27.

(134) Ehrenberg, A., and Reichard, P. (1972) Electron spin resonance of the iron-containing protein B2 from ribonucleotide reductase. *J. Biol. Chem. 247*, 3485-8.

(135) Barlow, T., Eliasson, R., Platz, A., Reichard, P., and Sjöberg, B. M. (1983) Enzymic modification of a tyrosine residue to a stable free radical in ribonucleotide reductase. *Proc. Natl. Acad. Sci. U. S. A. 80*, 1492-5.

(136) Fontecave, M., Eliasson, R., and Reichard, P. (1987) NAD(P)H:flavin oxidoreductase of *Escherichia coli* - a ferric iron reductase participating in the generation of the free-radical of ribonucleotide reductase. *J. Biol. Chem. 262*, 12325-12331.

(137) Covès, J., Laulhère, J. P., and Fontecave, M. (1997) The role of exogenous iron in the activation of ribonucleotide reductase from *Escherichia coli*. *J. Biol. Inorg. Chem. 2*, 418-426.

(138) Fieschi, F., Nivière, V., Frier, C., Décout, J. L., and Fontecave, M. (1995) The mechanism and substrate specificity of the NADPH:flavin oxidoreductase from *Escherichia coli*. *J. Biol. Chem. 270*, 30392-400.

(139) Nivière, V., Fieschi, F., Décout, J. L., and Fontecave, M. (1999) The NAD(P)H:flavin oxidoreductase from *Escherichia coli*. Evidence for a new mode of binding for reduced pyridine nucleotides. *J Biol Chem 274*, 18252-60.

(140) Covès, J., Nivière, V., Eschenbrenner, M., and Fontecave, M. (1993) NADPH-sulfite reductase from *Escherichia coli* - A flavin reductase participating in the generation of the free-radical of ribonucleotide reductase. *J. Biol. Chem. 268*, 18604-18609.

(141) Blazyk, J. L., Gassner, G. T., and Lippard, S. J. (2005) Intermolecular electron-transfer reactions in soluble methane monooxygenase: A role for hysteresis in protein function. *J Am Chem Soc 127*, 17364-17376.

(142) Wu, C. H., Jiang, W., Krebs, C., and Stubbe, J. (2007) YfaE, a ferredoxin involved in diferric-tyrosyl radical maintenance in *Escherichia coli* ribonucleotide reductase. *Biochemistry 46*, 11577-88.

(143) Hristova, D., Wu, C. H., Jiang, W., Krebs, C., and Stubbe, J. (2008) Importance of the maintenance pathway in the regulation of the activity of *Escherichia coli* ribonucleotide reductase. *Biochemistry 47*, 3989-99.

(144) Thelander, L., Gräslund, A., and Thelander, M. (1983) Continual presence of oxygen and iron required for mammalian ribonucleotide reduction: possible regulation mechanism. *Biochem Biophys Res Commun 110*, 859-865.

(145) Fontecave, M., Eliasson, R., and Reichard, P. (1989) Enzymatic regulation of the radical content of the small subunit of *Escherichia coli* ribonucleotide reductase involving reduction of its redox centers. *J. Biol. Chem. 264*, 9164-70.

(146) Sobrado, P., Lyle, K. S., Kaul, S. P., Turco, M. M., Arabshahi, I., Marwah, A., and Fox, B. G. (2006) Identification of the binding region of the [2Fe-2S] ferredoxin in stearoyl-acyl carrier protein desaturase: insight into the catalytic complex and mechanism of action. *Biochemistry 45*, 4848-58.

Chapter 2

The Discovery of YfaE and the Characterization of its Role in the Maintenance of the Diferric-Y• Cofactor

Adapted in part from Wu, C.-H., Jiang, W., Krebs, C., and Stubbe, J. (2007) YfaE, a Ferredoxin Involved in Diferric-Tyrosyl Radical Maintenance in *Escherichia coli* Ribonucleotide Reductase, *Biochemistry 46*, 11577–11588.

INTRODUCTION

In bacteria, genes involved in the same biosynthetic pathways are usually organized in operons. Examination of the bacterial genomes that contain *nrdAB* (coding for α_2 and β_2 for class Ia RNRs) revealed a conserved neighboring gene encoding a hypothetical 2Fe2S-ferredoxin, YfaE in *E. coli*. Because 2Fe2S-ferredoxins in biology mainly function as electron carriers, we speculated that YfaE could play a role in providing the reducing equivalents necessary for diferric-Y• cofactor assembly and maintenance. These potential roles of YfaE are further supported by the studies on methane monooxygenase (MMO) and Δ^9-desaturase (Δ9D), two proteins that are structurally and functionally homologous to β_2. Both enzymes use di-iron cofactors in which the inactive, diferric form of the cofactor needs to be reduced to the active, diferrous cofactor after each turn over, which is similar to the maintenance pathway for met-β_2 (*1, 2*). Reduction of the diferric cluster in MMO is carried out by methane monooxygenase reductase (MMOR), which consists of two domains: a 2Fe2S-ferredoxin (Fdx) domain and ferredoxin reductase (FdxR) domain that contains FAD and NADH binding sites (*3, 4*). The FdxR domain uses NADH to reduce its tightly bound FAD, and the resulting $FADH_2$ reduces the $[2Fe2S]^{2+}$ cluster of the Fdx domain. The reduced Fdx domain then provides the electrons required for reducing the diferric cluster of MMO to the active, diferrous form. The gene that encodes MMOR resides in the same operon as MMO.

The inactive diferric cluster in Δ9D must also be reduced to the active diferrous cluster by a plant Fdx (*5*). The real physiological partner for recycling Δ9D and the Fdx reductase partner for Fdx have not yet been established. The diferrous form of MMO and Δ9D react with O_2 and the cofactor acts catalytically to oxidize substrate (methane or stearoyl-ACP) to product (methanol or oleoyl-ACP). Thus the reduction of a diferric cluster to a diferrous cluster followed

by reaction with O_2 resembles the maintenance pathway proposed for β_2. The major difference between theses systems, however, is that the reduction of the ferric iron of β_2 is not required for each catalytic cycle and β_2, a protein, is the substrate, in which tyrosine 122 (*E. coli*) is oxidized to a tyrosyl radical (Y•).

If the catalytic cycles for MMO and Δ9D are models for cluster maintenance in β_2, a Fdx might be a likely candidate to deliver the reducing equivalents required to generate diferrous-β_2 in the maintenance pathway and to supply the extra reducing equivalent in the biosynthetic pathway (**Figure 1-10, Chapter 1**). The analogy might further suggest that Fre, a flavin-reducase proposed to be involved in the maintenance pathway could be part of a Fdx reductase that acts in conjunction with YfaE. In this chapter we report cloning, expression, refolding, and purification of YfaE. YfaE has been characterized by Fe and S quantitation, by UV-vis, EPR and Mössbauer spectroscopies and shown to be a [2Fe2S]-ferredoxin. The ability of the reduced form of YfaE to reduce the diferric cluster of met-β_2 has been examined by titration studies and by stopped flow (SF) spectroscopy under anaerobic conditions. Reassembly of the diferrous-β_2 to the diferric-Y• β_2 has also been examined. The studies together support the importance of reduced YfaE in the maintenance pathway. The quantitative analysis demonstrates that only 2 Fe^{2+} are required per Y• generated, suggesting that β itself supplies the required reducing equivalent. A comparison of the specific activities of β_2 produced in the absence/presence of excess YfaE suggests that YfaE can also supply the extra reducing equivalent required in the biosynthetic pathway.

MATERIALS AND METHODS

Genomic analysis of genes contiguous to *nrdAB*

A subsystem of ribonucletide reduction in the genome database SEED (http://theseed.uchicago.edu) was used to analyze the genes neighboring *nrdB*. For genes encoding unannotated hypothetical proteins neighboring *nrdB*, the amino acids sequences were analyzed by BLAST searches to see if the open reading frames contained interesting sequence motifs that might suggest their involvement in the biosynthesis or maintenance of the diferric-Y• cofactor of β_2. For genomes that contain *nrdB* but lack contiguous *yfaE*, PHI-BLAST analyses using the conserved Cys motif ($CX_{4,5}CX_2CX_{28\text{-}35}C$) for the binding of [2Fe2S] clusters were performed to identify other possible ferredoxins.

Cloning and expression of *yfaE*

YfaE was annotated in the *E. coli* K-12 genome as a putative 2Fe2S-ferredoxin. Two primers, 5′-CCGCAAGAATT**CATATG**GCCCGCGTTACCCTGCG-3′ and 5′-ACTACAGGATCCTCACATCTCGATTTCAATATC-3′ containing NdeI (bold) and BamHI (underlined) restriction enzyme sites were used to obtain *yfaE* from a single colony of wild type (wt) *E. coli* K-12 (Yale *E. coli* Genetic Stock Center, New Haven, CT) using Taq polymerase (Promega) and PCR following manufacturer's protocol. *yfaE* was then sub-cloned into pET11a (Novagen) via the NdeI and BamHI sites (New England Biolab) using T4 DNA ligase (Promega) with a vector to insert ratio of 1:8. The sequence of *yfaE* was confirmed by DNA sequencing at the MIT Biopolymers Lab.

To express YfaE, a single colony of BL21 Gold (DE3) cells (Stratagene) containing pET11a-*yfaE* was inoculated into 5 mL of LB (100 μg/mL ampicillin in all growths) and the

culture was grown at 37 ºC for 6 h in a roller drum. The 5 mL culture was then transferred into 2 L LB in 6 L flasks and grown at 37 ºC, 180 rpm overnight (~16 h). The overnight culture (A_{600nm} ~2) was harvested by centrifugation at 12,000 g for 20 min, 4 ºC. The cells from 6 L LB growth were suspended in 100 mL of 100 mM Tris-HCl, 5% glycerol, pH 8.0, rapidly frozen in liquid nitrogen, and stored at -80 ºC. A typical yield was ~4 g cell paste/L culture.

Purification of inclusion bodies containing YfaE

The overexpressed YfaE was not soluble and formed insoluble inclusion bodies. Modified procedures from the literature for the purification of inclusion bodies were followed (*6*). To purify YfaE inclusion bodies, the cell suspension (~20 g in 100 mL of 100 mM Tris-HCl, 5% glycerol, pH 8.0) was thawed and the cell walls broken by two passages through a French pressure cell at 16,000 psi followed by centrifugation at 17,000 g at 4 ºC for 20 min. The pellets were suspended in 120 mL of 100 mM Tris-HCl, 4% (v/v) Triton-X-100, 2M urea, pH 8.0 by sonication at 5 Watts output for 1 min in an ice-water bath (VirSonic 100, SP Industries Company, Gardiner, NY). The suspension was then pelleted by centrifugation at 17,000 g and 4 ºC for 20 min and the supernatant discarded. This process was repeated an additional two times. The pellet was then washed three times with 120 mL water. Aliquots of the purified inclusion bodies were stored at -20 ºC. Typically ~0.1 g inclusion bodies were obtained per g of cell paste.

Reconstitution and purification of YfaE under strictly anaerobic conditions

The reconstitution of 2Fe2S-YfaE and the following purification steps were carried out in a custom-designed glove box (M.Braun, Newburyport, MA) in a cold room at 4 ºC. All buffers and resins for chromatography were degassed on a Schlenk line (stirring and evacuation for ~1 h

followed by refilling with Ar for ~15 min, three times) before being brought into the glove box. Inclusion bodies (~0.4 g for a typical purification) were suspended in 80 mL of 100 mM Tris-HCl, 8 M urea and 100 mM DTT, at pH 7.8, stirred for 1.5 h for complete solubilization, followed by addition of 80 μL of $FeCl_3$ (100 mM stock solution in 10 mM HCl), 88 μL $Fe(NH_4)_2(SO_4)_2$ (90 mM of stock solution in H_2O) and 160 μL NaS (100 mM stock solution in 10 mM NaOH) over 10 min to give final concentrations of 100, 100, and 200 μM, respectively. The refolding of the protein was initiated by a rapid 4-fold dilution (from 80 mL to 320 mL) with 100 mM Tris-HCl, pH 7.8 and the refolding process was allowed to proceed for 18 h. The sample (320 mL) was then loaded onto a Q-Sepharose column (2.5 x 4 cm, High Performance, Pharmacia Biotech) in the glove box at a flow rate of 3 mL/min, washed with 200 mL 100 mM Tris-HCl, pH 7.8 and eluted with a 150 mL x 150 mL linear gradient from 0 to 1 M NaCl in 100 mM Tris-HCl, pH 7.8. Fractions of 5.5 mL were collected and those with an $A_{340/280nm} > 0.6$ were pooled and concentrated to ~3 mL by a Millipore Amicon concentrator using a 45 mm PLBC3 membrane that had washed before use with 30 mL of 100 mM sodium dithionite, dd-H_2O, and 100 mM Tris-HCl, pH 7.8 before use. The concentrate (3 mL) was then loaded onto a Sephadex G-75 column (2.5 x 45 cm, superfine, Sigma) at a flow rate of 25 mL/h and eluted overnight in 100 mM Tris-HCl, pH 7.8. Fractions of 6.3 mL were collected and those with an $A_{340/280nm} > 0.7$ were pooled and concentrated as above. The YfaE concentration was determined using ε_{420nm} = 11 $mM^{-1}cm^{-1}$ (*7*). The yield was typically ~80 mg YfaE/g inclusion bodies.

Preparation of a 1:1 mixture of $^{57}Fe^{2+}$:$^{57}Fe^{3+}$ for Mössbauer analysis of [^{57}Fe]-YfaE

To prepare the $^{57}Fe^{3+}$ stock solution, ^{57}Fe foil (~4 mg) was added to a mixture of 375 μL 12 N HCl and 125 μL 13 N HNO_3 in a 10 mL pear shape flask for ~1 h at RT. The solution was

then degassed in vacuo for ~1 min with stirring and brought into the glove box. The solution was then neutralized by addition of ~0.4 mL 10 N NaOH. To prepare the $^{57}Fe^{2+}$ stock solution, ^{57}Fe foil (~8 mg) was added into 800 μL 12N HCl in a 10 mL pear shaped flask fitted with a greased glass stopcock. The solution was degassed immediately for ~1 min on a Schlenk line and then stirred in a 70 ºC oil bath overnight with the glass stopper closed. The $^{57}Fe^{2+}$ solution was degassed again for ~1 min, brought into the glove box and neutralized by adding ~0.56 mL 10 N NaOH. The concentration of each solution was determined by the ferrozine assay (*8*) in the presence (Fe^{2+}) or in the presence of ascorbate (Fe^{3+}), respectively. The reconstitution and purification of ^{57}Fe YfaE were then carried out as described above.

Characterization of YfaE

UV-visible spectroscopy: Purified $[2Fe2S]^{1+}$-YfaE was placed into a 0.7 mL cuvette in the glove box and fitted with an air tight screw cap (Starna Cells, Atascadero, CA). The cuvette was removed from the glove box and the absorption spectrum was recorded using Varian Cary 3 spectrophotometer (Walnut Creek, CA). The screw cap was then removed and O_2 (Airgas, Radnor, PA) was blown over the surface of the sample for 5 sec and the sample mixed by inverting the cuvette. The spectrum was then again recorded.

Iron and sulfide quantitation: The amount of iron and sulfide per YfaE were determined following the published procedures (*8, 9*). To determine the amount of iron, concentrated proteins (0.5-1 mM) were diluted in water in 1.5 mL eppendorfs to reach a final volume of 500 μL. Two hundred and 50 μL of 0.6 N HCl, 2.25% (w/v) $KMnO_4$ (prepared freshly by mixing equal volume of 1.2 N HCl and 4.5% $KMnO_4$ dissolved in dd-H_2O) was then added, and the

reaction mixture was incubated in a 60 ºC water bath for 2 h. The samples were then cooled to RT (~5 min), and 50 μL of a freshly prepared solution containing 6.5 mM ferrozine, 13.1 mM neoupoine (Sigma), 2M ascorbic acid, 5M ammonium acetate was added followed by incubation at RT for 30 min. The iron concentrations were determined by A_{562nm} (ε_{562nm} = 27.9 $mM^{-1}cm^{-1}$).

To measure the amount of sulfide, protein samples (0.5-1 mM) were diluted in water to reach a final volume of 300 μL, followed by addition of 1 mL 1% (w/v) zinc acetate and 50 μL 12% (w/v) NaOH. The samples were mixed by vortexing and incubated for 2 h at RT before addition of 250 μL of 0.1% (w/v) N, N-dimethyl-p-phenylene-diamine (dissolved in 5 N HCl) and 50 μL of 23 mM $FeCl_3$ (dissolved in 0.4 N HCl). The samples were then incubated for 30 min at RT followed by centrifugation at 12,000 rpm for 5 min at RT. The concentration of sulfide is determined by A_{670nm} (ε_{670nm}= 28.54 $mM^{-1}cm^{-1}$).

EPR spectroscopy: The purified YfaE (1.8 mM) was placed in an EPR tube inside the glove box and frozen in liquid nitrogen. EPR spectra were recorded using a Bruker ESP-300 X-band spectrometer at 77 K. The spin quantitation was carried out using a $CuSO_4$ standard (*10*) and Win-EPR software (Bruker).

Mass spectrometry: The molecular mass of purified YfaE was determined by LC-MS with a QSTAR Elite quadrupole-time-of-flight mass spectrometer in the Proteomics Core Facility of the Koch Institute in MIT. A protein microtrap (Michrom BioResources) was used to bind the YfaE sample, which was subsequently desalted with aqueous HPLC buffer and then eluted isocratically (50% water, 50% acetonitrile, 0.1% formic acid) for MS analysis. The mass spectrometer was calibrated with horse myoglobin just prior to sample analysis.

Size exclusion chromatography (SEC): $[2Fe2S]^{1+}$-YfaE (50 μL, 155 μM) was centrifuged at 14000 *g* for 10 min before being brought out of the glove box and analyzed by SEC using a Superose 12 column (10/300 GL, 25 mL, 10 x 300 mm, GE Healthcare, Little Chalfont, U.K.) pre-equilibrated with 120 mL of 50 mM K_2PO_4, 150 mM NaCl, pH 7, which had been filtered with a 0.2 μm, 47 mm Nylon membrane, followed by degassing with Ar over 20 min. The flow rate was maintained at 0.5 mL/min by Waters 2480 HPLC system (Waters). Molecular mass standards (Low molecular weight gel filtration standard, Bio-Rad) were run prior to each experiment.

Mössbauer Spectroscopy: Mössbauer spectra were recorded on spectrometers from WEB Research (Edina, MN) operating in the constant acceleration mode in transmission geometry. Spectra were recorded with the temperature of the sample at 4.2 K maintained by a liquid helium cryostat. For low-field spectra, the sample was kept inside a SVT-400 dewar (Janis, Wilmington, MA) and a magnetic field of 53 mT was applied either parallel or perpendicular to the γ-beam. For high-field spectra, the sample was kept inside a 12SVT dewar (Janis, Wilmington, MA), which houses a superconducting magnet that allows for application of variable fields between 0 and 8 T parallel to the γ-beam. The isomer shifts quoted are relative to the centroid of the spectrum of a metallic foil of Fe at room temperature. Data analysis was performed using the program WMOSS from WEB Research (Edina, MN), using the spin Hamiltonian given in equation (1), in which all symbols have their usual meaning (*11*).

$$\mathbf{H} = \beta \mathbf{S} \bullet \mathbf{g} \bullet \mathbf{B} + \sum_{\mathbf{i}=1}^{2} \frac{\mathbf{eQV}_{ZZ,\,\mathbf{i}}}{4} \left[\mathbf{I}_{\mathbf{z,i}}^{2} - \frac{I_i(I_i+1)}{3} + \frac{\eta}{3}(\mathbf{I}_{\mathbf{x,i}}^{2} - \mathbf{I}_{\mathbf{y,i}}^{2}) \right] + \sum_{\mathbf{i}=1}^{2} \mathbf{S} \bullet \mathbf{A}_{\mathbf{i}} \bullet \mathbf{I}_{\mathbf{i}} - \sum_{\mathbf{i}=1}^{2} g_n \beta_{\mathrm{n}} \mathbf{B} \bullet \mathbf{I}_{\mathbf{i}} \qquad (1)$$

Simulations of the $[2Fe2S]^{1+}$ cluster were carried out with respect to the total spin of the ground state, $S = 1/2$. The **A**-tensors in eq 1 are given with respect to the total spin. They are related to the intrinsic **a**-tensors by eq 2, in which +7/3 and -4/3 are the vector coupling coefficients for the $S = 1/2$ ground state (*12, 13*).

$$\mathbf{A}_{Fe(III)} = +7/3 \cdot \mathbf{a}_{Fe(III)} \qquad \mathbf{A}_{Fe(II)} = -4/3 \cdot \mathbf{a}_{Fe(II)} \qquad (2)$$

It was assumed that the fluctuation of the electronic states is slow compared to the ^{57}Fe Larmor frequency.

Preparation of met-β_2: Wt-β_2 (1 mL, ~0.4 mM, specific activity of 6500 nmol/min/mg and 1.1 Y• (*14*)) was incubated with 200-fold excess of hydroxyurea (HU, 80 mM, Sigma) at 4 ºC for 30 min (*15*). The HU was removed by loading ~0.5 mL sample onto a Sephadex G-25 column (~7 mL, 1 x 10 cm, Sigma) in 100 mM Tris-HCl, pH 7.8. Fractions of the eluent were collected manually in a 96-well plate followed by measurements of A_{260}, A_{280nm} and A_{340nm} in a plate reader (Bio-Rad). The protein-containing eluent (~2 mL) was concentrated to ~1 mL by Microcon YM30 (Millipore), degassed with stirring on a Schlenk line and then brought into the glove box. The concentration of the met-β_2 was determined using $\varepsilon_{280nm} = 131\ mM^{-1}cm^{-1}$ (*14*). The removal of Y• was confirmed by A_{410nm} and the iron content was determined by the ferrozine assay (*8*).

Titration of met-β_2 with $[2Fe2S]^{1+}$-YfaE

Reduction of met-β_2 to diferrous-β_2: $[2Fe2S]^{1+}$-YfaE (100 μM in 100 mM Tris-HCl, pH 7.8) was placed into a 250 μL gas tight syringe fitted with a repeating dispenser (model PB600-1, Hamilton) and the needle passed through the septum (12 mm Teflon/Silicon, Pierce) of the 0.7 mL cuvette. The cuvette contained 360 μL of 10 μM met-β_2 in 100 mM Tris-HCl, pH 7.8. YfaE

was added in 5 μL aliquots. The spectra were recorded on Cary 3 spectrophotometer and a difference spectrum was recorded and examined between each titration step. The titration end point was reached when the difference spectrum indicated the presence of reduced YfaE. This experiment was repeated 10 times on two separate batches of $[2Fe2S]^{1+}$-YfaE.

Assembly of diferric-Y• β_2 from diferrous-β_2: Once an end point was reached in the reduction of β_2, O_2 was blown over the solution surface for ~ 5 sec and the sample was mixed by inversion of the cuvette. The spectrum was immediately recorded. The procedure was repeated and no further change in the spectrum was observed. The amount of Y• generated was determined by EPR spectroscopy and the specific activity of the enzyme was determined by the spectrophotometric assay (*14*).

Calculation of Fe reduced and YfaE oxidized at the titration end point: The amount of Fe reduced during the titration is calculated by equation 3, assuming diferrous-β_2 and met-β_2 are the only forms of β_2 in the sample. There are 3.4 irons/β_2. A_{320i} and A_{320f} are the absorption at 320 nm before and after the titration. $A_{320YfaE}$ equals $[YfaE]_f \times \varepsilon_{320nm}$ (ε_{320nm} = 13.3 $mM^{-1}cm^{-1}$, based on ε_{420nm} = 11 $mM^{-1}cm^{-1}$ (*7*); $[YfaE]_f$ is the concentration of YfaE at the end point of the titration). V_i and V_f are the initial and final volume of the titration (in μL). $\varepsilon_{320differous\beta2}$ and $\varepsilon_{320met\beta2}$ are 1.6 and 11 $mM^{-1}cm^{-1}$, based on ε_{280nm} of diferrous-β_2 and met-β_2 (120 and 131 $mM^{-1}cm^{-1}$, respectively)(*14, 16*).

$$\text{nmol Fe reduced} = 3.4V_f \bullet \left(\frac{(A_{320f} - A_{320YfaE} - (A_{320i} \bullet \frac{V_i}{V_f}))}{(\varepsilon_{320differous\beta2} - \varepsilon_{320met\beta2})} \right) \qquad (3)$$

Reduction of met-β_2 with YfaE and assembly of diferric-Y• cofactor–Analysis of Y• by EPR and activity: Met-β_2 (10 μM) was titrated with 14–200 μM YfaE in a final volume of 360 μL of 100 mM Tris-HCl, pH 7.8. The assembly of diferric-Y• cofactor, EPR spectroscopic analysis and determination of the specific activity of RNR were carried out as described above.

Quantitation of Fe^{2+} produced during reduction of met-β_2 with $[2Fe2S]^{1+}$-YfaE by the ferrozine assay

$[2Fe2S]^{1+}$-YfaE (100 μM in 100 mM Tris-HCl, pH 7.8) was titrated anaerobically into 360 μL containing 10 μM met-β_2 and 100 μM ferrozine (100 mM Tris-HCl, pH 7.8). The amount of Fe^{2+}-ferrozine complex formed was determined using $\varepsilon_{562nm} = 27.9\ mM^{-1}cm^{-1}$ (*8*). The A_{562nm} of Fe^{2+}-ferrozine generated concomitantly with $[2Fe2S]^{1+}$-YfaE oxidation was obtained by subtracting the A_{562nm} of a titration in the absence of ferrozine and thus allowed removal of the absorption features associated with YfaE and β_2.

Characterization of met-β_2 or wt-β_2 reduction by $[2Fe2S]^{1+}$-YfaE by UV-visible SF spectroscopy

The rates of met-β_2 reduction and $[2Fe2S]^{1+}$-YfaE oxidation were recorded on an Applied Photophysics SX20 SF spectrometer with the cell thermostated at 37ºC. The stopped flow lines were washed with 20 mL of a 100 mM dithionite solution, 20 mL of anaerobic water and 20 mL of anaerobic 100 mM Tris-HCl, pH 7.8. Degassed met-β_2 (10 μM in 100 mM Tris-HCl, pH 7.8) was loaded into one syringe and reduced YfaE (3 to 90 μM in 100 mM Tris-HCl, pH 7.8) was loaded into the second syringe in the glove box. The connections of the syringes to the

instrument were purged with nitrogen gas during the experiments. The reaction was carried out by mixing equal volumes from each syringe. The reactions were monitored at 320 nm and at 465 nm, the reduction of the diferric cluster of met-β_2 and the oxidation of YfaE, respectively, in the single-wavelength photomultiplier mode. Data (2000 points) were collected in a logarithmic time scale (20 sec) and analyzed in KaleidaGraph (v. 3.6, Synergy Software). Data points were best fit to two single exponentials: $A(t) = \Delta A_1 \times e^{-k1 \times t} + \Delta A_2 \times e^{-k2 \times t} + c$, in which ΔA_1 and ΔA_2 are the amplitudes for the observed rate constants k_1 and k_2, respectively, t represents time, and c is a constant which equals A (t) when $t \sim \infty$. Typically 6–10 shots were averaged in each set of experiments.

The amplitude of the kinetic traces at 320 nm and 465 nm were used to calculate the stoichiometry between the amount of YfaE oxidized and Fe reduced in met-β_2. The amount of YfaE oxidized was calculated from $\Delta A_{465nm}/(\varepsilon_{465oxidizedYfaE} - \varepsilon_{465reducedYfaE})$. The A_{465nm} associated with met-β_2 and diferrous-β_2 is ~2% of the total change at 465 nm and was excluded from the calculation. The amount of met-β_2 reduced was calculated from $\Delta A_{320nm}/(\varepsilon_{320diferrous\beta2} - \varepsilon_{320met\beta2})$, assuming at the end of the reaction, β_2 is in form of either met-β_2 or diferrous-β_2. The amount of iron reduced was calculated from the amount of met-β_2 reduced times 3.4, the iron content of met-β_2 (3.4 Fe/β_2).

The same procedures were carried out to determine rates of reactions between wt-β_2 (10 μM in 100 mM Tris-HCl, pH 7.8) and $[2Fe2S]^{1+}$-YfaE (90 μM in 100 mM Tris-HCl, pH 7.8) under anaerobic conditions at 37 ºC. Data (2000 points) were collected in a logarithmic time scale (1000 sec) and averages of 10-12 shots monitored at 465 or 320 nm were analyzed.

Reaction of YfaE-reduced met-β_2 with O_2 monitored by SF spectroscopy

To examine the formation of the transient $WH^{+\bullet}$ after YfaE-reduced met-β_2 is exposed to O_2, the SF instrument was made anaerobic as described above. The O_2 saturated buffer was prepared by purging O_2 into ~30 mL of 100 mM Hepes, 5% glycerol, pH 7.6 for ~1 h at 4 ºC, and then loaded into a Hamilton gastight syringe. To prepare YfaE-reduced met-β_2, 30 μM met-β_2 was incubated with 60 μM $[2Fe2S]^{1+}$-YfaE in 100 mM Hepes, 5% glycerol, pH 7.6 for ~15 min in the glove box at 4ºC and loaded into a 2 mL gastight syringe before being removed from the glove box. The reaction was carried out by mixing equal volumes of O_2-saturated buffer and YfaE-reduced met-β_2. The formation of the transient $WH^{+\bullet}$ was monitored at 560 nm (ε_{560nm} = 3000 $M^{-1}cm^{-1}$) (*17*) in the single-wavelength photomultiplier mode. Data (2000 points, average of 6 shots) were collected in a logarithmic time scale (20 sec) and analyzed in KaleidaGraph (v. 3.6, Synergy Software). The data analysis followed our published procedures (*18, 19*) using a sequential reaction model involving two consecutive, first-order reactions (**Scheme 2-1**) (R, reactants; I, intermediate; P, products. k_1 and k_2 represent the rate constants of the formation and decay of the intermediate I, respectively).

Scheme 2-1

$$R \xrightarrow{k_1} I\,(A_{560nm}) \xrightarrow{k_2} P$$

This sequential reaction model can then be described by **Eq 2-1**, in which A_0, A_∞, represent absorbance at t = 0 and ∞, respectively, and A_1 represents the amplitude for the observed rate constant k_1 (*18*).

Eq 2-1: $A_t = A_\infty + A_1 \times e^{-k1 \times t} + (A_0 - A_\infty - A_1) \times e^{-k2 \times t}$

RESULTS

Genomic analysis of genes contiguous to *nrdAB*

Comparison of 181 bacterial genomes that have a *nrdAB* operon revealed that in 29%, a gene encoding a hypothetical 2Fe2S ferredoxin was found 3′ to *nrdAB*. For the genomes that do not have an apparent ferredoxin adjacent to *nrdB*, a PHI-BLAST search using the YfaE sequence and the conserved ferredoxin iron binding motif ($CX_{4,5}CX_2CX_{28,35}C$) revealed that 38% contain ferredoxin-like proteins. For the remaining 33% of the genomes, alternative reductants such as [4Fe4S] proteins, glutaredoxins or flavoproteins may be available which could function in a capacity similar to YfaE.

The hypothetical 2Fe2S-ferredoxin, YfaE in *E. coli* has 84 amino acids with a molecular weight of 9.3 kDa. The size of YfaE is smaller than the Fd domain of MMOR (98 amino acids) and the plant Fd (99 amino acids) that reacts with Δ9D. Structural and biochemical information on the Fd of MMOR or Δ9D suggest that the four cysteines of the 2Fe2S cluster are described by a $CX_4CX_2CX_{28\text{-}31}C$ motif, which is also found in YfaE (*20, 21*). After examining additional annotated Fds in the *E. coli* genome, only the Fd in the *isc* operon, Fdx (111 amino acids), possesses a similar motif ($CX_5CX_2CX_{35}C$) (*22*).

Expression and purification of YfaE

To investigate the roles of YfaE, *yfaE* was cloned and the protein was overexpressed in *E. coli*. While over-expression of YfaE was successful, in all cases the protein was found in inclusion bodies. Efforts to obtain soluble YfaE by changing the growth temperature, adding iron to the growth media, making different constructs with different affinity tags at the C or N terminus (His_6, GST, NusA) of the protein and co-expression with *isc* operon proteins (*23*) were

all unsuccessful. We thus decided to purify YfaE from inclusion bodies and reconstitute soluble 2Fe2S-containing YfaE in vitro using protocols that have been successful with other iron-sulfur containing proteins (*24*). The inclusion bodies were purified by repeated washing and centrifugation steps and then brought into an anaerobic box and solubilized with 8 M urea. A 1:1:2 mixture of Fe^{2+} and Fe^{3+} and sulfide were added to the denatured YfaE under anaerobic conditions, rapidly diluted and refolded for ~18 h. The solution was then applied to a Q-Sepharose column, washed, and eluted using a salt gradient. **Figure 2-1A** shows a typical elution profile of YfaE. Two peaks usually appear in the elution profile. The fractions of the first peak containing $[2Fe2S]^{1+}$-YfaE were pooled and concentrated by the Amicon concentrator with a PLBC3 membrane pre-washed with dithionite solution. The concentrated sample was then loaded onto a Sephadex G-75 column and the protein was eluted as a single sharp peak (**Figure 2-1B**). The desired fractions were pooled and concentrated by the PLBC3 membrane. Washing the membrane with a dithionite solution prior to each concentration step is necessary to prevent YfaE oxidation. The yield of protein from each purification step is summarized in **Table 2-1**. Typically ~80 mg of $[2Fe2S]^{1+}$-YfaE can be isolated from 1 g of inclusion bodies. The success of the purification procedures was judged by SDS-PAGE (**Figure 2-2**). The LC-MS of the purified YfaE shows a major peak at 9161 Da (**Figure 2-3**), consistent with an apo form of YfaE with the first methionine having been cleaved off. The purified protein is stable for about a month in the glove box at 4 ºC.

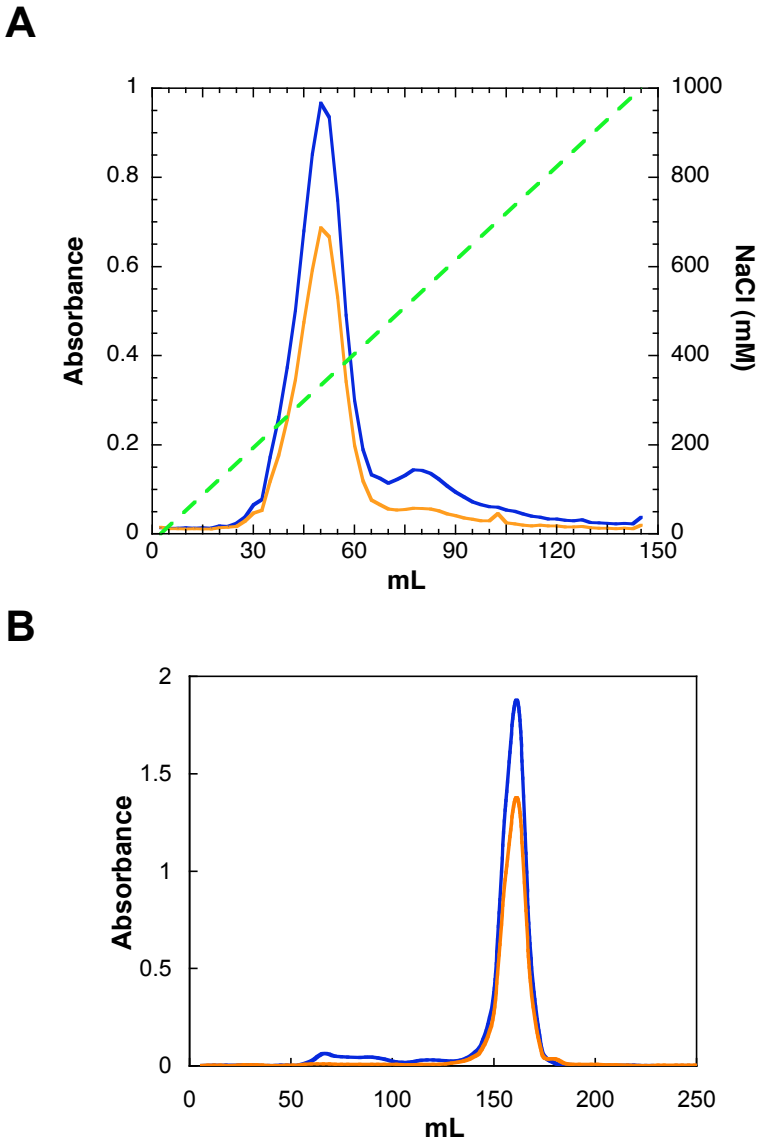

Figure 2-1. Purification of YfaE by anion-exchange and SEC under anaerobic conditions. (A) Elution profile of YfaE from a Q-Sepharose column. Blue: A_{280nm}, orange: A_{340nm}, green: NaCl gradient. (B) Elution profile of YfaE from a Sephadex G-75 column. Blue: A_{280nm}, orange: A_{340nm}.

Table 2-1. Summary of YfaE purification profile

Step	Yield (mg)	% yield	A_{340nm}/A_{280nm} [a]
Inclusion bodies	196	100	-
After Q-sehaprose	33	17	0.7
After Sephadex G-75	17	9	0.83

[a] oxidized form

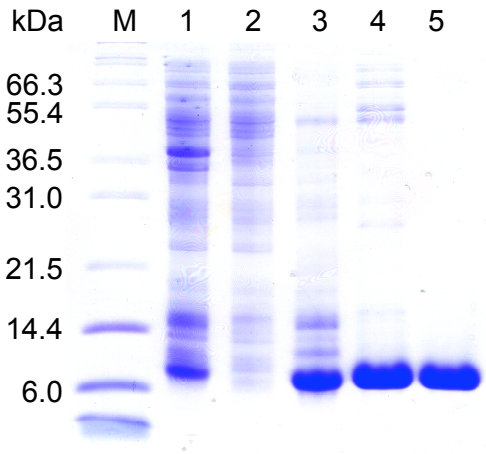

Figure 2-2. Purification of YfaE monitored by 15 % SDS-PAGE. M: molecular weight markers, lane 1, whole cells; lane 2, cell lysate; lane 3, purified inclusion bodies; lane 4, pooled protein from Q-Sepharose chromatography; lane 5, pooled protein from Sephadex G-75 chromatography.

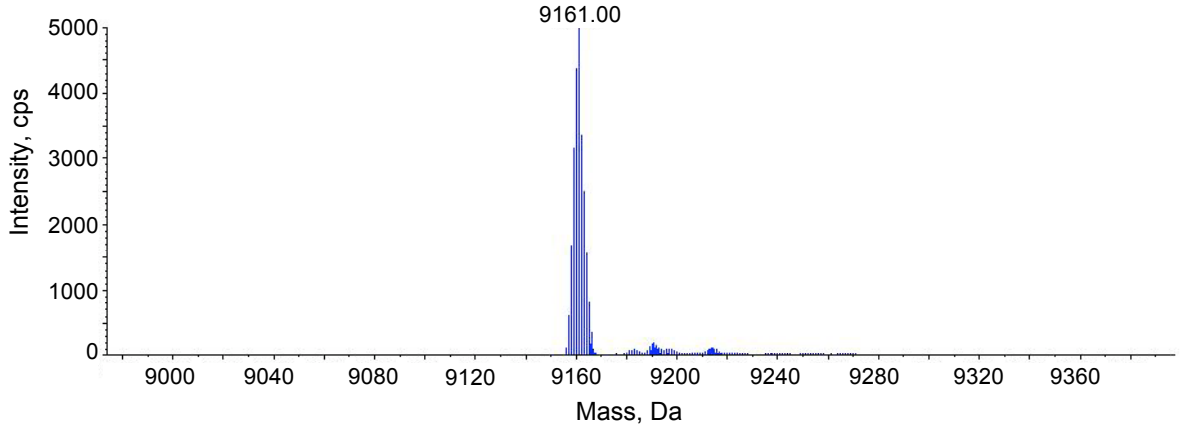

Figure 2-3. Molecular mass of the purified YfaE determined by LS-MS with a quadrupole-time-of-flight mass spectrometer. A molecular mass of 9161 Da was obtained for purified YfaE which is consistent with the mass of the apo form of YfaE with the first methionine at the N-terminus having been removed.

UV-visible spectra of $[2Fe2S]^{1+/2+}$-YfaE and sensitivity to O_2

YfaE as isolated has the absorption spectrum shown in **Figure 2-4** (blue line) which reveals shoulders at 350, 390, 470, 550 nm, typical of reduced $[2Fe2S]^{1+}$ clusters (*3*). To characterize the oxidized state of YfaE, O_2 was blown over to the surface of the sample followed with mixing by inverting the cuvette. The resulting spectrum is shown in **Figure 2-4** (red line). The oxidized form has absorption features at 340, 420, and 460 nm with a broad shoulder at 550 nm and ratios relative to A_{280nm} of 0.83, 0.60 and 0.60, respectively (*3, 24*). This spectrum and its isosbestic point (320 nm) are typical of previously reported 2Fe2S Fds (*3*).

In contrast with many oxidized Fds, however, $[2Fe2S]^{2+}$-YfaE is not stable under aerobic or anaerobic conditions. At room temperature under aerobic conditions, oxidized features associated with YfaE start to decrease after one hour and disappear over a 6 h period (**Figure 2-5**). During the oxidation, the oxidized YfaE aggregates. The aggregate can be separated from

reduced YfaE by Sephadex G-75 chromatography. While sodium dithionite can reduce oxidized YfaE to its reduced state after initial exposure to O_2, it fails to regenerate reduced YfaE from the aggregate. These results were the basis for our purification and storage of YfaE in an anaerobic chamber.

Quantitation of the amount of Fe and S in the reduced YfaE requires a knowledge of the extinction coefficient for the protein. Absorbance at 280 nm is not a reliable basis for calculating the protein concentration because the amounts and oxidation states of the FeS cluster affect the absorption in this region. Therefore, our quantitation is based on the reported extinction coefficients for $[2Fe2S]^{2+}$-Fds at 420 nm. The numbers range from 9,500 $M^{-1}cm^{-1}$ to 11,000 $M^{-1}cm^{-1}$ (*3, 7*). All subsequent quantitation is based on the latter, with numbers based on 9500 $M^{-1}cm^{-1}$ given in parenthesis. Iron quantitation gave 2.2 ± 0.2 (1.9 ± 0.2) Fe/YfaE based on 7 determinations from 3 different batches of purified YfaE. Sulfide quantitation gave 3.7 ± 0.2 (3.2 ± 0.2) S/YfaE based on 8 determinations from 3 different batches of purified YaE. The iron assay suggests the success of the reconstitution of one 2Fe2S cluster per YfaE. The iron content is also consistent with the Mössbauer analysis described subsequently. The cause of the greater than stoichiometric amount of sulfide observed is not understood, but could be associated with persulfide formation with cysteines at the C-terminus of YfaE.

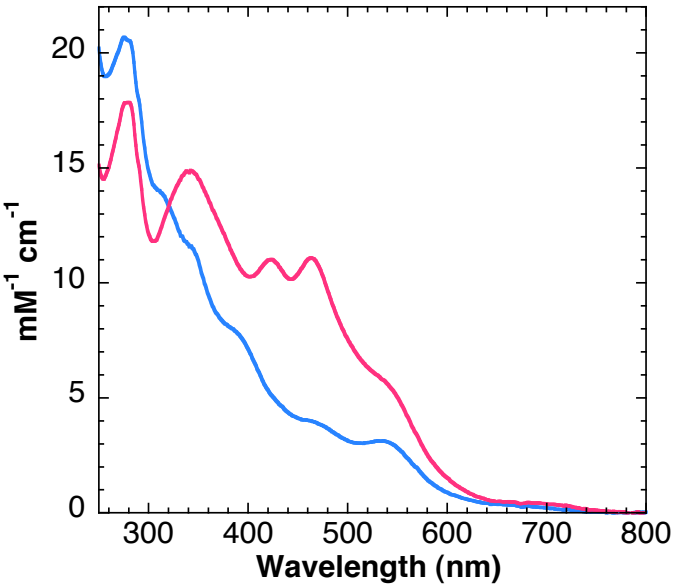

Figure 2-4. UV-visible spectra of oxidized (red) and reduced (blue) YfaE in units of mM^{-1} cm^{-1}.

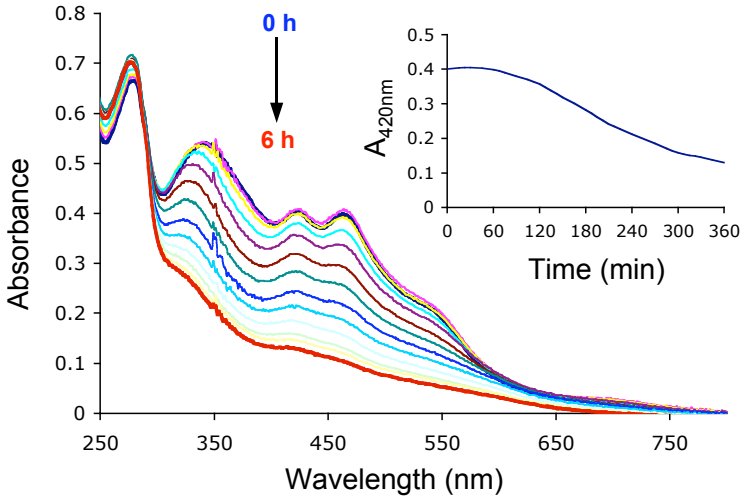

Figure 2-5. Lability of the [2Fe2S] cluster of oxidized YfaE. YfaE (35 μM) purified anaerobically was oxidized by blowing O_2 over the surface of the solution followed by mixing the solution by inverting the cuvette. UV-visible spectra of the YfaE after oxidation (thick blue line) were taken every 30 min (thin colored lines) for 6 h (thick red line) at 25 ºC. Inset: A_{420nm} at different time points after exposed to O_2. The decrease of A_{420nm} with time indicates the decomposition of the $[2Fe2S]^{2+}$ cluster in YfaE.

EPR spectrum of $[2Fe2S]^{1+}$-YfaE

A further quantitation of the iron cluster has been made by analyzing the EPR spectrum of $[2Fe2S]^{1+}$-YfaE. The result is shown in **Figure 2-6**. The spin quantitation using a $CuSO_4$ standard indicates 0.96 ± 0.03 (0.83 ± 0.03) spins per $[2Fe2S]^{1+}$-YfaE (*g* values of 2.036, 1.944 and 1.884, which is very similar to previously reported quantitation for the plant 2Fe2S Fd (*24*) and the Fd domain of MMOR (*3*)).

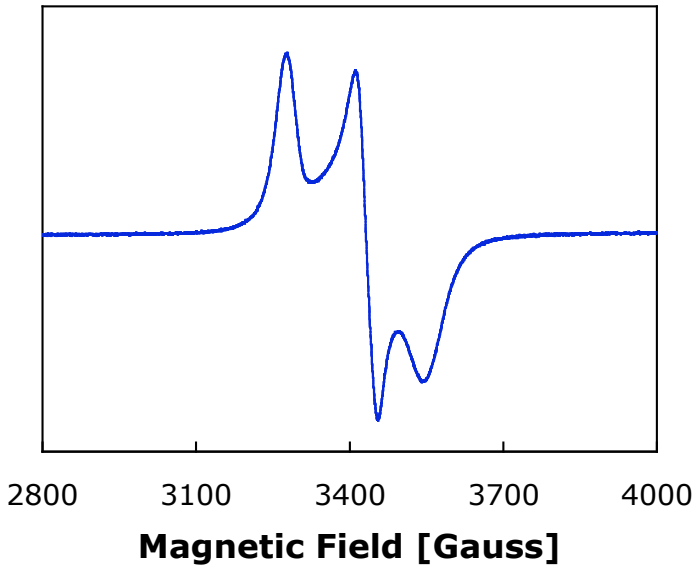

Figure 2-6. X-band EPR spectrum of $[2Fe2S]^{1+}$-YfaE (1.8 mM). Recorded at 77 K in a liquid nitrogen finger dewar, frequency = 9.4 GHz, microwave power = 1.0 mW, receiver gain = $3.17x10^4$, modulation amplitude = 10 G. The calculated g-values are 2.036, 1.944 and 1.844. Spin quantitation showed 0.96 $[2Fe2S]^{1+}$ cluster per YfaE.

Characterization of the FeS clusters in reduced and oxidized YfaE by Mössbauer spectroscopy

The types of FeS clusters in the reconstituted YfaE were further analyzed by Mössbauer spectroscopy. The Mössbauer spectra reveal that ~80% of total Fe is in the form of a $[2Fe2S]^{1+}$

cluster and ~20% of total Fe is in the form of a $[4Fe4S]^{2+}$ cluster (**figure 2-7**). From these numbers we conclude that 89% of YfaE harbors a $[2Fe2S]^{1+}$ cluster (80% of total iron), and 11% a $[4Fe4S]^{2+}$ cluster (20% of total iron). The 210-K/zero-field spectrum displays four lines corresponding to overlapping quadrupole doublets. The outer and inner lines have parameters reminiscent of tetrahedrally Cys_4-coordinated Fe^{2+} and Fe^{3+} sites, consistent with a $[2Fe2S]^{1+}$ cluster. The inner lines are broader and more intense, suggesting the presence of a third quadrupole doublet overlapping with the quadrupole doublet of the Fe^{3+} site. The high-energy line of the additional component can be seen as a distinct shoulder at ~1 mm/s (arrow in **Figure 2-7**). The low-energy lines of the Fe^{3+} site and the third quadrupole doublet overlap, resulting in the more intense second line. The spectrum can be analyzed as a superposition of three quadrupole doublets with parameters given in **Table 2-2**. The red and blue spectra in **Figure 2-7** have parameters expected for the Fe^{2+} and Fe^{3+} sites of a $[2Fe2S]^{1+}$ cluster, respectively, and their relative intensity was constrained to be the same during the fit. The quadrupole doublet shown in green has parameters reminiscent of $[4Fe4S]^{2+}$ clusters.

Spectra recorded at 4.2 K in varying externally applied fields corroborate this assignment. They can be analyzed as a superposition of 78% $[2Fe2S]^{1+}$ and of 21% $[4Fe4S]^{2+}$ subspectra (**Figure 2-8**, black lines). The individual contributions of the $[4Fe4S]^{2+}$ and of the Fe^{2+} and Fe^{3+} sites of the $[2Fe2S]^{+}$ cluster are shown for the 8-T and 53-mT spectra. The simulation parameters (**Table 2-2**) are similar to those observed for other $[4Fe4S]^{2+}$ and $[2Fe2S]^{1+}$ clusters (*25-27*). The isomer shift values decrease with increasing temperature, due to the second order Doppler effect (*11*), and the quadrupole splitting of the Fe^{2+} site of the $[2Fe2S]^{1+}$ cluster are slightly temperature-dependent, as was observed for the $[2Fe2S]^{1+}$ cluster from MMOR (*26*).

We note that the large number of variables does not allow all parameters to be determined unambiguously.

We also considered the possibility that the YfaE sample contained oxidized $[2Fe2S]^{2+}$ cluster. This cluster form exhibits a diamagnetic ground state and thus gives rise to quadrupole doublet spectra in zero or low applied fields. High-field spectra of $[2Fe2S]^{2+}$ clusters can be predicted with good accuracy. From analysis of the spectra, we can set an upper limit of ~7% for the fraction of $[2Fe2S]^{2+}$ in the sample. Including a small amount of this cluster type does not result in parameters significantly different from those in **Table 2-2** and does not improve the quality of the spectral simulations. The spectrum of reconstituted YfaE that was exposed to oxygen (**Figure 2-9**) exhibits a quadrupole doublet with parameters typical of a $[2Fe2S]^{2+}$ cluster (**Table 2-2**). The upper limit of the fraction of Fe in form of $[4Fe4S]^{2+}$ cluster in this sample is ~10%, suggesting that the amount of this cluster type is variable, but small. Thus the visible spectrum, EPR spectrum and Mössbauer analysis suggest that the reconstitution of a folded active YfaE has been successful.

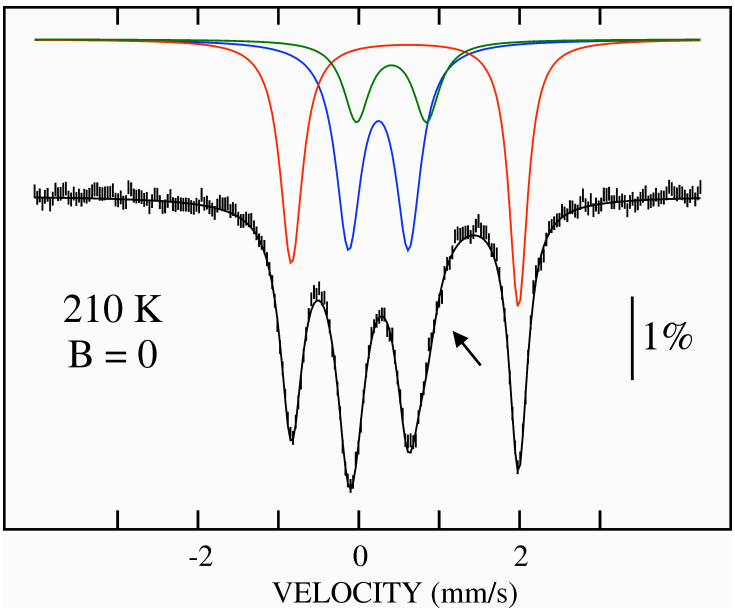

Figure 2-7. 210-K/zero-field Mössbauer spectrum of reconstituted $[2Fe2S]^{1+}$-YfaE. The simulations of the individual contributions of the Fe^{2+} and Fe^{3+} sites of the $[2Fe2S]^{1+}$ cluster (40% each) are shown in red and blue, respectively. The contribution of the $[4Fe4S]^{2+}$ cluster (20%) is shown in green. The sum of the simulations is shown in solid, black line overlaid with the data (see **Table 2-2** for parameters). The arrow indicates a tiny shoulder contributed by $[4Fe4S]^{2+}$ cluster. The vertical bar shows 1% of the magnitude of the γ-radiation source.

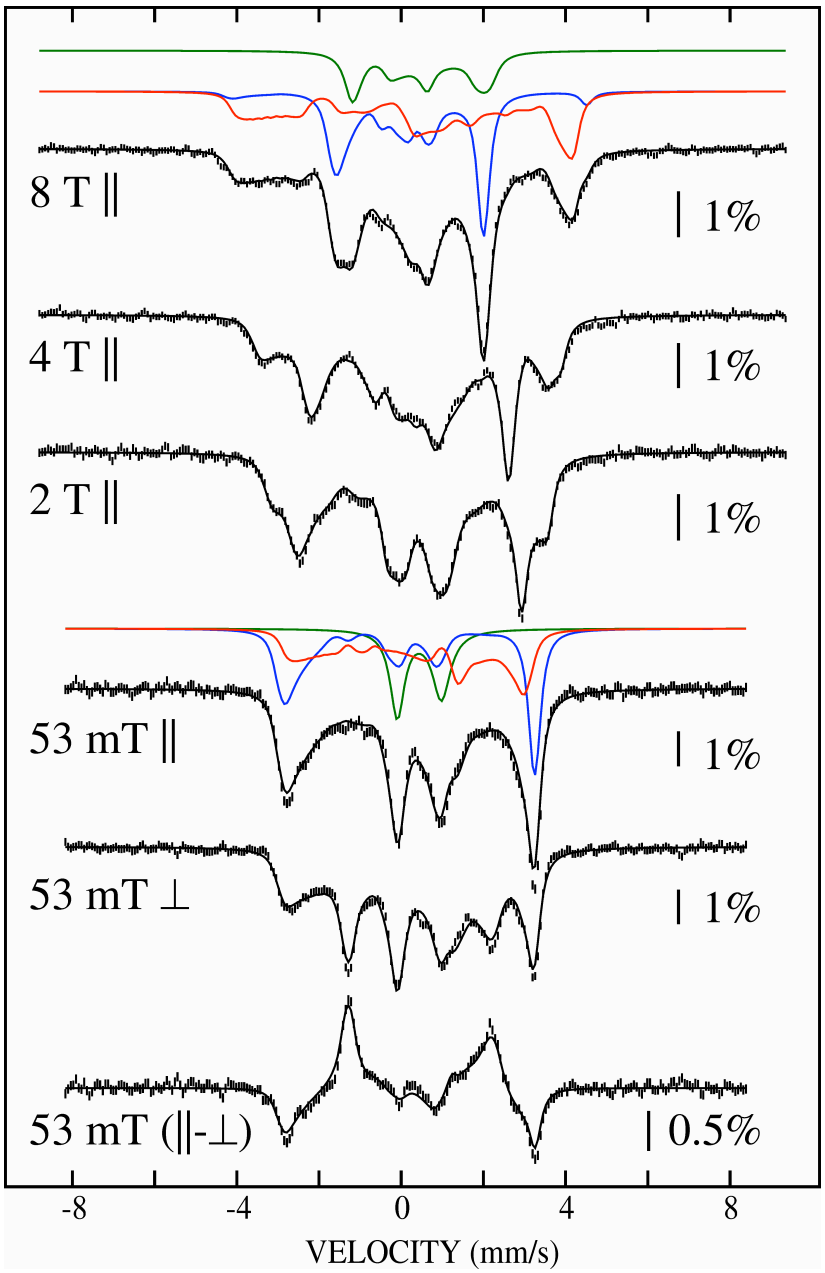

Figure 2-8. 4.2-K Mössbauer spectra of reconstituted YfaE acquired in varying external magnetic fields. Simulations of the individual contributions from the Fe^{2+} and Fe^{3+} sites of the $[2Fe2S]^{1+}$ cluster (39% each) are shown in red and blue, respectively. The contribution of the $[4Fe4S]^{2+}$ cluster (21%) is shown in green. The solid lines (black) are overlaid with the data and are the sum of the simulations (see **Table 2-2** for parameters). The vertical bar shows 1% of the magnitude of the γ-radiation source. The strength (T or mT) and orientation (parallel or perpendicular) of the magnetic field relative to the propagation direction of the γ-photons is indicated adjacent to each spectrum.

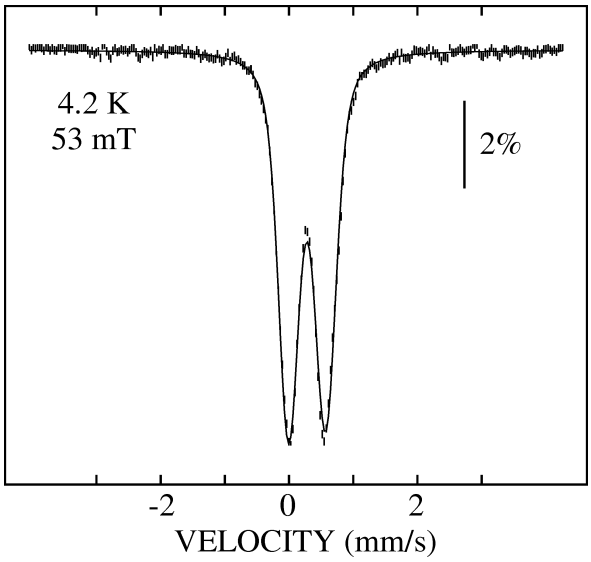

Figure 2-9. 4.2-K/53-mT Mössbauer spectrum of a sample of reconstituted $[2Fe2S]^{1+}$-YfaE that was exposed to O_2. The solid line is a simulation with parameters given in **Table 2-2**.

Table 2-2. Mössbauer simulation parameters of the $[4Fe4S]^{2+}$, $[2Fe2S]^{1+}$, and $[2Fe2S]^{2+}$ clusters of YfaE. The *g*-values of the $S = 1/2$ ground state of the $[2Fe2S]^{1+}$ cluster were taken from the EPR spectrum. The electric field gradient and hyperfine tensors were assumed to be collinear.

Sample	cluster	Ground state	Relative amount	site	T (K)	δ (mm/s)	ΔE_Q (mm/s)	η	$\mathbf{A}/g_N\beta_N$ (T)
Reconstituted YfaE	$[2Fe2S]^{1+}$	$S = 1/2$	80%	Fe^{3+}	4.2	0.33	0.78	-0.6	-38.5, -37.7, -30.9
					210	0.25	0.75	-	-
				Fe^{2+}	4.2	0.60	-3.13	-1	10.7, 10.1, 25.0
					210	0.57	2.82	-	-
	$[4Fe4S]^{2+}$	$S = 0$	20%	$Fe^{2.5}$	4.2	0.44	1.07	0	-
					210	0.41	0.87	-	-
Air-oxidized YfaE	$[2Fe2S]^{2+}$	$S = 0$	>90%	Fe^{3+}	4.2	0.28	0.58	n.d.	-

Size-exclusion chromatography of YfaE

In addition to spectroscopic analyses for YfaE, the oligomeric state of YfaE was examined by SEC to help us understand the reaction stoichiometries in the following experiments. Low molecular weight standards (1.35 to 670 kDa) from Bio-Rad were used to calibrate the Superose-12 column. There are small variations in the retention times of the same sample between each run, especially when the experiments were performed on different days. Thus the molecular weight standards were run each time before analysis of YfaE. **Figure 2-10** shows the elution profile of the gel filtration standards and the calibration curve generated by plotting the retention time against the logarithm of the molecular mass. The peaks that might be associated with aggregation or degradation of the gel filtration standards were excluded. YfaE was taken from the glove box and analyzed immediately by SEC analysis to prevent extensive formation of high molecular mass aggregates of oxidized YfaE. The elution profile of YfaE revealed a dominant single peak at 35.8 min, corresponding to a molecular mass of 9506 Da, which aggrees with the predicted molecular mass of a 2Fe2S containing-YfaE monomer (9337.5 Da) (**Figure 2-11**). The A_{340nm}/A_{280nm} of the dominant peak suggests YfaE is in its oxidized state. The small peak eluted in the void volume of the column (~15.5 min) could be aggregates of oxidized YfaE. The results from SEC suggested that YfaE, like most of the ferredoxins, is a monomer under physiological conditions.

A

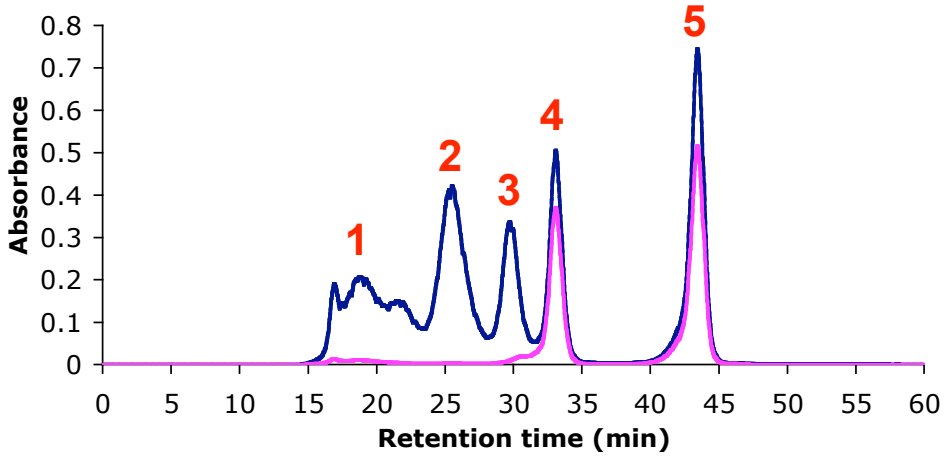

B

Standard	mw (Da)	retention time (min)	$\log_{10}$(Da)
1. Thyroglobulin (bovin)	670000	18.8	5.83
2. Gamma globulin (bovine)	158000	25.4	5.20
3. Ovalbumin (chicken)	44000	29.8	4.64
4. Myoglobin (horse)	17000	33.1	4.23
5. Vitamin B-12	1350	43.5	3.13

C

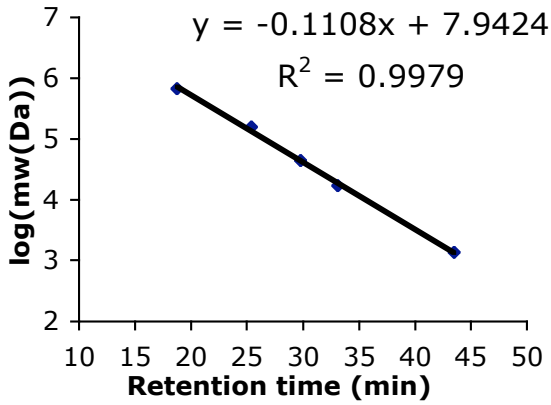

Figure 2-10. Standard curves for Superose-12 size-exclusion chromatography. (A) Elution profile of the standards. Blue, A_{280nm}; pink, A_{340nm}. Peaks of the corresponding standards listed in B are labeled in red. (B) List of the molecular weight, retention time and logarithm of molecular weight of each standard. (C) Standard curve generated by plotting retention time of each standard against logarithm of molecular weights.

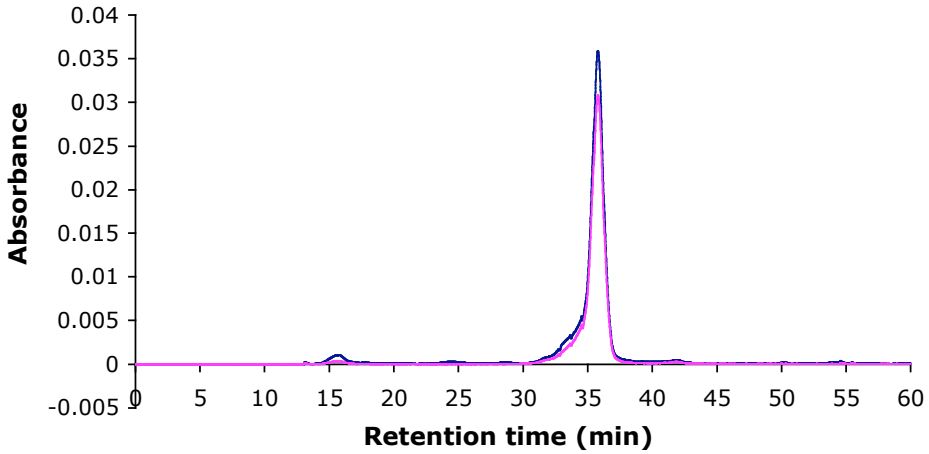

Figure 2-11. Superose-12 SEC of purified YfaE. Purified YfaE was taken from an anaerobic chamber and injected immediately onto a Superose-12 size-exclusion column. Blue, A_{280nm}; pink, A_{340nm}. The retention time of the dominant peak is 35.8 min, corresponds to a molecular weight of 9506 Da, which is consistent with a YfaE monomer with an intact [2Fe2S] cluster.

Titration of met-β_2 with $[2Fe2S]^{1+}$-YfaE

To determine if YfaE plays a role in the maintenance pathway of the diferric-Y• cofactor of β_2, we examined the ability of its $[2Fe2S]^{1+}$ to reduce met-β_2. Wt-β_2 (1.1 Y•, 3.4 Fe/β_2 and specific activity of 6500 nmol•min^{-1}•mg^{-1}) was reduced with hydroxyurea to produce met-β_2 (3.4 Fe/β_2). Met-β_2 in deoxygenated Tris buffer at pH 7.8 was then titrated under anaerobic conditions with $[2Fe2S]^{1+}$-YfaE. The titrations were repeated 17 times with a representative titration shown in **Figure 2-12**. The end point of the titration was assessed by monitoring the difference spectrum recorded subsequent to each addition of $[2Fe2S]^{1+}$-YfaE. When additional YfaE added remained in the reduced state, the titration was assumed to be complete. At this end point, YfaE reduced ~2.5 Fe^{2+} out of the 3.4 Fe^{3+} per met-β_2, that is, ~75% of the total iron.

Assuming that YfaE is 90-95% homogeneous based on the Mössbauer, 1 YfaE reduces 1 Fe (**Table 2-3**, Titration A, average of 3 representative titrations).

To further examine the stoichiometry of YfaE oxidation and iron reduction of met-β_2, a similar anaerobic titration in the presence of ferrozine was carried out (repeated 3 times) (**Figure 2-13**, **Table 2-3**, Titration B). After subtracting the absorption features associated with oxidized YfaE and met-β_2 at 562 nm, the analysis of the stoichiometry revealed that every YfaE oxidized resulted in one iron reduced. Control experiments in which YfaE was titrated into a solution with ferrozine demonstrated that the ferrous ion in $[2Fe2S]^{1+}$-YfaE is not chelated. Results from titration A and B (**Table 2-3**) indicate that YfaE is a chemically competent reductant of met-β_2.

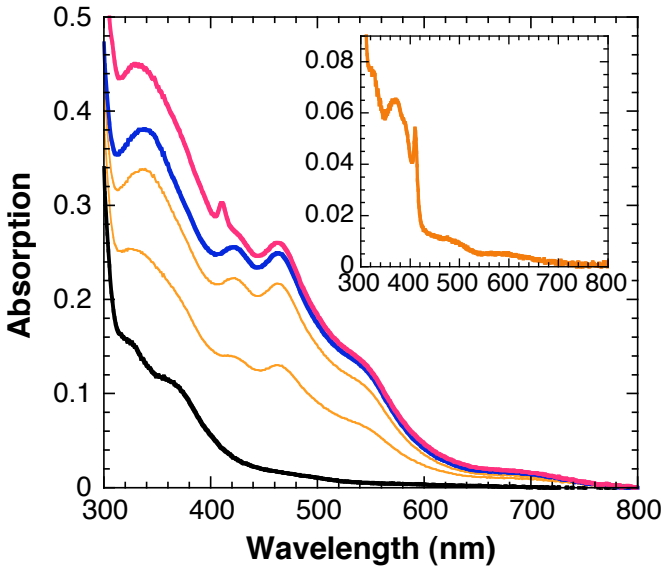

Figure 2-12. Titration of met-β_2 with $[2Fe2S]^{1+}$-YfaE under anaerobic conditions. Met-β_2 (10 μM, black) was titrated with $[2Fe2S]^{1+}$-YfaE (10 and 18 μM (final concetration), orange) to an end point with 22 μM $[2Fe2S]^{1+}$-YfaE (blue). Upon completion of the reduction, O_2 was added to monitor cluster assembly (pink). Insert: difference spectrum between the end point of the YfaE titration and the O_2 addition.

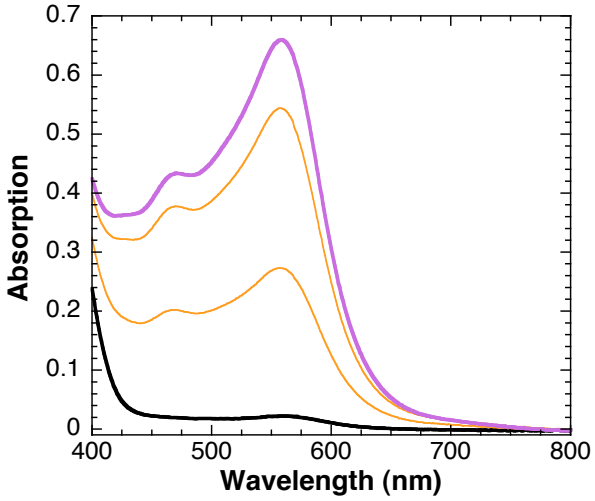

Figure 2-13. Ferrozine assay quantitation on the amount of iron reduced in met-β_2 during the titration with $[2Fe2S]^{1+}$-YfaE. In the presence of 100 μM ferrozine, met-β_2 (10 μM, black) was titrated with $[2Fe2S]^{1+}$-YfaE (final concentration, 10, 18 μM, (orange) and 22 μM (purple) under anaerobic conditions. The amount of the Fe^{2+}-ferrozine complex was determined by A_{562nm} (ε = 27.9 $mM^{-1}cm^{-1}$).

Table 2-3. Stoichiometry between Fe reduced in met-β_2 and the amount of YfaE oxidized.

Experiments	YfaE oxidized (nmol)	Fe reduced (nmol)	Fe reduced/YfaE oxidized	Activity (nmol•min^{-1}•mg^{-1})	Y•/β_2	Fe/Y•
Titration A[a]	10.3 ± 0.3	8.9 ± 1.5	0.9 ± 0.2	6200 ± 500	1.24 ± 0.04	2.0 ± 0.3
Titration B[a]	9.3 ± 0.3	9.3 ± 0.7[b]	1.0 ± 0.1	-	-	-
Stopped Flow	2.4 ± 0.6	2.4 ± 0.3	1.0 ± 0.2	-	-	-

[a] Average of three titrations of met-β_2 (3.6 nmol) with $[2Fe2S]^{1+}$-YfaE in the absence (A) or in the presence (B) of ferrozine. O_2 was added at the end point of the titration (A). Different batches of met-β_2 or YfaE were used in titrations A and B.

[b] The amount of Fe reduced was calculated from ferrozine-Fe^{2+} complex formed in the titration, assuming one Fe reduced per ferrozine-Fe^{2+} complex formed.

Reassembly of diferric-Y• cluster from reduced met-β_2

Once the end point for reduction of met-β_2 to the reduced state was identified, O_2 was added to the cuvette and the visible spectrum recorded (**Figure 2-12**, blue line). A difference spectrum was obtained by subtracting oxidized YfaE (amount added at the end point of the titration) from the spectrum generated in the presence of O_2. Diferric cluster absorption features at 325 and 365 nm and the Y• features at 390 and 410 nm are readily apparent (**Figure 2-12**, insert). The amount of Y• generated was determined by spin quantitation using EPR spectroscopy. From titration A in which 2.5 Fe^{2+}s were generated, 1.2 Y• were produced (**Table 2-3**). Thus, 2 Fe^{2+}s are sufficient to generate 1 Y•. Ten similar experiments were carried out giving 2.0 ± 0.4 Fe^{2+}/Y•. Our chosen experimental conditions and a ferrozine assay established that no excess reductant (such as Fe^{2+}) was present to deliver the reducing equivalent required for cluster assembly. Thus the reducing equivalent required for cluster assembly must be derived from β_2 itself with the most likely candidate being the W48 (*18, 19*).

The observation that only ~75% of the iron of met-β_2 had been reduced under these conditions suggested an equilibrium mixture of species. One would thus expect that addition of increased amounts of YfaE would shift the equilibrium to the right, reduce more Fe^{3+}s in met-β_2 and lead to additional formation of Y• after addition of O_2. To test this hypothesis, met-β_2 was titrated with increasing amounts of YfaE (**Table 2-4**). The amount of Fe^{2+} could not be quantified by the spectral subtraction method (eq 3) due to the size of the extinction coefficient of $[2Fe2S]^{1+/2+}$-YfaE relative to met and diferrous-β_2. However, spin quantitation of Y• generated subsequent to O_2 addition (**Table 2-4**) supports this proposal.

Table 2-4. Reduction of met-β_2 with increasing amounts of YfaE.

met-β_2 (nmol)	YfaE (nmol)	Activity (nmol•min^{-1}•mg^{-1})	Y•/β_2	Activity/(Y•/β_2)
3.6	5	2700 ± 400	0.61 ± 0.16	4600 ± 800
3.6	10	5100 ± 200	1.16 ± 0.06	4400 ± 400
3.6	20	8200 ± 400	1.33 ± 0.05	6100 ± 400
3.6	50	9300 ± 600	1.40 ± 0.06	6800 ± 600
3.6	72	10300 ± 400	1.5 ± 0.1	6900 ± 700

Comparisons of experiments with stoichiometric and excess [2Fe2S]$^{1+}$-YfaE might provide further insight about the source of the reducing equivalent required for diferric-Y• assembly. When no excess [2Fe2S]$^{1+}$-YfaE or Fe^{2+} is present, the reducing equivalent must come from β_2. However, when excess YfaE is present, it could provide the reducing equivalent. Measurement of the activity of β_2 produced in the presence and absence of excess [2Fe2S]$^{1+}$-YfaE could test this hypothesis. In the former case, one might expect to observe maximal enzymatic activity, unlike in the latter case, non-specific reduction of the $WH^{+\bullet}$ might reduce catalytic activity. The activity assay is an independent measure of the Y• concentration as previous studies have shown that the activity is directly correlated with the amount of Y• (*28*). The specific activity per Y• regenerated per β_2 was around 4000 nmol•min^{-1}•mg^{-1} per Y•/β_2 with stoichiometric amounts of YfaE and around 6000 nmol•min^{-1}•mg^{-1} per Y•/β_2 in the presence of excess YfaE (**Table 2-4**). Recall that the activity of the starting β_2 was 6500 nmol•min^{-1}•mg^{-1} (1.1 Y•s, ~6000 nmol•min^{-1}•mg^{-1} per Y•/β_2). Control experiments showed the presence of

oxidized YfaE causes no significant change in the activity of β_2. Thus the observed activities (**Table 2-4**) are in line with YfaE being able to protect β_2 from protein radical damage.

The titration studies have a number of mechanistic implications. First, the reduction of iron in β_2 by YfaE must occur cooperatively in one β. If iron was statistically reduced, the amount of Y• recovered, which requires a diferrous-β_2, would be lower than 2 Fe/Y• observed. Second, diferrous-β_2 itself, upon exposure to O_2, can rapidly deliver the reducing equivalent and convert all the reduced Fe^{2+} into differic-Y•, despite the time taken for the titrations that could potentially allow Fe^{2+} to dissociate from β. The YfaE thus may inhibit Fe^{2+} dissociation and/or enhance β's delivery of the reducing equivalent. Thus the assembly of the diferrous cluster without excess reductant can now be studied. Finally, the method of cluster assembly has resulted in high levels of Y• as well as the highest specific activity to date and suggests that if 4 Fe^{2+}s could be loaded into β_2, 2 Y• could be generated.

The difference spectrum (**Figure 2-12**, insert) from the assembly process requires further comment. The spectrum reveals absorption features between 400 and 600 nm in addition to the diferric Y• cofactor. We found that these features varied when different batches of YfaE were used in the titrations. Thus these features are unlikely to be associated with an oxidized amino acid residue in β. They are most reasonably associated with the heterogeneity of the FeS clusters in YfaE from the in vitro reconstitutions and the multiple spectral subtractions required to access this spectrum.

SF kinetics to monitor reactions between met-β_2 and [2Fe2S]$^{1+}$-YfaE

To provide further support for the role of YfaE in vivo, the kinetics of the reduction of met-β_2 by [2Fe2S]$^{1+}$-YfaE have been examined by SF spectroscopy. The reactions were carried out under anaerobic conditions and monitored at 320 and 465 nm. Changes at 320 nm, the isosbestic point between oxidized and reduced YfaE, provide the best way to monitor the reduction of the diferric cluster in β_2. Oxidation of YfaE was monitored at 465 nm as this wavelength represents the biggest difference in absorption between reduced and oxidized YfaE.

In a typical experiment met-β_2 is mixed with variable amounts of [2Fe2S]$^{1+}$-YfaE under anaerobic conditions at 37 °C. To make the SF system anaerobic, extensive incubation of sodium dithionite solutions followed by anaerobic water and anaerobic buffer washes of the SF mixing lines are essential. The results of a typical experiment are shown in **Figure 2-14**. The data from analysis of the first 5 sec at each wavelength were fit to two single exponentials giving rise to $k_{obs\text{-}fast}$ of ~5 s^{-1} (50% of total amplitude) and $k_{obs\text{-}slow}$ ~2 s^{-1} (50% of total amplitude) at 465 nm and $k_{obs\text{-}fast}$ of ~4 s^{-1} (83% of total amplitude) and $k_{obs\text{-}slow}$ ~1 s^{-1} (17% of total amplitude) at 320 nm. From the amplitudes of the SF data, the reaction stoichiometry between the amount of YfaE oxidized and met-β_2 reduced can also be calculated. Consistent with the titration experiments, the results suggest one Fe reduced per YfaE oxidized (**Table 2-3**).

To examine whether the observed rate constants are dependent on the concentrations of [2Fe2S]$^{1+}$-YfaE and met-β_2, the reactions between 1.5, 2.5, 5 and 10 μM [2Fe2S]$^{1+}$-YfaE and 5 μM met-β_2 monitored by the SF at 37 ºC under anaerobic conditions. Similar to the experiment in **Figure 2-14**, the kinetic traces at A_{465nm} can be well fit to two single exponentials (**Figure 2-15**). However, in contrast to the observations at higher [YfaE] in which the two observed rate constants had similar amplitudes, the absorbance changes were dominated by the slower phase

(**Table 2-5**). Furthermore, the rate constants of the fast phase varied from ~7 s^{-1} to ~100 s^{-1}, which contributed to ~3-14% of the total amplitude. Because of the inconsistency of the fast rate constants with the concentrations of YfaE, these $k_{obs\text{-}fast}$ are likely to be artifacts from the SF instrument. We thus focus analysis on $k_{obs\text{-}slow}$.

Figure 2-16 shows the correlations between $k_{obs\text{-}slow}$ and the concentration of YfaE. The results indicate that the observed rate constant is saturated at YfaE concentrations as low as 1.5 μM. The same SF experiment was carried out at lower concentrations of YfaE (0.25 μM and 0.5 μM), but the signal was too noisy to analyze. Therefore, 1.5 μM YfaE was determined to be the lower limit of detection for the SF experiments.

Even though the reason for distinct $k_{obs\text{-}fast}$ and $k_{obs\text{-}slow}$ after different [YfaE] is not understood, the rate constants for reduction of met-β_2 are considerably faster than those previously reported with Fre, Fraction B, DTT and NADPH (*29*) or with chemical reductants (*30-32*), suggesting YfaE may be the physiologically relevant reducant for met-β_2. Because inside the cells there are other potential substrates for $[2Fe2S]^{1+}$-YfaE such as wt-β_2 and oxygen that could potentially compete with met-β_2 for the availability of reduced YfaE, the rates of oxidation of YfaE by wt-β_2 and air-saturated buffer were investigated by SF.

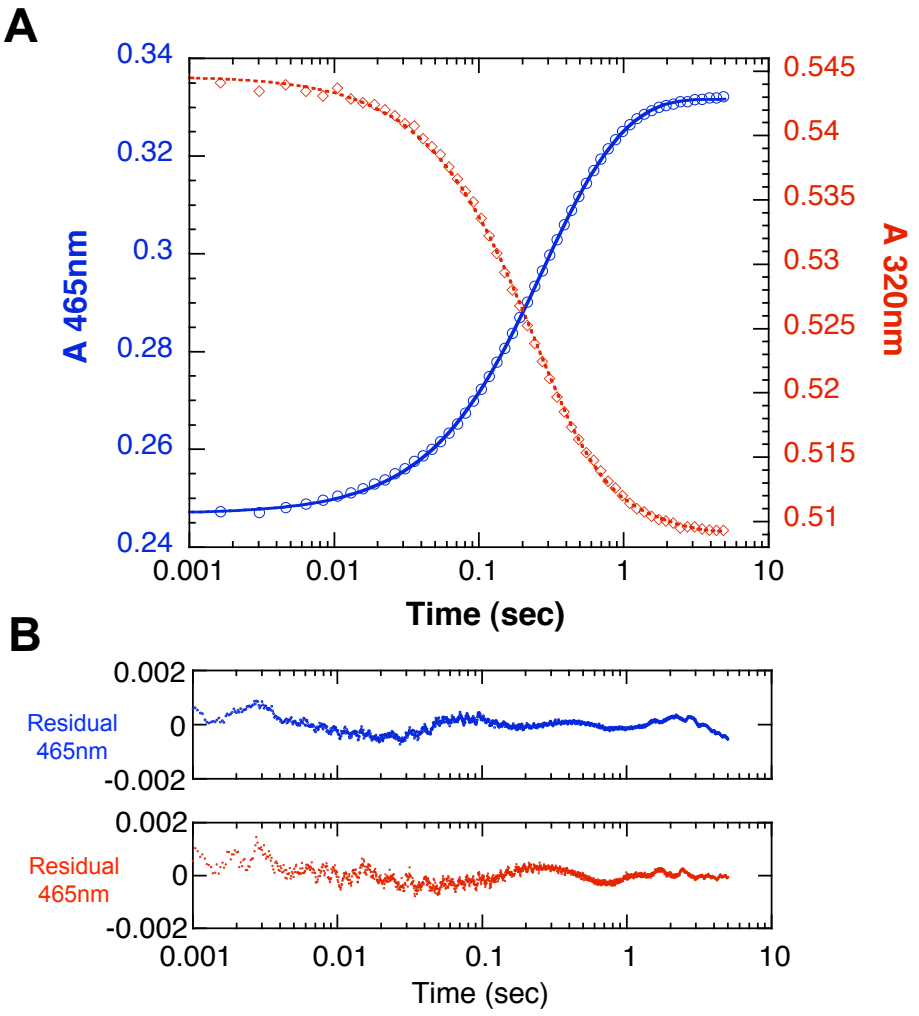

Figure 2-14. Reduction of met-β_2 (5 μM) with 37.5 μM $[2Fe2S]^{1+}$-YfaE monitored by stopped flow spectroscopy. A: Oxidation of $[2Fe2S]^{1+}$-YfaE was monitored at 465 nm (blue circles); reduction of met-β_2 was monitored at 320 nm (pink circles). The data were fit in both cases to two exponentials (blue line: 465 nm, pink line: 320 nm). B. The residuals of the fitting are shown.

Table 2-5. Kinetic parameters of YfaE oxidation by 5 μM met-β_2.

μM YfaE	ΔA_{465nm}	$k_{obs\text{-}fast}$ (s^{-1})	% ΔA	$k_{obs\text{-}slow}$ (s^{-1})	% ΔA
1.5	0.0064	49	14	1.7	86
2.5	0.014	17	10	1.8	90
5	0.031	101	3	1.8	97
10	0.057	6.7	9	1.6	91

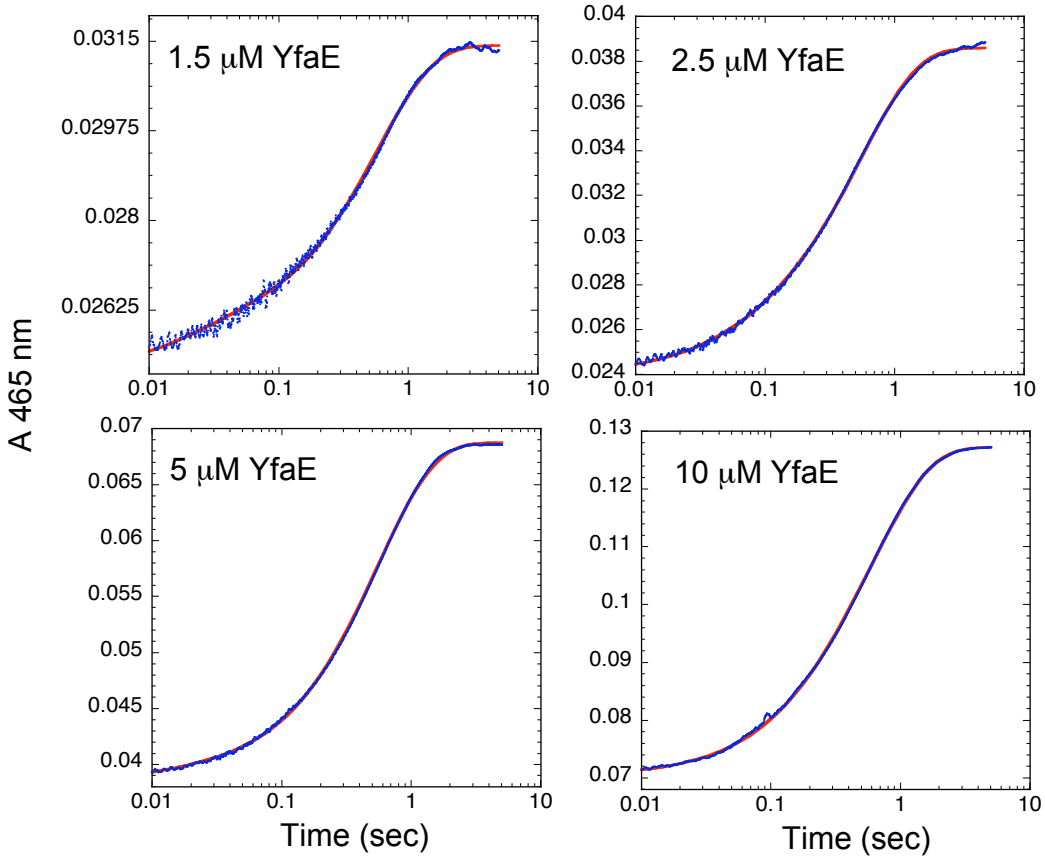

Figure 2-15. Stopped flow kinetics of $[2Fe2S]^{1+}$-YfaE oxidized by met-β_2 (5 μM) at 37 ºC under anaerobic conditions. The same experimental procedures and data analysis for the anaerobic SF experiments in Chapter 2 were followed. Oxidation of $[2Fe2S]^{1+}$-YfaE was monitored at 465 nm. Data points (blue, ~10 shots, 2000 points in logarithmic time scale for 20 sec) were averaged and the data of the first 5 sec were fit to two single exponentials (red line). Traces within the first one second are shown. The concentrations of $[2Fe2S]^{1+}$-YfaE (1.5, 2.5, 5 and 10 μM) are indicated.

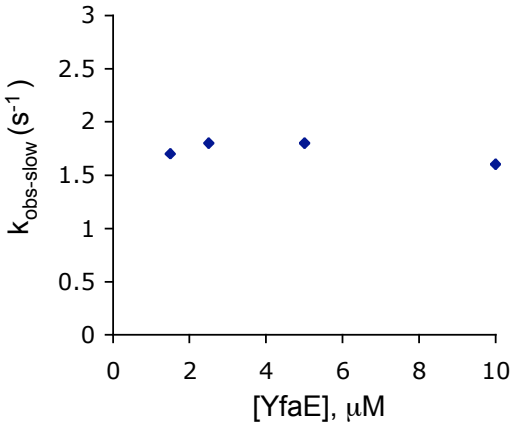

Figure 2-16. Concentration dependence of the rate of reaction between met-β_2 (5 μM) and $[2Fe2S]^{1+}$-YfaE (1.5, 2.5, 5, 10 μM) under anaerobic conditions. The oxidation of $[2Fe2S]^{1+}$-YfaE by met-β_2 was monitored at 465 nm by UV-visible stopped flow spectroscopy. The data in **Figure 2-15** were analyzed by Kaleidagraph to generate kinetic parameters listed in **Table 2-5**. The observed rate constants from the dominant ΔA_{465nm} (> 90%) were plotted against the concentrations of $[2Fe2S]^{1+}$-YfaE.

SF kinetics to monitor oxidation of $[2Fe2S]^{1+}$-YfaE by wt-β_2 or O_2

The rate of oxidation of $[2Fe2S]^{1+}$-YfaE (15 μM) by air-saturated buffer at 37ºC is shown in **Figure 2-17**. The data was best fit to two single exponentials even though the product(s) of the reactions and consequently the mechanism are unknown. Nevertheless, the k_{obs} from the dominant amplitude (96%) is 0.018 s^{-1}, which is much slower than the reactions with met-β_2, and suggests O_2 does not compete with met-β_2 for reduced YfaE.

Experiments of wt-β_2 (5 μM) and $[2Fe2S]^{1+}$-YfaE (45 μM) were also carried out as described for met-β_2 (**Figure 2-18**). The oxidation of YfaE (blue circle), was best fit to two single exponetials: $k_{obs-fast}$ = 0.03 s^{-1} and $k_{obs-slow}$ = 0.007 s^{-1}. Both reactions are ~100 fold slower than those with met-β_2. Analysis of the lost in A_{320nm} also was fit to two exponentials (**Figure 2-**

18). The fits to changes at 320 nm are in general more difficult to interpret as many changes occur in this region and the sensitivity of instrument at this λ is poor. From the total changes observed at each wavelength, 16.7 μM of YfaE ($\Delta\varepsilon_{465nm}$ = 6.6 $mM^{-1}cm^{-1}$) and 4.1 μM of wt-β_2 ($\Delta\varepsilon_{320nm}$ = 9.7 $mM^{-1}cm^{-1}$) were oxidized and reduced, respectively. At face value, 4.1 equivalent of YfaE were oxidized per wt-β_2 reduced. Given that there are 3.4 Fe and 1.1 Y• per wt-β_2, theoretically 4.5 equivalents of YfaE could be reduced, which is in fair agreement with the experimental results.

The slower oxidation rates of YfaE by wt-β_2 and O_2 suggest that met-β_2 is the more favored substrate in vivo. This result supports our proposal that YfaE functions in cluster maintenance for β_2 in vivo.

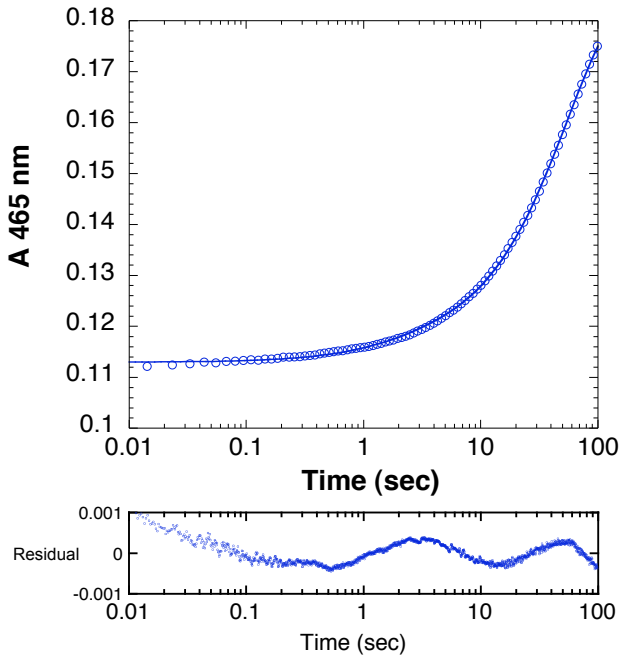

Figure 2-17. Oxidation of $[2Fe2S]^{1+}$-YfaE (15 μM) by air-saturated buffer monitored at A_{465nm}, 37 ºC by SF spectroscopy. Data points (2000 points in 100 sec, average of 5 shots) were fitting with two single exponentials with a k_{0bs1} = 0.6 s^{-1} (4% of total amplitude) and k_{0bs2} = 0.018 s^{-1} (96% of total amplitude). The residual of the fitting is shown.

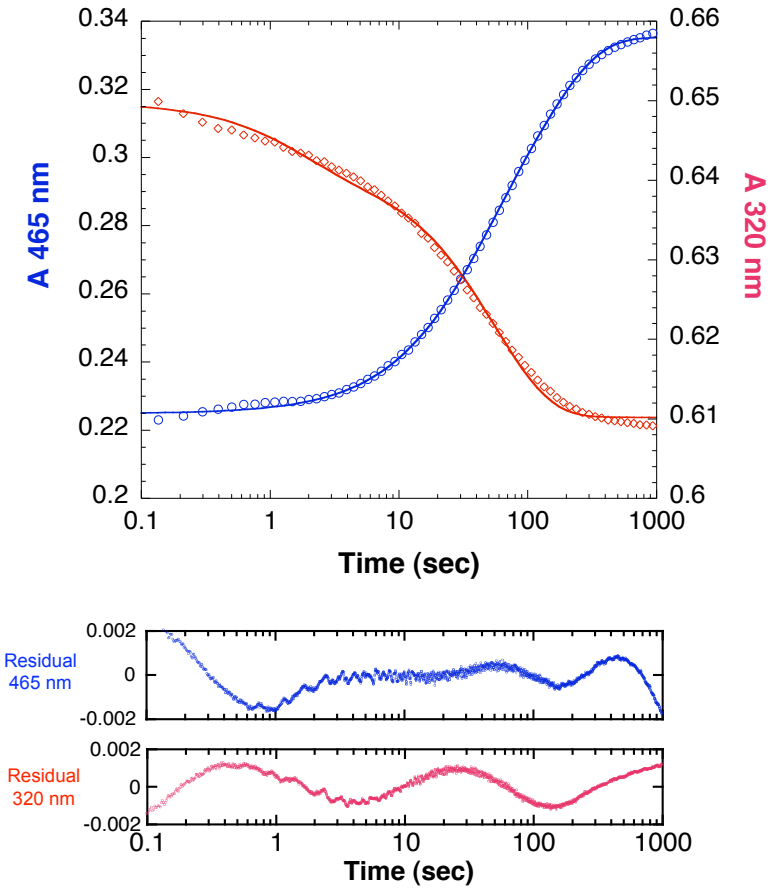

Figure 2-18. Reduction of wt-β_2 (5 μM) with 45 μM $[2Fe2S]^{1+}$-YfaE monitored by SF spectroscopy at 37 ºC. Oxidation of $[2Fe2S]^{1+}$-YfaE and reduction of wt-β_2 were monitored at 465 nm (blue) and 320 nm (red), respectively. Data points (~10 shots, 2000 points in 20 sec, logarithmic scale) were averaged and fitted with two single exponentials (blue line: 465 nm, red line: 320 nm). The kinetic parameters determined from changes at 465 nm are $k_{obs\text{-}fast}$ = 0.05 s^{-1} (27% of total amplitude), $k_{obs\text{-}slow}$ = 0.009 s^{-1}, 73% of total amplitude) and at 320 nm are $k_{obs\text{-}fast}$ = 0.6 s^{-1} (23% of total amplitude), $k_{obs\text{-}slow}$ = 0.02 s^{-1} , 77% of total amplitude). The residuals of the fitting are shown.

Formation of transient $WH^{+\bullet}$ monitored by SF spectroscopy in the reactions between YfaE-reduced met-β_2 and O_2

To further support the proposal that the reducing equivalent required for cluster assembly in β_2 is provided by W48, the formation of the transient $WH^{+\bullet}$ is monitored by SF spectroscopy at A_{560nm} (*18*). Met-β_2 was pre-reduced by $[2Fe2S]^{1+}$-YfaE followed by reaction with O_2-saturated buffer at 4 ºC. Because the oxidation of YfaE also changes A_{560nm}, the reaction was carried out using substoichiometric amounts of YfaE to reduce met-β_2 (YfaE : met-β_2 = 2 : 1). From experiments of met-β_2 titrated with $[2Fe2S]^{1+}$-YfaE, the reaction is close to completion at this ratio, therefore, a maximum of 60 μM of Fe^{2+} (30 μM of Fe after being mixed with O_2-saturated buffer in SF) can be generated in met-β_2 (3.4 Fe/β_2, total ~102 μM Fe in 30 μM met-β_2) concomitant with complete oxidation of $[2Fe2S]^{1+}$-YfaE.

The assembly of the diferric-Y• cofactor from diferrous-β_2 was initiated by reacting with equal volume of O_2 saturated buffer and A_{560nm} was monitored by SF (**Figure 2-19**). The result shows a rapid increase of A_{560nm} that reaches a maximum at ~20 ms, followed by a slower decrease until 0.5 s. The data can be well fit to **Eq 2-1** derived from a two consecutive, first-order reaction model (**Scheme 2-1**), and generates two rate constants, k_1 = 162 s^{-1} and k_2 = 10 s^{-1}, in good agreement with the reported rate constants (k_1 = 200 s^{-1} and k_2 = 12 s^{-1}) observed for the $WH^{+\bullet}$ formed in the reactions between diferrous-β_2 (pre-loaded with Fe^{2+}) and O_2 (*19*). Using ε_{560nm} = 3000 $M^{-1}cm^{-1}$ determined from pulse radiolysis experiments (*17*), we can calculate that ~11 μM $WH^{+\bullet}$ was formed, which is ~73% of the theoretical value, 15 μM, assuming 2 Fe^{2+} in β_2 generate one $WH^{+\bullet}$ after reacting with O_2. These results support the proposal that the reducing equivalent required for diferric-Y• cofactor assembly is provided by a W, likely W48 of β_2.

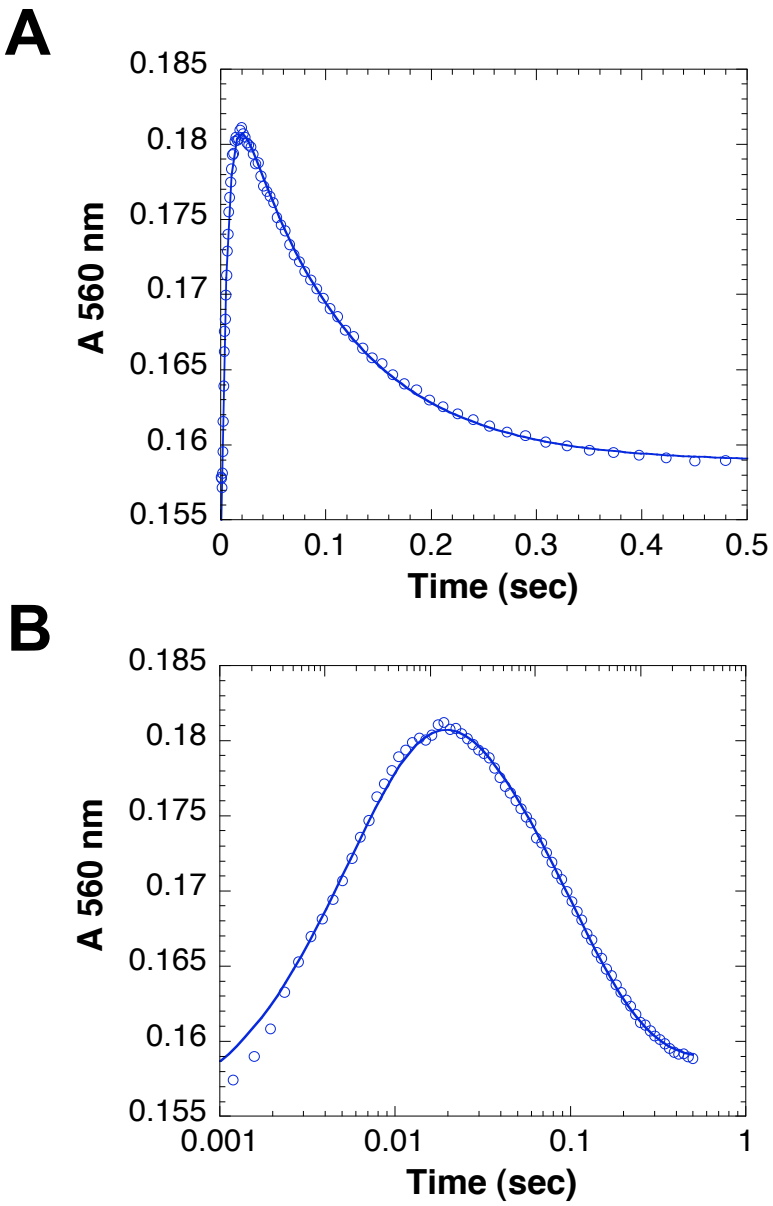

Figure 2-19. Reaction of YfaE-reduced met-β_2 with O_2-saturated buffer monitored by SF spectroscopy at 4 ºC. Met-β_2 (15 μM) was pre-reduced by 30 μM $[2Fe2S]^{1+}$-YfaE anaerobically and mixed with O_2-saturated buffer. Data points were fit to a sequential R→I→P model (blue line, **Scheme 2-1, Eq 2-1**). The rate of the formation and decay of the intermediate I is 162 and 10 s^{-1}, respectively. Linear time scale (A) and logarithmic time scale (B) of the plots are shown.

DISCUSSION

The high occurrence of a conserved putative 2Fe2S-ferredoxin gene adjacent to the *nrdAB* operon suggests that it might be a key player in generating and maintaining the diferric-β_2 cofactor of active β_2 in RNR. The cloning and overexpression of this ferredoxin, YfaE in *E. coli* was successful but the purification proved to be a challenge as the overexpressed protein formed inclusion bodies. Several attempts to express soluble protein were not successful thus we chose to refold and reconstitute YfaE under strictly anaerobic conditions. The protein was purified to homogeneity judged by SDS-PAGE. It was then characterized by quantitation of the amount of iron and sulfide and by UV-visible, EPR and Mössbauer spectroscopies. YfaE is predominantly a monomer, but oxidized YfaE forms aggregate irreversibly.

Once the challenges of protein purification were overcome, we set out to investigate whether YfaE might be involved in the biosynthesis and maintenance of the diferric-Y• cofactor. As mentioned in the introduction, this hypothesis was derived in part due to the striking similarity of the structure and chemistry of MMO and Δ9D (*1, 2, 33*). YfaE shares ~29% sequence identity with both the plant Fdx that can reactivate Δ9D and the ferredoxin domain in MMOR (*4, 5, 20*). This functional analogy and the studies with MMOR/MMO and Fdx/Δ9D, provide compelling support for our proposed function of YfaE.

To study the ability of YfaE to reduce met-β_2 to diferrous-β_2, titration experiments under anaerobic conditions were carried out. These studies revealed the ability of YfaE to play this role. Quantitative analysis showed that every YfaE oxidized resulted in one iron reduced (**Table 2-3**). Parallel titration experiments analyzing for Fe^{2+} using the ferrozine assay supported this conclusion. Thus YfaE is a chemically competent reductant of met-β_2. After the titration end point was reached, the sample was exposed to O_2 and the formation of diferric-Y• was observed

within the 2 min required to scan the spectrum (**Figure 2-12**). This cluster assembly occurred in the absence of exogenous reducing reagents. To further characterize the resulting diferric-Y• cofactor, the amount of Y• generated from the titration experiments was quantitated by EPR spectroscopy. Interestingly, a stoichiometry of two iron reduced (two YfaE oxidized) per one Y• generated was observed. This result requires the reducing equivalent is provided by β_2 and not by Fe^{2+} that has dissociated from β_2 during the titration. From our previous studies on cluster assembly in vitro, the W48 in β_2 is the best candidate for the reducing equivalent, generating a $WH^{+\bullet}$ (*18, 19*). This proposal is further supported by SF experiments in which YfaE-reduced met-β_2 was reacted with O_2, generating a transient intermediate at A_{560nm}, a typical absorption feature of a $WH^{+\bullet}$ (*18, 19*).

Furthermore, in the presence of excess YfaE, the amount of Y• generated is greater than the amount of Y• observed in our way in reconstitution experiments for β_2. This result suggests that YfaE reduction will allow us to generate Y• equivalent to half of the amount of iron. The met-β_2 used in our experiments contained 3.4 irons, which means a theoretical maximum of 1.7 Y•/β_2 could be obtained if all the iron is reduced. Under conditions where the concentration of $[2Fe2S]^{1+}$-YfaE was 20× that of [met-β_2], a reduction of 88% of the iron center and formation of 1.5 Y•/β_2 was observed (**Table 2-4**).

While the titration data have clearly defined the reaction stoichiometry between YfaE and met-β_2, the rates of reaction must be determined to provide convincing support for the role of YfaE. SF kinetics monitoring both the reduction of met-β_2 and the oxidation of $[2Fe2S]^{1+}$-YfaE under anaerobic conditions were carried out. Since there are 3.4 irons in the met-β_2 used in this experiment and $[2Fe2S]^{1+}$-YfaE can only deliver one electron at a time, the kinetics are inherently complex (*4*). The data in **Figure 2-14** have been fit for the first 5 sec during which

80% of the irons are reduced. Two single exponentials give rate constants of 4 to 5 s^{-1} and 1 to 2 s^{-1} with similar amplitudes. These numbers compare favorably with similar experiments carried out on Δ9D and MMO. In the former case when reduced Fdx is incubated with oxidized Δ9D, the rate of product formation (1.5 products/dimer) is 3.4 s^{-1} in which the reduction step is likely the rate-limiting step even though this has not been unambiguously verified (*33*). In the case of MMO, studies with the Fdx domain only (residues 1-98) show that it reduces oxidized MMO with rate constants of 1 s^{-1} and 0.2 s^{-1} (*4*). When both domains in MMOR are present, the rates are greatly enhanced to 95 s^{-1}, even though 10-40% of the MMO is not reduced in the in vitro studies (*4*).

Our results, however, suggest the rates of reduction of met-β_2 are rapid, relative to other reductants previously reported (*29, 31, 32*). There have been many studies investigating the reduction of met-β_2 to the diferrous-β_2 using chemical reductants and "protein reductants" (*29-32, 34, 35*). Unfortunately, the actual rate constants are not readily accessible from the published information. In the case of the chemical reductants, dithionite and a dye mediator, deazaflavin and light, DTT and Fe^{2+} etc, the rates of reduction are very slow on the order of several minutes (*30-32, 34*). In the case of a protein reductant, Fre, the reported data for reduction suggested that the rate is also very slow (less than 0.001 s^{-1}) (*29, 32*). These results support the proposal that YfaE is a physiologically relevant reductant for met-β_2.

Inside the cell, active-β_2 and O_2 might compete with met-β_2 for reduced YfaE, so their rates of reduction by $[2Fe2S]^{1+}$-YfaE were examined as control experiments. In order to mimic physiological conditions, oxidation of YfaE by O_2 was carried out in air-saturated buffer at 37 ºC. The results indicate that the rate is slow (~0.02 s^{-1}) relative to rates of oxidation by met-β_2 under similar conditions. We then examined the oxidation of YfaE by the diferric-Y•-β_2. The

rate of oxidation of YfaE was 0.05 s^{-1}. Analysis of the UV-vis spectra during the reduction process showed the diferric-cluster is lost concomitant with Y• reduction. This behavior has been observed in earlier studies with the chemical reductants hydrazine and phenylhydrazine (*36*). The proposed mechanism involves reduction of one Fe^{3+} to Fe^{2+} to form a transient mixed valent cluster, which is then rapidly oxidized back to the diferric cluster concomitant with Y• reduction (*37*). The resulting met-β_2 is then reduced as to diferrous-β_2 as described above. These results imply that met-β_2 may be the more favored substrate for $[2Fe2S]^{1+}$-YfaE in vivo.

In summary, we have identified a 2Fe2S-ferredoxin, YfaE, which can function in reactivating met-β_2 by reducing the diferric cluster to diferrous form. The presence of O_2, the diferrous-β_2 reassembles to form diferric-Y• cluster. The immediate electron source for the cluster assembly is provided by β_2, possibly through formation of a $W^{+\bullet}$. The kinetic studies suggest YfaE can reduce met-β_2 at a rate faster than reductants previously examined for this role (*30-32, 34*). Based on these results, the role of YfaE is incorporated into our model for maintenance and biosynthesis pathways (**Figure 2-20**).

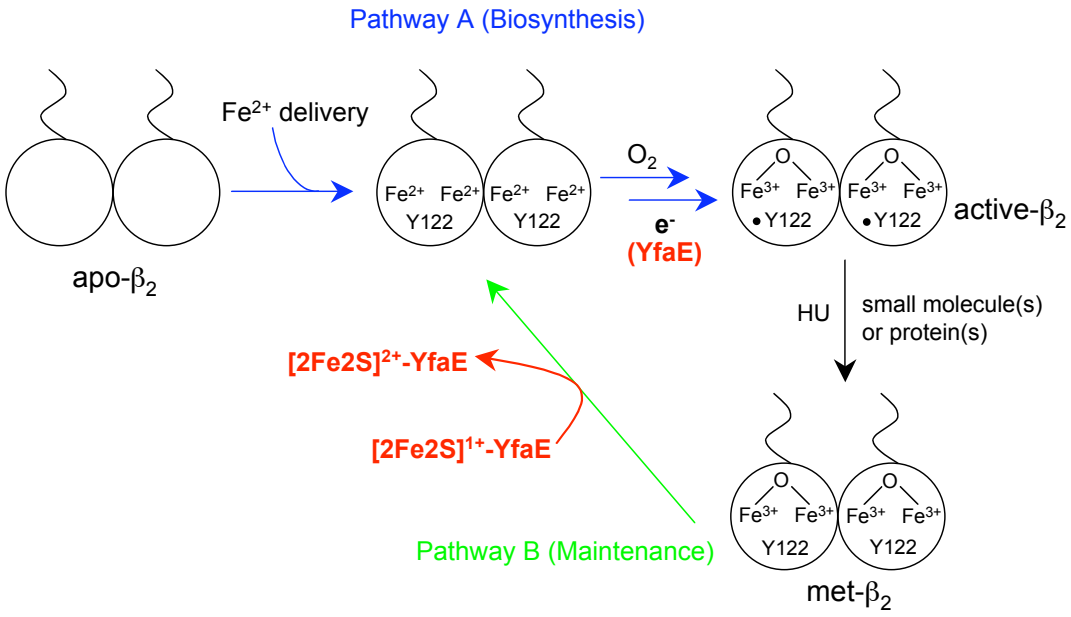

Figure 2-20. Model for the postulated roles of YfaE (red) in the maintenance and biosynthesis of diferric-Y• cofactor (see Chapter 1).

REFERENCES

(1) Baik, M. H., Newcomb, M., Friesner, R. A., and Lippard, S. J. (2003) Mechanistic studies on the hydroxylation of methane by methane monooxygenase. *Chem. Rev. 103*, 2385-419.

(2) Fox, B. G., Lyle, K. S., and Rogge, C. E. (2004) Reactions of the diiron enzyme stearoyl-acyl carrier protein desaturase. *Acc. Chem. Res. 37*, 421-9.

(3) Blazyk, J. L., and Lippard, S. J. (2002) Expression and characterization of ferredoxin and flavin adenine dinucleotide binding domains of the reductase component of soluble methane monooxygenase from *Methylococcus capsulatus* (Bath). *Biochemistry 41*, 15780-94.

(4) Blazyk, J. L., Gassner, G. T., and Lippard, S. J. (2005) Intermolecular electron-transfer reactions in soluble methane monooxygenase: A role for hysteresis in protein function. *J. Am. Chem. Soc. 127*, 17364-76.

(5) Sobrado, P., Lyle, K. S., Kaul, S. P., Turco, M. M., Arabshahi, I., Marwah, A., and Fox, B. G. (2006) Identification of the binding region of the [2Fe-2S] ferredoxin in stearoyl-acyl carrier protein desaturase: Insight into the catalytic complex and mechanism of action. *Biochemistry 45*, 4848-58.

(6) Cafaro, V., Scognamiglio, R., Viggiani, A., Izzo, V., Passaro, I., Notomista, E., Piaz, F. D., Amoresano, A., Casbarra, A., Pucci, P., and Di Donato, A. (2002) Expression and purification of the recombinant subunits of toluene/o-xylene monooxygenase and reconstitution of the active complex. *Eur. J. Biochem. 269*, 5689-99.

(7) Gunsalus, I. C., and Wagner, G. C. (1978) Bacterial P-450cam methylene monooxygenase components: Cytochrome m, putidaredoxin, and putidaredoxin reductase. *Methods Enzymol. 52*, 166-188.

(8) Fish, W. W. (1988) Rapid colorimetric micromethod for the quantitation of complexed iron in biological samples. *Methods Enzymol. 158*, 357-364.

(9) Beinert, H. (1983) Semi-micro methods for analysis of labile sulfide and of labile sulfide plus sulfane sulfur in unusually stable iron-sulfur proteins. *Anal. Biochem. 131*, 373-8.

(10) Broman, L., Malmström, B. G., Aasa, R., and Vanngard, T. (1962) Quantitative electron spin resonance studies on native and denatured ceruloplasmin and laccase. *J. Mol. Biol. 5*, 301-10.

(11) Münck, E. (2000) in *Physical Methods in Bioinorganic Chemistry* (Que, L., Jr., Ed.) pp 287-319, University Science Books, Sausalito, CA.

(12) Gibson, J. F., Hall, D. O., Thornley, J. H., and Whatley, F. R. (1966) The iron complex in spinach ferredoxin. *Proc. Natl. Acad. Sci. U. S. A. 56*, 987-90.

(13) Bencini, A., and Gatteschi, D. (1990) *EPR of exchange coupled systems*, Springer-Verlag, Berlin.

(14) Ge, J., Yu, G., Ator, M. A., and Stubbe, J. (2003) Pre-steady-state and steady-state kinetic analysis of *E. coli* class I ribonucleotide reductase. *Biochemistry 42*, 10071-83.

(15) Barlow, T., Eliasson, R., Platz, A., Reichard, P., and Sjöberg, B. M. (1983) Enzymic modification of a tyrosine residue to a stable free radical in ribonucleotide reductase. *Proc. Natl. Acad. Sci. U. S. A. 80*, 1492-5.

(16) Atkin, C. L., Thelander, L., Reichard, P., and Lang, G. (1973) Iron and free-radical in ribonucleotide reductase - exchange of iron and Mössbauer-spectroscopy of protein-B2 subunit of *Escherichia coli* enzyme. *J. Biol. Chem. 248*, 7464-7472.

(17) Solar, S., Getoff, N., Surdhar, P. S., Armstrong, D. a., and Singh, a. (1991) Oxidation of tryptophan and N-methylindole by $N_3^{\cdot}$, Br_2^{-}, and $(Scn)_2^{-}$ radicals in light-water and heavy-water solutions - a pulse-radiolysis study. *J. Phy. Chem. 95*, 3639-3643.

(18) Bollinger, J. M., Jr., Tong, W. H., Ravi, N., Huynh, B. H., Edmondson, D. E., and Stubbe, J. (1994) Mechanism of assembly of the tyrosyl radical-diiron(III) cofactor of *Escherichia coli* ribonucleotide reductase. 3. Kinetics of the limiting Fe^{2+} reaction by optical, EPR, and Mössbauer spectroscopies. *J. Am. Chem. Soc. 116*, 8024-8032.

(19) Baldwin, J., Krebs, C., Ley, B. A., Edmondson, D. E., Huynh, B. H., and Bollinger, J. M. J. (2000) Mechanism of rapid electron transfer during oxygen activation in the R2 subunit of *Escherichia coli* ribonucleotide reductase. 1. Evidence for a transient tryptophan radical. *J. Am. Chem. Soc. 122*, 12195-12206.

(20) Müller, J., Lugovskoy, A. A., Wagner, G., and Lippard, S. J. (2002) NMR structure of the [2Fe-2S] ferredoxin domain from soluble methane monooxygenase reductase and interaction with its hydroxylase. *Biochemistry 41*, 42-51.

(21) Rypniewski, W. R., Breiter, D. R., Benning, M. M., Wesenberg, G., Oh, B. H., Markley, J. L., Rayment, I., and Holden, H. M. (1991) Crystallization and structure determination

to 2.5-A resolution of the oxidized [2Fe-2S] ferredoxin isolated from *Anabaena* 7120. *Biochemistry 30*, 4126-31.

(22) Ta, D. T., and Vickery, L. E. (1992) Cloning, sequencing, and overexpression of a [2Fe-2S] ferredoxin gene from *Escherichia coli*. *J. Biol. Chem. 267*, 11120-5.

(23) Zheng, L., Cash, V. L., Flint, D. H., and Dean, D. R. (1998) Assembly of iron-sulfur clusters. Identification of an *iscSUA-hscBA-fdx* gene cluster from *Azotobacter vinelandii*. *J. Biol. Chem. 273*, 13264-72.

(24) Cheng, H., Xia, B., Reed, G. H., and Markley, J. L. (1994) Optical, EPR, and ^{1}H NMR spectroscopy of serine-ligated [2Fe-2S] ferredoxins produced by site-directed mutagenesis of cysteine residues in recombinant *Anabaena* 7120 vegetative ferredoxin. *Biochemistry 33*, 3155-64.

(25) Dunham, W. R., Bearden, A. J., Salmeen, I. T., Palmer, G., Sands, R. H., Orme-Johnson, W. H., and Beinert, H. (1971) The two-iron ferredoxins in spinach, parsley, pig adrenal cortex, *Azotobacter vinelandii*, and *Clostridium pasteurianum*: Studies by magnetic field Mössbauer spectroscopy. *Biochim. Biophys. Acta 253*, 134-52.

(26) Fox, B. G., Hendrich, M. P., Surerus, K. K., Andersson, K. K., Froland, W. A., Lipscomb, J. D., and Münck, E. (1993) Mössbauer, EPR, and ENDOR studies of the hydroxylase and reductase components of methane monooxygenase from *Methylosinus trichosporium* Ob3b. *J. Am. Chem. Soc. 115*, 3688-3701.

(27) Münck, E., Debrunner, P. G., Tsibris, J. C., and Gunsalus, I. C. (1972) Mössbauer parameters of putidaredoxin and its selenium analog. *Biochemistry 11*, 855-63.

(28) Bollinger, J. M., Jr. (1993) On the chemical mechanism of assembly of the tyrosyl radical-dinuclear iron cluster cofactor of *E. coli* ribonucleotide reductase. Thesis Ph. D. Massachusetts Institute of Technology. Department of Chemistry. pp 369 leaves.

(29) Fontecave, M., Eliasson, R., and Reichard, P. (1989) Enzymatic regulation of the radical content of the small subunit of *Escherichia coli* ribonucleotide reductase involving reduction of its redox centers. *J. Biol. Chem. 264*, 9164-70.

(30) Sahlin, M., Gräslund, A., Petersson, L., Ehrenberg, A., and Sjöberg, B. M. (1989) Reduced forms of the iron-containing small subunit of ribonucleotide reductase from *Escherichia coli*. *Biochemistry 28*, 2618-25.

(31) Fontecave, M., Gerez, C., Mansuy, D., and Reichard, P. (1990) Reduction of the Fe(III)-tyrosyl radical center of *Escherichia coli* ribonucleotide reductase by dithiothreitol. *J. Biol. Chem. 265*, 10919-24.

(32) Covès, J., Delon, B., Climent, I., Sjöberg, B. M., and Fontecave, M. (1995) Enzymic and chemical reduction of the iron center of the *Escherichia coli* ribonucleotide reductase protein R2. The role of the C-terminus. *Eur. J. Biochem. 233*, 357-63.

(33) Lyle, K. S., Haas, J. A., and Fox, B. G. (2003) Rapid-mix and chemical quench studies of ferredoxin-reduced stearoyl-acyl carrier protein desaturase. *Biochemistry 42*, 5857-66.

(34) Covès, J., Laulhère, J. P., and Fontecave, M. (1997) The role of exogenous iron in the activation of ribonucleotide reductase from *Escherichia coli*. *J. Biol. Inorg. Chem. 2*, 418-426.

(35) Fontecave, M., Eliasson, R., and Reichard, P. (1987) NAD(P)H:flavin oxidoreductase of *Escherichia coli* - a ferric iron reductase participating in the generation of the free-radical of ribonucleotide reductase. *J. Biol. Chem. 262*, 12325-12331.

(36) Han, J. Y., Swarts, J. C., and Sykes, A. G. (1996) Kinetic studies on the hydrazine and phenylhydrazine reductions of the *Escherichia coli* R2 subunit of ribonucleotide reductase. *Inorg. Chem. 35*, 4629-4634.

(37) Twitchett, M. B., Dobbing, A. M., and Sykes, A. G. (2000) New mechanistic insights into the reactivity of the R2 protein of *E. coli* ribonucleotide reductase (RNR). *J. Inorg. Biochem. 79*, 59-65.

Chapter 3:

Studies on the Interactions between YfaE and β_2 and the Physiological Role of YfaE

INTRODUCTION

In Chapter 2 we demonstrated the chemical competence of YfaE in reducing met-β_2 and regenerating the Y• in the presence of oxygen. We were next interested in determining the binding affinity and investigating the nature of interaction between the two proteins, which can set the stage for designing kinetic experiments and evaluating the physiological relevance of the proposed functions of YfaE. The approaches we applied and the design of our experiments are heavily based on the studies on MMO and Δ9D, the structural and functional analogues of β_2.

In MMO, the reduction of the di-ferric center is carried out by MMOR, which contains a [2Fe2S]-ferredoxin domain (MMOR-Fdx) and a reductase domain (MMOR-FAD) that has a tightly bound FAD and a NADH binding site. Lippard and coworkers have separated these two domains and studied the interaction between the two domains and between MMOR-Fdx and MMO in great detail (*1-3*). By isothermal titration calorimetry (ITC), they have shown that two MMOR-Fdxs bind to one MMO ($\alpha_2\beta_2\gamma_2$) with two binding constants of 0.6 and 3.2 μM (*1*). Similar results were observed for binding between MMOR and MMO, with two dissociation constants of 0.4 and 0.7 μM (*4*). It should be noted that the ITC experiments were carried out at ~4 ºC under aerobic conditions, thus the iron in both proteins are in +3 state. Furthermore, only ~70% of the MMO participated the binding to MMOR or MMOR-Fdx. Kinetic studies of reactions between dithionite-reduced MMOR-Fdx and MMO by SF spectroscopy under anaerobic conditions have demonstrated that the reactions are bi-phasic with two observed rate constants of 1.0 and 0.24 s^{-1}. Quantitative analysis revealed that 10-40% of MMO was not reduced by MMOR-Fdx, similar to the observations in the ITC studies.

The nature of interaction between MMOR-Fdx and MMO was revealed by structural studies of MMOR-Fdx by NMR spectroscopy (*5*). By examination of line broadening in NMR

spectra of MMOR-Fdx in the presence of MMO, a binding surface on MMOR-Fdx composed of charged residues surrounded by hydrophobic patches was proposed. Studies using MMOR D26A and E73A mutants further showed that the binding affinity to MMO decreased 2-fold and 3-fold, respectively (*1*), suggesting the importance of electrostatic interactions between MMOR and MMO.

The importance of electrostatic interactions between a diiron protein and its redox partner has also been demonstrated in the studies by Fox and coworkers on the binding interface between Δ^9-desaturase (Δ9D) and a plant ferredoxin (p-Fdx) (*6*). By chemical cross-linking, site-directed mutagenesis, steady state kinetics and molecular docking studies, they identified three surface lysines (K56, K60, K230) on Δ9D that are important for interacting with p-Fdx. Single alanine mutation on K56, K60 and K230 decreased the k_{cat}/K_m for p-Fdx by 22-, 4- and 2400-fold, respectively. The K56A/K60A double mutant and K56A/K60A/K230A triple mutant decreased the k_{cat}/K_m for p-Fdx by 250- and 700,000-fold, respectively, indicating their roles for interacting with the p-Fdx (*6*). These lysines are located in close proximity to the postulated electron transfer pathway (W62, H146, D228) to the iron center of Δ9D, which is structurally conserved in β_2 (W48, H118, D237). Furthermore, a molecular docking model suggested a conserved glutamate (E31) in p-Fdx that directly interacts with K60 in Δ9D, supporting the proposal that the binding between Δ9D and p-Fdx is governed by electrostatic interactions.

One key difference between the studies on MMO and Δ9D is that for MMO, the physiological redox partner is MMOR in which the Fdx domain is reduced by the FAD domain, whereas for Δ9D, the physiological relevant Fdx and Fdx-reductase have not yet been established. If the analogy between MMO and β_2 still holds for the mechanism by which the diferric center of β_2 is reduced, YfaE is likely to be cycled by a Fdx-reductase in vivo.

Our candidate for a YfaE-reductase came from experiments by Reichard, Fontecave, and their coworkers. Their studies on the identification of components in crude extracts of *E. coli* that can reduce and regenerate the Y• in β_2 have led to the isolation of Fre, which is proposed to regenerate the Y• in the presence of flavin, NAD(P)H, DTT and a "fraction B" (*7-9*). Despite heroic efforts, the components in fraction B that facilitated the reduction of met-β_2 could not be purified (*10*). Furthermore, it was found that fraction B could be replaced by Fe^{2+}, thus a model was proposed that Fe^{2+}, which could be generated by reduced flavins generated inturn by Fre, is responsible for reduction of met-β_2. However, this model is questionable given the reactivity of both Fe^{2+} and reduced flavins with O_2 to generate toxic O_2 species. Evidence for the involvement of Fre in reactivation of the Y• in vivo was provided by studies on a *Δfre E. coli* K-12 strain grown in the presence of hydroxyurea (HU), a radical scavenger specific for the Y• of β_2 (*11, 12*). The results showed that when the deletion strain was grown in M9 minimal medium, the *Δfre* is three times more sensitive to HU (~40 mM) than the wild type cells, supporting a role for Fre in the regeneration of the Y• in vivo (*13, 14*). From these observations, we proposed a model that in vivo met-β_2 is directly reduced by YfaE, which can then be cycled by Fre (*15*).

Based on the studies on MMO and Δ9D, we have applied several methodologies in an effort to determine the binding constant between YfaE and met-β, and used K→A mutants of β_2 or a E→A mutant of YfaE to examine the role of electrostatic interactions between these two proteins. Fre was cloned and purified, and its ability in reducing $[2Fe2S]^{2+}$-YfaE catalytically was established. Growth experiments using *ΔyfaE* in the presence of HU suggest that YfaE plays a major role in the maintenance pathway.

MATERIALS AND METHODS

Materials

E. coli BW25113 wt and isogenic strains with an in frame single gene deletion of *yfaE*, *fre, fdx* or *fpr* were obtained from the Keio collection in the National Institute of Genetics, Mishima, Japan (*16*). DNA primers were purchased from Invitrogen (**Table 3-1**). Plasmids pET24a, pET3a, pET28a and pET9d were purchased from Novagen (**Table 3-1**). PfuUltraII DNA polymerase, *E. coli* BL21(DE3) and TOP10 cells were from Stratagene. Restriction enzymes were from New England Biolaboratory. Tris(hydroxymethyl)aminomethane hydrochloride (Tris-HCl) was from J.T. Baker. Isopropyl-β-D-thiogalactopyranoside (IPTG) was from Promega. Immun-Blot Poly(vinylidene) difluoride (PVDF) membrane (0.2 μm), 10%, 15% and 18% Tris-HCl SDS-PAGE (1.0 mm) Criterion Precast Gels and Silver Stain Plus Kit were from Bio-Rad. Polyclonal rabbit antibodies (Abs) against β_2, YfaE and Fre were produced by Covance (Denver, PA). Secondary Abs (Goat anti-rabbit conjugated horseradish peroxidase), chemiluminescence reagent SuperSignal West Femto and Slide-A-Lyzer dialysis cassettes (0.5 mL capacity, 3.5 kDa cut-off) were from Thermo Scientific. Protease inhibitors cocktail (Complete Mini, EDTA-free) were from Roche. Strep-Tactin Sepharose resin was from IBA GmbH. Amicon and Microcon ultrafiltration membranes (YM30, PM30, YM10, YM3, YM50 and PLBC3) were purchased form Millipore. Bradford reagent and all other chemicals were obtained in the highest purity available from Sigma-Aldrich.

Verification each gene deletion strain obtained from the Keio collection

The success of the gene deletion was verified by either sequencing the genomic DNA purified from the knockout strains or by PCR using primers annealed ~50 bp upstream and

downstream of the deleted gene and the purified genomic DNA as a template. The cell growth and the purification of genomic DNA were carried out according to manufacturer's protocol (Bacterial Genomic DNA purification kit, Sigma). The sequences were confirmed at the MIT Biopolymers Laboratory. For PCR verification, the success of a deletion was judged using agarose gels by the appearance of a ~1.5 kb PCR product containing the kanamycin resistance gene and the disappearance of the target gene. Lists of verification primers are shown in **Table 3-1**. All knockout strains were confirmed.

Site-directed mutagenesis of β_2 and YfaE

Mutants of β_2 and YfaE were made by site-directed mutagenesis (SDM) PCR using pBAD-C-S-nrdB (*17*) and pET11a-yfaE (*15*) as PCR templates, and PfuUltraII DNA polymerases according to manufacturer's protocol (Stratagene). The PCR primers are listed in **Table 3-1**.

Homology modeling of YfaE

Structures of β_2 (pdb: 1AV8), Δ9D (pdb: 1AFR), and Fdx-Δ9D (pdb: 1FXA) were drawn using the program PyMol (*18*). A homology model of YfaE was generated by Swiss-Model (http://swissmodel.expasy.org) by submitting the amino acid sequence of YfaE and the pdb file of Fdx-Δ9D to the web site. The generated homology model of YfaE was drawn using PyMol.

Anaerobic Stopped-flow (SF) spectroscopy

The purification of YfaE inclusion bodies and the refolding, reconstitution and purification of YfaE were described in Chapter 2. The protein production and purification of N-

or C-terminus StrepII-tagged β_2 followed our published protocols (*17*). Procedures for the preparation of met-β_2 and stopped flow (SF) kinetics under anaerobic conditions were described in Chapter 2. The kinetic traces were fitted with single-, double- or multiple-exponential equations using program KaleidaGraph.

SF spectroscopic studies on the concentration dependence of the observed rate of reaction between met-β_2 and [2Fe2S]$^{1+}$-YfaE

Reactions between met-β_2 (0.75 μM) and [2Fe2S]$^{1+}$-YfaE (5, 12.5, 25, 50 and 100 μM) were monitored by SF spectroscopy at 37 ºC under anaerobic conditions (*15*). Kinetic traces were fit to a double-exponential equation using KaleidaGraph: $A_{465nm}(t) = \Delta A_{465nm\text{-}1} \times e^{-k1 \times t} + \Delta A_{465nm\text{-}2} \times e^{-k2 \times t} + c$, in which $\Delta A_{465nm\text{-}1}$ and $\Delta A_{465nm\text{-}2}$ are the amplitudes for the observed rate constants k_1 and k_2, respectively, t represents time, and c is a constant which equals $A_{465nm}(t)$ when $t \sim \infty$. The observed rate constants, k_{obs}, for the oxidation of [2Fe2S]$^{1+}$-YfaE were plotted as a function of [YfaE]. To test the possibility of obtaining binding constants between met-β_2 and [2Fe2S]$^{1+}$-YfaE from the plot (k_{obs} v.s. [YfaE]), the data were fit to equations derived from a two-step reaction model (**Scheme 3-1**). This model only considers the binding of one YfaE to one subunit of β_2 (step 1) and the reduction of one Fe^{3+} in β (step 2). In the SF experiment, ΔA_{465nm} comes from the redox reaction in step 2.

Scheme 3-1

$$YfaE_{red} + Fe^{3+}\text{-}\beta \underset{k_{-1}}{\overset{k_1}{\rightleftharpoons}} YfaE_{red}{:}Fe^{3+}\text{-}\beta \underset{k_{-2}}{\overset{k_2}{\rightleftharpoons}} YfaE_{ox}{:}Fe^{2+}\text{-}\beta$$

The association and dissociation rate constants are k_1 and k_{-1}, respectively, between β and [2Fe2S]$^{1+}$-YfaE, whereas k_2 and k_{-2} represents the forward and reverse rate constants of the redox

reaction. Under conditions in which [YfaE] >> [β] and the interaction between YfaE and β_2 is described by a rapid binding equilibrium: $k_1[YfaE] + k_{-1} >> k_2 + k_{-2}$ (**Scheme 3-1**), k_{obs} is described by **Eq 1** in which $K_1 = k_1/k_{-1} = 1/K_d$ (K_d: dissociation constant) (*19-21*). **Eq 1** predicts a hyperbolic relationship between k_{obs} and [YfaE]. Under saturation conditions ($K_1[YfaE] >> 1$), $k_{obs} = k_2 + k_{-2}$.

On the other hand, if the redox reaction is much faster than the rate of binding ($k_2 + k_{-2} >> k_1[YfaE] + k_{-1}$), k_{obs} is described by **Eq 2**, which predicts a linear relationship between k_{obs} and [YfaE]. The slope is k_1 and the intercept is $k_{-1}/(K_2 + 1)$, where $K_2 = k_2/k_{-2}$.

Finally, if the rate of reaction in the two steps are similar (**Scheme 3-1**), k_{obs} is described by a generic equation (**Eq 3**). **Eq 3** also predicts a hyperbolic relationship between k_{obs} and [YfaE]. Among these cases, only under rapid binding equilibrium conditions (**Eq 1**) can the binding affinity between YfaE and β be determined.

Eq 1 $$k_{obs} = k_2K_1[YfaE]/(K_1[YfaE] + 1) + k_{-2}$$

Eq 2 $$k_{obs} = k_1[YfaE] + k_{-1}k_{-2}/(k_2 + k_{-2})$$

Eq 3 $$k_{obs} \approx (k_1[YfaE](k_2 + k_{-2}) + k_{-1}k_{-2})/(k_1[YfaE] + k_{-1} + k_2 + k_{-2})$$

Binding affinity between $[2Fe2S]^{1+}$-YfaE and apo-β_2 monitored by anaerobic ITC

Sample preparations were performed in a glove box in a 4 ºC cold room. Purification of $[2Fe2S]^{1+}$-YfaE and apo-β_2 are described in Chapter 2 and Chapter 4, respectively. MOPS (50 mM, pH 7.4) and apo-β_2 (259 μM, 0.5 mL) were degassed on a Schlenk line according to the procedures in Chapter 2. Dialysis cassettes (Slide-A-Lyzer, 3.5 kDa cut-off, 0.5 mL size, Thermo Scientific) were pre-soaked in 10 mM dithionite solution in the glove box for 1.5 h

followed by incubation with stirring in 800 mL anaerobic water and 800 mL of 50 mM MOPS, pH 7.4 for 12 and 6 h, respectively to remove residual dithionite. Purified $[2Fe2S]^{1+}$-YfaE and apo-β_2 (~0.5 mL) were then transferred into the dialysis cassettes and dialyzed in 2 L 50 mM MOPS, pH 7.4 for 16 h. The samples were then transferred into pear-shape flasks with glass stopcocks (with vacuum grease) and taken out of the glove box.

To measure the binding constant under anaerobic conditions, the protein samples and the ITC instrument (VP-ITC, MicroCal, Inc., Northampton, MA) were placed inside a glove bag (Aldrich, AtomsBag polyethylene handbag) followed by 5 cycles of evacuation and refilling with Ar to minimize the amount of O_2. The glove bag showed no sign of deflation after 2 h, suggesting minimal leakage. Apo-β_2 (9.8 μM) was then transferred into a sample cell (1.430 mL) and titrated with 10 μL of 489 μM $[2Fe2S]^{1+}$-YfaE every 5 min at 4 ºC with a stirring speed of 310 rpm.

Attempts to use ultrafiltration to determine the K_d between $[2Fe2S]^{1+}$-YfaE and apo-β_2

Inside the glove box, 300 μL of 30 μM $[2Fe2S]^{1+}$-YfaE was added to a YM30 (or YM3, YM10, YM50) Microcon (0.5 mL size, Millipore, pre-washed with 350 μL of sodium dithionite, water and 100 mM Tris-HCl, pH 7.8 buffer). The YM30 Microcons were then centrifuged at 10,000*g* until more than 200 μL of filtrate was obtained (~7 min). Filtrate (200 μL) and concentrate (100 μL) were transferred into a new Eppendorf and the concentration of YfaE in the filtrate and concentrate were measured by Bradford assay. The integrity of YfaE before and after centrifugation was monitored by UV-visible spectroscopy and no oxidation was found during the centrifugal ultrafiltration.

Cloning of Fre, YqjH, Fdx and Fpr

To generate pET24a-fre, pET24a-yqjH, pET9d-fpr, pET3a-fdx and pET28a-fdx constructs, genes encoding Fre, YqjH, Fpr and Fdx were PCR amplified from *E. coli* K-12 wt (without isolation of genomic DNA) using the primers listed in **Table 3-1**. To prepare PCR templates, about 25 mg of the cell paste of *E. coli* K-12 wt was suspended in 1 mL water and incubated in 100 ºC sand bath for 30 min followed by centrifugation at 14,000*g* for 10 min at RT. The PCR reaction mixture (total 50 μL) contained 23 μL of the supernatant, 1 μM forward primer, 1 μM reverse primer, and 25 μL of 2X PCR MasterMix™ (Promega). A temperature touch down PCR program was used: 95 ºC, 30 sec, 1 cycle; 95 ºC, 30 sec, 65 ºC, 30 sec, 72 ºC, 60 sec, 2 cycles; 95 ºC, 30 sec, 63 ºC, 30 sec, 72 ºC, 60 sec, 2 cycles; 95 ºC, 30 sec, 61 ºC, 30 sec, 72 ºC, 60 sec, 2 cycles; 95 ºC, 30 sec, 59 ºC, 30 sec, 72 ºC, 60 sec, 2 cycles; 95 ºC, 30 sec, 57 ºC, 30 sec, 72 ºC, 60 sec, 2 cycles; 95 ºC, 30 sec, 55 ºC, 30 sec, 72 ºC, 60 sec, 20 cycles; 72 ºC, 10 min, 1 cycles.

The PCR products were purified by a commercial PCR purification kit (Qiagen) and digested with 10 U of restriction enzymes and ligated with purified pET24a, pET9d, pET3a and pET28a vectors (Novagen) pretreated with restriction enzymes using T4 DNA ligase (Promega) in a vector to insert ratio of 1:3. The sequences of the mutant proteins and the cloning constructs were confirmed at the MIT Biopolymers Laboratory.

Purification of Fre

A single colony of BL21(DE3)-pET24a-fre was inoculated into 7 mL of LB-Kanamycin (70 μg/mL) and grown overnight (~16 h) at 37 ºC in a roller drum. The overnight culture (5 mL) was inoculated into 2.6 L LB-kanamycin (70 μg/mL) and grown at 37 ºC, 200 rpm. The protein

production was induced by addition of 1 mM IPTG when the A_{600nm} reached ~0.4. The cells were allowed to grow for additional 4 h before being harvested at 7,000*g* for 10 min at 4 ºC. The cell paste (10.2 g, 3.9 g/L) was flash frozen in liquid N_2 and stored at –80 ºC.

Purification of Fre followed published procedures (*14*) with some modification. The cell paste of BL21(DE3)-pET24a-fre was suspended in 5 mL buffer F/g cell paste (**buffer F:** 25 mM Tris-HCl, pH 7.5, 10% (v/v) glycerol, 30% (w/v) ammonium sulfate) and the cells were disrupted by two passages through the French Press at 14,000 psi. The cell debris was removed by centrifugation at 48,000*g*, 4 ºC for 30 min. The supernatant was loaded at a flow rate of 2 mL/min onto a 20 mL Phenyl Sepharose 6 Fast Flow column (2.5 × 4 cm, Amersham) pre-equilibrated in buffer F. The column was then washed with 200 mL buffer F followed by an additional 160 mL buffer F containing 5% (w/v) ammonium sulfate. The protein was eluted with 25 mM Tris-HCl, pH 7.5, 10% (v/v) glycerol and fractions of 2.8 mL were collected and assayed for activity.

Fractions with activity >15 U from the Phenyl Sepharose column were combined and concentrated using an Amicon YM10 concentrator to a final volume of 2.6 mL. The concentrate was then loaded at a flow rate of 10 mL/h onto a 100 mL Sephadex G-75 column (1.5 × 57 cm, Sigma) pre-equilibrated with 25 mM Tris-HCl, pH 7.5, 10% (v/v) glycerol. Fractions of 3.8 mL were collected and those containing activity >200 U were combined and concentrated using a YM10 Centricon (Millipore) to a final volume of 1.2 mL. The concentration of the purified protein was determined by ε_{280nm} = 27.0 mM^{-1} cm^{-1} and the concentration of samples from each purification steps were determined by Bradford assay using BSA as a standard. Aliquots of the protein were stored at –80 ºC. A yield of 1.8 mg of purified Fre per g of cell paste was obtained.

To assay Fre activity, the rate of NADPH reduction was monitored. The assay was performed in 25 mM Tris-HCl, pH 7.5 containing 200 μM NADPH (Sigma, ε_{340nm} = 6.22 mM^{-1} cm^{-1}) and 25 μM riboflavin (Aldrich R170-6, ε_{373nm} = 10.0 mM^{-1} cm^{-1}) in a total volume of 500 μL. The rate of Δ_{A340nm} was measured before and after 2 μL of each fraction was added. One unit is defined as 1 nmol NADPH oxidation/min. The specific activity of the purified Fre is 120,000 U/mg, which is the same as reported in the literature (*14*).

Western blotting on *E. coli* whole cells to determine the concentrations of YfaE, Fre and β_2

Overnight cultures from a single colony of *E. coli* K-12 wt (2 mL) were inoculated into 500 mL LB without antibiotic and grown at 37 ºC, 200 rpm until A_{600nm} reached 0.7 to 0.8. The cells were then spun down by centrifugation at 8500*g* for 10 min at 4 ºC. The supernatant was discarded and the cell paste was suspended in 5 mL PBS/g cell paste. For cell counting, 10 fold serial dilutions of the cell suspension into PBS at 4 ºC were made, plated onto LB-agar plates without antibiotic and grown overnight at 37 ºC. To prepare whole cell samples for Western blotting, the cell suspension was mixed in a 1:1 ratio with 2× Laemmli buffer followed by incubation in a 100 ºC sand bath for 10 min before flash freezing in liquid N_2 and storage at –80 ºC. The cell counting indicated 1.4 ± 0.1 x 10^7 cells per μL of the whole cell Laemmli samples (8 measurements from two independent serial dilutions).

The quantitative Western blotting was performed by following our published procedures (*17*). Purified wt-β_2, $[2Fe2S]^{1+}$-YfaE or Fre and the whole cell samples in Laemmli buffer were loaded onto an 18-well Tris-HCl, SDS-PAGE (1.0 mm) Criterion Precast gels (Bio-Rad) (10%, 18% and 15% gel for blotting of wt-β_2, YfaE and Fre, respectively). The SDS-PAGE was run at 200 V for 40 min at 4 ºC. The gel was then incubated in the blotting buffer (25 mM Tris, 195

mM glycine, 15% (v/v) methanol, and 0.01% SDS for 30 min before blotting onto a PVDF membrane (Bio-Rad) at 200 mA for 60 min at 4 ºC. To examine the efficiency of transfer, a second PVDF membrane was included and the gels after transfer were stained by Silver Stain Plus (Bio-Rad). The PVDF membranes were blocked in 3% casein in TAE buffer (40 mM Tris, 20 mM acetate, 1 mM EDTA, pH 8.0) for 30 min before treatment with primary antibodies (10,000x, 500x and 5000x dilution of antibodies against wt-β_2, YfaE and Fre) for 1 h followed by washing with 100 mL PBS, 3 times. Secondary antibodies solutions (HRP-conjugated goat anti-rabbit antibodies, ThermoScientific, 2000x dilution in 3% casein in TAE buffer) were then added to the membranes followed by 1 h incubation at room temperature. After the PVDF membranes were washed with 100 mL PBS 3 times, the membranes were developed using FemtoWest chemiluminescence reagents (Thermo Scientific) and the Western signals were detected using a CCD camera and quantified by QuantityOne program (Bio-Rad).

Reduction of YfaE and met-β_2 in the presence of flavins, Fre and NADPH

Reduction of [2Fe2S]$^{2+}$-YfaE by photoreduced FMN: To prepare $FMNH_2$, 0.4 mL of 0.2 mM FMN, 2 mM sodium oxalate in 100 mM Tris-HCl, pH 7.8 was placed in a 0.7 mL quartz cuvette fitted with an air-tight screw cap. The cuvette was removed from the glove box, exposed to a 150-watts Kramer microscope lamp (Burlington, MA) for 3 min at room temperature and brought back into the glove box (*22*). To prepare oxidized YfaE, 800 μL of 36 μM [2Fe2S]$^{1+}$-YfaE in 100 mM Tris-HCl, pH 7.8 was removed from the glove box, exposed to oxygen, followed by 5 cycles of evacuation with refill with argon on a Schlenk line and brought into the glove box. Similar anaerobic titration procedures to these described in detail in Chapter 2 were followed. In an anaerobic cuvette, [2Fe2S]$^{2+}$-YfaE (360 μL, 39 μM in 100 mM Tris-HCl, pH

7.8) was titrated with 216 μM $FMNH_2$ (10 μL aliquots) until an end point was reached. O_2 was then blown over the surface of the sample and the sample was mixed by inverting the cuvette. The UV-visible spectrum was recorded on Cary 3 spectrophotometer (Varian).

Reduction of $[2Fe2S]^{2+}$-YfaE by Fre, riboflavin and NADPH: Fre, riboflavin and NADPH solution were degassed on a Schlenk line following the procedures described in the previous section. No precipitation of Fre was observed after the evacuation and refill cycles. Inside a glove box, a 0.7 mL quartz cuvette fitted with an air-tight screw cap and a Teflon/silicon septum (Thermo Scientific) was filled with 506 μL of 18.5 μM $[2Fe2S]^{2+}$-YfaE, 0.8 μM riboflavin and 0.8 μM Fre in 100 mM Tris-HCl, pH 7.8. The cuvette was removed from the glove box and the sample was titrated with 1 mM NADPH (2-10 μL aliquots) under anaerobic conditions. At the titration end point, the sample was oxidized as in the previous section.

Reduction of met-β_2 by NADPH in the presence of catalytic amounts of YfaE, Fre and riboflavin: In a 0.7 mL quartz cuvette fitted with an air-tight screw cap and a Teflon/silicon septum, 360 μL of 20 μM met-β_2, 0.5 μM $[2Fe2S]^{1+}$-YfaE, 0.5 μM riboflavin and 0.5 μM Fre in 100 mM Tris-HCl, pH 7.8 were titrated with 1 mM NADPH (2-10 μL aliquots) under anaerobic conditions. At the titration end point, the sample was oxidized as in the previous section. A control titration in the absence of YfaE was also carried out.

Determination of the growth rate of BW25113-ΔyfaE, Δfre, Δfdx, Δfpr in the presence of hydroxyurea (HU)

An overnight culture (150 μL from 5 mL culture) from a single colony of BW25113-pET9a, BW25113-*ΔyfaE*, BW25113-*Δfre*, BW25113-*Δfdx* or BW25113-*Δfpr* was inoculated into 30 mL M9 minimal medium (42 mM Na_2HPO_4, 22 mM KH_2PO_4, 19 mM NH_4Cl, 9 mM NaCl, 0.4% glucose, 20 mM $MgSO_4$) or LB medium containing 30 μg/mL kanamycin in 125 mL flasks and grown at 37 ºC, 200 rpm until A_{600nm} reached ~0.1. An aliquot of each culture (1 mL) was then transferred into 24-well tissue culture plates (Corning) and HU (10, 30 and 50 μL of 1 M stock solution) was added into each well to reach a final concentration of 0, 10, 30 or 50 mM. The cells were further grown at 37 ºC, 200 rpm and A_{630nm} was recorded on a microplate reader (Bio-Rad) every 30 min and 10 min for cells grown in M9 and LB media, respectively,. Four to six replicates of each condition were carried out.

Western blotting on *E. coli* whole cells to determine the concentration of YfaE, β_2 and Fre in the presence of HU

To examine the levels of expression of YfaE, β_2 and Fre in the presence of HU, an overnight culture (2.5 mL) from a single colony of *E. coil* BW25113-pET9d was inoculated into 500 mL of LB-kanamycin (30 μg/mL) in a 2.8 L baffled flask and grown at 200 rpm, 37 ºC until A_{600nm} ~ 0.55. Aliquots (100 mL) of the culture were then transferred into 500 mL baffled flasks and HU (1 M stock solution) was added to a final concentration of 10 and 30 mM. The cells were grown at 200 rpm, 37 ºC and at 1 h after addition of HU, 20 mL aliquots of the culture were transferred into 50 mL Falcon tubes and incubated on ice for > 30 min followed by recording of A_{600nm}.

To prepare whole cell samples in the Laemmli buffer, cultures containing 4×10^9 cells (assuming 1 mL of cell culture at $A_{600nm} = 2 \times 10^8$ cells) were centrifuged at 3000 rpm at 4 ºC for 20 min. The supernatant was removed and the cell paste was suspended in 200 μL of 2× Laemmli buffer (2×10^7 cell/μL Laemmli sample), followed by incubation in a sand bath at 100 ºC for 10 min. The same procedures described above for the determination of the concentration of YfaE, β_2 and Fre by Western blot analysis were carried out, using 5 μL of the whole cell Laemmli sample (1×10^8 cells).

Table 3-1. List of primers used in this chapter

Site-directed mutagenesis primers[a, b, c]	
β_2-K38A	CGCTACGATCAGCAAAAATATGACATCTTCGAA**GCG**CTGATCGAAAAGCA GCTCTCTTTCTTCTGGC
β_2-K42A	CTTCGAAAAGCTGATCGAA**GCG**CAGCTCTCTTTCTTCTGGC
β_2-K38A/K42A	CGCTACGATCAGCAAAAATATGACATCTTCGAA**GCG**CTGATCGAA**GCG**CA GCTCTCTTTCTTCTGGCGTCCG
β_2-K229A	CGCGAATTGATGGAAGGCAACGCC**GCA**ATTATTCGCCTGATTGCCCG
YfaE-E26A	TTCCCTTCTGGCGGCGCTG**GCG**TCCCACAATGTGGCGGTT
Cloning primers[a, d]	
Fre-5-NdeI	GAGAAAG**CATATG**ACAACCTTAAGCTGTAAAGTG
Fre-3-XhoI	TTTTTT**CTCGAG**TCAGATAAATGCAAACGCATC
YqjH-5-NdeI	GCGATA**CATATG**AATAACACCCCCCGCTAC
YqjH-3-XhoI	TTTATA**CTCGAG**TTACTTTGCGTGCCAGTAAGC
Fpr-5-NcoI	CAGGAGAAAA**CCATGG**CTGATTGGGTAACAGGCAAAG
Fpr-3-BamHI	TAAGT**GGATCC**TTACCAGTAATGCTCCGCTG
Fdx-5-NdeI	CGAGGTTT**CCTATG**CCAAAGATTGTTATTTTGC
Fdx-3-BamHI	ACTAA**GGATCC**TTAATGCTCACGCGCATGGT
Knockout strain verification primers[a]	
ΔyfaE-5′	ATTGACTCGGAAGTGGACAC
ΔyfaE-3′	TAAGCGTTGTATCTGGCACT
Δfre-5′	GATGCGCGTTTGTTTTGCCCT
Δfre-3′	CGCCTGTCAGGGGCGGGTTTT
Δfdx-5′	GTCGGTTCGTCGTGCGCTG
Δfdx-3′	GGTCCACTTAAGTCCCATAC
Δfpr-5′	GTTCGGAGAACGAAGATAAG
Δfpr-3′	CATCGTGCCGTTTATCGATA

a. sequences of all primers drawn from 5′ to 3′
b. The primers shown and their complementary pair were used for SDM
c. sites of mutations are in bold
d. restriction enzyme digestion sites are in bold; the start or stop codon are underlined

RESULTS

Efforts to determine the K_d between $[2Fe2S]^{1+}$-YfaE and met-β_2 by SF kinetics

In the reactions between $[2Fe2S]^{1+}$-YfaE and met-β_2, the mechanism(s) is (are) complicated because the reduction of met-β_2 (3.4 Fe/β_2) to diferrous-β_2 requires multiple association and dissociation steps between two proteins. The possibility of cooperative binding of two YfaEs with β_2 or intramolecular electron transfer between β_2 monomers to generate reduced iron in the same β monomer, further complicate kinetic analysis (*23*). A simplified model for the redox reaction between $[2Fe2S]^{1+}$-YfaE and met-β_2 is shown in **Scheme 3-1**. This model represents the binding of YfaE to one subunit of met-β_2 (step 1) and reduction of one ferric iron in met-β_2 (step 2). In the SF spectroscopic experiments, the absorbance changes monitor the redox chemistry in step 2.

Assuming this model, the k_{obs} can be described by the four microscopic rate constants, k_1, k_{-1}, k_2, and k_{-2} using different equations formulated under different assumptions (**Eq 3-1 to 3-3**). Under conditions in which [YfaE] >> [met-β_2] and there is a rapid binding equilibrium between YfaE and met-β_2, the k_{obs} can be described by **Eq 3-1**, which predicts a concentration dependence of YfaE on k_{obs} that follows a hyperbolic relationship. The association constant K_1 can be derived directly if such a relationship is observed. To examine whether the redox reaction between $[2Fe2S]^{1+}$-YfaE and met-β_2 fulfills the criteria in **Eq 3-1**, SF spectroscopic experiments using 0.75 μM met-β_2 and increasing amounts 5, 12.5, 25, 50 and 100 μM $[2Fe2S]^{1+}$-YfaE (~7-130 fold excess) under anaerobic conditions were carried out (**Figure 3-1**). Due to lower signal to noise ratio at A_{320nm}, which monitors the reduction of met-β_2, only the A_{465nm} changes, which represents the oxidation of $[2Fe2S]^{1+}$-YfaE, were analyzed. The kinetic traces were best fit to a

double-exponential equation. The kinetic parameters from these fittings are summerized in **Table 3-2**.

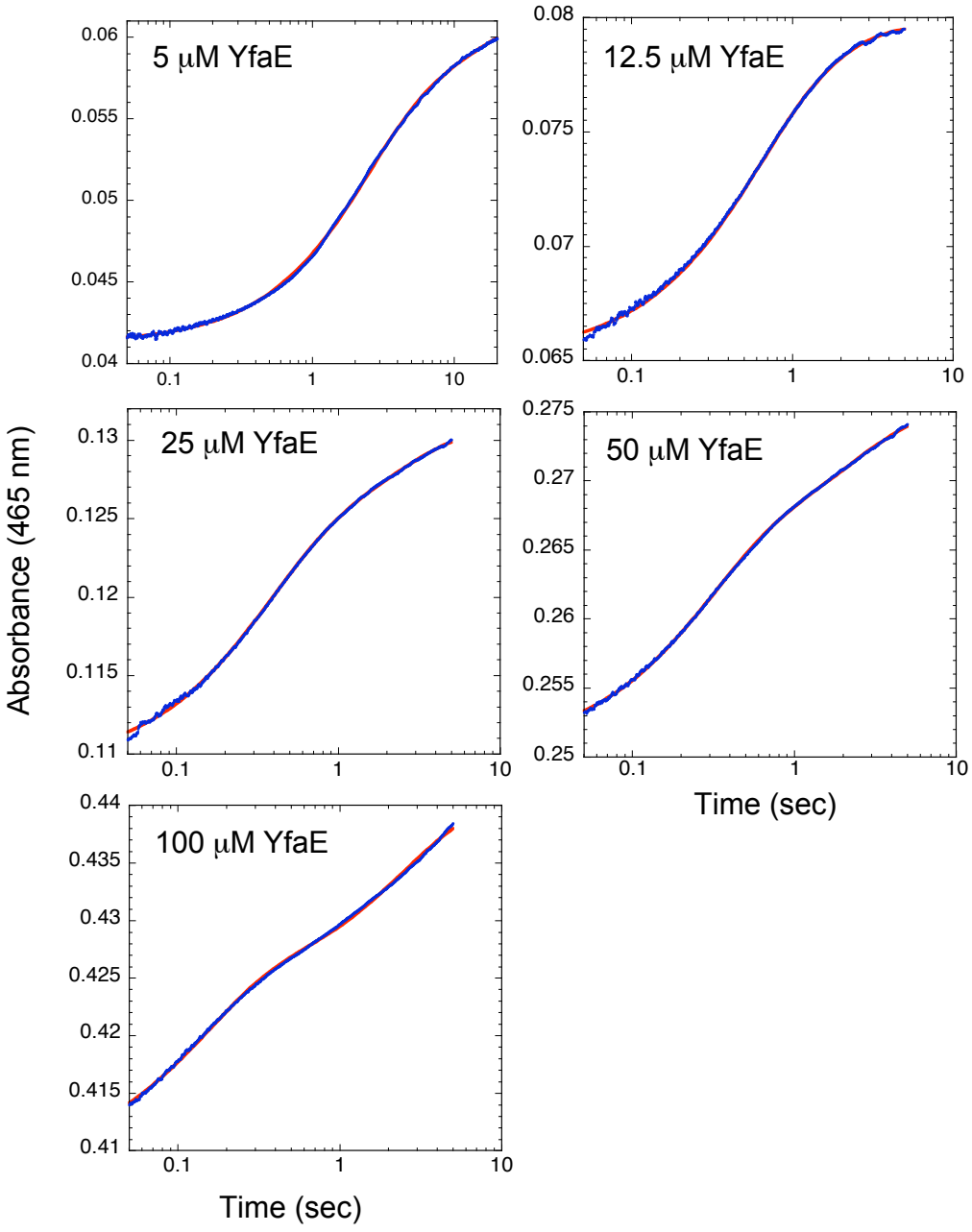

Figure 3-1. Stopped flow kinetics of $[2Fe2S]^{1+}$-YfaE oxidized by met-β_2 (0.75 μM) at 37 ºC under anaerobic conditions. Oxidation of $[2Fe2S]^{1+}$-YfaE was monitored at 465 nm. Data points (blue, average of 10 shots, 2000 points per shot collected in logarithmic time scale for 20 sec) of the first 5 sec were fit to two single exponentials (red line). The concentrations of $[2Fe2S]^{1+}$-YfaE (5, 12.5, 25, 50 and 100 μM) are indicated.

Table 3-2. Kinetic parameters of YfaE oxidation by 0.75 μM met-β_2.

[YfaE], μM	$k_{obs\text{-}fast}$ (s^{-1})	ΔA_{465nm}	$k_{obs\text{-}slow}$ (s^{-1})	ΔA_{465nm}
5	0.46	0.014	0.08	0.006
12.5	1.76	0.011	0.60	0.004
25	3.03	0.013	0.46	0.008
50	3.7	0.014	0.42	0.010
100	7.4	0.015	0.39	0.016

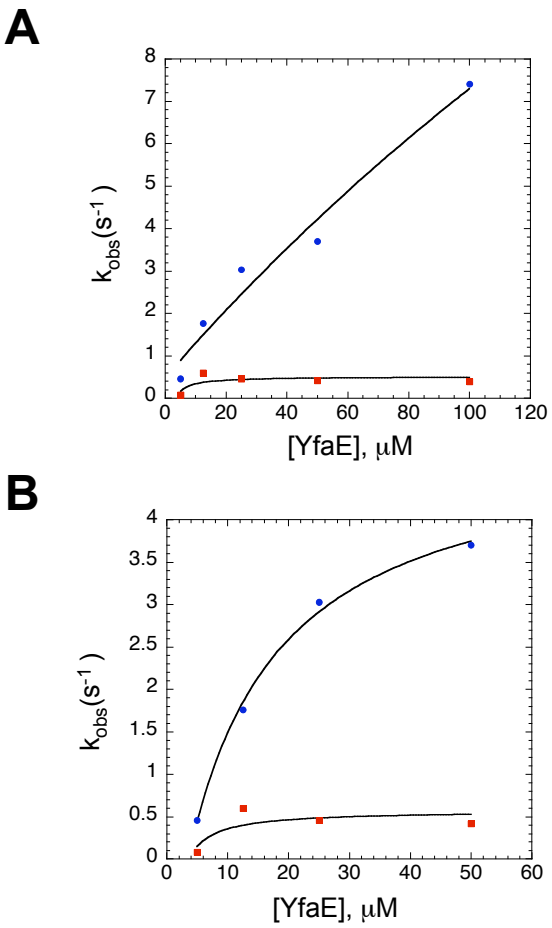

Figure 3-2. Concentration dependence of the k_{obs} from reactions between met-β_2 (0.75 μM) and $[2Fe2S]^{1+}$-YfaE (5, 12.5, 25, 50, 100 μM) under anaerobic conditions. The k_{obs} (blue, $k_{obs\text{-}fast}$; red, $k_{obs\text{-}slow}$) from in **Table 3-2** are plotted against [YfaE] and fit to **Eq 3-1** (black line). (A) the k_{obs} are plotted against 5-100 μM YfaE, (B) the k_{obs} are plotted against 5-50 μM YfaE.

Table 3-2 shows the $k_{obs\text{-}fast}$ increases with the [YfaE] with no sign of saturation, and the $k_{obs\text{-}slow}$ increases with the [YfaE] at lower [YfaE] but decreases slightly at higher [YfaE]. The amplitudes from the fast phase are very similar and represent ~90% reduction of the total iron in met-β_2. The amplitudes of the slower phase increase with the [YfaE], and reach ~50% of total amplitude at [YfaE] = 100 μM. The source of oxidant that is responsible for this slower phase is not clear. It may be associated with multiple FeS species in the reconstituted YfaE.

To examine whether the concentration dependence of k_{obs} follows a hyperbolic trend defined by **Eq 3-1**, the k_{obs} were plotted against [YfaE] and fit to **Eq 3-1** (**A, Figure 3-2**). The results show that there is no good correlation between the data points and the trend lines. A K_d of 500 μM can be derived from the fitting on $k_{obs\text{-}fast}$, which is highly unlikely given the known [β_2] in vivo (~2 μM) (*17*). A negative k_{-2} was derived from fitting on $k_{obs\text{-}slow}$, which indicates the inaccuracy of the equation. The k_{obs} from a different range of [YfaE] (5-50 μM) were also fit to **Eq 3-1 (B, Figure 3-2)**. Even though the $k_{obs\text{-}fast}$ in this concentration range show a better correlation with **Eq 3-1**, in both fast and slow k_{obs}, a negative k_{-2} was derived, indicating the inaccuracy of the equation.

The $k_{obs\text{-}fast}$ and $k_{obs\text{-}slow}$ were also fit to **Eq 3-2** and **Eq 3-3.** In neither case a correlation between the data and curve fits were observed, suggesting that the simplified model in **Scheme 3-1** is insufficient to describe the complicated redox reaction between $[2Fe2S]^{1+}$-YfaE and met-β_2. These results suggest that it is not feasible to derive the binding constants between $[2Fe2S]^{1+}$-YfaE and met-β_2 from this simple kinetic analysis.

Efforts to determine the K_d between $[2Fe2S]^{1+}$-YfaE and apo-β_2 by ITC

Due to the inability to determine the binding affinity between $[2Fe2S]^{1+}$-YfaE and met-β_2 by SF kinetic analysis, we decided to explore isothermal titration calorimetry (ITC) to determine the K_d. This method has been utilized to measure the K_d between MMOR and MMO, and between a 2Fe2S-putidaredoxin and its redox partners, NADH-putidaredoxin reductase and cytochrome P450cam (*1, 24*). These experiments were carried out under aerobic conditions using the oxidized form of 2Fe2S-proteins. The instability of oxidized YfaEs suggested however, that our titrations would need to be carried out under anaerobic conditions. Anaerobic ITC has been successful in determining the binding affinity of ferrous iron with frataxin (*25, 26*), and our experimental approach was modeled based on these methods.

Since the reduced YfaE reduces met-β_2, producing heat exchange not related to the binding, the met-β_2 was substituted with apo-β_2. Structural studies suggest that the overall structure of apo-β_2, diferrous-β_2 and met-β_2 are similar, so apo-β_2 was used in the initial ITC experiments (*27-29*). In addition, Mn^{2+}-loaded β_2 was considered as an alternative for the ITC experiments (*23*). Initial experiments used conditions employed in the successful determination of K_d between oxidized MMOR-Fdx and MMO (*1*).

Figure 3-3 shows the results of titrating ~10 μM apo-β_2 with ~500 μM $[2Fe2S]^{1+}$-YfaE. The baseline is not stable (see first 30 min) and the signals from the injections are overwhelmed by the drifting of the baseline. After about 40 min, the baseline looks more stable but the signals from each injection do not form the sharp peaks typically seen in ITC titration curves. The titration was carried out over 2 h and the sample was then transferred to a quartz cuvette fitted with a gas-tight screw cap and the UV-visible spectrum was recorded (**B, Figure 3-3**). The spectrum indicated a mixture of apo-β_2 and completely oxidized YfaE. It is possible that the

substantial baseline drift in first 30 min is associated with oxidation of YfaE, and subsequent to its oxidation, the protein started to form insoluble aggregates judged observable precipitation. This precipitation could explain the slow heat exchange observed in the signal between 40 to 120 min. We suspected that the O_2 contamination were from the impurities of the N_2, so the N_2 was replaced by high-purity argon for the evacuation-refill cycles. However, oxidation of YfaE still occurred during the titration, causing an unstable baseline, which made data analysis impossible. Even though there was no leakage observed in the glove bag, it is possible that the space inside the ITC instrument may have trapped air that was difficult to exchange during the ~2 h evacuation-refill cycles.

These results suggest the challenges in maintaining a strictly anaerobic environment to measure the binding constant between $[2Fe2S]^{1+}$-YfaE and apo-β_2. However, recent discoveries that oxidized YfaE is relatively stable in the presence of DTT and that certain YfaE mutants might remain soluble in the oxidized state could make the determination of binding affinity between oxidized YfaE and mt-β_2 by ITC possible (see Chapter 5).

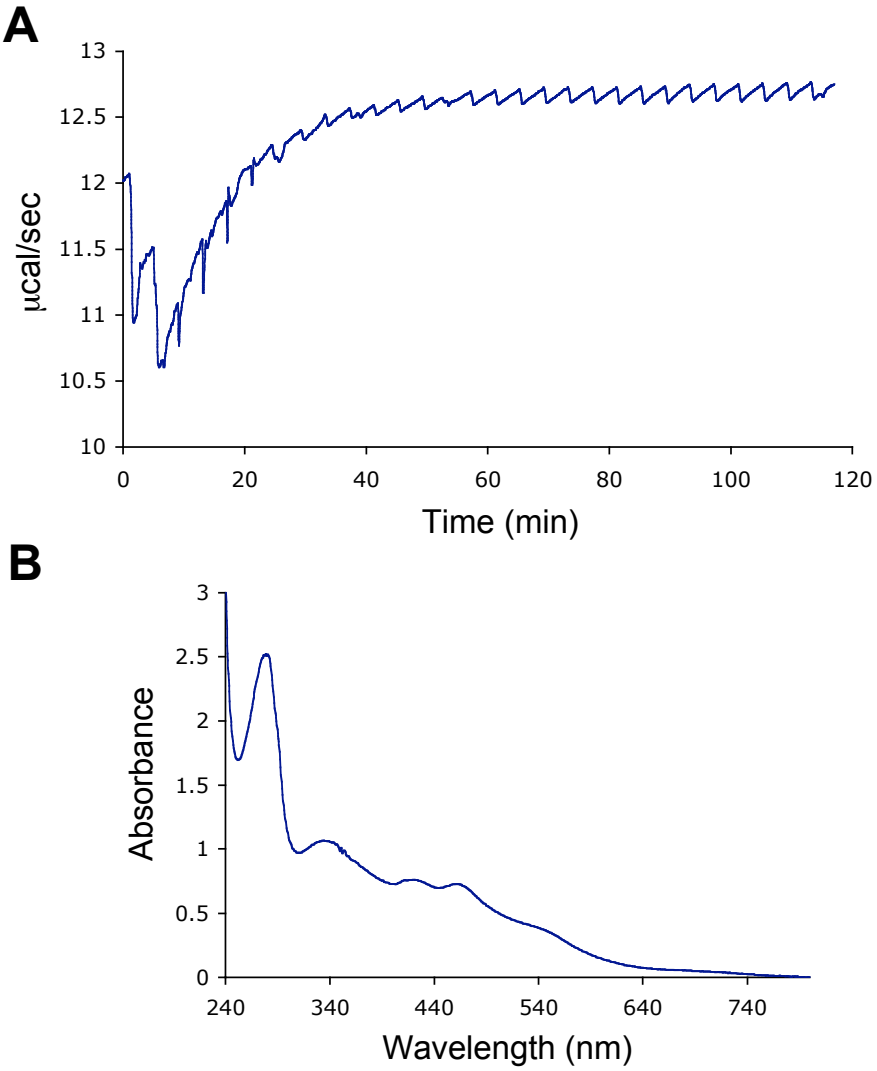

Figure 3-3. Efforts to determine the binding constant between $[2Fe2S]^{1+}$-YfaE and apo-β_2 by anaerobic ITC. (A) Apo-β_2 (10 µM, 1.430 mL in the calorimeter cell) was titrated with $[2Fe2S]^{1+}$-YfaE (489 µM in a 300 µL injection syringe) at 4 ºC in an anaerobic glove bag filled with N_2. Each heat pulse corresponds to a 10 µL injection of YfaE in 5 min intervals into the calorimeter cell. (B) UV-visible spectrum of the sample at the end of the titration.

Efforts to determine the K_d between $[2Fe2S]^{1+}$-YfaE and apo-β_2 by centrifugal ultrafiltration

A third method to measure the binding constant is centrifugal ultrafiltration (30). For this method to be applicable in the determination of the binding constant between $[2Fe2S]^{1+}$-YfaE and apo-β_2, a semi-permeable membrane that can separate YfaE from apo-β_2 and YfaE-apo-β_2 complex needs to be found. Furthermore, the membrane cannot have any non-specific binding to the proteins (30, 31). We first tested whether YfaE could freely flow through a YM30 membrane, which is reoutinely used to concentrate β_2. Since YfaE is a monomer of ~9 kDa, it was expected to pass freely through the YM30 membrane, which allows filtration of molecules less than 30 kDa. **Figure 3-4** shows the results of the centrifugal ultrafiltration carried out in the glove box in the cold room. Unfortunately, most of the YfaE remained in the concentrate after centrifugation. The UV-visible spectra of the concentrate indicated that YfaE stayed in the reduced form, therefore, the possibility of YfaE aggregates due to oxidation of YfaE can be ruled out. Furthermore, about 10% of YfaE was lost, probably due to non-specific binding to the membrane. Other membranes with different molecular mass cutoff (YM3, YM10 and YM50) were also tested and the same results were obtained, suggesting that this method is not practical for measuring the binding constant between YfaE and β_2.

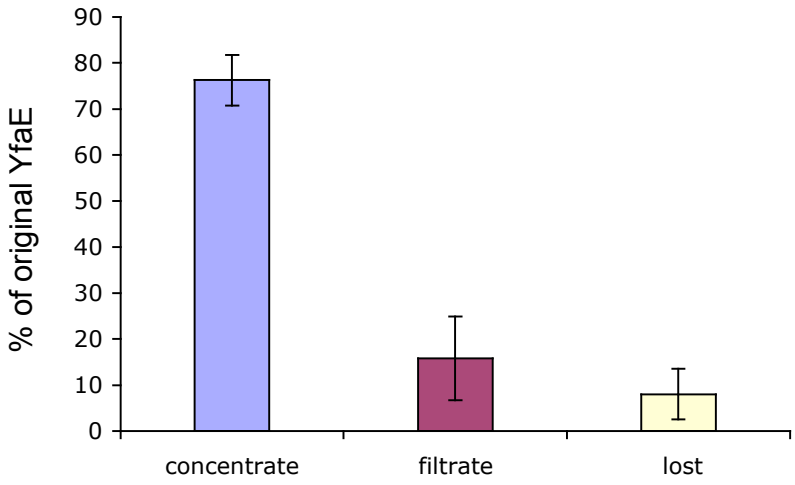

Figure 3-4. Evaluation of the anaerobic centrifugal ultrafiltration method for determination of the binding constant between $[2Fe2S]^{1+}$-YfaE and apo-β_2. In an anaerobic chamber at 4 ºC, 30 μM $[2Fe2S]^{1+}$-YfaE was loaded into YM30 microcon pre-washed with sodium dithionite solution and centrifuged at 10,000*g* for 7 min. The amount of the protein retained above the membrane and in the flow through were determined by Bradford assay using BSA as a standard. The amount of the protein that precipitates on the membrane was calculated by subtracting the original amount of YfaE from the amount that was retained and eluted. Results in percentage of original amount of YfaE are shown (four independent measurements).

Probing the binding sites between YfaE and β_2 by site-directed mutagenesis

After failed attempts to determine the binding affinity between YfaE and β_2, we were next interested in understanding the surfaces defining the interactions of the two protein using mutagenesis. Previous studies of Fox et al established the binding surface between Δ9D and a plant ferredoxin (*6*). The similarities of the electron transfer (ET) to Δ9D reduction and that for β_2, provided the basis for this proposal that the surfaces interactions between YfaE and β_2 might be similar and largely governed by electrostatic interactions. Studies on the surfaces interactions between MMOR-Fd(1-98) and MMO also suggest the importance of electrostatic interactions (*1, 5*). **Figure 3-5** shows the structural model of Δ9D (*32*) with the three key lysines that have been established to be important for interaction with p-Fdx and the proposed electron transfer pathway to reduce the diferric center highlighted. Two lysines, K56 and K60, are located in the same unstructured strand with W62, a surface tryptophan in the proposed ET pathway. A double K56A/K60A mutant caused a 250-fold decrease in k_{cat}/K_m of Δ9D (250-fold increase in K_m) when using a p-Fdx as an electron donor. A third conserved lysine, K230 is located on a neighboring α-helix that also contains D228, which is proposed to modulate the reduction potential of W62 in the ET pathway. A single K230A mutation decreased the k_{cat}/K_m by 2400 fold (2100-fold increase in K_m). The triple mutant, K56A/K60A/K230A diminished the k_{cat}/K_m of Δ9D by 700,000 fold (*6*). These studies provided the basis for Fox's proposal of the docking surface between the two proteins.

Based on these observations, we examined the 16 lysines in β_2 (**Figure 3-6**). We established by sequence alignments that 9 of these 16 lysines are conserved (**Figure 3-7**). Three of these lysines (K38, K42 and K229) are located in close proximity to the diferric-oxo cluster and the conserved amino acids in the proposed ET pathway (**B, Figure 3-6**). K42 and K229 are

conserved, while K38 is highly conserved. Analogous to the K56 and K60 in Δ9D, the K38 and K42 in β_2 are located in the α-helix connected to an unstructured region containing W48. A third lysine, K229, is located on the same α-helix as D237 in β_2, the residue that hydrogen bonds with W48. The relative arrangements of the three conserved lysines are obviously not the same in β_2 and Δ9D. This variation may define the specificity of each diiron protein for a specific ferredoxin.

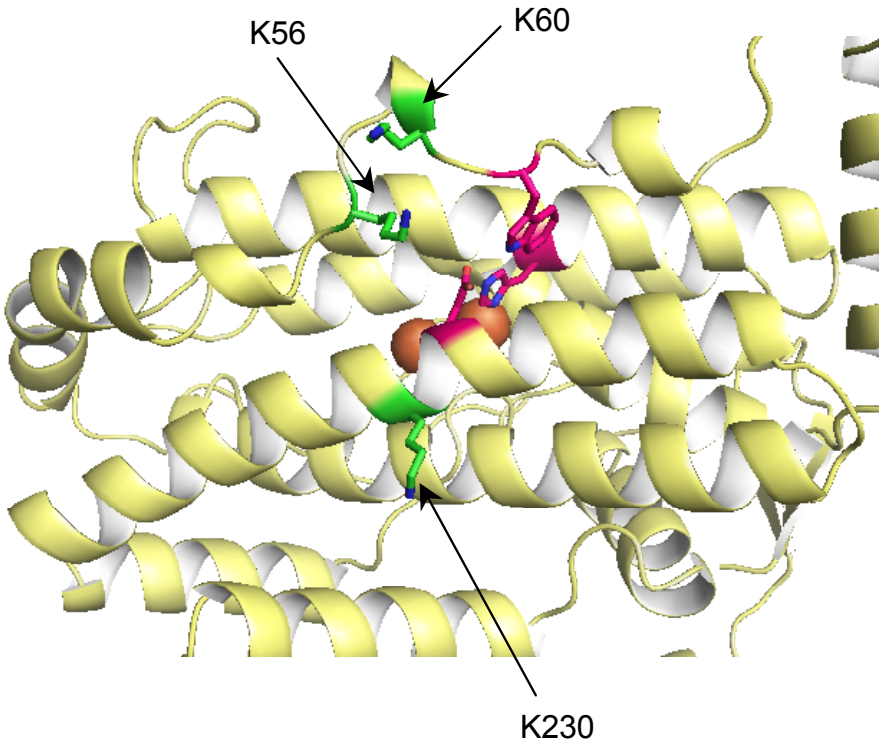

Figure 3-5. Key lysines in Δ9D (pdb file 1AFR) identified for interaction with Fdx. Green: the conserved lysines proposed for binding with Fdx. Red: proposed electron transfer pathway consist of W, H and D. Orange CPK: ferric irons.

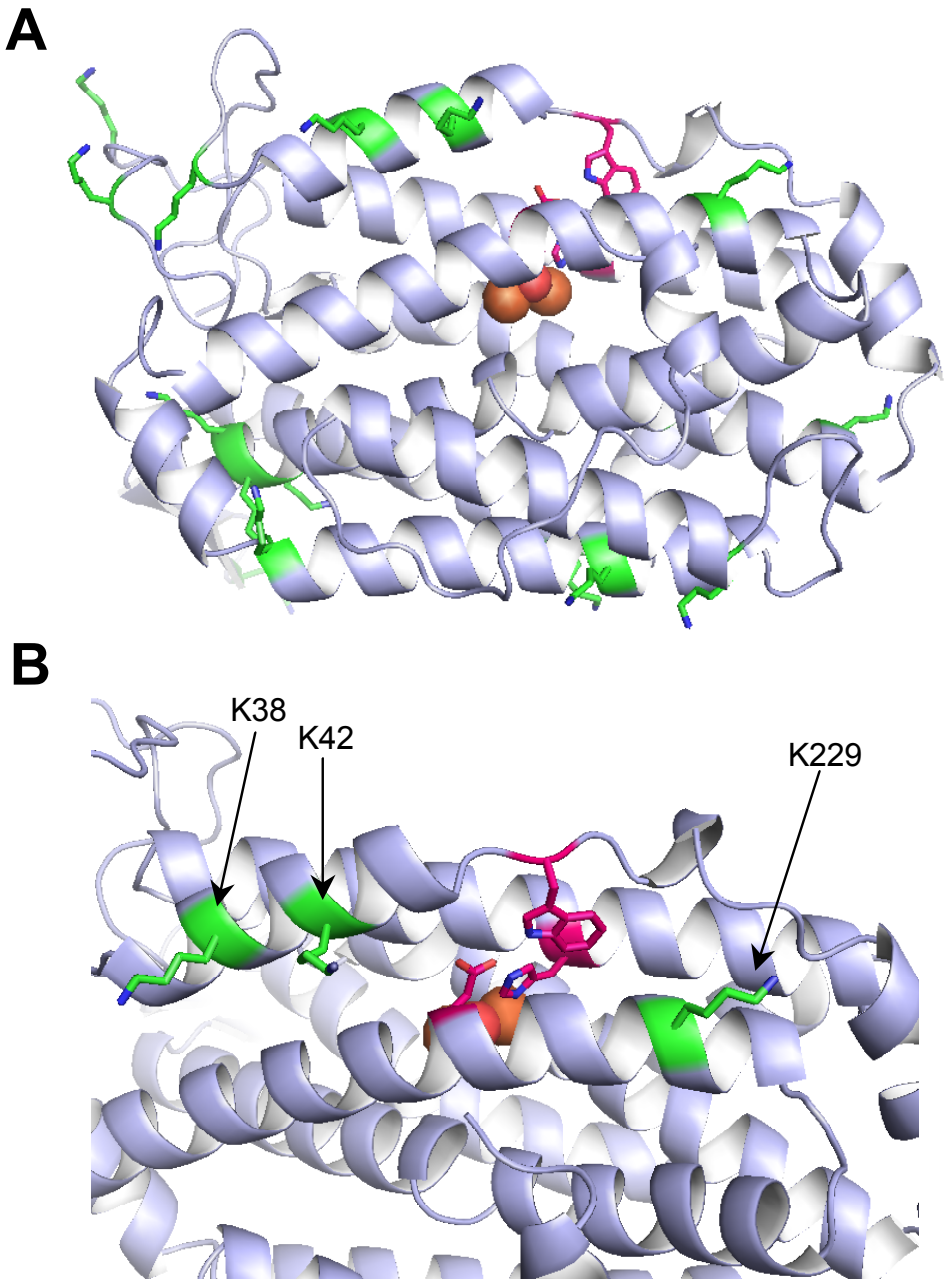

Figure 3-6. Lysines (green) in β_2 (pdb file 1AV8) to determine a putative interaction surface with YfaE. Red: proposed electron transfer pathway composed of W, H and D. Orange CPK: ferric irons. Red CPK: oxygen atom. (A) shows all 16 lysines in β_2. (B) shows the three conserved lysines near the diferric-oxo cluster and the proposed electron transfer pathway.

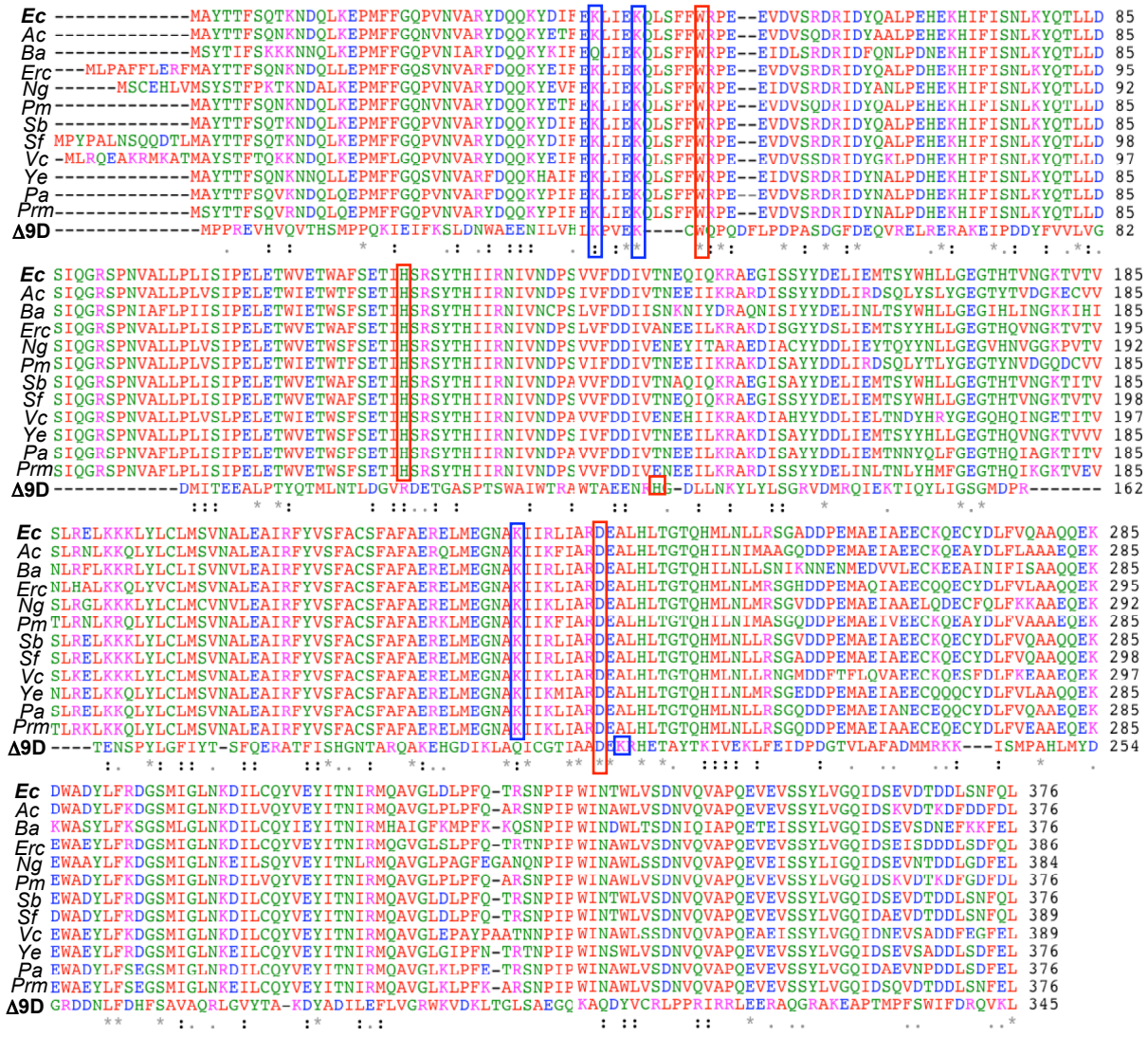

Figure 3-7. Sequence alignment between Δ9D and a number of class Ia β_2s. ClustalW2 (http://www.ebi.ac.uk/tools/clustalw2) was used to align protein sequences of Δ9D and class Ia β_2s. The conserved surface lysines (K38, K42, K229 in *E. coli* β_2; K56, K60, K230 in Δ9D) proposed to interact with ferredoxins are indicated in blue boxes. The conserved residues (W48, H118, D237 in *E. coli* β_2; W62, H144, D228 in Δ9D) proposed to be in the electron transfer pathways are labeled in red boxes. *Ec: Escherichia coli, Ac: Actinobacillus actinomycetemcomitans, Ba: Buchnera aphidicola, Erc: Erwinia carotovora, Ng: Neisseria gonorrhoeae, Pm: Pasteurella multocida, Sb: Salmonella bongori, Sf: Shigella flexneri, Vc: Vibrio cholerae, Ye: Yersinia enterocolitica, Pa: Photorhabdus asymbiotica, Prm: Proteus mirabilis.*

From the same binding studies by Fox and coworkers, a glutamate (E31) in the p-Fdx was proposed to interact with K60 in Δ9D. However, no experiment has been carried out to verify this proposal. Sequence alignments between YfaEs and the p-Fdx indicated that only one glutamate is conserved (E26 inYfaE). In addition, four cysteines proposed to be ligands with 2Fe2S cluster are also conserved (**Figure 3-8**). To gain some insights as to whether E26 is structurally conserved with the E31 in Fdx, a homology model of YfaE based on the crystal structure of the p-Fdx was generated (**Figure 3-9**). The four conserved cysteinyl ligands in YfaE align in the same orientations as those in p-Fdx. The conserved glutamate (**red, Figure 3-9**) is located in a small α-helix at the same relative position to the FeS cluster in both YfaE and p-Fdx, suggesting the E26 in YfaE could function in a similar capacity as that proposed for E31 in p-Fdx. Interestingly, the C-terminus of p-Fdx forms a small helix that is located adjacent to the FeS cluster (**red arrows, B, Figure 3-9**). This C-terminal α-helix does not exist in YfaE (**red arrows, A, Figure 3-9**) as most of the YfaEs have only ~80 amino acids, compared to other ferredoxins that commonly have ~100 amino acid. This small C-terminal α-helix may contribute to the stability of the 2Fe2S clusters in other ferredoxins.

In order to test the role of these surface charged residues in β_2 and YfaE, site-directed mutagenesis was performed and rates of the oxidation of YfaE and reduction of met-β_2 were measured by SF spectroscopy. If these residues play a role in binding of the two proteins, a decrease of the observed rate constant should be observed where YfaE does not saturate β_2. To examine this model, StrepII-tagged β_2 single (K38A, K42A and K229A), double (K38A/K42A) and triple (K38A/K42A/K229A) mutants and a YfaE-E26A mutant were prepared.

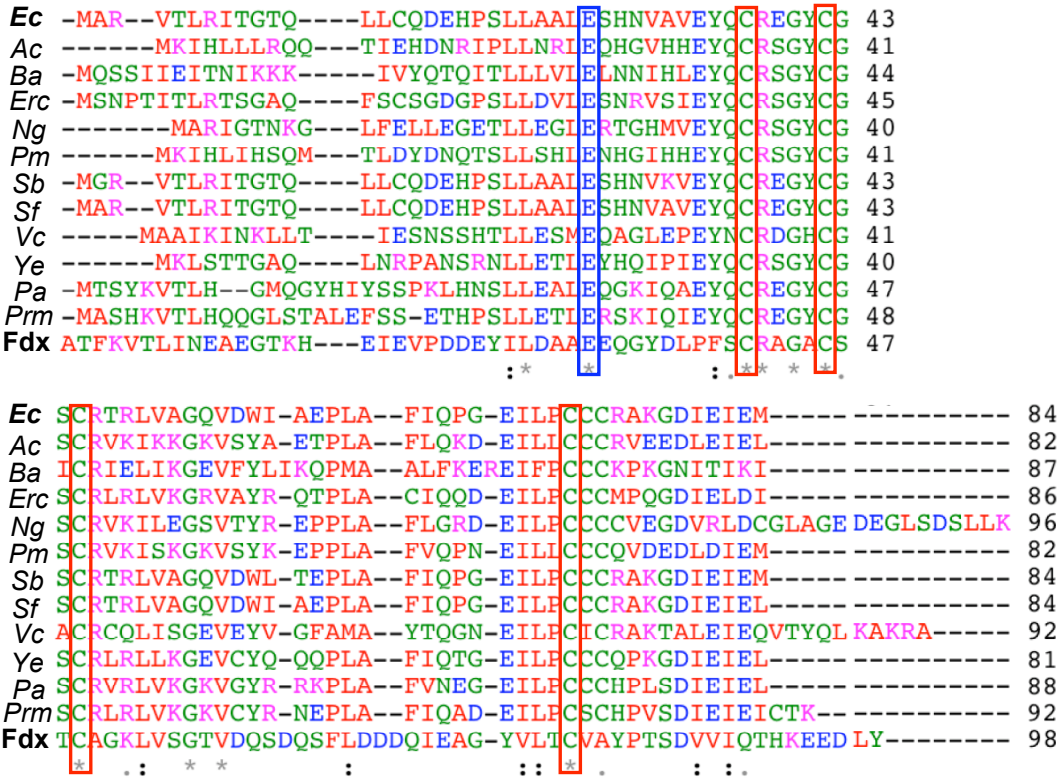

Figure 3-8. Sequence alignment between YfaEs and Δ9D-ferredoxin. Program ClustalW2 (http://www.ebi.ac.uk/tools/clustalw2) was used to align the protein sequence of plant ferredoxin and YfaE-like ferredoxins. The conserved cysteines for [2Fe2S] cluster are labeled in red boxes. The conserved glutamate proposed for interaction with β_2 or Δ9D are labeled in blue box. *Ec: Escherichia coli, Ac: Actinobacillus actinomycetemcomitans, Ba: Buchnera aphidicola, Erc: Erwinia carotovora, Ng: Neisseria gonorrhoeae, Pm: Pasteurella multocida, Sb: Salmonella bongori, Sf: Shigella flexneri, Vc: Vibrio cholerae, Ye: Yersinia enterocolitica, Pa: Photorhabdus asymbiotica, Prm: Proteus mirabilis*

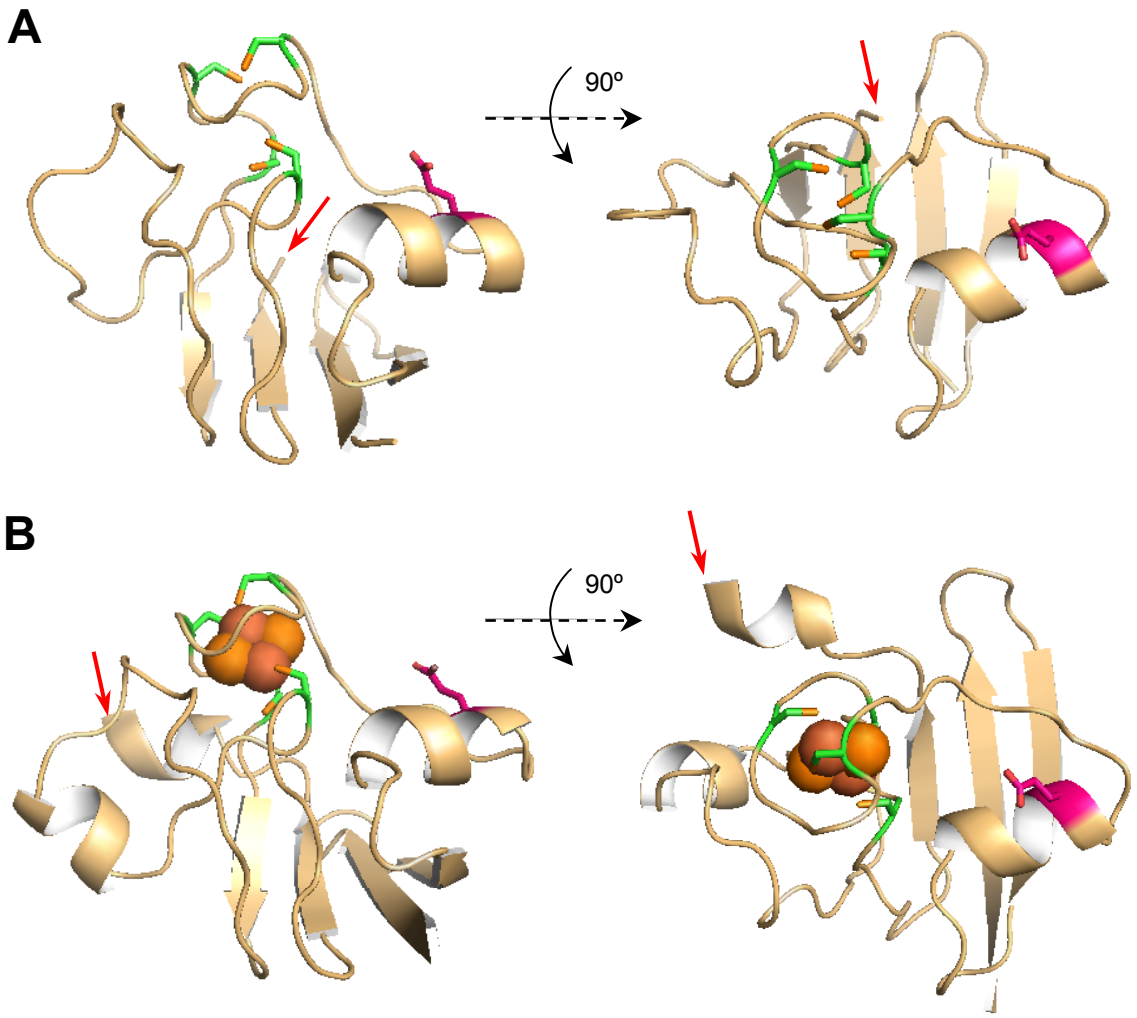

Figure 3-9. A homology model of YfaE (A) generated by the software Swiss-Model (http://swissmodel.expasy.org) using the crystal structure of the plant ferredoxin (B, pdb: 1FXA) as a template for modeling. Green: four conserved cysteine ligands for the 2Fe2S cluster; red: conserved glutamate predicted to be important for interacting with β_2 or Δ9D; orange CPK: 2Fe2S cluster. Red arrows indicate the C-terminal ends of YfaE and plant Fdx.

YfaE-E26A isolation and characterization: As with the wt, YfaE-E26A was expressed in inclusion bodies. It was solubilized in 8 M urea and refolded in the presence of Fe^{2+}, Fe^{3+} and S^{2-} under strictly anaerobic conditions. However, unlike wt-YfaE, the E26A mutant was very unstable. Efforts to further purify the protein via Sephadex G-75 chromatography were unsuccessful as the process typically takes ~1.5 days. Under these chromatographic conditions, the cluster was found to decompose. Therefore, YfaE-E26A was concentrated and characterized immediately after elution from the Q-Sepharose column. The UV-visible spectrum of YfaE-E26A after anion-exchange chromatography is shown in **Figure 3-10**. Features of the absorption from the reduced YfaE-E26A are very similar to those observed for the wt YfaE. The oxidized YfaE-E26A showed absorption peaks at 330, 419 and 458 nm, in contrast to the wt enzyme with features at 340, 420 and 460 nm. Furthermore, ratio of the A_{280nm} to 330, 419 and 458 nm were 0.67, 0.47 and 0.41, respectively, compared to 0.83, 0.60 and 0.60 for the wild type. The lower ratios for this mutant could be due to lower purity of the mutant because of the omission of the Sephadex G-75 column. Another distinguishing feature was ratio of A_{419nm}:A_{458nm} of 1.16, compared with A_{420nm}:A_{460nm} of 1 in the wt enzyme (**Figure 2-4**).

Despite the purity of the mutant, its ability to reduce met-β_2 was examined by SF spectroscopy. The protein concentration was determined from the A_{419nm}, assuming an ε_{419nm} = 11 $mM^{-1}cm^{-1}$. The maximum absorption difference and the isosbestic point between oxidized and reduced YfaE-E26A were shifted from the wt wavelengths to 460 and 317 nm, respectively. Therefore, the oxidation of YfaE-E26A and the reduction of met-β_2 were monitored at 460 and 317 nm in the SF experiments.

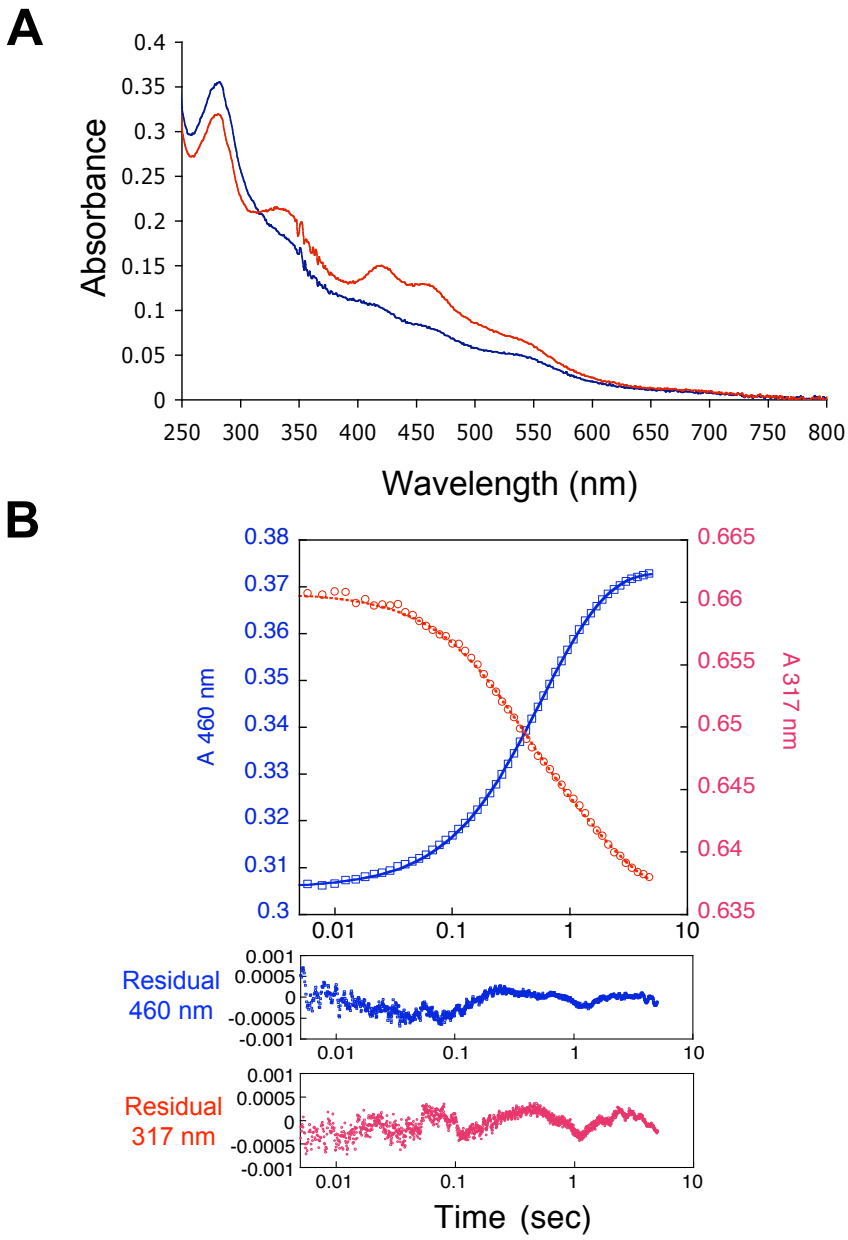

Figure 3-10. UV-visible spectrum of oxidized (red) and reduced (blue) YfaE-E26A (A) and SF kinetics of reactions between 5 μM met-β_2 and 45 μM of Q-Sepharose purified $[2Fe2S]^{1+}$-YfaE-E26A at 37 ºC (B). The same data collection and analysis as **Figure 3-1** were followed except that the oxidation of YfaE and reduction of met-β_2 were monitored at 460 and 317 nm, respectively.

The results of oxidation of $[2Fe2S]^{1+}$-YfaE-E26A and reduction of met-β_2 are shown in **Figure 3-10 (B)** and the kinetic parameters are summarized in **Table 3-3**. Similar to wt YfaE, the SF traces were best fit to two single exponential functions. The $k_{obs\text{-}fast}$ and $k_{obs\text{-}slow}$ at 460 and 317 nm were both 1-2 seconds slower than the corresponding k_{obs} for wt-β_2. These results indicate that under these conditions, the E26A mutation does not alter the reduction of met-β_2 dramatically, suggesting affinity is not altered. Because of the instability of YfaE-E26A, the focus changed to lysine mutants of β_2.

Preparation of K→A β_2 mutants and characterization of their redox properties: To facilitate the rapid purification of β_2 mutants, plasmid pBAD-C-S-*nrdB* with a C-terminal StrepII tag (*17*) was used as the PCR template for site-directed mutagenesis. The mutant proteins were expressed in *E. coli* TOP10 cells by induction with 0.5 mM arabinose for 2 h and purified by our published procedure (*17*). Typically 0.7-1.0 Y•/β_2 and ~3.0-3.4 Fe/β_2 were obtained from the purified wt and mutant β_2 without in vitro reconstitution of the cluster. Each purified β_2 was then treated with HU for ~30 min at 4 ºC to reduce the Y•, passed through a Sephadex G-25 column and brought into the glove box after being degassed on a Schlenk line. Met-β_2 (5 μM) and $[2Fe2S]^{1+}$-YfaE (45 μM) were used as the initial conditions for the SF spectroscopic experiments because a significant ΔA is expected, which facilitates the data analysis.

Figure 3-11 shows the SF kinetics traces between $[2Fe2S]^{1+}$-YfaE and met-β_2 (wt and mutants) under anaerobic conditions. In all cases the data are best fit to two single exponentials. Kinetic parameters obtained from Kaleidagraph analysis are summarized in **Table 3-3**. The data indicate that the single K→A β_2 mutants have lower k_{obs} (2 to 10 fold) monitored by ΔA_{465nm} and ΔA_{320nm}, in contrast with observations in Δ9D single mutants (**Table 3-4**). In most cases the k_{obs}

for the slower phase is affected more by the single mutations than the fast phase. A similar trend is observed with β_2-K38A/K42A double mutant. The $k_{obs\text{-}slow}$ decreased by ~20 fold relative to wt in both YfaE oxidation and met-β_2 reduction, whereas the $k_{obs\text{-}fast}$ are similar to those in wt. In the β_2-K38A/K42A/K229A triple mutant, both $k_{obs\text{-}fast}$ and $k_{obs\text{-}slow}$ are decreased 80 to 250 fold. Nevertheless, the decrease is not as dramatic as in the Δ9D triple mutant in the steady state measurements (**Table 3-4**). These results suggest that the three conserved surface lysines in β_2 play a role in redox reaction which could be related to binding to YfaE.

Table 3-3. Summary of kinetic parameters from stopped-flow experiments of reactions between $[2Fe2S]^{1+}$-YfaE (45 μM) and met-β_2 (5 μM).

Sample	$k_{obs\text{-}fast,\ 460nm}$	$\Delta A_{460nm\ -fast}$	$k_{obs\text{-}slow,\ 460nm}$	$\Delta A_{460nm\ -slow,}$	$k_{obs\text{-}fast,\ 317nm}$	$\Delta A_{317nm\ -fast}$	$k_{obs\text{-}slow,\ 317nm}$	$\Delta A_{317nm\ -slow,}$
YfaE-E26A	2.9	0.028	1.0	0.039	3.5	0.011	0.57	0.012
Sample	$k_{obs\text{-}fast,\ 465nm}$	$\Delta A_{465nm\ -fast}$	$k_{obs\text{-}slow,\ 465nm}$	$\Delta A_{465nm\ -slow,}$	$k_{obs\text{-}fast,\ 320nm}$	$\Delta A_{320nm\ -fast}$	$k_{obs\text{-}slow,\ 320nm}$	$\Delta A_{320nm\ -slow,}$
NS-β_2	7.0	0.035	2.4	0.047	4.6	0.025	0.79	0.006
CS-β_2	4.3	0.068	1.3	0.030	6.2	0.023	1.3	0.017
CS-β_2-K38A	1.3	0.049	0.61	0.045	4.0	0.008	0.44	0.021
CS-β_2-K42A	1.5	0.019	0.26	0.080	1.7	0.005	0.21	0.034
CS-β_2-K229A	2.3	0.084	0.10	0.011	4.0	0.026	1.0	0.009
CS-β_2-K38A/K42A	3.8	0.016	0.06	0.045	2.6	0.006	0.052	0.019
CS-β_2-K38A/K42A/K229A	0.047	0.081	0.017	0.047	0.025	0.036	0.016	0.009

Table 3-4. Steady state kinetics for the Δ9D-catalyzed conversion of 18:0-ACP to 18:1-ACP measured at varying concentrations of p-Fdx (**Adapted from Ref. (*6*)**).

Δ9D isoform	k_{cat} (min^{-1})	K_m (mM)	k_{cat}/K_m ($mM^{-1}min^{-1}$)
wt	28	0.56	50
K56A	42	18	2.4
K60A	40	3.2	12
K230A	24	1194	0.02
K56A/K60A	30	140	0.2
K56A/K60A/K230A	ND[a]	ND[a]	0.00007

a: ND, not determined

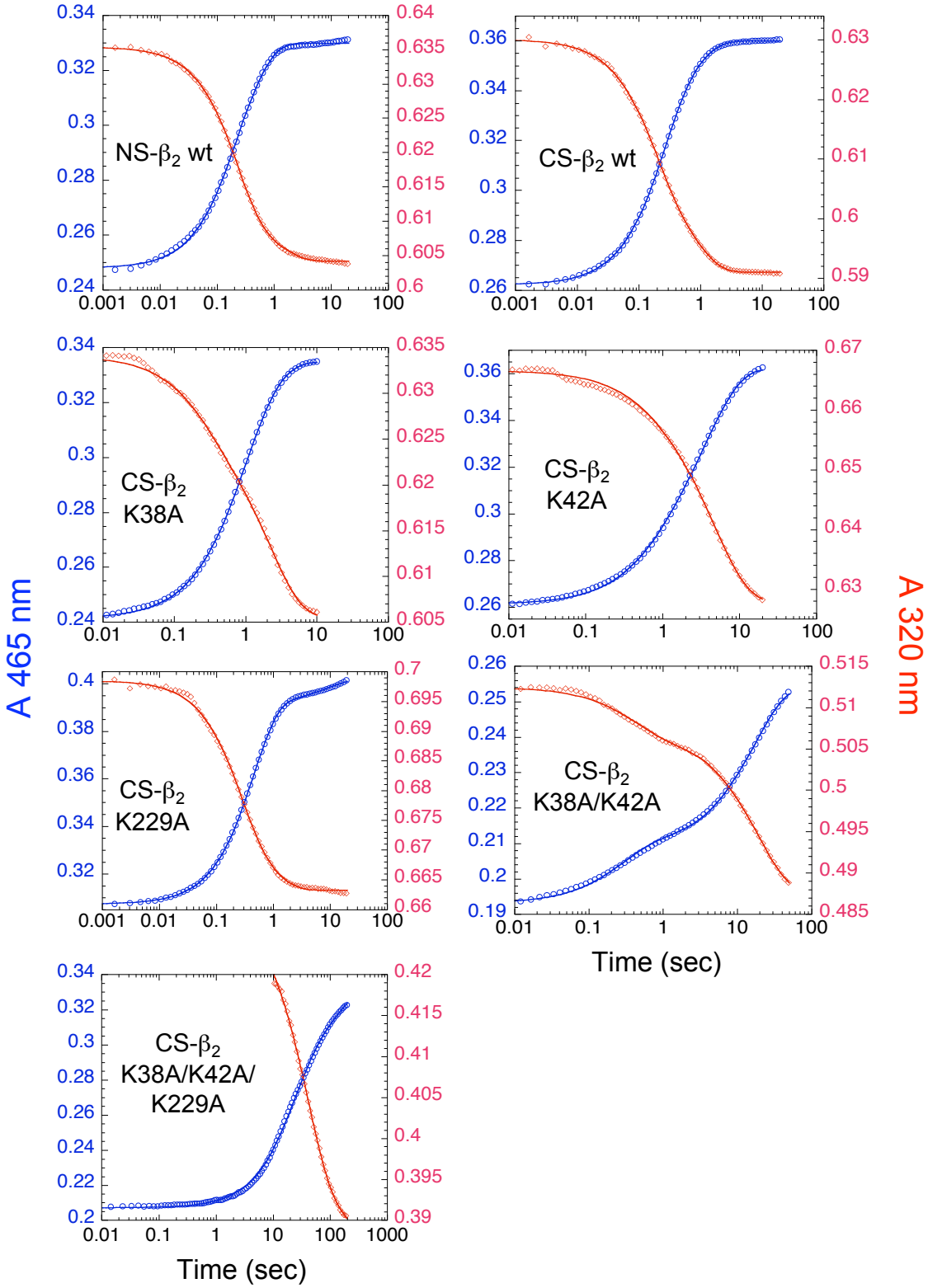

Figure 3-11. SF kinetics of 5 μM met-β_2 wt or mutants react with 45 μM $[2Fe2S]^{1+}$-YfaE at 37 ºC under anaerobic conditions. The same data collection conditions and analysis as **Figure 3-1** were followed. The kinetic parameters are summarized in **Table 3-3**. Notice the different time scales between experiments.

Determination of concentration of YfaE in *E. coli* by quantitative Western blotting

There are several studies on ferredoxins and their corresponding protein substrates in vivo, however, few have determined the concentrations of the two proteins inside the cells. In one study on chloroplasts and root plastids in maize, the molar ratios of Fdx I (leaf) and Fdx III (root) to a substrate, sulfite reductase were found to be 30:1 and 3:1, respectively, therefore, these ferredoxins are likely to act stoichiometrically in reducing sulfite reductase in vivo (*33*). Thus, prior to characterizing the YfaE/β_2 interaction in detail, we decided to determine if YfaE acts stoichiometrically or catalytically in vivo, and to investigate the proposal that Fre is the Fdx reductase.

The method of choice for analysis of number of molecules of proteins under different growth conditions is quantitative Westerns (*17, 34*). Antibodies (Abs) to β_2 have previously been obtained and Abs to purified $[2Fe2S]^{1+}$-YfaE were raised in rabbits. *E. coli* K-12 wt cells were grown in LB medium at 37 ºC until the culture reached mid-log phase (A_{600nm} ~0.8), during which the rapid cell division may demand higher [Y•] that can be activated/maintained by YfaE. The cells were then harvested by centrifugation, suspended and serial diluted in PBS at 4 ºC for cell counting. The standard deviation was 7%, which contrast with 30% we previously reported. The major difference is that in previous studies cells were grown to A_{600nm} ~ 1.8. It is possible that the viability of the cells decreases after the culture is saturated, causing a higher standard deviation in cell counting (*17*).

Because of the instability of oxidized YfaE that could aggregate and precipitate during the preparation of crude cell lysate, the suspended *E. coli* K-12 wt cells were lysed directly and completely in the Laemmli buffer and loaded directly onto gels for SDS-PAGE analysis. To verify the reliability of this procedure, the in vivo concentration of β_2 was determined and

compared to our published results. **Figure 3-12** shows a typical quantitative Western blot for β_2. Purified β_2 was used to generate a standard curve following our published procedures (*17*). Cells were suspended and lysed in Laemmli buffer (1.4×10^7 cells/μL Laemmli buffer) and loaded (1 to 30 μL) onto the gel. Western signals that fell within the range of the standard curve were analyzed. The results indicate the [β_2] is 3.1 ± 0.3 μM (assuming 0.85 fL per cell) (*35*) or 1562 ± 150 β_2 molecules per cell, which is in good agreement with our previous results (2.2 ± 0.4 μM) (*17*).

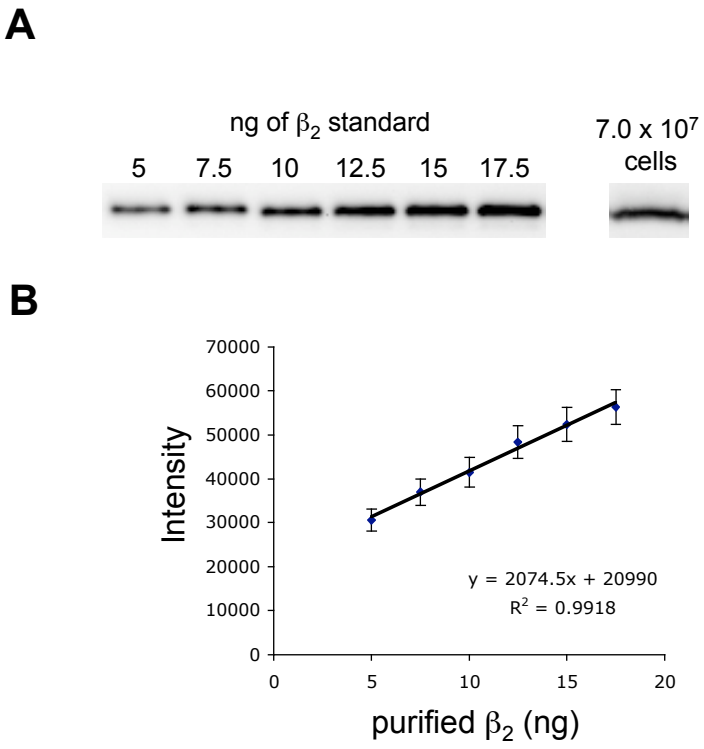

Figure 3-12. Quantitative Western blot analysis to determine the in vivo concentration of β_2 in wt *E. coli* cells. Growth in LB to mid-log phase (A) Western signals of purified β_2 standards and whole cells of wt *E. coli*. The amount of the protein standards in each lane and the number of cells loaded are indicated above each lane. (B) A standard curve generated from densitometry analysis of the signals from purified β_2 standards.

The determination of [YfaE] in vivo turned out to be challenging due to the very poor YfaE Abs. Even at a 500-fold dilution of the YfaE Abs, the Western signal from 10 ng of purified YfaE was very weak. Attempts to increase the titer of the Abs through acetone powder purification using *ΔyfaE* cells were unsuccessful. Because [2Fe2S]-YfaE is ~9.4 kDa, too small to generate sufficient immune response in rabbits, it was conjugated through its Cys or Lys to Keyhole Limpet Hemocyanin and injected into rabbits with Freund's Complete Adjuvant (FCA). The conjugation and injection were performed by Covance. It is possible that $[2Fe2S]^{1+}$-YfaE oxidized and precipitated during shipment or during preparation of the conjugated immunogen. To avoid the problem associated with the instability of oxidized YfaE, purified $[2Fe2S]^{1+}$-YfaE was loaded onto 15% SDS-PAGE and the acrylamide gel bands of YfaE were sent to Covance to mix with FCA directly for generating immune response in rabbits. This alternative procedure proved to be more effective and the new antibodies have much better affinity to YfaE under the same dilution (500-fold).

Figure 3-13 shows the results of the quantitative Western blots for YfaE. The new YfaE antibodies can detect 1 ng of purified YfaE and the Western signals are linear to 12.5 ng. However, in the whole cell samples suspended in Laemmli buffer that contain as high as 4.2×10^8 cells, no signal of YfaE was detected. Based on this result, the [YfaE] in vivo is < 0.3 μM (~160 YfaE molecules per cell). If this number is correct, then YfaE must act catalytically in reducing met-β_2 in vivo.

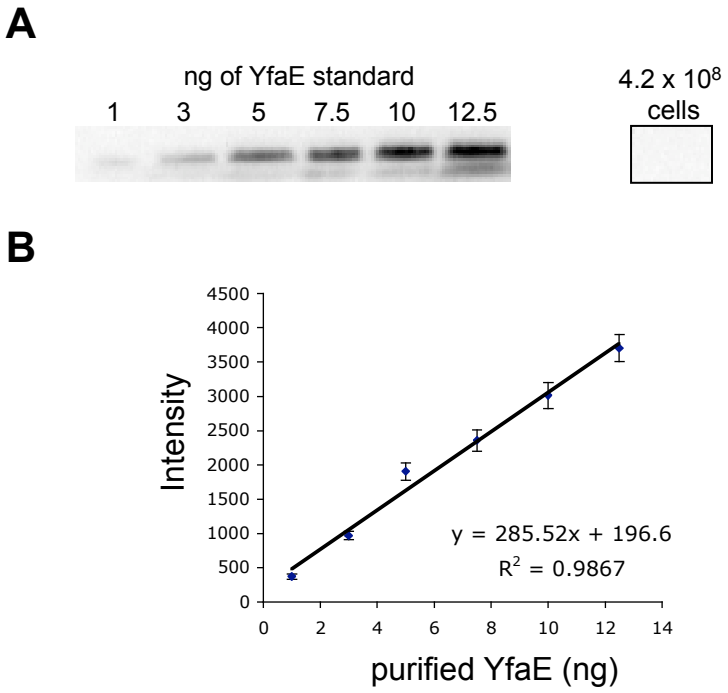

Figure 3-13. Quantitative Western blot analysis to determine the concentration of YfaE in wt *E. coli* cells. (A) Western signals of purified YfaE standards and wt *E. coli* cells. The amount of the protein standard and the number of cells loaded are indicated above each lane. (B) A standard curve generated from densitometry analysis of the signals from purified YfaE standards.

Cloning, expression and purification of Fre

In order to further examine whether YfaE can catalytically reduce met-β_2, we cloned three possible candidates, Fre, Fpr and YqjH that might be able to function as a YfaE-reductase. Fre (233 a.a.) has been identified as a flavin reductase, which was proposed to play a role in the maintenance of β_2 diferric-Y• cofactor (*7-9*). Ferredoxin-NADP reductase, Fpr (248 a.a., also called Fnr, flavodoxin reductase) is an FAD containing protein that reduces ferredoxin and flavodoxin by consumption of NADPH (*36, 37*). YqjH (254 a.a.) is also an FAD-containing protein that is postulated to be a cytoplasmic ferric-siderophore reductase (*38*). Because of the implications of Fre's involvement in the cofactor maintenance from previous studies, we first focused on determining whether Fre is able to reduce YfaE.

Fre was amplified from the genome of wt *E. coli* K-12 by PCR and cloned into pET24a. The plasmid was transformed into BL21(DE3) cells grown in LB-kanamycin medium and the protein expression was induced by 1 mM IPTG for 4 h. Published protocols were followed for purification of Fre (*14*). Crude cell lysate was loaded onto a Phenyl Sepharose column and washed with a buffer containing 30% ammonium sulfate followed by a second wash with buffer containing 5% ammonium sulfate. Fre was then eluted with buffer containing 0% ammonium sulfate. Fractions were collected and the activity of the eluent was determined by the rate of NADPH consumption in the presence of riboflavin (**Figure 3-14**). Based on the A_{280nm}, the majority of the protein eluted before fraction 20. However, the activity assay indicates that the majority of the "Fre" elutes in fractions 30 to 100. Fractions 29 to 95 with activity higher than 15 units, were combined and concentrated by YM10 membranes.

Concentrated protein (13 mg/mL) was further purified by Sephadex G-75 chromatography. The protein elution and activity profile are shown in **Figure 3-14**. Fractions

14 to 16 from the major peak, with highest activity, were combined and concentrated. SDS-PAGE analysis indicates that Fre is nearly homogeneous and a UV-visible spectrum reveals that it does not co-purify with flavin, consistent with previous reports (**Figure 3-15**). **Table 3-5** summarizes the purification protocol. The specific activity of purified Fre is 120 µmol NADPH·min^{-1}·mg^{-1}, which is consistent with the literature value (*14*).

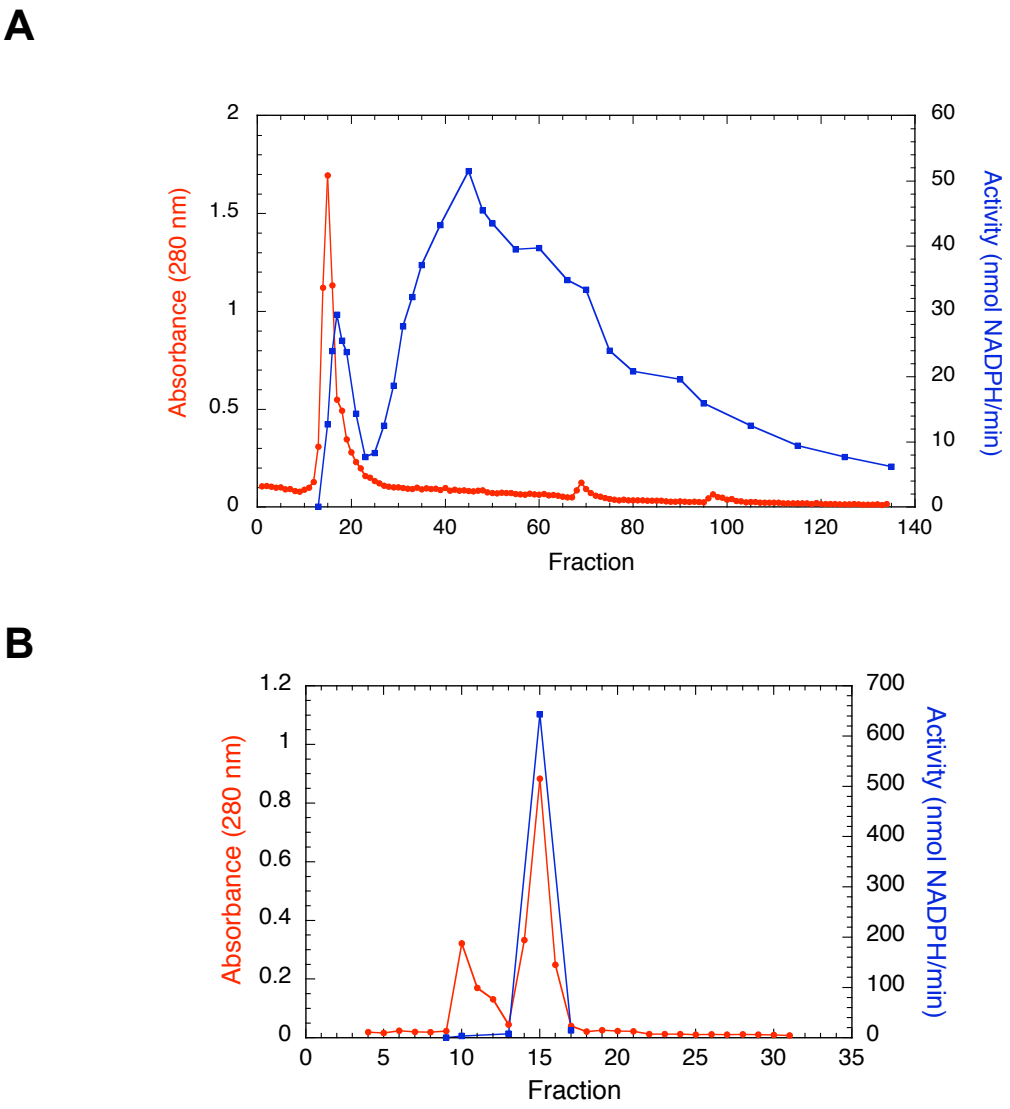

Figure 3-14. Purification of Fre by Phenyl Sepharose 6 Fast Flow (A) and Sephadex G-75 (B) chromatography. Fractions were monitored by A_{280nm} (red) and by activity (blue) monitoring NADPH consumption (A_{340nm}).

A

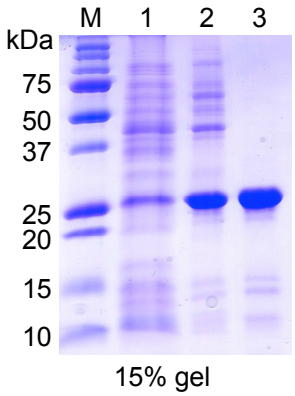

B

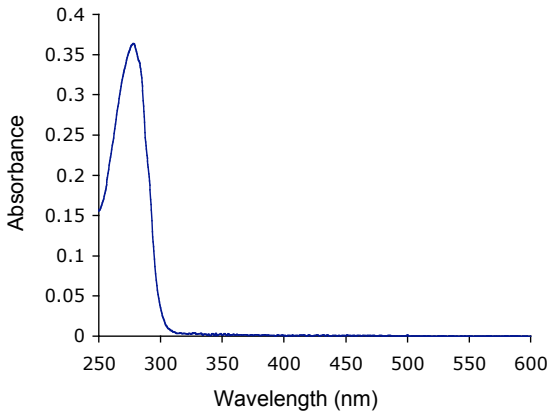

Figure 3-15. SDS-PAGE gel (15%) and UV-visible spectrum of Fre. (A) Each purification step was examined. M, molecular mass standards; lane 1, crude cell lysate; lane 2, after Phenyl Sepharose; lane 3, Sephadex G-75. (B) UV-visible spectrum of Fre after Sephadex G-75 purification.

Table 3-5. Purification Table of Fre

	volume (mL)	concentration (mg/mL)	yield (mg)	% yield (mg)	activity	% yield (activity)	specific activity [b]
cell lysate	42	9.5	399	100	5600000	100	14
flow through	42	1.1	46.2	12	66000	1.2	1,400
wash 1[a]	200	0.04	8	2	13000	0.2	1.6
wash 2[a]	160	0.7	112	28	13000	0.2	0.12
Phenyl Sepharose	2.6	13	34	8	2550000	46	75
G-75	1.2	15	18	5	2150000	38	120

[a] Buffers (25 mM Tris-HCl, pH 7.5, 10% glycerol) containing 30% and 5% ammonium sulfate were used for wash 1 and wash 2 from the Phenyl Sepharose column, respectively.
[b] $\mu mol \cdot min^{-1} \cdot mg^{-1}$

Reduction of YfaE by Fre

The capability of Fre to reduce oxidized YfaE was examined. To prepare oxidized YfaE, purified $[2Fe2S]^{1+}$-YfaE was removed from the glove box and exposed to O_2. All solutions including $[2Fe2S]^{2+}$-YfaE, riboflavin, NADPH and Fre were then degassed and brought into the glove box to prevent reoxidation of reduced YfaE and reduced flavin during the titration. Riboflavin and NADPH were chosen as substrates for Fre as previous studies had shown that this combination gives the highest k_{cat} and k_{cat}/K_m (*7, 14*). To examine whether Fre can catalytically reduce YfaE, a mixture of $[2Fe2S]^{2+}$-YfaE (18.5 μM), riboflavin (0.8 μM) and Fre (0.8 μM) was titrated with 1 mM NADPH in 2 to 10 μL aliquots under anaerobic conditions. The concentration of each reagent was chosen for ease in monitoring the disappearance of oxidized YfaE at 420 nm with minimal interference from riboflavin.

The results of this titration are shown in **Figure 3-16**. The results establish that YfaE is reduced upon addition of NADPH. The amount of YfaE (9.4 nmol) reduction was complete after addition of 24 nmol NADPH, which theoretically can provide 48 nmol electrons. Surprisingly no NADPH absorption at 340 nm was detected despite its presence in excess of that required for reduction. This result suggests that "O_2" was not completely during degassing on the Schlenk line and that reduced flavin was reoxidized by O_2 and re-reduced by NADPH to consume all the NADPH. At the end point of the titration, the sample was exposed to oxygen and features of the oxidized YfaE reappeared, indicating the redox cycle is reversible.

Despite the defect of O_2 contamination in this experiment, the results establish that YfaE can be catalytically reduced by the Fre reduction system.

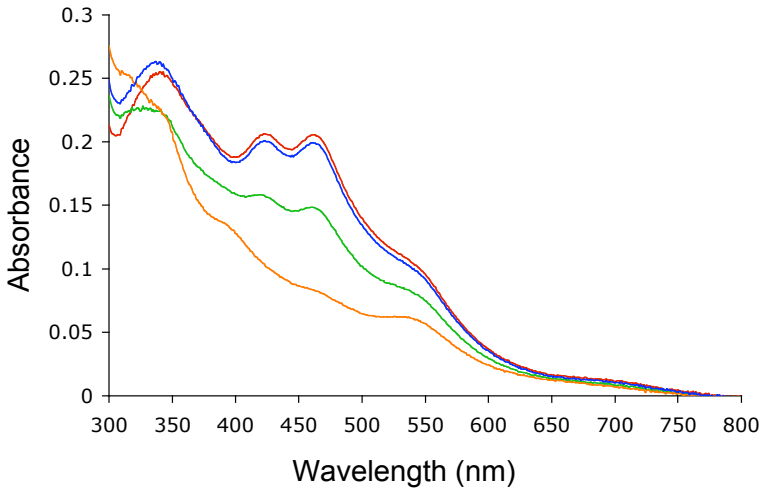

Figure 3-16. Reduction of oxidized YfaE by NADPH, riboflavin, and Fre under anaerobic conditions. Oxidized YfaE (9.4 nmol, 18.5 μM) was incubated with 0.8 μM Fre and 0.8 μM riboflavin (red) followed by titration with NADPH until an end point was reached. Spectra after addition of 12 nmol/24 μM (green) or 24 nmol/48 μM (orange, end point) NADPH are shown. After the titration end point was reached, the sample was oxidized by re-addition of an O_2 atmosphere to the cuvette (blue). Changes in absorbance due to dilution were normalized to the original volume.

Reduction of YfaE by photoreduced FMN

The flavin in Fre is not tightly bound, thus it is possible that the reductant of $[2Fe2S]^{2+}$-YfaE is free reduced riboflavin (RFH_2) and not Fre•RFH_2. To examine whether $[2Fe2S]^{2+}$-YfaE can directly be reduced by reduced flavins, FMN was incubated with sodium oxalate under anaerobic conditions and exposed to light to generate $FMNH_2$ (**Figure 3-17**) (*22*). Time course studies indicated an exposure time of 3 min was sufficient to completely reduce FMN.

Oxidized YfaE (14 nmol) was then titrated with $FMNH_2$ under anaerobic conditions. Since FMN species do not absorb at $\lambda > 510$ nm, the reduction of YfaE was monitored at 550 nm. The [YfaE] was chosen to have an $A_{550nm} > 0.2$. Upon addition of $FMNH_2$, the absorbance at 550 nm decreased concomitant with an increase at ~460 nm region, indicating reduction of YfaE and oxidation of $FMNH_2$, respectively (**Figure 3-17**). A titration end point was reached after addition of 16 nmol $FMNH_2$ (32 nmol of e^-). Exposure to oxygen after the end point resulted in complete re-oxidation of YfaE as judged by A_{550nm}. The oxidized sample also showed a strong increase in absorption at the 460 nm region, indicating a proportion of $FMNH_2$ added was still in the reduced state and became oxidized after exposure to oxygen. This is supported by the stoichiometry observed in this titration in which 16 nmol $FMNH_2$ was needed to reduce 14 nmol YfaE, suggesting an equilibrium mixture of $FMNH_2$ and FMN existed during the course of titration. Semi-quinone FMNH• has absorption features around 600 nm region and was not observed during the course of titration, judging from the spectra (*39*). This experiment demonstrates that YfaE is reduced directly by reduced flavins, suggesting direct contact with Fre is not required during the Fre-mediated reductions.

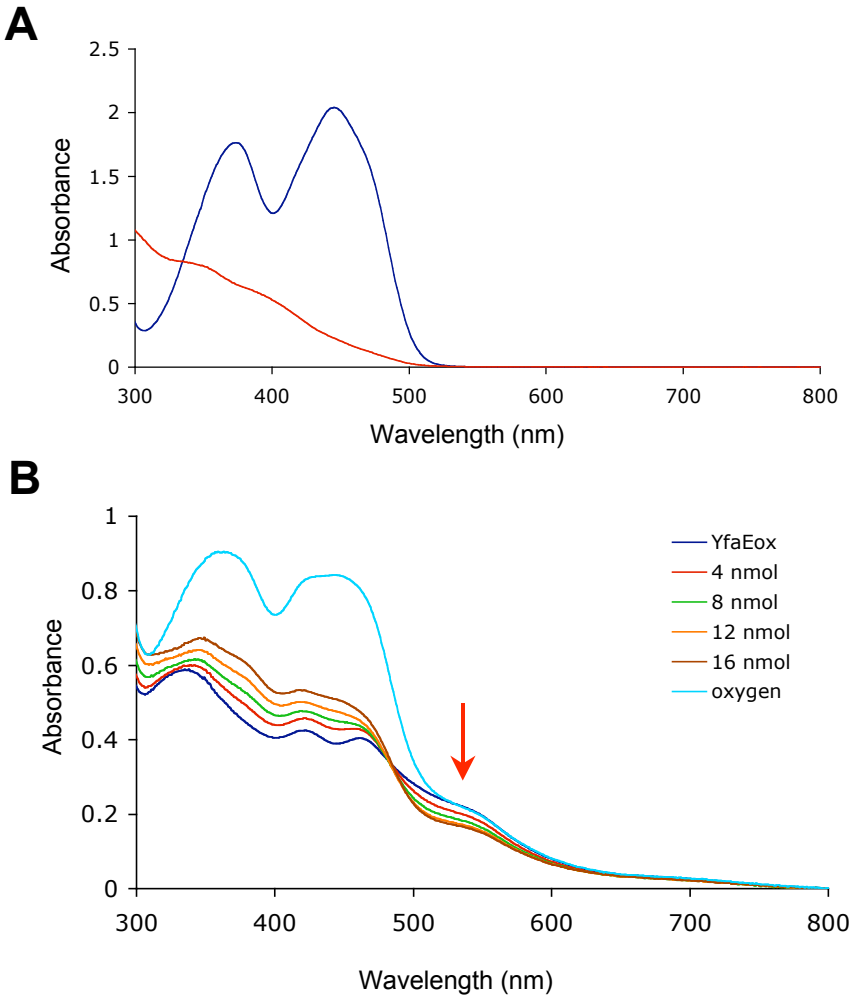

Figure 3-17. Photoreduction of FMN by oxalate (A) and reduction of 39 μM (14 nmol) oxidized YfaE by 216 μM $FMNH_2$ (B). (A) A mixture of 0.2 mM FMN and 2 mM sodium oxalate was exposed to 150 W-tungsten lamp for 3 min to generated $FMNH_2$. Spectra before (blue) and after (red) exposure to light are shown. (B) Oxidized YfaE (blue) was titrated with $FMNH_2$ under anaerobic conditions. Reduction of YfaE was monitored at ~550 nm region in which FMN does not absorb (red arrow). A titration end point was reached after addition of 16 nmol $FMNH_2$, at which point, exposure to oxygen resulted a complete oxidation of YfaE judged by A_{550nm}. The absorption between 300 to 500 nm region indicates features from oxidized YfaE and FMN. Spectra have been normalized for dilution.

Reduction of met-β_2 in the presence of YfaE, Fre, riboflavin and NADPH

After showing that YfaE can be reduced by NADPH in the presence of catalytic amounts of Fre and riboflavin, we investigated whether met-β_2 can be reduced by a catalytic amount of YfaE in the presence of the Fre reducing system. Met-β_2 (20 μM) was mixed with $[2Fe2S]^{1+}$-YfaE (0.5 μM), Fre (0.5 μM) and riboflavin (0.5 μM) and titrated with 1 mM NADPH in 1-2 μL aliquots under anaerobic conditions. The concentrations of each reagent were chosen to have clear absorption features associated with met-β_2 ($A_{370nm} > 0.15$) and minimal interference from YfaE, Fre or riboflavin ($A_{370nm} < 0.01$).

Figure 3-18 shows the results of the titration. Upon addition of 5 nmol NADPH, ~2.6 nmol met-β_2 (~8.8 nmol Fe, as 3.4 Fe/β_2) was reduced as judged from ΔA_{370nm}. The reaction was complete within the 2 min, the time required to obtain the spectrum. The titration end point was reached after addition of 11 nmol NADPH. Exposure to oxygen at this point resulted a generation of 1.4 Y•/β_2 quantitated by the dropline method (**orange line, A, Figure 3-18**) (*40*). Because 11 nmol NADPH can provide 22 nmol reducing equivalent, the generation of 10.1 nmol Y• implies a stoichiometry of 2 Fe reduced per Y• generated. From the iron content of the original β_2 (3.4 Fe/β_2), about 82% ((10.1 nmol Y• ×2)/(7.2 nmol met-β_2 × 3.4)) of the total iron in met-β_2 was reduced at the titration end point, similar to results from the titration experiments with $[2Fe2S]^{1+}$-YfaE in Chapter 2. Since there was no excess reductant, the extra reducing equivalent required for generating the diferric-Y• cofactor was provided by β_2 itself, which is also consistent with the observations in Chapter 2. Furthermore, unlike the previous two experiments (**Figure 3-16, 3-17**) in which more than 50% of the reductants remained in reduced form, more than 92% of NADPH added was oxidized, suggesting that in the presence of met-β_2, the equilibrium was shifted to favor the reduction of met-β_2.

To examine whether the reduction of met-β_2 was mediated by YfaE or by reduced flavin generated by Fre, a control experiment minus YfaE was carried out (**B, Figure 3-18**). In contrast to the results observed when the titration was done in the presence of YfaE, the addition of 5 nmol NADPH followed immediately by recording the spectrum (~2 min) resulted in an increase of the absorption at 340 nm, suggesting that most of the NADPH remained reduced. The difference spectrum from the reaction mixture before and after addition of NADPH revealed 96% in the reduced state. The 4% of NADPH oxidized (~0.2 nmol) could have been used to reduce the 0.18 nmol riboflavin by Fre and not for the reduction of met-β_2. After 10 min of incubation, a slight decrease of the absorption features between 320 to 375 nm was observed (**B, Figure 3-18**). If this absorption decrease was completely due to oxidation of NADPH, 0.85 nmol NADPH (~17% of total) was oxidized during the 10 min incubation time, in contrast to ~100% oxidation in less than 2 min in the presence of YfaE (**A, Figure 3-18**).

These results support the idea that the reduction of met-β_2 in the presence of the Fre reducing system is mediated by YfaE instead of direct reduction by reduced flavin generated by Fre. Furthermore, 20 μM met-β_2 was reduced by 0.5 μM YfaE, 40-fold less, implying YfaE acts catalytically in reducing met-β_2 in the presence of the Fre reducing system.

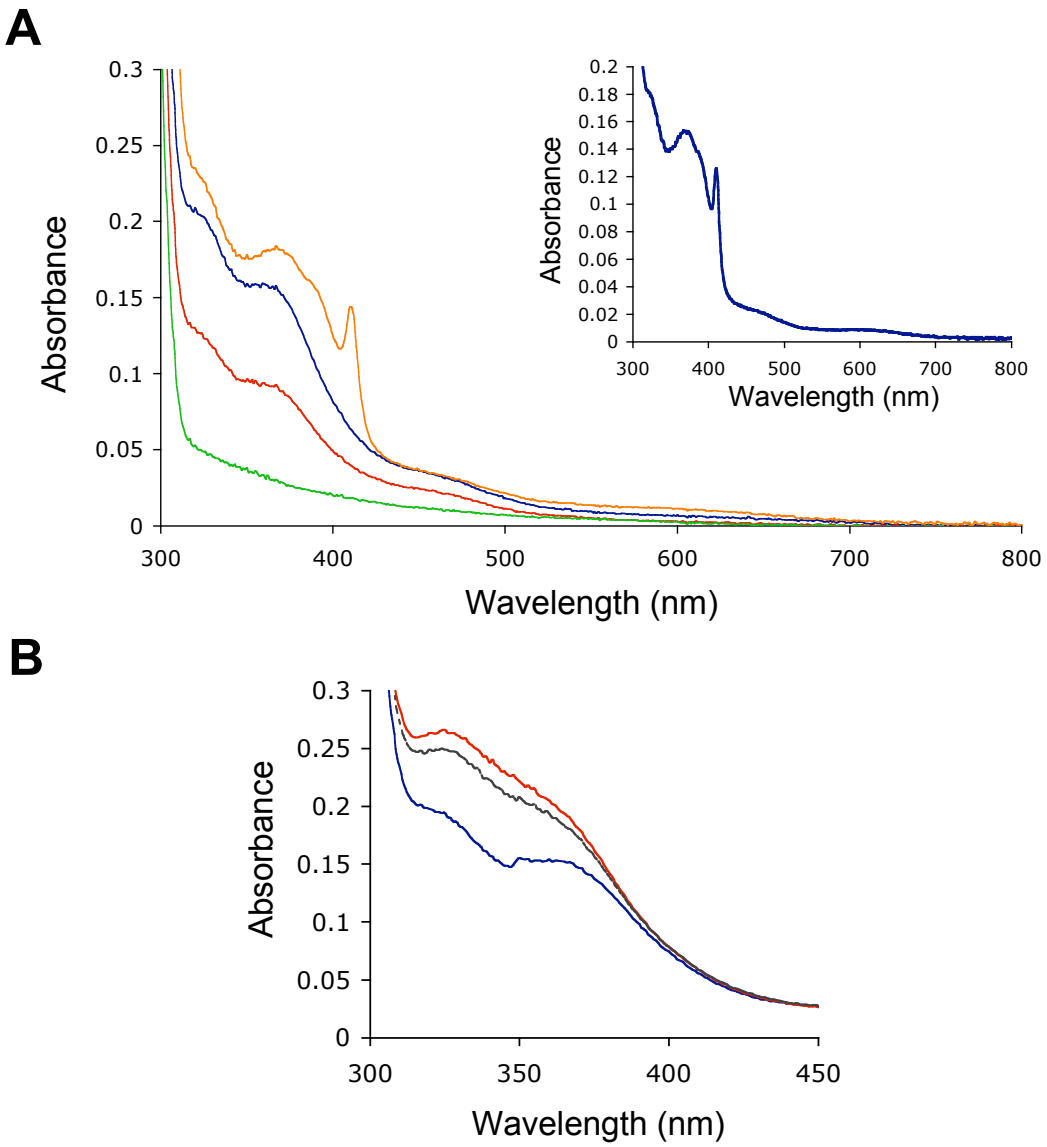

Figure 3-18. Reduction of met-β_2 by catalytic amounts of YfaE and Fre. (A) Under anaerobic conditions, 20 μM of met-β_2 (7.2 nmol) was mixed with 0.5 μM (0.18 nmol) of YfaE, Fre, and riboflavin (blue), followed by titration with 1 mM NADPH until an end point was reached. Spectra after addition of 5 nmol (14 μM) (red) or 11 nmol (31 μM) (green, end point) NADPH are shown. After the end point was reached, the sample was oxidized by exposure to O_2 (orange). Changes in absorbance due to dilution were normalized to the original volume. Inset: Difference spectrum between the end point of NADPH titration (green) and the oxygen addition (orange). (B) A control experiment, with the same conditions as in (A), except that YfaE was omitted. A mixture of met-β_2 (7.2 nmol), riboflavin (0.18 nmol) and Fre (0.18 nmol) (blue) was titrated with 5 nmol NADPH (red) under anaerobic conditions. Ten minute after addition of 5 nmol NADPH (black).

Determination of in vivo concentration of Fre by quantitative Western blotting

The titration experiment implies that the Fre reducing system catalytically cycles YfaE, which reduces met-β_2. Because of the complexity of the reactions, which involve multiple enzymes and reagents, knowing the relative ratio between Fre, YfaE and met-β_2 in vivo could help design in vitro kinetic experiments that reflect physiological conditions inside the cells. The concentration of Fre in vivo was determined by quantitative Western blots using the whole cell samples of wt *E. coli* K-12 grown in LB to mid-log phase. **Figure 3-19** shows the results of the quantitative Western blots. From the densitometry analysis, the concentration of Fre is 3.6 ± 0.3 μM (1814 ± 151 Fre molecules per cell, four measurements). This result implies YfaE is limiting in the cell grown under these conditions and the maintenance of the Y• may be controlled by regulating the expression of YfaE in vivo.

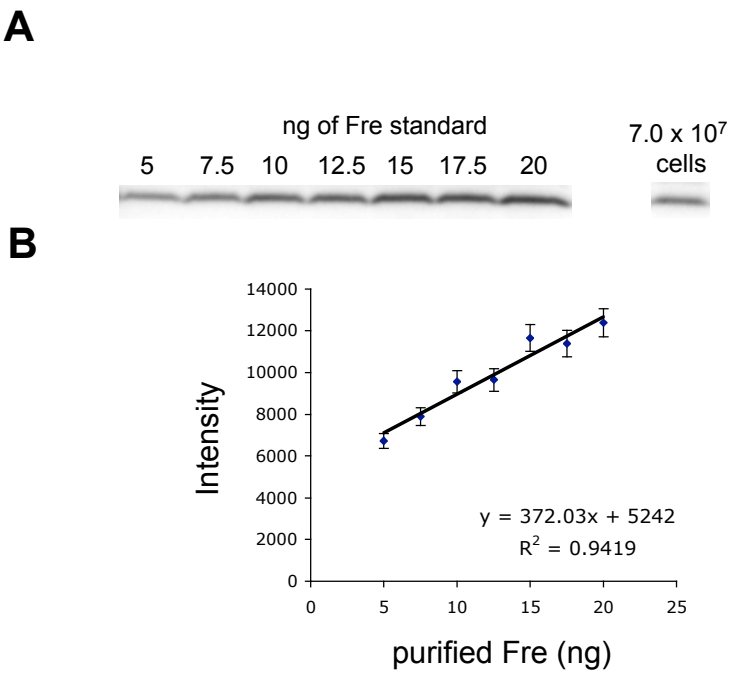

Figure 3-19. Quantitative Western blot analysis to determine the in vivo concentration of Fre in wt *E. coli* K-12. (A) Western signals of purified Fre standards and whole cells of wt *E. coli*. The amount of the protein standard and the number of cells loaded are indicated above each lane. (B) A standard curve generated from densitometry analysis of the signals from purified Fre standards.

Effects of HU on the growth of BW25113-*ΔyfaE*

One common way to examine the role of a protein in vivo is to delete the gene and see the effect of the gene deletion on the cell growth under different growth conditions. In order to examine the role of YfaE in vivo, *E. coli* K-12 BW25113-*ΔyfaE* was obtained from the National Institute of Genetics, Japan. The deletion was confirmed by PCR and DNA sequencing. The *ΔyfaE* was then grown in M9 minimal or LB medium in the presence of varying concentrations of hydroxyurea (HU), an anti-tumor reagent used clinically that specifically reduces the Y• of active β_2, generating inactive met-β_2. If YfaE is involved in regenerating the Y• in vivo as suggested from the in vitro experiments, the deletion of *yfaE* should lead to higher sensitivity to HU. In addition to *ΔyfaE*, effects of HU on the growths of BW25113-*Δfre*, *Δfdx* and *Δfpr* were also examined. The isogenic wt strain, *E. coli* K-12 BW25113 was included as a control.

Cell growth under these different conditions was measured with 4-6 replicates using the following protocol. An overnight culture from a single colony of a specific strain was inoculated into M9 minimal or LB medium and grown at 37 ºC until early log-phase of growth (A_{600nm} ~0.1). Aliquots of the cell culture (1 mL) were then transferred into a 24-well plate containing 0-50 mM HU and the cells were grown at 37 ºC with shaking (200 rpm). The cell growth was monitored at A_{630nm}. Since the deletion strains all contain a kanamycin resistant gene, 30 μg/mL kanamycin was also included in media. In order to avoid changes in growth rate associated with kanamycin, the wt control was transformed with plasmid pET9d (empty) which contains the kanamycin resistant gene.

Figure 3-20 shows the growth curves of wt *E. coli* and *ΔyfaE, Δfre, Δfdx* and *Δfpr* grown in M9 or LB medium in the presence of HU (0. 10, 30 and 50 mM). The cell growth in M9 medium was much slower so the A_{630nm} was measured every 30 min for ~9 h after addition of

HU. For the cells grown in LB medium, the A_{630nm} was measured every 10 min for ~4.5 h after addition of HU.

In M9 medium in the presence of 10 mM HU, a significant difference on the cell growth was observed in *ΔyfaE* and *Δfre*, with the *ΔyfaE* having the largest response. The effect of 10 mM HU on *Δfre* seems to be diminished at the later stage of growth. In the presence of 30 mM HU, the wt, *Δfdx*, and *Δfpr* started to show sensitivity to HU and in the *ΔyfaE* and *Δfre*, the growth was completely stopped. In the presence of 50 mM HU, all the strains showed no sign of cell growth.

In normal LB medium the addition of 10 mM HU caused a dramatic decrease in the growth rate of *ΔyfaE*, whereas no significant difference was observed in *Δfdx* and *Δfpr*. The wt and *Δfre* showed a similar response to 10 mM HU. The addition of 30 or 50 mM HU caused similar responses among all the strains except for *ΔyfaE*, which had minimal growths as in the presence of 10 mM HU.

In order to make a more quantitative comparison, the doubling times of each strain grown under different conditions were analyzed. **Figure 3-21** shows the analysis of the effect of HU on the doubling times. Because at 30 and 50 mM HU, the cells basically stopped growing, only the doubling times in the presence of 0 and 10 mM HU are reported.

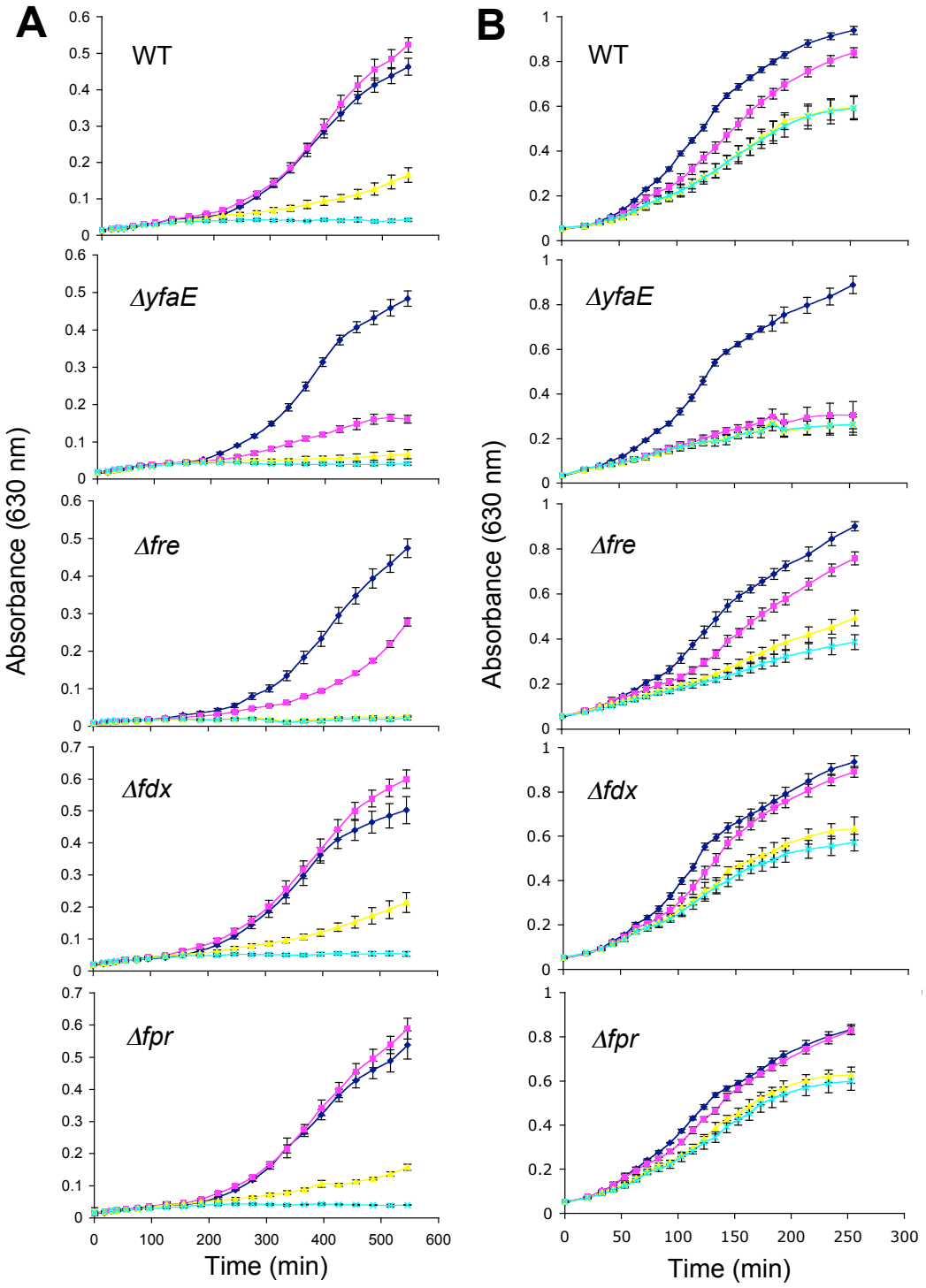

Figure 3-20. Growth curves of wt *E. coli* and *ΔyfaE, Δfre, Δfdx* and *Δfpr* grown in M9 minimal medium (A) or LB rich medium (B) in the presence of varying concentrations of HU. Wt *E. coli* and its isogenic gene deletion strains were grown in 24-well plates at 37 ºC, 200 rpm in the presence of 0 mM (◆), 10 mM (■), 30 mM (▲) and 50 mM (×) hydroxyurea. Cell growth was monitored at A_{630nm}. Averages of 4-6 independent growths are shown.

In M9 medium (**A, Figure 3-21**), the *ΔyfaE* shows ~75% increase in its doubling time in the presence of 10 mM, whereas other strains show only ~10% increase. Similar trends were observed when the cells are grown in LB medium except for *Δfre*, in which the doubling time is already longer than the other strains even in the absence of HU (**B, Figure 3-21**). To normalize for growth rate differences inherent to each strain, the growth rates (inverse of doubling times) at 10 mM HU were compared to that at 0 mM HU in each individual strain. In this way, only the effects associated with HU are highlighted (**C, Figure 3-21**). The results show that under 10 mM HU, the cells demonstrated similar responses in M9 and LB medium. The percentages of growth rate decrease in the presence of 10 mM HU were between 5-20% in all strains except for *ΔyfaE* which was ~40%.

These results support the role of YfaE in regenerating the Y• in vivo. Furthermore, the fact that the *Δfre* did not show as dramatic sensitivity to HU as *ΔyfaE* implies that YfaE may be recycled by other ferredoxin reductases. It is noticed that the sensitivity to HU of the *Δfre* observed in this experiment is not as dramatic as the response reported in the literature using *E. coli* K-12 L1312 (*fre::kan*) (*13, 14*). About 35% decrease in the growth rate was reported, in contrast to our observation (~20%) (both in M9 minimal medium, 10 mM HU). However, no detailed growth conditions were reported, so we have not been able to reproduce their results.

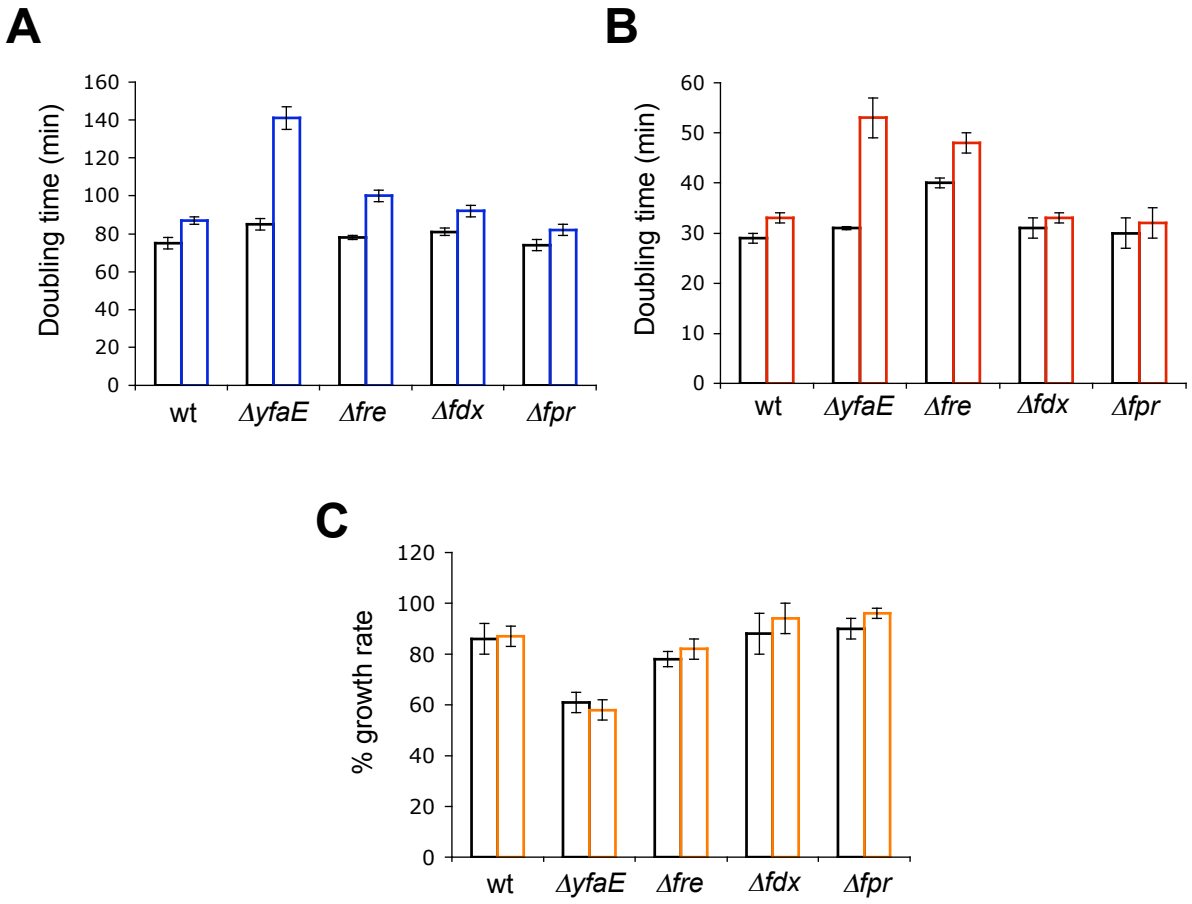

Figure 3-21. Doubling times of wt E. coli and ΔyfaE, Δfre, Δfdx and Δfpr strains grown in M9 minimal medium or LB medium in the presence of HU. (A) Doubling times of cells grown in M9 minimal medium. Black: 0 mM HU, blue: 10 mM HU. (B) Doubling times of cells grown in LB medium. Black: 0 mM HU, red: 10 mM HU. (C) Effect of HU on the rate of cell growth in different strains. The growth rates (inverse of doubling time) of each strain at 10 mM HU are compared to cells with no HU (normalized to 100%). Black: cells grown in M9 medium, orange: cells grown in LB medium.

Effects of HU on the expression of YfaE, β_2 and Fre

The slower growth rates of *ΔyfaE* and *Δfre* compared to that of wt in the presence of HU suggest the involvement of the two proteins in the maintenance of the Y• of β_2 in vivo. To further examine this proposal, the expression levels of YfaE and Fre in the presence of HU were examined. If YfaE and Fre play roles in the reactivation of the Y• of β_2, it is likely that the expression of these two proteins is up-regulated inside the cell in the presence of HU to counteract the detrimental effect of HU and to ensure cell survival.

Quantitative Western blot analysis on whole cells was employed to examine the expression levels of YfaE, β_2 and Fre. Wild type *E. coli* BW25113 cells were grown in LB until the early log growth phase was reached (A_{600nm} ~ 0.55). Different amounts of HU (10 and 30 mM) were then added into the culture and the cells were grown for another 1 h before the cell growth was stopped by incubation on ice for > 30 min. This time point was chosen based on the observation that the differences in cell growth in LB (**Figure 3-20**) start to become more prominent at ~ 1 h after addition of HU, after enough time has elapsed for HU to enter the cell and reduce the Y•, and the time for the cell to respond to the diminished [Y•]. Since HU could dramatically change the viability of the cell, the amounts of cells loaded on the SDS-PAGE were quantitated based on A_{600nm} instead of cell counting on LB-agar plates.

Figure 3-22 shows the results of Western blots. In the absence of HU or in the presence of 10 mM HU, no YfaE can be detected in the whole cells, which is similar to our previous observations. However, after treatment of 30 mM HU for 1 h, an observable signal appears, suggesting a higher expression of YfaE under such conditions. Based on the signal intensity of YfaE (30 mM HU, 1 h) relative to YfaE standards (**A, Figure 3-22**), we can estimate that the concentration of YfaE in vivo is ~ 1.3 μM (~655 molecule/cell) under these conditions, assuming

a cell volume of 0.85 fL/cell (*35*). Therefore, the concentration of YfaE has been up-regulated at least 4-fold compared to in the absence of HU.

The Western signals of [β_2] in the whole cells show that in the presence of 10 mM HU, in contrast to YfaE, the expression of β_2 increases (~2 fold) compared to without HU (**Figure 3-22**). The increased amount of HU (30 mM) does not seem to cause a further increase of the expression of β_2. In the case of Fre, the expressions of Fre are very similar between 0 and 10 mM HU. In the presence of 30 mM HU, ~2-fold increase of the Western signal is observed, suggesting an up-regulation of expression of Fre under these conditions (**Figure 3-22**). These results indicate that in response to the diminished [Y•] in vivo caused by HU, cells are able to up-regulate the expression of β_2, YfaE and Fre, supporting the role of YfaE and Fre in vivo in the regeneration of the Y• of β_2.

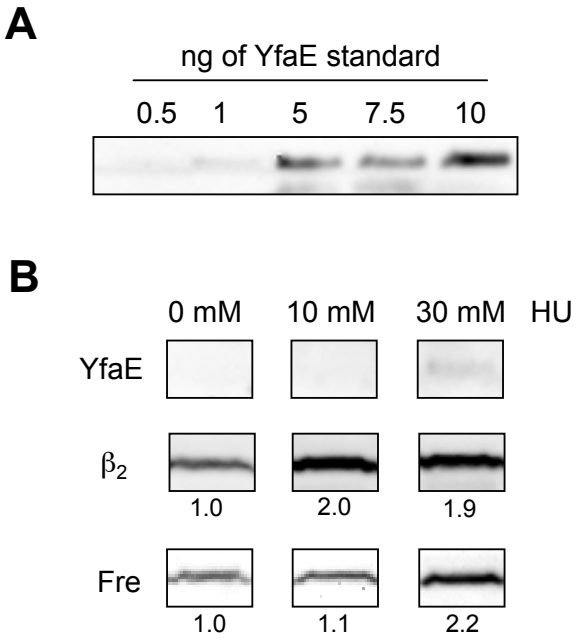

Figure 3-22. Western blot analysis to determine the level of expression of YfaE, β_2 and Fre in wt *E. coli* cells grown in LB the presence of HU. (A) Western signals of purified YfaE standards (B) Western signals of YfaE, β_2 and Fre of the whole cells grown in the absence or presence of HU (10 and 30 mM) for 1 h. Each lane represents ~1×10^8 cells estimated by A_{600nm}. The relative intensity of the Western signal is indicated.

DISCUSSION

Structural and kinetic studies on the interactions between Δ9D and a p-Fdx or MMO and MMOR-Fdx have provided a rich paradigm for us to think about how β_2 and YfaE might interact (*1-6, 41, 42*). Furthermore, in order to study reactions that are physiologically relevant, an understanding of the binding affinity and the concentrations of each protein in vivo are critical in evaluating whether the proposed functions from in vitro experiments are important in vivo. Several strategies have been applied to determine the binding constant between YfaE and β_2. We first examined the possibility of deriving K_d from a kinetic analysis of the redox reaction between $[2Fe2S]^{1+}$-YfaE and met-β_2 monitored by SF spectroscopy. The advantage of this method is that the K_d is obtained from two proteins in the physiologically relevant oxidation states, in contrast to the K_d measured from an ITC experiment in which both proteins are oxidized to avoid the redox chemistry which would give rise to heat exchange associated with chemistry in addition to binding.

In order to derive the K_d from kinetic analysis, the reaction between $[2Fe2S]^{1+}$-YfaE and met-β_2 needs to meet certain criteria. First, the reaction mechanism needs to be able to be described by a simple two-step reaction (**Scheme 3-1**). Second, the [YfaE] needs to be >> [met-β_2] to create a pseudo first order reaction conditions. Third, the binding equilibrium between $[2Fe2S]^{1+}$-YfaE and met-β_2 needs to be fast enough so that the observed rate constant can be described as a function of the association constant. Only the second condition can be controlled experimentally, whereas the other two criteria are restricted by the inherent nature of the reaction between YfaE and met-β_2. To examine whether the reaction between YfaE and met-β_2 meet these criteria, a 7 to 130 fold excess of $[2Fe2S]^{1+}$-YfaE was reacted with met-β_2 under anaerobic conditions and the k_{obs} was obtained from fitting the kinetic traces with two single exponentials.

The results suggest that reaction between $[2Fe2S]^{1+}$-YfaE and met-β_2 does not follow the rapid binding equilibrium and the simple two-step reaction model, therefore, the K_d could not be derived from this kinetic analysis.

Because of our inability to determine this K_d by SF spectroscopy and the successful example of measuring the K_d between MMOR-Fdx and MMO by isothermal titration calorimetry (*4*), we next tried to measure the binding affinity between $[2Fe2S]^{1+}$-YfaE and apo-β_2 by ITC. The major challenge for use of ITC is that unlike other oxidized ferredoxins, $[2Fe2S]^{2+}$-YfaE, during the time course required for such measurements, is unstable. Efforts to set up ITC under anaerobic conditions failed because of difficulty in removing contaminating O_2, which could potentially come from inside of the ITC instrument. However, recent discoveries have shown that oxidized YfaE remains stable in the presence of DTT (see Chapter 5). Furthermore, sequence alignments of YfaEs and homology modeling of YfaE with known ferredoxin structures have revealed a highly conserved cysteine residue that might be responsible for the instability of oxidized YfaE (see Chapter 5). If this is true, we might be able to measure the binding constant by ITC using these YfaE C→S mutants or by addition of DTT. The ability to use stabilized YfaE for ITC would also be valuable in determination of binding constant between YfaE and Fre, Fpr or YqjH, which may help us identify the ferredoxin reductase that is the physiological partner for YfaE.

To further understand the nature of binding between YfaE and β_2, site-directed mutagenesis coupled with SF spectroscopy were employed. These studies were modeled after studies on Δ9D by Fox et al (*6*). We postulated the importance of three surface lysines in β_2 (K38, K42 and K229) for electrostatic interaction with YfaE. Single, double and triple mutants of K→A were generated and their effect on the observed rate constants for oxidation of YfaE

was used as a criteria for their importance in the reduction process. Structural studies on the Fdx domain of MMOR also suggest that in addition to hydrophobic interactions, electrostatic interactions play a major role for interacting with MMO, which is distinct from the interactions between MMO and its regulatory partner MMOB that is mainly hydrophobic (*4, 5, 41*). However, comparisons between structural models of β_2 and Δ9D indicate that the relative positions of the predicted key lysines are not the same (**Figure 3-5, 3-6**), which may provide the basis for distinguishing between different redox partners inside the cell (*43, 44*). Sequence alignments of YfaEs and homology modeling of YfaE indicate a conserved Glu that may be the binding partner for the lysines in β_2. NMR titration studies on MMOR-Fdx domain also show that an Asp (D26) on the same α-helix near the FeS cluster participates the interaction with MMO (**Figure 3-9**) (*5*). However, a YfaE-E26A mutant proved to be unstable, probably through interference with the binding loops for the FeS cluster (*5*), making purification and SF spectroscopic measurements difficult.

Kinetic studies on the β_2 lysine mutants suggest the three conserved lysines are important for interaction with YfaE. The triple Lys mutant of β_2 showed a 250-fold decrease in the observed rate constants compared to wt under the same reaction conditions. This change is not as dramatic as reported in the Δ9D triple Lys mutant (~700,000 fold decrease in k_{cat}/K_m) (**Table 3-4**). This difference could be due to distinct lysine positions between Δ9D and β_2. Interestingly, from **Table 3-3**, the k_{obs} from the slower phase seems to be affected more by the lysine mutations compared to k_{obs} in the fast phase. It is tempting to speculate that the two phases may be associated with the binding of YfaE to each subunit of met-β_2, and these binding on one subunit affects the binding on the other subunit. Similar observations were reported that the binding of MMOR or MMOB (*1, 41, 45*).

Insight into the stoichiometric v.s. catalytic function of YfaE might be garnered by measuring the concentrations of YfaE, β_2 and Fre under a variety of growth conditions. Quantitative Western blots revealed that for cells in mid-log phase, concentrations of β_2 and Fre are both ~3 μM and the concentration of YfaE is less than 0.3 μM. If the dissociation constant between YfaE and β_2 is similar to that between MMOR-Fd and MMO, the maximum concentration of YfaE-β_2 complex in vivo is estimated to be 0.22 μM, assuming a K_d of 1 μM and no binding competition from α_2. From the k_{obs} in the SF experiment, if we assume the rate of redox reaction between YfaE and β_2 at physiological concentrations is ~0.1 s^{-1}, a pool of 0.22 μM YfaE-met-β_2 complex can regenerate an equivalent of 13 μM Y• in 20 min (0.1 s^{-1} × 0.22 μM × 60 sec × 20 min × 1 Y• generated/2 Fe reduced), which is much higher than the concentration of β_2 in vivo, implying that YfaE is kinetically competent to maintain Y• in vivo. These estimations could also explain the low [YfaE] in vivo. One assumption we made in the calculation is that 0.3 μM YfaE is maintained in the reduced state, which means oxidized YfaE needs to be recycled at a rate comparable to the rate of redox reaction with met-β_2.

To look for evidence of the function of YfaE in regenerating the Y• in vivo, knockout strains *ΔyfaE*, *Δfre*, *Δfdx*, and *Δfpr* were grown in minimal media and in LB in the presence of HU and the growth rates were measured. The results reveal in the former case that in the presence of 10 mM HU, *ΔyfaE* and *Δfre* showed about 40% and 20% decrease in the growth rates, respectively, whereas *Δfdx* and *Δfpr* showed similar sensitivity to HU as wt. These observations support the idea that YfaE plays a major role in the maintenance of the Y•. Similar experiments by Fontecave et al indicated that in M9 medium in the presence of 10 mM HU, *Δfre* showed ~35% decrease in the growth rates, which is higher than our observation (20% decrease)

(*14*). Unfortunately details of conditions of cell growth conditions and determination of growth rates were not reported, so we were not able to reproduce their results.

The role of YfaE in the maintenance of the Y• in vivo is further supported by the Western analysis of the whole cells grown in the presence of HU. The results show that for the first time, a detectable Western signal of YfaE in the whole cells was observed when the cells were treated with 30 mM HU and grown for an additional 1 h. Analysis on the expression level of β_2 and Fre also indicate a higher expression level of these two proteins in the presence of HU, suggesting cells could respond to the toxicity of HU by increasing the expression of β_2 and the machineries involved in regeneration of the Y•. Based on the experiments in this chapter, another piece of the puzzle for the maintenance of the diferric-Y• cofactor can be fit to the model (**Figure 3-23**).

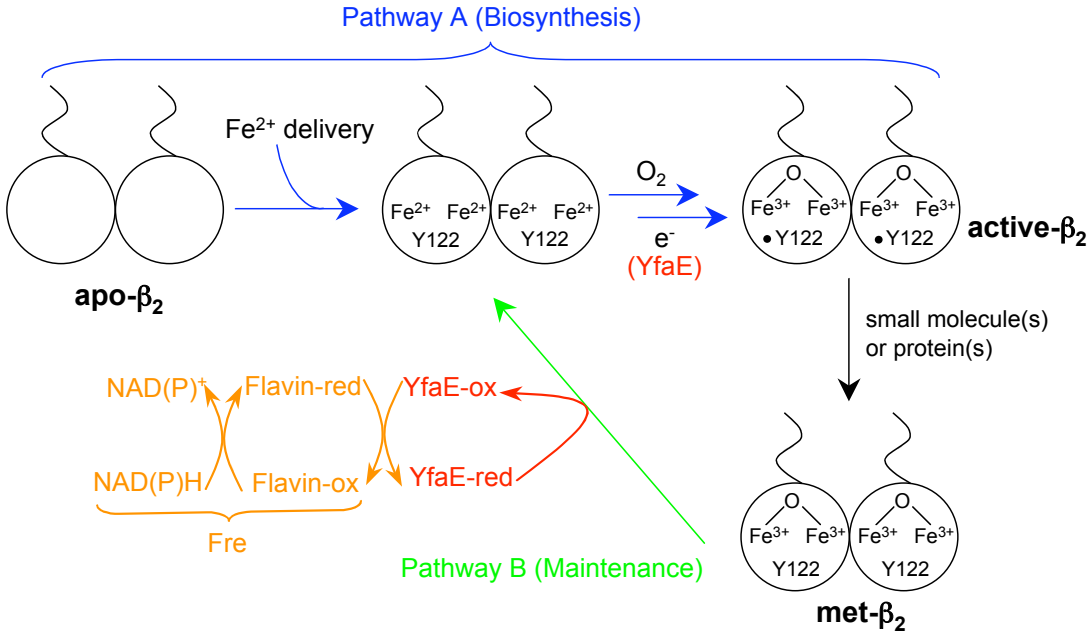

Figure 3-23. Our model for the maintenance of the diferric-Y• cofactor of β_2. A mechanism for recycling YfaE by Fre is added to the model (orange). Oxidized YfaE can be reduced by reduced flavin (either in solution or bound to Fre) generated by Fre with consumption of NAD(P)H.

REFERENCES

(1) Blazyk, J. L., Gassner, G. T., and Lippard, S. J. (2005) Intermolecular electron-transfer reactions in soluble methane monooxygenase: a role for hysteresis in protein function. *J Am Chem Soc 127*, 17364-76.

(2) Blazyk, J. L., and Lippard, S. J. (2002) Expression and characterization of ferredoxin and flavin adenine dinucleotide binding domains of the reductase component of soluble methane monooxygenase from *Methylococcus capsulatus* (Bath). *Biochemistry 41*, 15780-94.

(3) Blazyk, J. L., and Lippard, S. J. (2004) Domain engineering of the reductase component of soluble methane monooxygenase from *Methylococcus capsulatus* (Bath). *J Biol Chem 279*, 5630-40.

(4) Gassner, G. T., and Lippard, S. J. (1999) Component interactions in the soluble methane monooxygenase system from *Methylococcus capsulatus* (Bath). *Biochemistry 38*, 12768-85.

(5) Müller, J., Lugovskoy, A. A., Wagner, G., and Lippard, S. J. (2002) NMR structure of the [2Fe-2S] ferredoxin domain from soluble methane monooxygenase reductase and interaction with its hydroxylase. *Biochemistry 41*, 42-51.

(6) Sobrado, P., Lyle, K. S., Kaul, S. P., Turco, M. M., Arabshahi, I., Marwah, A., and Fox, B. G. (2006) Identification of the binding region of the [2Fe-2S] ferredoxin in stearoyl-acyl carrier protein desaturase: insight into the catalytic complex and mechanism of action. *Biochemistry 45*, 4848-58.

(7) Fontecave, M., Eliasson, R., and Reichard, P. (1987) NAD(P)H:flavin oxidoreductase of *Escherichia coli* - a ferric iron reductase participating in the generation of the free-radical of ribonucleotide reductase. *J. Biol. Chem. 262*, 12325-12331.

(8) Fontecave, M., Eliasson, R., and Reichard, P. (1989) Enzymatic regulation of the radical content of the small subunit of *Escherichia coli* ribonucleotide reductase involving reduction of its redox centers. *J. Biol. Chem. 264*, 9164-70.

(9) Barlow, T., Eliasson, R., Platz, A., Reichard, P., and Sjöberg, B. M. (1983) Enzymic modification of a tyrosine residue to a stable free radical in ribonucleotide reductase. *Proc. Natl. Acad. Sci. U. S. A. 80*, 1492-5.

(10) Covès, J., Laulhère, J. P., and Fontecave, M. (1997) The role of exogenous iron in the activation of ribonucleotide reductase from *Escherichia coli*. *J. Biol. Inorg. Chem. 2*, 418-426.

(11) Brown, N. C., Eliasson, R., Reichard, P., and Thelander, L. (1969) Spectrum and iron content of protein B2 from ribonucleoside diphosphate reductase. *Eur. J. Biochem. 9*, 512-8.

(12) Ehrenberg, A., and Reichard, P. (1972) Electron spin resonance of the iron-containing protein B2 from ribonucleotide reductase. *J. Biol. Chem. 247*, 3485-8.

(13) Covès, J., Nivière, V., Eschenbrenner, M., and Fontecave, M. (1993) NADPH-sulfite reductase from *Escherichia coli.* A flavin reductase participating in the generation of the free radical of ribonucleotide reductase. *J Biol Chem 268*, 18604-9.

(14) Fieschi, F., Nivière, V., Frier, C., Décout, J. L., and Fontecave, M. (1995) The mechanism and substrate specificity of the NADPH:flavin oxidoreductase from *Escherichia coli*. *J. Biol. Chem. 270*, 30392-400.

(15) Wu, C. H., Jiang, W., Krebs, C., and Stubbe, J. (2007) YfaE, a ferredoxin involved in diferric-tyrosyl radical maintenance in *Escherichia coli* ribonucleotide reductase. *Biochemistry 46*, 11577-88.

(16) Baba, T., Ara, T., Hasegawa, M., Takai, Y., Okumura, Y., Baba, M., Datsenko, K. A., Tomita, M., Wanner, B. L., and Mori, H. (2006) Construction of *Escherichia coli* K-12 in-frame, single-gene knockout mutants: the Keio collection. *Mol. Syst. Biol. 2*, 2006 0008.

(17) Hristova, D., Wu, C. H., Jiang, W., Krebs, C., and Stubbe, J. (2008) Importance of the maintenance pathway in the regulation of the activity of *Escherichia coli* ribonucleotide reductase. *Biochemistry 47*, 3989-99.

(18) DeLano, W. L. (2002) *The Pymol Molecular Graphysics System*, Delano Scientific LLC, San Carlos, CA.

(19) Johnson, K. A. (1992) *Transient-State Kinetics Analysis of Enzyme Reaction Pathways*, Vol. 20, Academic Press, New York.

(20) Bernasconi, C. (1976) *Relaxation Kinetics*, Academic Press, New York.

(21) Licht, S. S., Lawrence, C. C., and Stubbe, J. (1999) Thermodynamic and kinetic studies on carbon-cobalt bond homolysis by ribonucleoside triphosphate reductase: the importance of entropy in catalysis. *Biochemistry 38*, 1234-42.

(22) Massey, V., and Hemmerich, P. (1977) A photochemical procedure for reduction of oxidation-reduction proteins employing deazariboflavin as catalyst. *J Biol Chem 252*, 5612-4.

(23) Pierce, B. S., and Hendrich, M. P. (2005) Local and global effects of metal binding within the small subunit of ribonucleotide reductase. *J Am Chem Soc 127*, 3613-23.

(24) Aoki, M., Ishimori, K., Fukada, H., Takahashi, K., and Morishima, I. (1998) Isothermal titration calorimetric studies on the associations of putidaredoxin to NADH-putidaredoxin reductase and P450cam. *Biochim Biophys Acta 1384*, 180-8.

(25) Kondapalli, K. C., Kok, N. M., Dancis, A., and Stemmler, T. L. (2008) *Drosophila* frataxin: an iron chaperone during cellular Fe-S cluster bioassembly. *Biochemistry 47*, 6917-27.

(26) Shi, H., Bencze, K. Z., Stemmler, T. L., and Philpott, C. C. (2008) A cytosolic iron chaperone that delivers iron to ferritin. *Science 320*, 1207-10.

(27) Nordlund, P., Sjoberg, B. M., and Eklund, H. (1990) Three-dimensional structure of the free radical protein of ribonucleotide reductase. *Nature 345*, 593-8.

(28) Aberg, A., Nordlund, P., and Eklund, H. (1993) Unusual clustering of carboxyl side chains in the core of iron-free ribonucleotide reductase. *Nature 361*, 276-8.

(29) Logan, D. T., Su, X. D., Aberg, A., Regnstrom, K., Hajdu, J., Eklund, H., and Nordlund, P. (1996) Crystal structure of reduced protein R2 of ribonucleotide reductase: the structural basis for oxygen activation at a dinuclear iron site. *Structure 4*, 1053-64.

(30) Whitlam, J. B., and Brown, K. F. (1981) Ultrafiltration in serum protein binding determinations. *J Pharm Sci 70*, 146-50.

(31) Ormo, M., and Sjoberg, B. M. (1990) An ultrafiltration assay for nucleotide binding to ribonucleotide reductase. *Anal Biochem 189*, 138-41.

(32) Lindqvist, Y., Huang, W., Schneider, G., and Shanklin, J. (1996) Crystal structure of delta9 stearoyl-acyl carrier protein desaturase from castor seed and its relationship to other di-iron proteins. *Embo J 15*, 4081-92.

(33) Yonekura-Sakakibara, K., Onda, Y., Ashikari, T., Tanaka, Y., Kusumi, T., and Hase, T. (2000) Analysis of reductant supply systems for ferredoxin-dependent sulfite reductase in photosynthetic and nonphotosynthetic organs of maize. *Plant Physiol 122*, 887-94.

(34) Ortigosa, A. D., Hristova, D., Perlstein, D. L., Zhang, Z., Huang, M., and Stubbe, J. (2006) Determination of the in vivo stoichiometry of tyrosyl radical per betabeta' in Saccharomyces cerevisiae ribonucleotide reductase. *Biochemistry 45*, 12282-94.

(35) Neidhardt, F. C., and Ingraham, J. L. (1987) *Escherichia coli and Salmonella typhimurium: cellular and molecular biology*, American Society for Microbiology, Washington, D.C.

(36) Arakaki, A. K., Ceccarelli, E. A., and Carrillo, N. (1997) Plant-type ferredoxin-NADP+ reductases: a basal structural framework and a multiplicity of functions. *FASEB J. 11*, 133-40.

(37) Ceccarelli, E. A., Arakaki, A. K., Cortez, N., and Carrillo, N. (2004) Functional plasticity and catalytic efficiency in plant and bacterial ferredoxin-NADP(H) reductases. *Biochim Biophys Acta 1698*, 155-65.

(38) Bamford, V. A., Armour, M., Mitchell, S. A., Cartron, M., Andrews, S. C., and Watson, K. A. (2008) Preliminary X-ray diffraction analysis of YqjH from *Escherichia coli*: a putative cytoplasmic ferri-siderophore reductase. *Acta Crystallogr Sect F Struct Biol Cryst Commun 64*, 792-6.

(39) Cotruvo, J. A., Jr., and Stubbe, J. (2008) NrdI, a flavodoxin involved in maintenance of the diferric-tyrosyl radical cofactor in *Escherichia coli* class Ib ribonucleotide reductase. *Proc Natl Acad Sci U S A 105*, 14383-8.

(40) Bollinger, J. M., Jr., Tong, W. H., Ravi, N., Huynh, B. H., Edmondson, D. E., and Stubbe, J. (1994) Mechanism of assembly of the tyrosyl radical-diiron(III) cofactor of *Escherichia coli* ribonucleotide reductase. 2. Kinetics of the excess Fe^{2+} reaction by optical, EPR, and Mössbauer spectroscopies. *J. Am. Chem. Soc. 116*, 8015-8023.

(41) Sazinsky, M. H., Dunten, P. W., McCormick, M. S., DiDonato, A., and Lippard, S. J. (2006) X-ray structure of a hydroxylase-regulatory protein complex from a hydrocarbon-oxidizing multicomponent monooxygenase, *Pseudomonas* sp. OX1 phenol hydroxylase. *Biochemistry 45*, 15392-404.

(42) Lyle, K. S., Haas, J. A., and Fox, B. G. (2003) Rapid-mix and chemical quench studies of ferredoxin-reduced stearoyl-acyl carrier protein desaturase. *Biochemistry 42*, 5857-66.

(43) Wan, J. T., and Jarrett, J. T. (2002) Electron acceptor specificity of ferredoxin (flavodoxin):NADP+ oxidoreductase from *Escherichia coli*. *Arch Biochem Biophys 406*, 116-26.

(44) Martinez-Julvez, M., Medina, M., and Gomez-Moreno, C. (1999) Ferredoxin-NADP(+) reductase uses the same site for the interaction with ferredoxin and flavodoxin. *J Biol Inorg Chem 4*, 568-78.

(45) Liu, K. E., and Lippard, S. J. (1991) Redox properties of the hydroxylase component of methane monooxygenase from *Methylococcus capsulatus* (Bath). Effects of protein B, reductase, and substrate. *J Biol Chem 266*, 12836-9.

Chapter 4:

Investigating How the Iron Required for Cofactor Assembly is Delivered into Apo-β_2

Adapted in part from Hristova, D., Wu, C.-H., Jiang, W., Krebs, C., and Stubbe, J. (2008) Importance of the Maintenance Pathway in the Regulation of the Activity of *Escherichia coli* Ribonucleotide Reductase, *Biochemistry 47,* 3989-3999.

INTRODUCTION

In the previous three chapters we reported the discovery and characterization of YfaE, a ferredoxin that can provide the reducing equivalents for the maintenance and biosynthetic pathways for assembly of the diferric-Y• cofactor of β_2. Another unknown component in the assembly of cofactor is the iron source. In this chapter, we utilize several strategies to investigate possible iron sources for β_2 cluster assembly. The experiments include: 1. study of an iron chaperone candidate, CyaY; 2. development of a sensitive colorimetric assay that can monitor Fe delivery to β_2 from fractionated crude cell lysate that may contain iron chaperones; 3. search for iron chaperons that co-purify with affinity tagged β_2; 4. use of iron transport pathway deletion strains and whole cell EPR spectroscopy to monitor Y• generation in an effort to identify source of iron; and 5. use of whole cell Mössbauer spectroscopy to monitor the migration of iron pools within the cell and specifically into the diferric center of β_2.

Drawing on the extensive studies of FeS cluster biosynthesis and the literature on cofactor biosynthesis in general, a protein chaperone may be required for cluster assembly in β_2. Same specific targets are assessed, such as CyaY, a frataxin analogue of the *S. cerevisiae* iron chaperone involved in the FeS cluster biosynthesis. Details of CyaY have been described in Chapter 1.

In addition to investigation of specific iron chaperone candidates for β_2 cluster assembly, two generic "fishing" methods to look for iron chaperone are also explored. To identify machinery that might be involved in delivery of iron to β_2, one needs a robust assay to allow purification of this machinery from crude cell lysate and column chromatographies. The method we have investigated to monitor cluster assembly is based on the observation of Sjöberg and coworkers that an iron catechol-like cluster is generated subsequent to loading of apo-β_2-F208Y

with iron and O_2 (**Eq 4-1**) (*2, 3*). The formation of this cluster does not require the reducing equivalent necessary in the wt β_2 cluster assembly. Furthermore, the absorption peak of this cluster is at ~660 nm, where the background absorption features from crude cell lysate are minimal. A more recent study has shown that the double mutant (β_2-W48F/F208Y) in which the critical W48 is replaced with F, also generates a Fe^{3+}-catechol complex (ε_{660nm} ~3 $mM^{-1}cm^{-1}$, 3 times the amount of Fe^{3+}-catechol in β_2-F208Y) (*4*). The suitability of β_2-W48F/F208Y for the task of factor purification is explored.

Eq 4-1

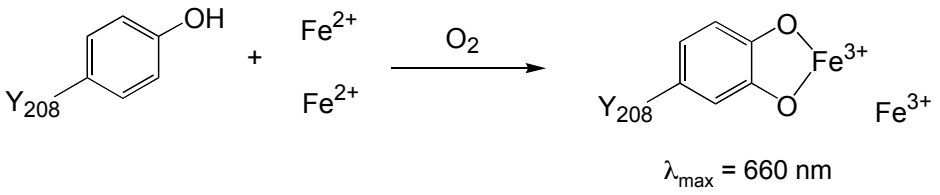

The second generic method in fishing iron chaperones involves incorporation of an "affinity" tag in β_2 and look for potential protein binding partners that co-purify with β_2. Identification of binding partners would be carried out by SDS-PAGE separation, in-gel trypsin digestion and mass spectrometry (LC-ESI/MS). This strategy has been successful employed to identify many protein-protein interactions (*5-7*). In order to increase the probability of identifying protein binding partners, the type and location of affinity tags and the expression level of affinity tagged proteins need to be examined. Therefore, a pBAD vector in which the expression of the protein of interest can be modulated by concentration of arabinose was selected (*8*). A StrepII tag (WSHPQFEK) was chosen for its small size, its lack of metal binding ligands, and high specificity for Strep-Tactin resin and consequently ease of purification (*9, 10*). Furthermore, because the nature of interaction of β_2 with its potential partners is unknown, the

affinity tag was placed in three different positions, the N-terminus, C-terminus and between N179 and G180 of β_2 (*1*), to preserve the interaction surface for binding of potential chaperones (**Figure 4-1**).

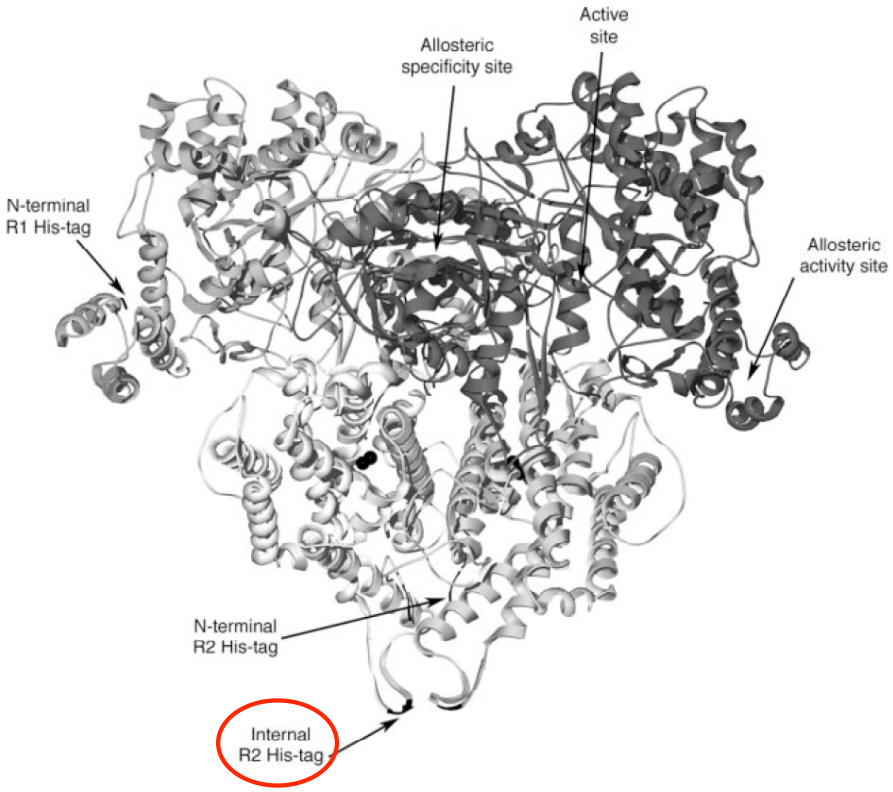

Figure 4-1. The position of the internal 6×His tag (red) in β_2. The structure of the modeled class Ia RNR complex is shown. An internal 6×His tag is inserted between N179 and G180 of β_2 (dark black line). **Adapted from reference (1)**.

To enhance the probability of detecting weakly bound chaperones, in vivo cross-linking with formaldehyde (FA) was examined. This method has been utilized in identifying binding

partners in protein-protein and protein-DNA interactions in the yeast, mammalian cells and prokaryotes (*11-13*). FA is cell wall-permeable and reacts with two proper amino acid side chains such as Lys that are within ~3 Å, forming a methylene bridge. This reaction can be reversed by incubation in electrophoresis buffer (Laemmli buffer) at 100 ºC (*14, 15*). In this strategy, different concentrations of FA is titrated into cell culture and the cells are grown for different periods of time until the reactions are quenched by addition of glycine. The effectiveness of cross-linking can then be monitored by SDS-PAGE or Western blots. After reversing the cross-links, the identity of the binding partners can be determined by mass spectrometry (*7*).

The affinity tag and ability to modulate β_2 expression levels have also been used to allow us to probe the concentration of Y• per β_2 by rapid purification from crude cell lysate. Specifically one potential mechanism of regulation of RNR activity is to control the concentration of Y•. The amount of Y•/β_2 can also be assessed using whole cell EPR spectroscopy, cell counting and quantitative Westerns. These types of studies all have successfully been carried out in different *S. cerevisiae* strains. In contrast to our whole cell EPR studies on *S. cerevisiae* and EPR studies by Sjöberg et al. on the *E. coli* β_2 over-producing strain, KK546, we were not able to quantitate the Y• in wt *E. coli* due to its low concentration (*16, 17*). To overcome this problem, the levels of expression of β_2 (μM to mM) were modulated by concentrations of arabinose (*18*). The ability of modulating the levels of expression of β_2 made the quantitation of Y• in vivo by EPR spectroscopy feasible. Using isogenic strains of *E. coli* with deletion strains in transporters or iron storage proteins, the concentration of Y• in these deletion strains containing pBAD-*nrdB* could now be examined by whole cell EPR spectroscopy.

Under conditions in which mM concentrations of β_2 was expressed, whole cell EPR spectroscopy revealed a very strong Y• signal. This signal implies high iron loading in β_2, suggesting that monitoring the iron incorporation in β_2 which has a unique diferric cluster by whole cell Mössbauer spectroscopy might be feasible. Conditions have been found where whole cell Mössbauer spectroscopy can be applied to monitor iron movement within the cell into β_2 (*19-21*). With the development of these strategies together, we may be able to establish how under different growth conditions apo-β_2 obtains ferrous iron inside the cell as a first step in active β_2 formation.

MATERIALS AND METHODS

Materials

Plasmid pET-*cyaY* was kindly provided by Dr. Pastore at the National Institute for Medical Research, UK (*22*). The sequence of the plasmid was confirmed by DNA sequencing by the MIT Biopolymers Laboratory. pR2-F208Y and pR2-W48F/F208Y were obtained from Prof. Martin Bollinger Jr. at Pennsylvania State University (*4*). The plasmids were amplified in *E. coli* DH5α (pR2-F208Y) and BL21 (pR2-W48F/F208Y) and the sequences were determined. The pR2-W48F/F208Y was correct based on the wt *E. coli* K-12 genome sequence, whereas the pR2-F208Y has an additional mutation at V141I. *E. coli* W3110 with a variety of iron transporter gene deletions (**Table 4-2**) were kindly provided by Prof. Rensing at the University of Arizona (*23*). *E. coli* BW25113 wt and isogenic strains with a variety of in frame single gene deletions were obtained from the Keio collection in the National Institute of Genetics, Mishima, Japan **(Table 4-2**) (*24*). The gene deletion was verified following the procedures in Chapter 3. The primers used for sequence verification are listed in **Table 4-3**. All gene deletion strains were missing the appropriate gene. Tris(hydroxymethyl)aminomethane hydrochloride (Tris-HCl) and glycine (acid form) was from J.T. Baker. Isopropyl-β-D-thiogalactopyranoside (IPTG) was from Promega. Protease inhibitors cocktail (Complete Mini, EDTA-free) was from Roche. Strep-Tactin Sepharose resin was from IBA GmbH. Formaldehyde (37%) was from Mallinckrodt. Bradford reagent and all other chemicals were obtained in the highest purity available from Sigma-Aldrich.

Purification and characterization of CyaY

Cell growth: Published procedures were followed for the purification of CyaY (*22*). A single colony of BL21(DE3)-pET-*cyaY* was inoculated into 30 mL LB-kanamycin (70 μg/mL) and grown at 37 ºC, 150 rpm overnight (~16 h). The overnight culture (20 mL) was inoculated into 2 L of LB-kanamycin (70 μg/mL) at 37 ºC, 180 rpm until A_{600nm} reached ~0.8, at which point the protein expression was induced by 0.5 mM IPTG and the cells were further grown for an additional 4 h (A_{600nm} ~1.7) before being harvested by centrifugation at 7000*g* for 30 min at 4 ºC. The cell paste was stored at –80 ºC after flash freezing in liquid nitrogen. Typically 2.5 g of cell paste/L culture was obtained.

Purification of CyaY by affinity chromatography: pET-*cyaY* contains a GST affinity tag followed by a 6×His tag at the N-terminus of CyaY. The published procedure to purify the protein on a Ni-column was followed. The cell paste (~4.9 g) was suspended in 25 mL of 20 mM Na_2HPO_4, 0.5 M NaCl, 10 mM imidazole, pH 7.4 including 1250 U of DNaseI (Roche). The cells were cracked open by two passages through the French Press at 14,000 psi, 4 ºC followed by centrifugation at 15,000 rpm for 30 min at 4 ºC. The supernatant was transferred into a 50 mL centrifuge tube containing 10 mL Ni-iminoacetic acid resin (Sigma) and the tube was shaken gently at 4 ºC for 2 h. The slurry was then loaded into a column (1.5 × 6 cm), washed with 400 mL of 20 mM Na_2HPO_4, 0.5 M NaCl, 10 mM imidazole, pH 7.4 and eluted with 20 mM Na_2HPO_4, 500 mM imidazole, 0.5 M NaCl, pH 7.4. The eluent (~3.2 mL/fraction) was assayed by Bradford reagent (Sigma) and A_{630nm} was recorded on a multi-plate reader (Bio-Rad). Protein-containing fractions (3-8) were combined and loaded onto a Sephadex G-25 column (2.5 × 42 cm, 210 mL) pre-equilibrated in 50 mM Tris-HCl, pH 7.6, followed by elution

in the same buffer at a flow rate of 2.6 mL/min. The protein-containing fractions (10-16) judged by the Bradford assay were combined and concentrated using an Amicon concentrator with a YM30 membrane. The protein was found to flow through the YM30 membrane despite its predicted molecular mass of ~40 kDa. The protein solution was concentrated again using an Amicon concentrator with a YM3 membrane until reaching a final volume of 6.5 mL. Aliquots of the sample (60 mg/mL) were flash frozen in liquid nitrogen and stored at –80 ºC. The iron content of the purified GST-His-CyaY was determined by ferrozine assay (*25*).

Removal of a GST-His affinity tag from CyaY: To cleave off the GST-His affinity tag from CyaY, recombinant TEV protease (250 U, Invitrogen) was added to 275 mg of GST-His-CyaY in a digestion buffer (50 mM Tris-HCl, 1 mM DTT, 0.5 mM EDTA, pH 8.0) and incubated in a 30 ºC water bath for ~24 h. The digested sample (~6 mL) was loaded onto a Superdex-75 column (150 mL, 2.5 × 32.5 cm, Amersham, prep-grade) and eluted with 50 mM Tris-HCl, 100 mM NaCl, pH 7.6 at a flow rate of 0.85 mL/min. The CyaY-containing fractions (12-14), judged by 15% SDS-PAGE, were concentrated using an Amicon concentrator with a YM3 membrane to ~6 mL and re-chromatograph on the same Superdex-75 column under the same conditions to completely remove residual GST-His tag contaminants. Fractions (13-14) were combined and concentrated by the Amicon concentrator with a YM3 membrane to ~2.5 mL. Aliquots of the protein were flash frozen in liquid nitrogen and stored at –80 ºC. A final yield of ~6.5 mg CyaY was obtained.

UV-visible spectroscopy and Mass spectrometry analysis: The concentration of CyaY was determined by A_{280nm} (ε_{280nm} = 29,970 $M^{-1}cm^{-1}$) (*26*). The molecular mass of CyaY was

determined by LC-ESI-MS in the MIT Biopolymers Laboratory (instrument: ABI 140C, column: Michrom PLRP-S).

Reconstitution of CyaY under anaerobic conditions: To reconstitute purified CyaY with Fe^{2+} under anaerobic reconstitution, 1 mL of purified CyaY (2.5 mM, in 10 mL pear shape flask), 800 mL of **buffer A** (50 mM Tris-HCl, 150 mM NaCl, pH 7.6) (in 2L round bottom flask), 0.392 g of $Fe(NH_4)_2(S0_4)_2 \cdot 6H_2O$ (in 10 mL pear shape flask) and 5 g of Sephadex G-25 powder (in 200 mL round bottom flask) were degassed by three cycles of evacuation and refill with Ar (~30 min/cycle, except for CyaY, which was degassed by 10 cycles of evacuation (~30 sec) and refill (~10 sec)) on a Schlenk line. The samples were then moved into a glove box (M. Braun, Newburyport, MA). The Sephadex G-25 powder was suspended in buffer A and packed into a column (~20 mL resin volume, 1 × 27 cm) followed by equilibration with 200 mL of buffer A. The $Fe(NH_4)_2(S0_4)_2 \cdot 6H_2O$ was dissolved in 5 mL buffer Y and the concentration (180 mM) was determined by the ferrozine assay (*25*).

To load CyaY with Fe^{2+}, 110 μL of 180 mM Fe^{2+} (10× molar excess, assuming 2 Fe^{2+}/CyaY) was added into 370 μL of 2.5 mM CyaY and the sample was mixed by pipetting followed by incubation for 30 min at room temperature in the glove box. The sample was then loaded onto the Sephadex G-25 column (~20 mL resin volume, 1 × 27 cm) to separate the excess Fe^{2+}. A_{280nm} of the eluent (50× dilution) was recorded on a multi-plate reader (Bio-Rad) and the iron content of the eluent (10× dilution) was determined by the ferrozine assay.

Purification of apo-β_2-W48F/F208Y

Cell growth: Published procedures were followed for the purification of apo-β_2-W48F/F208Y (*4*). A single colony of BL21(DE3)-pR2-W48F/F208Y was inoculated into 50 mL LB-ampicillin (150 μg/mL) and grown at 37 ºC, 180 rpm for ~16 h. The overnight culture (25 mL) was inoculated into 2 L of LB-ampicillin (150 μg/mL) in a 6 L flask and grown at 37 ºC, 180 rpm for ~3 h until A_{600nm} reached ~1.0. The iron chelator, 1,10 phenanthroline (100 mM stock, dissolved in 0.1 N HCl) was then added into the culture to reach a final concentration of 100 μM. The cells were grown for another 20 min before being induced with 0.2 mM IPTG for 4 h. The cells were then harvested by centrifugation at 7000*g* for 20 min at 4 ºC. About 2.8 g/L of cell paste was obtained. The cell paste was flash frozen in liquid nitrogen and stored at –80 ºC.

Protein purification: To purify apo-β_2-W48F/F208Y, 14 g of the cell paste was suspended in 56 mL of buffer B (50mM Tris-HCl, 5% (w/v) glycerol, 1 mM 1,10-phenanthroline, 0.25 mM PMSF, pH 7.6 at 4 ºC). One tablet of Roche complete mini protease inhibitor cocktail was added into the cell suspension. The cells were then disrupted by two passages through the French Press at 14,000 psi followed by centrifugation at 15,000 rpm for 20 min at 4 ºC. About 71 mL of crude cell lysate was collected. Streptomycin sulfate (15 mL, 6% (w/v) stock) was then added into the cell lyaste to a final concentration of 1% followed by stirring for 20 min before centrifugation at 21,000 rpm for 20 min at 4 ºC. About 83 mL of the supernatant was obtained. Ammonium sulfate (32.4 g) was then added slowly (~10 min) into the supernatant to reach 60% saturation (0.39 g/mL) at 4 ºC. The sample was stirred for another 30 min before being centrifuged at 18,000 rpm for 20 min at 4 ºC. The supernatant was discarded and the pellet was dissolved in 12 mL buffer C. An extra step of centrifugation was performed (21,000 rpm for 20 min at 4 ºC) to

remove un-dissolved pellet. A total of 15 mL supernatant was loaded onto a Sephadex G-25 column (2.5 × 45 cm, ~220 mL) at a flow rate of 4.5 mL/min. Protein fractions (~93 mL, monitored by the Bradford assay) were combined and loaded onto a DEAE Sepharose CL-6B (5 × 14 cm, ~280 mL), washed with 300 mL buffer B, then with 300 mL buffer B containing 80 mM NaCl. The protein was eluted with a 900 × 900 mL linear gradient of buffer B with 80-600 mM NaCl. Protein fractions (12 mL/fraction, 260 mL, monitored by 10% SDS-PAGE) were then concentrated to ~100 mL using an Amicon concentrator with a YM30 membrane. The sample was then centrifuged at 21,000 rpm for 20 min at 4 ºC to remove the protein precipitate. The supernatant was then diluted in 60 mL buffer B to reach a final [NaCl] of ~250 mM before being loaded onto a Q-Sepharose column (5.5 × 4 cm, 75 mL). The column was washed with 250 mL buffer B containing 250 mM NaCl followed by elution with a 750 × 750 mL linear gradient of buffer B with 250-750 mM NaCl. Protein-containing fractions (12 mL/fraction, ~60 mL) determined by Bradford assay and 10% SDS-PAGE were collected and concentrated by an Amicon concentrator with a PM30 membrane to 20 mL before being loaded onto a Sephadex G-25 column (2.5 × 45 cm, ~200 mL) pre-equilibrated with 100 mM HEPES buffer, pH 7.6. Protein fractions (44 mL) were concentrated using an Amicon concentrator with a PM30 membrane to 9.3 mL, before flash freezing in liquid nitrogen and storage at –80 ºC. The final concentration of the apo-β_2-W48F/F208Y is 0.48 mM determined by A_{280nm} (ε_{280nm} = 111 $mM^{-1}cm^{-1}$) (*4*).

Examination of iron incorporation in apo-β_2-W48F/F208Y

In HEPES buffer: To test whether the purified apo-β_2-W48F/F208Y is capable of forming an Fe-catechol cluster upon addition of Fe^{2+}, 50 μM apo-β_2-W48F/F208Y was mixed aerobically at

room temperature with 0, 100, 200 and 400 μM $Fe(NH_4)_2(SO_4)_2$ (prepared freshly in the glove box by following the procedures in the previous section) in 100 mM HEPES, pH 7.6 in a total volume of 100 μL. Subsequent to the addition of Fe^{2+}, the UV-visible spectrum of each sample was recorded on a Varian Cary 3 spectrophotometer.

In crude cell lysate prepared by the French Press: To prepare crude cell lyaste from *E. coli* K-12 wt, an overnight culture (20 mL) from a single colony was inoculated into 1.2 L of LB medium (w/o antibiotics) and grown at 37 ºC, 180 rpm for ~3.5 h (A_{600nm} ~1.8), followed by centrifugation at 4000 rpm for 10 min at 4 ºC. Aliquots of the cell paste (~1g cell paste/tube) were flash frozen in liquid nitrogen and stored at –80 ºC. A yield of 5 g cell paste /L was obtained. The cell paste of wt *E. coli* K-12 (~1 g) was then suspended in 4 mL of 100 mM HEPES, pH 7.6 (containing Roche protease inhibitor cocktail, without EDTA) and disrupted by one passage through the French Press at 14,000 psi. The cell debris was spun down at 21,000 rpm for 20 min at 4 ºC. About 10 mg/mL crude cell lysate was obtained (by the Bradford assay using BSA as a standard).

To monitor the iron incorporation in the presence of crude cell lysate, in a final volume of 100 μL, 50 μM of apo-β_2-W48F/F208Y was incubated with ~15 mg/mL crude cell lysate (both in final concentrations) at room temperature for 5 min and the UV-visible spectrum was recorded. To examine whether exogenous Fe^{2+} could be incorporated into apo-β_2-W48F/F208Y in the presence of crude cell lysate, 5 or 10 μL of 180 mM Fe^{2+} was added into the sample and the UV-visible spectrum was recorded.

In crude cell lyaste prepared by sonication: Cell paste of wt *E. coli* K-12 (1.07 g) was suspended in 2.14 mL 100 mM HEPES, pH 7.6 (containing Roche protease inhibitor cocktail, without EDTA) followed by sonication using VirSonic 100 (SP Industries Co., Gardiner, NY) at a power level 6 for 3 min in a 50 mL centrifuge tube in ice-water bath with stirring. The cell debris was removed by centrifugation at 21,000*g* for 10 min at 4 ºC. About 12.4 mg/mL of crude cell lysate was obtained (Bradford assay using BSA standards). The same procedures as described above were followed to monitor iron incorporation into apo-β_2-W48F/F208Y.

In crude lysate prepared under anaerobic conditions: To prepare oxygen-free samples, 10 mL Novagen Bugbuster solution (with 1 tablet of Roche protease inhibitor cocktail, without EDTA, 250 U of Benzonase nuclease (Novagen, 25 unit/μL)) and ~190 μL of 0.48 mM apo-β_2-W48F/F208Y were degassed on a Schlenk line following the procedures in the section above. The solutions were brought into the glove box in a 4 ºC cold room. About 1 g cell paste of *E. coli* K-12 wt was placed in a 50 mL tube and brought into the glove box with a hole on the cap (punctured with an 18-G needle). The cell paste was suspended in 5 mL Bugbuster solution and transferred into a 35 mL centrifuge tube with a screw cap fitted with a vacuum-greased O-ring. The cell suspension was shaken gently on a vortex mixer for 30 min, removed from the glove box and centrifuged at 16,000*g* for 20 min at 4 ºC. The centrifuge tube was brought back into the glove box and the supernatant was transferred into a 15 mL tube. The concentration of the crude cell lysate was ~10 mg/mL determined by the Bradford assay using BSA as a standard.

To monitor iron incorporation into apo-β_2-W48F/F208Y, in a final volume of 100 μL, 50 μM apo-β_2-W48F/F208Y was mixed with ~10 mg/mL anaerobic crude cell lyaste with or without a 400 μM Fe^{2+} (90 mM stock solution) in a 1.5 mL eppendorf tubes (final concentrations

are indicated in all cases). The eppendorf tubes were removed from the glove box and exposed to oxygen. The UV-visible spectrum was then immediately recorded.

Iron incorporation in wt apo-β_2

WT apo-β_2 was prepared by following published procedures (*27*). Similar procedures for monitoring iron incorporation in buffer or in the presence of crude cell lysates were followed as described in the previous section. WT apo-β_2 (50 μM) was mixed with 1 mM $Fe(NH_4)_2(SO_4)_2$ in 100 mM HEPES, pH 7.6 under aerobic conditions and the UV-visible spectrum was recorded (final concentrations are indicated in all cases). Alternatively, wt apo-β_2 (50 μM) was mixed with ~10 mg/mL of crude cell lysate (prepared by sonication) under aerobic conditions and the UV-visible spectrum was recorded (final concentrations are indicated in all cases). $Fe(NH_4)_2(SO_4)_2$ solution was then added to this mixture to a final concentration of 1 mM and the UV-visible spectrum was recorded again. The quantitation of the tyrosyl radical was made by the dropline method using $\varepsilon_{410nm} = 1.7\ mM^{-1}cm^{-1}$ (*28*).

Cloning of *nrdB* with different affinity tags

pTB2-R2 was used as a PCR template (*29*). To generate pBAD-N-S-*nrdB* (N-terminal StrepII-tagged β_2), a 5' primer containing a StrepII-tag (WSHPQFEK) and a five amino acid linker (ALGGH) was used (5'-AAT TAA **CCA TGG** CG*T GGA GCC ACC CGC AGT TCG AAA AA*T CTC TGG GCG GCC ATA TGG CAT ATA CCA CCT TTT CAC-3'. The *Nco*I restriction site including the start codon is in bold, the five amino acid linker is underlined, and the StrepII-tag is shown in italics. The 3' primer was 5'-AAC GC**C TCG AG**T CAG AGC TGG AAG TTA CTC AAA TCG-3' (*Xho*I restriction site (bold) and the last 25 nucleotides of *nrdB*

including the stop codon are underlined). Pfu-Ultra DNA polymerase was used for PCR following the manufacturer's protocol (Invitrogen). The PCR product and the pBAD-myc-HIS-A vector (Invitrogen) were digested with a 10 fold excess of *Nco*I and *Xho*I and ligated with T4 DNA ligase (Promega) in a vector to insert ratio of 1:2.

To make pBAD-C-S-*nrdB* (C-terminal StrepII-tagged β_2), the forward primer, 5'-AGG ACA CAC **CCA TGG** CAT ATA CCA CCT TTT CAC-3' which contains a *Nco*I site (bold) and the first 22 nucleotides of the *nrdB* (underlined) was used. The reverse primer was 5'-AAC GC**C TCG AG**T CA*T TTT TCG AAC TGC GGG TGG CCC A*GA GCT GGA AGT TAC TCA AAT C-3' which contains a *Xho*I site (bold) followed by a stop codon, a StrepII tag gene (italics) and the last 21 nucleotides of *nrdB* excluding the stop codon (underlined). The cloning procedures were the same as for the pBAD-N-S-*nrdB*. To make pBAD-*nrdB* (with no tag), the forward primer used to make pBAD-C-S-*nrdB* and the reverse primer to make pBAD-N-S-*nrdB* were used, cut with the appropriate restriction enzymes and cloned into pBAD-myc-HIS-A.

To construct the internal affinity tagged *nrdB*, pBAD-*nrdB* was used as a PCR template and the genes encoding affinity tags were introduced into *nrdB* (between N179 and G180 of β) (*1*) by site-directed mutagenesis (SDM) PCR following the manufacturer's protocol (Stratagene). To make pBAD-I-S-*nrdB* (internal StrepII-tagged β_2), a forward primer 5'-GTA CCC ACA CCG TTA ACT GGA GCC ACC CGC AGT TCG AAA AAG GTA AAA CTG TGA CCG-3' (underlined: StrepII tag gene) and its complementary reverse primer were used for SDM. To make pBAD-I-H-*nrdB* (internal His-tagged β_2), a forward primer 5'-GTA CCC ACA CCG TTA ACC ATC ATC ATC ATC ATC ATG GTA AAA CTG TGA CCG-3' (underlined: 6xHis tag gene) and its complementary reverse primer were used for SDM.

The *nrdB* constructs containing the E115A mutation, were made by using the corresponding wild type plasmids (pBAD-N-S-*nrdB*, pBAD-C-S-*nrdB*, pBAD-I-S-*nrdB*, pBAD-I-H-*nrdB*) as templates and a forward primer 5'-CCT GGG CGT TCT CAG CGA CGA TTC ATT CCC GTT CC-3' and its complementary reverse primer for SDM PCR. The sequences of all constructs were confirmed by DNA sequencing at the MIT Biopolymers Laboratory.

Protein co-purification

Cell growth: Overnight cultures (0.25 mL, 16 h growth) from a single colony of TOP10 cells containing plasmid pBAD-N-S-nrdB, pBAD-C-S-nrdB, pBAD-I-S-nrdB, or pBAD-I-H-nrdB (wt or E115A mutant) (**Table 4-2**) were inoculated into 50 mL LB-ampicillin (100 μg/mL) in 250 mL flasks and grown at 37 ºC, 200 rpm until A_{600nm} was between 0.5 to 1.0. Unless otherwise specified, the expression of proteins was induced by 0.01 mM L-arabinose and grown for another 2 h before the cells were harvested by centrifugation at 4,000 rpm for 20 min at 4 ºC. About 0.3 to 0.4 g of cell paste was obtained. The cells were flash frozen in liquid nitrogen and stored at –80 ºC.

Protein co-purification under aerobic conditions: The protein purifications were performed at 4 ºC. **Buffer C** (100 mM Tris, pH 8.0 at 4 ºC, 150 mM NaCl, 5% glycerol) supplemented with protease inhibitor cocktail (Roche, EDTA-free) was prepared. The cell paste (~0.5 g) was suspended in 5 mL buffer C/g of cell paste and cracked open by one passage through the French Press at 16,000 psi followed by centrifugation at 21,000*g* for 30 min at 4 ºC. The supernatants were loaded onto Strep-Tactin Sepharose columns (0.2 mL resin volume, 0.4 × 1.5 cm, IBA GmbH, St. Louis, MO) by gravity flow. The column was washed with 2 mL of buffer C before

being eluted with 2 mL of buffer C containing 2.5 mM desthiobiotin (Sigma). Fractions (0.5 mL) of the wash and of the eluent (0.3 mL) were collected and analyzed on 15% SDS-PAGE and the UV-visible spectra were recorded. The iron content of the fractions with the highest protein concentration was determined by the ferrozine assay (*25*).

Protein co-purification under anaerobic conditions: To test for proteins that co-purify with affinity tagged β_2 under anaerobic conditions, the following four reagents were degassed with stirring by three cycles of evacuation (~30 min) and refill with Ar (~10 min) on a Schlenk line before being brought into the glove box in a cold room at 4 ºC: **1.** Wash buffer: 100 mL of 100 mM Tris-HCl pH 8.0, 20% glycerol, **2.** Elution buffer: 50 mL of buffer C with 2.5 mM desthiobiotin, **3.** Lysis buffer: 10 mL Bugbuster solution (Novagen) containing one tablet of protease inhibitor cocktail (Roche, complete-mini, EDTA-free) and benzonase nuclease (250 U, Novagen), **4.** 5 mL of Strep-Tactin resin (50% suspension in 100 mM Tris-HCl, 150 mM NaCl, 1 mM EDTA, pH 8.0).

About 0.5 g of the cell paste of TOP10-pBAD-C-S-*nrdB* (wt or E115A mutant; in 50 mL Falcon tubes with a hole in the caps made by an 18-G needle) were brought into the glove box after three cycles of evacuation (~10 min)-refill (with N_2) in the antechamber. The cell pastes were suspended in 2.5 mL Bugbuster solution, transferred into 35 mL centrifuge tubes with screw caps fitted with greased O-rings and shaken gently on a vortex mixer for 30 min in the glove box before being taken out and centrifuged at 16,000*g* for 20 min at 4 ºC. After the centrifugation, the centrifuge tubes were brought back into the glove box and the supernatants were loaded onto Strep-Tactin columns (~0.35 mL resin). The columns were then washed with 5 mL 100 mM Tris-HCl, pH 8.0, 20% glycerol (1 mL/fraction) and eluted with 3.6 mL buffer C

containing 2.5 mM desthiobiotin (0.6 mL/fraction). From the cell lysis to elution of the protein took ~1.5 h. The fractions were analyzed by 15% SDS-PAGE and the Bradford assay.

Non-specific cross-linking by addition of formaldehyde into cell cultures: An overnight culture (0.75 mL, 16 h growth) from single colonies of TOP10-pBAD-N-S-nrdB or TOP10-pBAD-C-S-nrdB (wt or E115A mutant) was inoculated into 150 mL LB-ampicillin (100 μg/mL) in 500 mL flasks and grown at 37 ºC, 200 rpm until A_{600nm} ~ 0.6. At this point 5 mM L-arabinose was added and the cells were grown for an additional ~3 h before 1% formaldehyde (Mallinckrodt, 37% stock) was added into the culture. Aliquots (50 mL) of the cell culture were taken 20 or 40 min after addition of formaldehyde and glycine (acid form) was added to a final concentration of 0.125 M. The samples were mixed in a roller drum at 37 ºC for 20 min followed by centrifugation at 3,000 rpm for 10 min at 4 ºC. The cells were lysed by the French Press and the proteins were purified by the Strep-Tactin columns as described above.

Non-specific cross-linking by addition of formaldehyde to crude cell lysate: To prepare the cell lysis buffer, 10 mL of Bugbuster (primary amine-free, Novagen 70923) was added with 250 U benzonase nuclease and one tablet of protease inhibitor cocktails (Roche, complete mini EDTA-free). Cell paste (~0.5 g) of TOP10-pBAD-C-S-nrdB (wt or E115A mutant) was suspended with 50 mL of PBS (Invitrogen) at 4 ºC followed by centrifugation at 4000 rpm for 15 min at 4 ºC. The supernatant was discarded and the cell paste was suspended in 2.5 mL of the lysis buffer. The cell suspension was shaken gently at room temperature for 20 min before centrifugation at 16,000g for 20 min at 4 ºC. The cell crude lysate was then mixed with 3% formaldehyde (Mallinkrodt, 37% stock) followed by incubation at room temperature for 20 min before addition

of 0.125 M glycine (acid form, 2 M stock solution in water). The crude cell lysate was incubated at room temperature for another 1 h before being centrifuged at 4,000 rpm for 15 min at 4 ºC. The supernatant was filtered through a 0.45 μm disc filter (Millipore) fit to a 3 mL syringe before being loaded onto a Strep-Tactin column (0.2 mL resin). The column was washed with 5 mL PBS and 1 mL fractions were collected. The protein was then eluted with 2.5 mL buffer C with 2.5 mM desthiobiotin and 0.5 mL fractions were collected. The fractions were analyzed by the Bradford assay and 15% SDS-PAGE.

Cell growth and protein co-purification with I-H-β_2: An overnight culture (0.3 mL, 16 h growth) from a single colony of TOP10-pBAD-I-H-nrdB (wt or E115A mutant) was inoculated into 60 mL LB-ampicillin (100 μg/mL) in 250 mL flasks and grown at 37 ºC, 200 rpm until A_{600nm} reached ~0.9. The protein expression was induced by 0.5 mM L-arabinose and the cells were grown for another 3.5 h before being harvested at 3,500 rpm for 10 min at 4 ºC. The cell paste (0.3 g) was flash frozen in liquid nitrogen and store at –80 ºC.

To look for proteins that co-purify with I-H-β_2, the cell paste was suspended in 1.5 mL **buffer D** (50 mM Na_2HPO_4, pH 7.0, 10 mM imidazole) and the cells were cracked open by one passage through the French Press at 14,000 psi, followed by centrifugation at 21,000g for 20 min at 4 ºC. The crude cell lysate was mixed with ~0.5 mL Ni-NTA agarose resin (Qiagen) and shaken gently at 4 ºC for ~1 h before being loaded onto an empty column (0.5 cm diameter). The column was washed with 4 mL buffer D (1 mL fractions were collected) and eluted with 2.5 mL buffer D containing 250 mM imidazole (0.5 mL fractions were collected). The eluents were analyzed by Bradford assay and 15% SDS-PAGE.

Non-specific cross-linking of internal His-tagged β_2 by addition of formaldehyde into the cell culture: An overnight culture (2.5 mL, ~16 h of growth) from a single colony of TOP-pBAD-I-H-nrdB (wt or E115A mutant) was inoculated into 500 mL LB-ampicillin (100 μg/mL) in a 2.8 L baffled flask and grown at 37 ºC, 200 rpm until A_{600nm} reached ~0.5, at which point 0.05 mM L-arabinose was added and the cells were grown for another 2 h. Aliquots (45 mL) of the cell culture were transferred into 250 mL flasks and formaldehyde was added to final concentrations of 0.4, 1 and 3%. The cells were grown for 15, 30 and 50 min at 37 ºC before the addition of glycine (0.1, 0.5 and 1 mM, corresponding to the concentration of formaldehyde). The culture was grown for an additional 20 min at 37 ºC before centrifugation at 5,000 rpm for 10 min at 4 ºC. Cell paste, 0.2~0.4 g, was obtained.

Because of the quantity of the samples, Ni-NTA spin columns (Qiagen) were used for rapid co-purification. The lysis buffer (**buffer E:** 50 mM NaH_2PO_4, 300 mM NaCl, 10 mM imidazole, pH 8.0) was supplemented with the Roche protease inhibitor cocktail (complete mini, EDTA-free) and the cell paste was suspended in 4 mL buffer E/g of cell paste followed by two passages through the French Press at 14,000 psi. The cell debris was spun down at 12,500 rpm for 20 min at 4 ºC. The supernatant (0.6 mL) was then loaded onto the spin columns (~0.2 mL Ni-NTA resin, Qiagen), washed with 1.8 mL of buffer E containing 20 mM imidazole and eluted with 0.4 mL of buffer E containing 250 mM imidazole. The eluents were analyzed by Bradford assay and 4-20% gradient SDS-PAGE.

Protein bands of cross-linked species on the SDS-PAGE were excised and sent to Proteomics Core Facility of the Koch Institute in MIT for in-gel trypsin digestion and LC-MS/MS analysis.

Measuring Y• concentration in the whole cells by EPR spectroscopy

To prepare the cells for EPR spectroscopy, a single colony of cells (wt or deletion strains) harboring pBAD-nrdB was inoculated into 7 mL LB-ampicillin (100 μg/mL) and grown at 37 ºC in a roller drum for ~16 h. The overnight culture (2.5 mL) was inoculated into 500 mL LB-amp (100 μg/mL) in a 2.8 L baffled flask containing ~5 drops of antifoam reagent (Sigma) and grown at 37 ºC, 200 rpm. When A_{600nm} reached ~0.8, L-arabinose was added to a final concentration of 0.5 mM and the cells were grown for additional 2 h before being harvested by centrifugation at 8500g for 20 min at 4 ºC. The cell paste was then transferred into a 50 mL centrifuge tube and centrifuged at 2000 rpm for 5 min at 4 ºC. Residual liquid was removed by a pipetman before the mass of cell paste was measured. The cell paste was then suspended in 1 mL buffer C/g cell paste by pipetting repetitively for ~2-3 min to ensure complete suspension. The cell suspension was then transferred into EPR tubes using a 12-inch Pasteur pipette followed by flash freezing in liquid nitrogen before analysis.

In order to measure the consistency of the cell packing in the EPR tubes, the cell suspension of the EPR samples was serial diluted 2000 fold and A_{600nm} was measured on the HP diode-array spectrophotometer (Agilent 8453). The average A_{600nm} from six different EPR samples is 0.38 with a standard deviation of ~1.6% ($A_{600nm} \pm 0.01$), indicating the cell packing in the EPR tubes was reproducible between samples. The level of overexpression of β_2 upon arabinose induction was monitored by 4-20% gradient SDS-PAGE.

EPR spectra were recorded using a Bruker ESP-300 X-band (9.4 GHz) spectrometer at 77 K using a liquid nitrogen cooled finger dewar. Typical parameters used to record the spectra were: 9.38 GHz frequency, 0.05 mW power, 1.5 G modulation amplitude, time constant 2.52 ×

10^3, and 10 to 20 scans. The spin quantitation was carried out using a $CuSO_4$ standard (30) and Win-EPR software (Bruker).

Monitoring the iron loading in overexpressed β_2 by whole cell Mössbauer spectroscopy

Preparation of whole cell Mössbauer sample: A $^{57}Fe^{3+}$ stock solution (158 mM) was prepared as previously described in Chapter 2. TOP10 cells were grown in LB media which contains ~12 μM ^{56}Fe determined by the ferrozine assay. An overnight culture of TOP10-pBAD-*nrdB* (1 mL) was inoculated into 500 mL LB supplemented with 100 μg/mL ampicillin and 50 μM $^{57}Fe^{3+}$ in a 2.8 L baffled flask. The cells were grown at 37 ºC, 200 rpm until A_{600nm} was ~0.5. Arabinose (0.5 mM) was added into the culture and the cells were grown for another 2 h (A_{600nm} ~ 1.7) before being harvested by centrifugation at 7000*g* for 20 min at 4 ºC. The cell pastes were packed directly into custom-designed Mössbauer cups (~450 μL, filled up to the top marker inside the Mössbauer cups). **Scheme 4-1** shows the steps of packing the cell paste into Mössbauer cups. To ensure consistency of cell packing, a small aliquot of the cell paste was taken using a metal spatula and transferred into the bottom of the Mössbauer cup. This small aliquot of the cell paste was then pushed gently to the corner of the Mössbauer cup to ensure no bubbles were trapped inside the cup. This step was repeated several times until the cell paste was filled up to the first marker of the Mössbauer cup. A control experiment was carried out under identical growth conditions, but no arabinose was added.

Scheme 4-1

Mössbauer spectroscopy: Mössbauer spectra were recorded on a spectrometer from Web Research (Edina, MN), equipped with a SVT-400 cryostat from Janis Research Company (Wilmington, MA). Spectra were collected in constant acceleration mode in transmission geometry. Isomer shifts are quoted relative to the centroid of α-Fe at room temperature. Spectra were analyzed with the program WMOSS from Web Research (Edina, MN).

Whole cell Mössbauer samples taken at different time points after arabinose induction

Test of different growth conditions for optimal β_2 expression in short periods of time: In order to monitor the change of iron populations inside the cells during the early stage of β_2 over-production, optimal induction conditions which result in maximum increase of [Y•] with minimum cell growth needed to be found. Therefore, experiments with cells induced at different growth stages by addition of 0.5 mM arabinose with growth continued for different amounts of time were carried out. An overnight culture (2 mL) from a single colony of TOP10-pBAD-*nrdB* was inoculated into 500 mL LB-ampicillin (100 μg/mL) supplemented with 50 μM $FeCl_3$ (50 mM stock in 0.01 N HCl) and grown in a 2.8 L baffled flask at 37 ºC, 200 rpm. β_2 expression was induced by 0.5 mM L-arabinose at A_{600nm} ~ 0.5, 1.0, and 1.5. After 10 and 20 min (and 2 h for the A_{600nm} ~ 0.5 sample), aliquots (200 mL) of the culture were centrifuged at 8000*g* for 10 min at 4 ºC. The cell paste was suspended in 1 mL buffer C/g cell pastes and loaded into EPR tubes for analysis.

Preparation of whole cell Mössbauer samples: An overnight culture (7 mL) from a single colony of TOP10-pBAD-*nrdB* was inoculated into 1.2 L LB-Amp (100 μg/mL) supplemented

with 50 μM ^{57}Fe and grown in a 6 L flask at 37 ºC, 200 rpm until A_{600nm} reached ~1.5. Part of the culture (300 mL) was taken as the zero time point sample before L-arabinose addition. The remaining 0.9 L of the cell culture was induced with 0.5 mM L-arabinose and grown for an additional 10, 20, and 40 min. For Mössbauer spectroscopy analysis, 250 mL of the cell culture was centrifuged at 8,000*g* for 10 min at 4 ºC and the cell paste was packed directly into custom-designed Mössbauer cups (~450 μL, filled up to the top marker inside the Mössbauer cups) as described above. For EPR analysis, 50 mL cell culture was centrifuged at 4,000 rpm for 15 min at 4 ºC and the cell paste was resuspended in 1 mL buffer C/g cell paste and loaded into EPR tubes. Recordings of the Mössbauer and EPR spectra were carried out as described above.

Table 4-1. List of common buffers used in this chapter

Buffers	***Composition***
A	50 mM Tris-HCl, 150 mM NaCl, pH 7.6
B	50mM Tris-HCl, 5% (w/v) glycerol, 1 mM 1,10-phenanthroline, 0.25 mM PMSF, pH 7.6 at 4 ºC
C	100 mM Tris, pH 8.0 at 4 ºC, 150 mM NaCl, 5% glycerol
D	50 mM Na_2HPO_4, pH 7.0, 10 mM imidazole
E	50 mM NaH_2PO_4, 300 mM NaCl, 10 mM imidazole, pH 8.0

Table 4-2. List of *E. coli* strains and plasmids used in this chapter.

Strain or plasmid	Description	Reference
***E. coli* strains**		
K-12	Wild type (F^+)	*E. coli* genetic stock center #7296
W3110	Wild type (F^- λ^- IN(*rrn*D-*rrn*E)1 rph^{-1})	(*31*)
BW25113	K-12 derived: (*lacI*q *rrnB*T14 Δ*lacZ*WJ16 *hsdR514* Δ*araBAD*AH33 Δ*rhaBAD*LD78)	(*32*)
TOP10	F^- *mcr*A Δ(*mrr-hsd*RMS-*mcr*BC) ϕ80*lacZ*ΔM15 Δ*lac*X74 *deo*R *rec*A1 *ara*D139 Δ(*ara-leu*)7697 *gal*U *gal*K *rps*L (Str^R) *end*A1 *nup*G	(*33*, *34*)
BL21(DE3)	F^- *omp*T *gal dcm lon hsd*S_B(r_B^- m_B^-) λ(DE3 [*lac*I *lac*UV5-T7 gene 1 *ind*1 *sam*7 *nin*5])	(*35*)
GR536	W3110 *fecABCDE*::*kan zupT*::*cat mntH entC feoABC*	(*23*)
GR537	W3110 *fecABCDE*::*kan mntH*::*cat entC feoABC*	(*23*)
GR538	W3110 *fecABCDE*::*kan zupT*::*cat entC feoABC*	(*23*)
GR499	W3110 *zupT*::*cat mntH feoABC entC*	(*23*)
ΔfepA	BW25113 *fepA::kan* (ferric-enterobactin outer membrane transporter)	(*24*)
ΔfecA	BW25113 *fecA::kan* (ferric-citrate outer membrane transporter)	(*24*)
ΔfhuA	BW25113 *fhuA::kan* (ferric-hydroxamate outer membrane transporter)	(*24*)
ΔfhuE	BW25113 *fhuE::kan* (ferric-hydroxamate outer membrane transporter)	(*24*)
ΔfeoB	BW25113 *feoB::kan* (ferrous iron inner membrane permease)	(*24*)
ΔmntH	BW25113 *mntH::kan* (divalent cation inner membrane permease)	(*24*)
ΔzupT	BW25113 *zupT::kan* (divalent cation inner membrane permease)	(*24*)
Plasmids		
pBAD-*nrdB*	pBAD containing β	(*18*)
pBAD-N-S-*nrdB*	pBAD containing N-terminal StrepII-β	(*18*)
pBAD-C-S-*nrdB*	pBAD containing N-terminal StrepII-β	(*18*)
pBAD-I-S-*nrdB*	pBAD containing interal StrepII-β (inserted between N179 and G180 of β)	This study
pBAD-I-H-*nrdB*	pBAD containing interal 6×His-β (inserted between N179 and G180 of β)	This study
pET-*cyaY*	pET containing GST-6xHis-CyaY	(*22*)
pR2-W48F/F208Y	*E. coli* β_2 W48F/F208Y mutant	(*4*)
pR2-F208Y	*E. coli* β_2 F208Y mutant (with an additional V141I mutation)	(*4*)

Table 4-3. List of primers for verification of single gene deletion strains[a].

Target gene	primers	Note
ΔfepA-5′	CTGCGTGTCTTTCAGGATCA	Ferric-enterobactin outer
ΔfepA-3′	CGCACTTTGTCAACAATCTG	membrane transporter
ΔfecA-5′	TCGTTCGACTCATAGCTGAA	Ferric-citrate outer
ΔfecA-3′	AAAAGCCCGGCAAGCCGGGC	membrane transporter
ΔfhuA-5′	ATCATTCTCGTTTACGTTAT	Ferric-hydroxamate outer
ΔfhuA-3′	GCACGGAAATCCGTGCCCCA	membrane transporter
ΔfhuE-5′	CCTCCTCCGGCATGAGCCTG	Ferric-hydroxamate outer
ΔfhuE-3′	CAGATGGCTGCCTTTTTTAC	membrane transporter
ΔfeoB-5′	CTTATTAGAAGTGGAAGCGG	Ferrous iron plasma
ΔfeoB-3′	CAAATCGCGCACCTGAATAA	membrane transporter
ΔmntH-5′	TTGGCATAGCATGAAACATA	Divalent cation plasma
ΔmntH-3′	CAATAGTGCCAGATGCGACG	membrane transporter
ΔzupT-5′	ATCCGGGTTCTTACTCCGCC	Divalent cation plasma
ΔzupT-3′	ACCGGATGGCACTCGCCATC	membrane transporter

[a]Sequences of all primers depicted from 5′ to 3′

RESULTS

I. Purification and characterization of *E. coli* frataxin, CyaY

Because of the recent discoveries of the roles of frataxin in the iron delivery for ferrochelatases, aconitases, or proteins requiring FeS clusters, we decided to evaluate whether a Fe^{2+}-loaded frataxin (CyaY in *E. coli*) can function as an iron chaperone in *E. coli* to deliver iron to apo-β_2 (*36-38*). A construct, pET-*cyaY*, was obtained (*22*), that contains a GST tag, a 6xHis tag, and a TEV (tobacco etch virus) protease restriction site before *cyaY*. DNA sequencing results revealed that the amino acid sequence in the N-terminal region of CyaY is -ENLYFQGA**M**GND-, with the TEV protease site underlined and the first amino acid (Met) of CyaY in bold. An additional amino acid, Gly, was inserted between the first (Met) and the second (N) amino acid of CyaY, probably for the purpose of cloning. After TEV protease treatment to cleave off the affinity tag, the N-terminus of CyaY contains **GA**M**G**ND-, with the additional amino acids indicated in bold. The calculated molecular mass is 12416.6 Da with a total of 109 amino acids including the three additional amino acids.

The pET-*cyaY* plasmid was transformed into *E. coli* BL21(DE3) cells and protein expression was induced at A_{600nm}~0.8 by addition of 0.5 mM IPTG and grown for an additional 4 h. The induction gel is shown in **Figure 4-2**: leakage of protein expression was observed before IPTG induction and the protein was further expressed after induction. The predicted molecular mass of GST-His-CyaY is ~40 kDa. The GST-His-CyaY was purified on a Ni-affinity column followed by a Sephadex G-25 column to remove the imidazole in the elution buffer for the Ni-column. The eluents from the G-25 column were first concentrated by an Amicon concentrator with a YM30 membrane; most of the protein was found in the filtrate. Therefore, an Amicon concentrator with a YM3 membrane was used to concentrate the protein. The purity and yield of

protein purified in each chromatography step is shown in **Figure 4-2** and **Table 4-4.** A total of 390 mg of GST-His-CyaY was obtained from 2 L of LB culture (~4.9 g of cell paste).

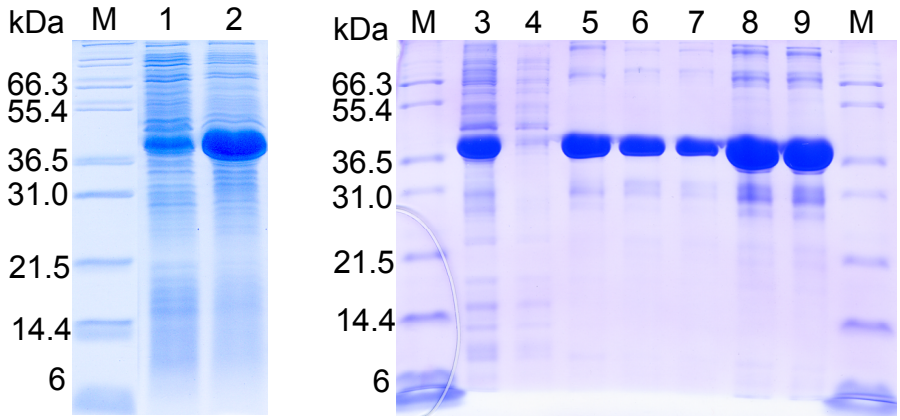

Figure 4-2. Induction and purification of GST-His-CyaY monitored by 15% SDS-PAGE. M: marker, lane 1: before induction, lane 2: after induction (0.5 mM IPTG), lane 3: crude cell lysate, lane 4: Ni-column flow through, lane 5: after Ni-column, lane 6: after Sephadex G-25, lane 7: YM30 filtrate, lane 8 and 9: YM3 concentrate.

Table 4-4. Efficiency of each purification step for GST-His-CyaY

	Volume (mL)	Concentration (mg/mL)	Total protein (mg)	Yield (%)
Crude cell lysate	32	38.2	1222	
Flow through	46	5.4	248	20
Ni column	19	36.8	699	57
G-25	54	10.5	567	46
YM30 filtrate	45	9.6	432	35
YM3 concentrate	6.5	60	390	32

Removal of the ~28 kDa GST-His tag was accomplished by TEV protease digestion. According to the manufacturer's protocol, one unit of TEV protease cleaves 85% of a 3 μg control substrate in 1 h at 30 ºC. Because the actual cleavage efficiency depends on the substrates, different amounts of TEV protease and GST-His-CyaY were tested for complete digestion and the results examined by 15% SDS-PAGE. The optimal digestion condition was found to be 0.7 unit of TEV per mg of GST-His-CyaY. A large-scale digestion was performed and the cleaved GST-His tag was separated from CyaY by passage through a Ni-column. The purification of CyaY was not successful due to incomplete digestion of the protein.

A higher TEV:GST-His-CyaY ratio was tested (1 U TEV/mg GST-His-CyaY) but incomplete digestion, (~55 mg scale) still persisted. Therefore, size-exclusion chromatography was used to purify CyaY. **Figure 4-3** shows the elution profile and the components of eluent analyzed by SDS-PAGE. In order to completely remove the residual GST-His tag contaminant, the concentrated CyaY was re-chromatographed on the same column; highly pure CyaY was isolated (**Figure 4-4**).

The purified CyaY was characterized by UV-visible spectroscopy and LC-ESI-MS spectrometry (**Figure 4-5**). The UV-visible spectrum showed no feature at ~350 nm that is indicative of Fe^{3+}-binding (*38*) and a ferrozine assay analysis detected no Fe. The LC-ESI-MS spectrometry shows a single peak corresponding to a CyaY monomer. The measured molecular mass (12418.5 Da) is about 2 Da higher than the predicted molecular mass (12416.6 Da, including the three extra amino acids), which could be due to a different protonation state of the protein or errors from calibration of the instrument.

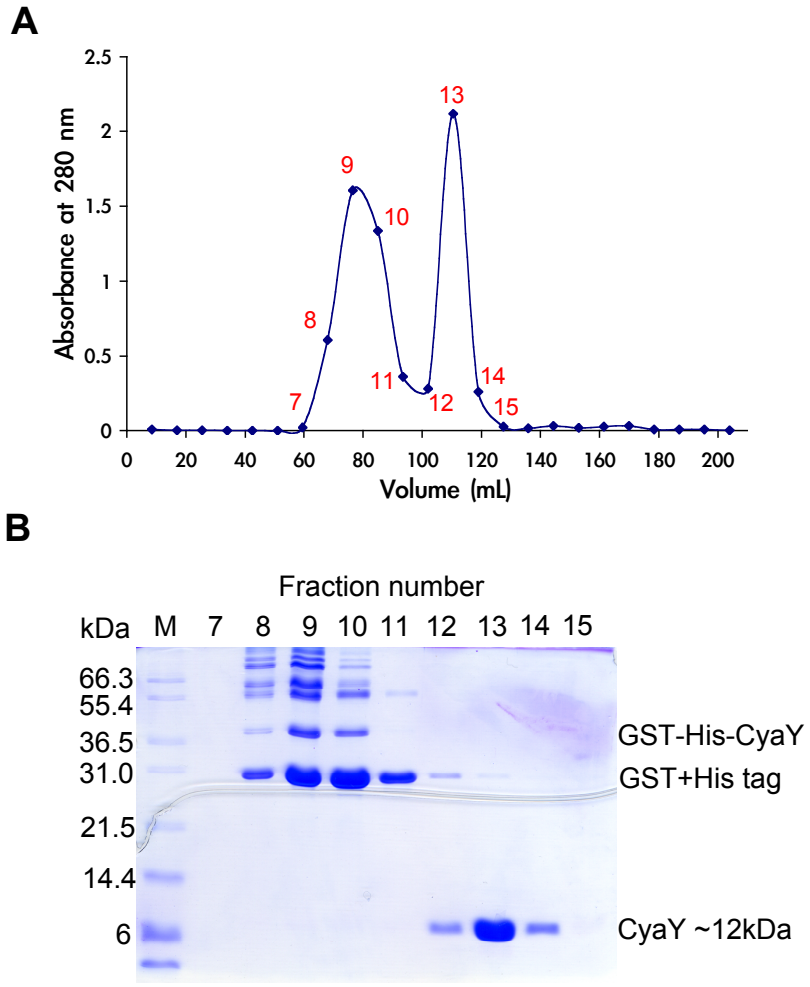

Figure 4-3. Purification of CyaY from GST-His tag by size-exclusion chromatography. Purified GST-His-CyaY was treated with rTEV protease to cleave the GST-His affinity tag. The protein was purified on a Superdex-75 column (A) and the eluents were examined on a 15% SDS-PAGE (B). Fractions in (A) that were loaded onto the SDS-PAGE are labeled in red.

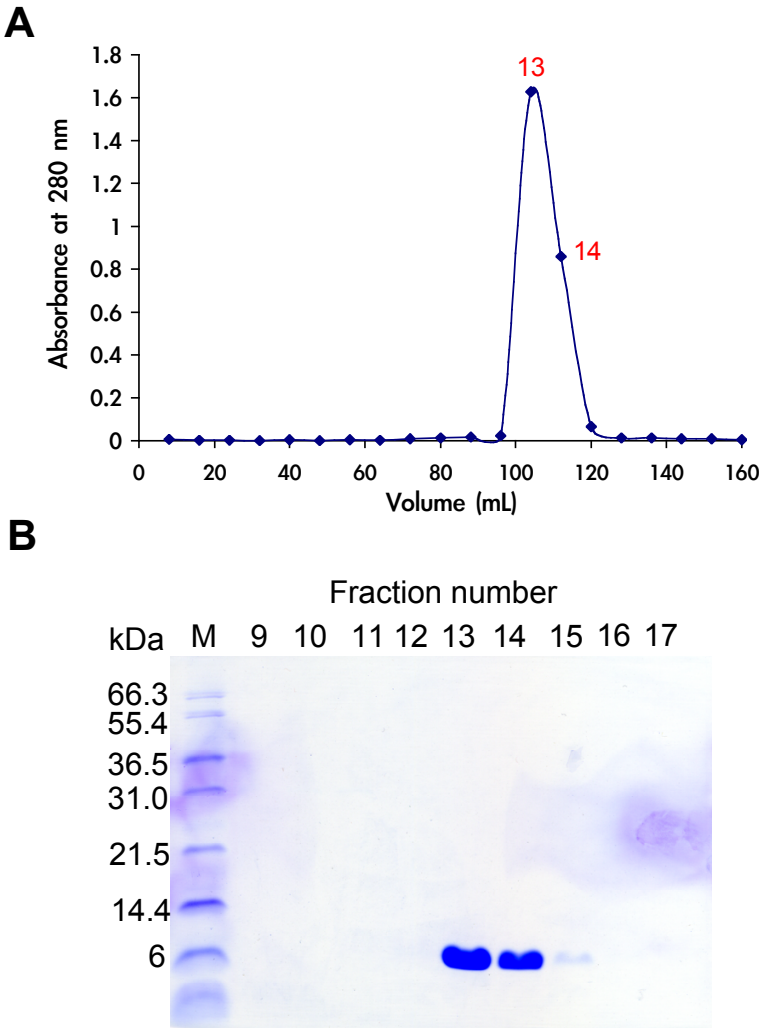

Figure 4-4. Re-chromatography of CyaY on a Superdex-75 column. Fractions (12 to 14) in **Figure 4-3** were combined, concentrated and loaded on to the same size-exclusion column to completely remove the residual GST-His tag in the sample. The eluents were analyzed by A_{280nm} (A) and 15% SDS-PAGE (B). The corresponding fractions in (B) are labeled on (A) in red.

A

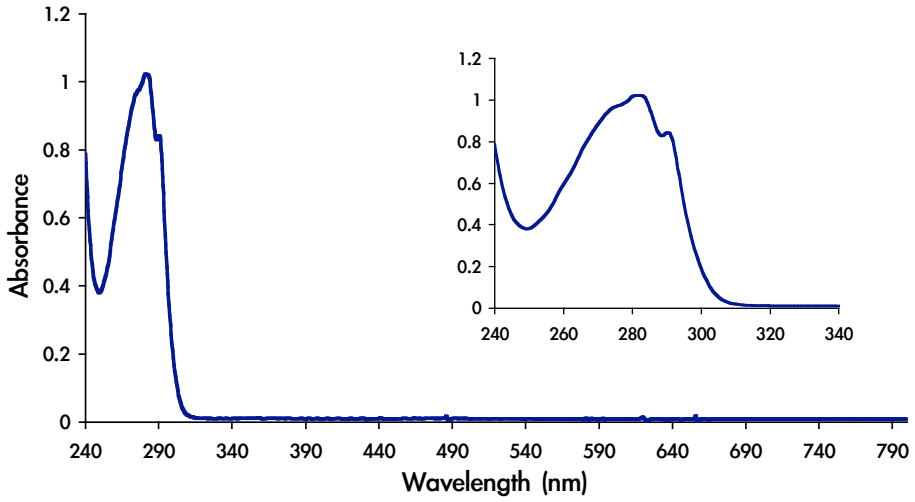

B

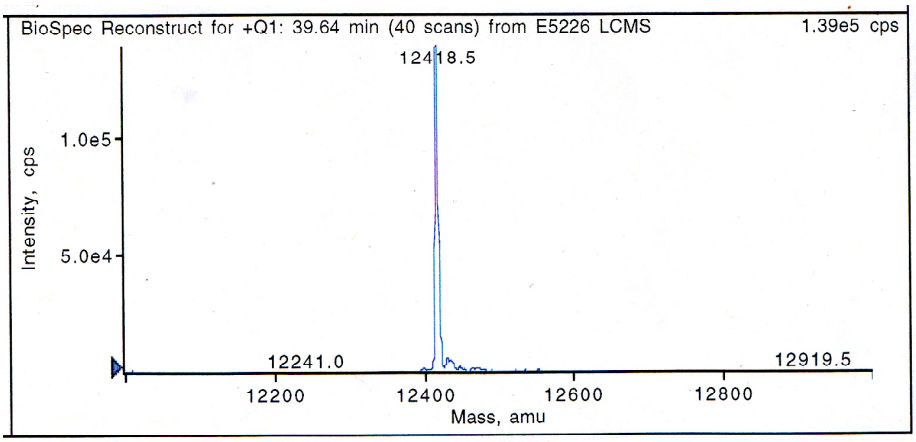

Figure 4-5. UV-visible (A) and LC-MS (B) spectra of CyaY. (A) No feature that may be associated with Fe-binding was observed in the UV-visible spectrum of CyaY. Inset: blow up at the UV region. (B) LC-ESI-MS of CyaY shows a single peak at 12418.5 Da, which is close to the theoretical molecular mass of CyaY (12416.6 Da).

Because the iron delivered to apo-β_2 needs to be in the ferrous form, we first tested whether a ferrous iron-loaded CyaY could be isolated. CyaY was incubated with a 10-fold excess Fe^{2+} (assuming 2 Fe^{2+} bind to 1 CyaY) in 50 mM Tris-HCl, 150 mM NaCl, pH 7.6, for 30 min at room temperature under strict anaerobic conditions. The sample was then passed through a Sephadex G-25 column to remove unbound Fe^{2+}. A_{280nm} of the eluents was recorded on a multi-plate reader and a ferrozine assay of each fraction was carried out. No Fe was detected in the protein fractions, suggesting that Fe^{2+} had dissociated from CyaY during the Sephadex G-25 chromatography due to its high K_d (~4 μM) (*26*).

Even though the purification of Fe^{2+}-CyaY was not successful in our hands, isolation of Fe^{2+}-CyaY was reported a year later by incubation of a 15-fold molar excess Fe^{2+} with CyaY for 2 h at 4 ºC followed by passage through a commercial Sephadex G-25 column (NAP-10, GE Healthcare) (*38*). The successful isolation of Fe^{2+}-CyaY could be due to higher [Fe^{2+}] (15-fold vs 10-fold), longer incubation time (2 h vs 30 min), lower incubation temperature (4 ºC vs room temperature), or a smaller Sephadex G-25 column (1 mL (sample size unknown) vs 20 mL (0.48 mL sample)). A ferrozine assay showed a stoichiometry of ~2.5 Fe^{2+}/CyaY. However, the Fe^{2+} was found to dissociate from CyaY upon repeated dilutions (1.5-fold each time, three times), or treatment with 60-fold excess EDTA or citrate; therefore, an Fe^{3+}-loaded CyaY in the presence of chemical reductants was used to demonstrate its iron chaperone activity by these workers (see Chapter 1) (*38*).

More recently, an Fe^{2+}-loaded frataxin from *Drosophila* was shown to deliver its Fe^{2+} into ISU, an FeS cluster scaffold protein (*39*). However, the Fe^{2+}-frataxin was prepared by 1:1 mixture of 100 μM Fe^{2+} and frataxin (K_d ~6 μM) without further purification. In their case, a faster observed rate constant of the formation of $[2Fe2S]^{2+}$-ISU was observed in the presence of

frataxin (~0.1 min^{-1}) relative to its absence (< 0.02 min^{-1}), suggesting a frataxin-mediated iron delivery into apo-ISU. However, given the fast self-assembly of apo-β_2 in the presence of Fe^{2+} and O_2, it may be challenge to distinguish whether the incorporation of Fe^{2+} in apo-β_2 is mediated by CyaY or delivered from Fe^{2+} in solution that has dissociated from CyaY. Therefore, the Fe^{3+}-CyaY with different reductants may be a better choice for investigation whether CyaY can be an iron chaperone for apo-β_2. These studies warrant further investigation given these evidence for the role of frataxin as an iron chaperone.

II. Developing assays for detection of iron incorporation into apo-β_2

A classical biochemical method for finding factor(s) required for diferric-Y• assembly in vivo, require a sensitive assay for fractionation of cell lysate. Two approaches for assay development were taken: both involved monitoring color changes associated with iron cluster assembly. A β_2 double mutant, W48F/F208Y, was previously shown to generate a Fe^{3+}-catechol complex upon addition of Fe^{2+} and O_2. The long wavelength absorption features of this Fe^{3+}-catechol (λ_{max} = 660 nm, ε_{660nm} = 3 $mM^{-1}cm^{-1}$) allow monitoring of its formation even with "colored" crude cell lysate. As a first step, experiments were carried out to examine the suitability of this approach. Apo-β_2-W48F/F208Y was overexpressed in *E. coli* BL21(DE3) cells subsequent to induction with 0.2 mM IPTG for 4 h in the presence of an iron chelator, 1,10-phenanthroline (100 μM) (**Figure 4-6**).

The protein was purified and a final yield of ~500 mg protein was obtained from 14 g of cell paste (5 L culture in LB) (**Figure 4-6, Table 4-5**). It should be noted that during when concentrating the protein, an Amicon concentrator with a PM30, rather than a YM30 membrane should be used to avoid precipitation.

To test for formation of a Fe^{3+}-catechol complex, Fe^{2+} was added to apo-β_2-W48F/F208Y under aerobic conditions (**A, Figure 4-7**). The solution turned purple immediately, and the UV-visible spectrum showed a broad peak at A_{660nm}. From the published spectrum, this absorption feature extended to over 960 nm: no baseline was observed (*4*). Several minutes after addition of Fe^{2+}, Fe^{3+} precipitated. To test the stoichiometry of Fe^{3+}-catechol formation, different amounts of Fe^{2+} were titrated into apo-β_2-W48F/F208Y under aerobic conditions and the increased A_{660nm} was measured (**B, Figure 4-7**). The results revealed that the maximal amount of Fe-catechol complex is formed at a ratio of four ferrous irons per apo-β_2-W48F/F208Y.

A number of experiments were carried out to determine if Fe^{3+}-catechol formation could be detected when crude cell lysate was added to apo-β_2. Experiments with extract generated via cell wall disruption with a French Press or by sonication gave no Fe^{3+}-catechol product. Even when Fe^{2+} was added to the crude cell lysate, which was in turn added to apo-β_2, no 660 nm feature was detected. To eliminate the possibility that endogenous or exogenous Fe^{2+} was oxidized, preventing binding to apo-β_2, the experiment was repeated under anaerobic conditions, followed by O_2 addition. The experiment was also unsuccessful.

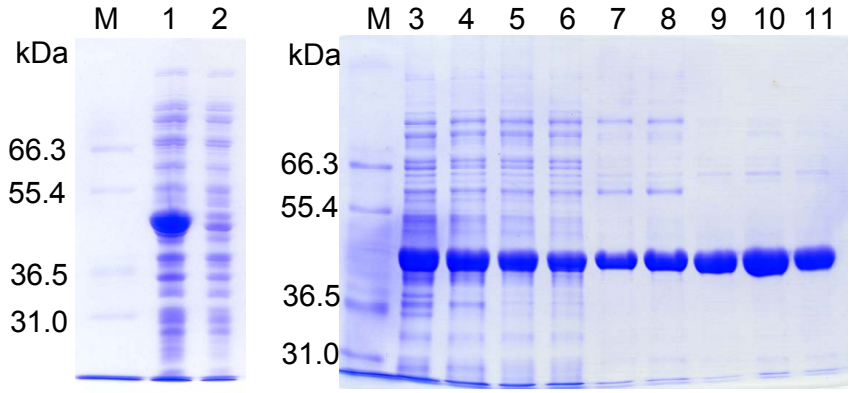

Figure 4-6. Induction and purification of apo-β_2-W48F/F208Y monitored by 10% SDS-PAGE. M: maker, lane 1: after 0.2 mM IPTG induction for 4 h, lane 2: before induction, lane 3: crude cell lysate, lane 4: after purification by streptomycin sulfate, lane 5: after purification by ammonium sulfate precipitation, lane 6: after desalting by Sephadex G-25, lane 7: after purification by DEAE ion-exchange chromatography, lane 8: after concentration by an Amicon concentrator with a YM30 membrane, lane 9: after purification by Q-Sepharose chromatography and concentration by an Amicon concentrator with a PM30 membrane, lane 10: after buffer exchange by Sephadex G-25, lane 11: after concentration by an Amincon concentrator with a PM30 membrane.

Table 4-5. Purification of apo-β_2-W48F/F208Y.

Sample	concentration (mg/mL)	volume (mL)	yield (mg)	% yield
crude cell lysate	13	71	923	
after streptomycin sulfate	11	83	913	74
after ammonium sulfate	57	15	855	70
after Sephadex G-25	12	93	1116	91
after DEAE	2.2	260	572	47
DEAE concentrate (YM30)	3	156	468	38
Q-Sepharose concentrate (PM30)	11	20	220	18
after G-25	9.9	44	436	35
G-25 concentrate (PM30)	53	9.3	493	40

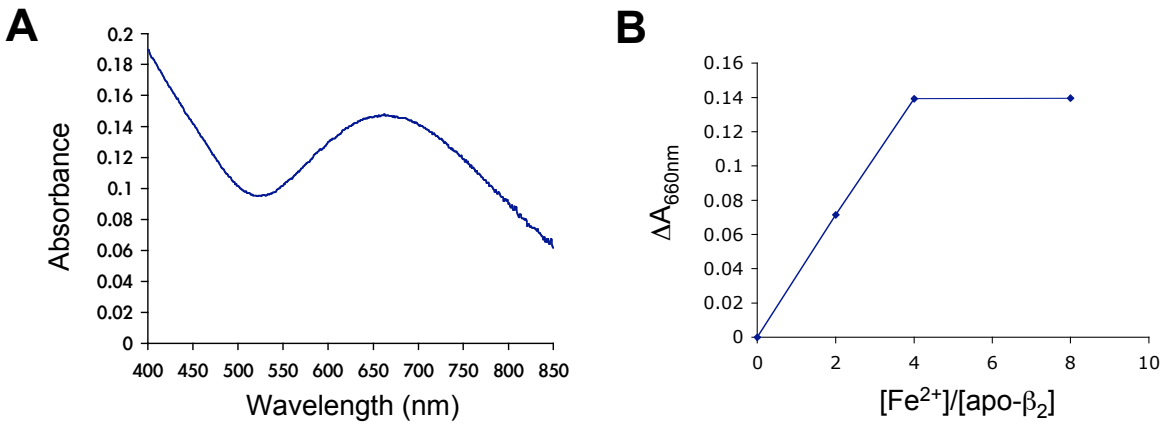

Figure 4-7. Looking for iron incorporation into apo-β_2 by monitoring Fe^{3+}-catechol formation at 660 nm in apo-β_2-W48F/F208Y. (A) Test the formation of Fe-catechol by adding Fe^{2+} (400 μM) into 50 μM apo-β_2-W48F/F208Y under aerobic conditions. After addition of Fe^{2+}, a peak with A_{660nm} was observed. (B) Determining the stoichiometry of the formation of Fe-catechol complex. Different amounts of Fe^{2+} (0, 100, 200, 400 μM) were added to 50 μM apo-β_2-W48F/F208Y under aerobic conditions and the A_{660nm} was measured. An absorption maximum was reached when the ratio of Fe^{2+} to apo-β_2-W48F/F208Y is 4 to 1.

One possible explanation for the failure to detect Fe^{3+}-catechol formation is that the components that can deliver Fe^{2+} to apo-β_2 can differentiate mutant from wt. To test this possibility the mutant was replaced by apo-β_2 wt and the experiments were repeated. Fe^{2+} added to apo-β_2 under aerobic conditions revealed the diferric-Y• cofactor formation (**Figure 4-8**) (*28*). Quantitation of the Y• by the drop-line method (*28*) indicated ~1 Y•/β_2. Apo-β_2 wt was then added to crude cell lysate prepared by sonication and the formation of the diferric-Y• was monitored (**Figure 4-8**). No significant changes of the spectrum after addition of apo-β_2 wt were observed initially; however, after spectra normalization for dilutions and subtraction of spectrum of crude cell lysate, features of the Y• were observed (**B, Figure 4-8, inset**). These results suggest that endogenous iron in the crude cell lysate can be incorporated into apo-β_2 wt. For the addition of ferrous iron to crude cell lysate resulted in a further increase in the A_{410nm}, indicative of increased formation of Y•. These results imply that there are unknown components inside the cells that can distinguish mutant apo-β_2 from wt apo-β_2 and can deliver iron specifically to the wt apo-β_2. While the sharp absorption feature at 410 nm from the formation of diferric-Y• cofactor could provide a means of fractioning factors capable of delivery of iron to apo-β_2, the sensitivity is very low. Thus this method was abandoned.

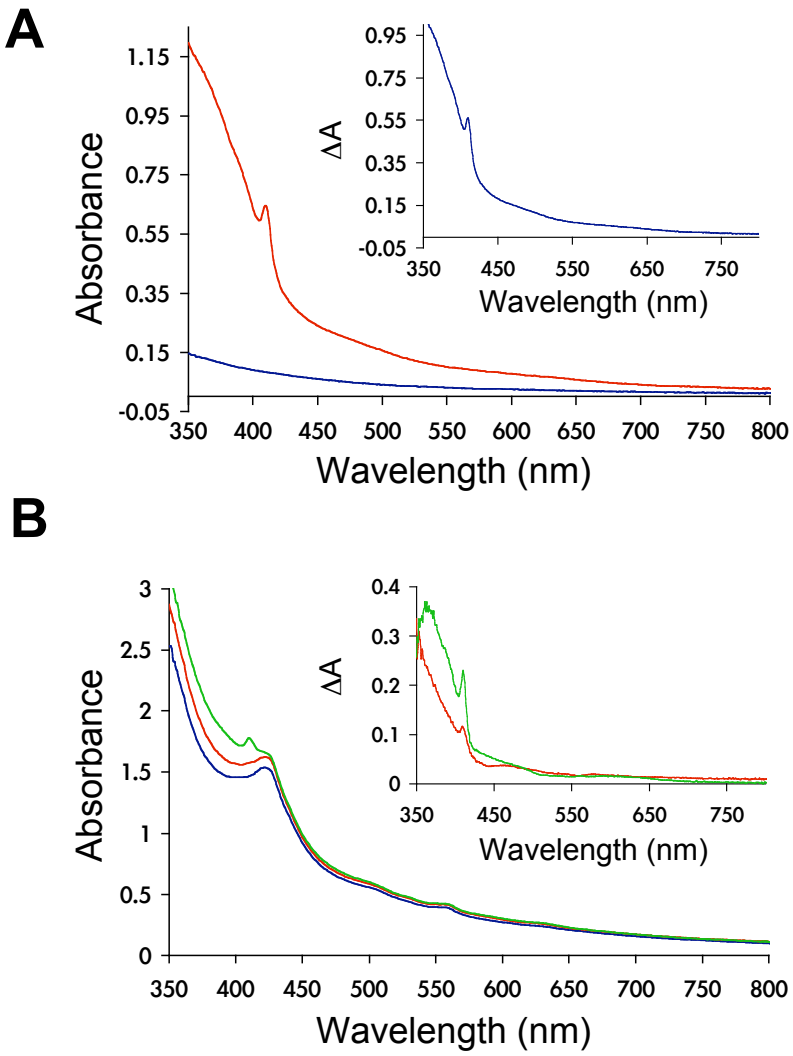

Figure 4-8. Looking for iron incorporation into wt apo-β_2 by monitoring the Y• formation at 410 nm. (A) WT apo-β_2 (50 μM, blue line) was added with $Fe(NH_4)_2(SO_4)_2$ (1 mM, red line) under aerobic conditions. Inset: Difference spectra between before and after addition of Fe^{2+}. (B) Looking for iron incorporation into wt apo-β_2 from crude cell lysate. Crude cell lysate from *E. coli* K-12 wt (~10 mg/mL) was mixed with 50 μM wt apo-β_2 followed by addition of 1 mM $Fe(NH_4)_2(SO_4)_2$ under anaerobic conditions. The UV-vis spectra of crude cell lysate (blue) and after addition of apo-β_2 (red) or 1 mM Fe^{2+} (green) are shown. The absorbance was adjusted for dilution. Inset: Difference spectra between after and before addition of apo-β_2 (red) and between after and before addition of Fe^{2+} (green) are shown. Features of the Y• were observed in both cases.

III. Looking for iron chaperone by protein co-purification

In addition to developing sensitive colorimetric assays to monitor iron delivery to apo-β_2, we have also developed techniques to monitor protein co-purification. Our working hypothesis is that iron loaded chaperone protein(s) is(are) likely to have a higher affinity for apo-β_2 than iron-loaded β_2. It is also likely that iron is transferred from the "iron chaperone" to apo-β_2 in its +2 oxidation state. In addition, from studies of the FeS cluster biosynthesis, the interaction between scaffold proteins and apo-recipient proteins appears to be weak (*40*). Therefore, we designed our affinity purification schemes to maximize detection of a co-purified protein.

(a) used a β_2-E115A mutant that is isolated in the apo-form to increase the chance of binding to iron loaded chaperone protein(s).

(b) placed affinity tags in three different positions within β_2 to prevent possible interference of tags on binding to a chaperone protein(s).

(c) eluted proteins from an affinity column with buffers containing different [NaCl] to maximize the prospects of finding a weakly bound protein.

(d) prepared crude cell lysate under anaerobic conditions to minimize Fe^{2+} oxidation.

(e) used non-specific formaldehyde cross-linking to increase the chance of co-purifying proteins with weak interactions.

A. Construction of wt and E115A β_2 with different affinity tags at various positions: An eight-amino acid StrepII tag was placed at the N- and, in a separate construct, the C-terminus of β_2 wt or E115A mutant to facilitate protein co-purification. To prevent potential interference of tags at the ends of β_2, constructs with an internal StrepII or independently a 6×His tag inserted between N179 and G180 of β_2 was also prepared. In order to be able to control the level of protein

expression, these tagged constructs were inserted into an arabinose-inducible pBAD vector and expressed in *E. coli* TOP10 cells in which the arabinose metabolism was abolished (**Table 4-2**) (*8, 18, 41*). The cells with the different constructs were grown in LB at 37 ºC until early log phase, at which time various concentrations of arabinose were added into the cell culture, to induce the expression of affinity tagged β_2. The cells were then grown for different amounts of time. The protein was purified by affinity chromatography. **Figure 4-9** shows the UV-visible spectrum of purified wt and E115A C-S-β_2. The spectrum of E115A β_2, as expected, does not have features associated with the diferric-Y• cofactor, in contrast to the spectrum of wt β_2. A ferrozine assay of E115A β_2 indicates a low iron content (< 0.1 Fe/β_2).

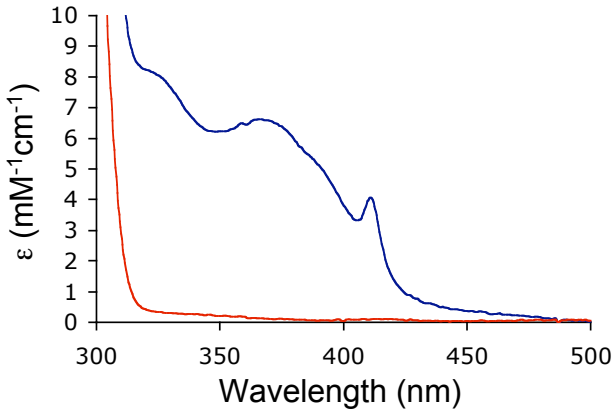

Figure 4-9. UV-visible spectra of purified C-terminal StrepII-tagged β_2. The expression of C-S-β_2 was induced by 0.01 mM ara for 2 h and the protein purified by Strep-Tactin affinity chromatography. Extinction coefficients of C-S-β_2 wt (blue) and C-S-β_2-E115A (red) were calculated using ε_{280nm} from wt-β_2 (131 $mM^{-1}cm^{-1}$) and apo-β_2 (120 $mM^{-1}cm^{-1}$). No feature from the diferric cluster was observed in the E115A mutant. Only the region between 300 nm and 500 nm was recorded.

B. Protein co-purification with StrepII-tagged β_2: We next tested the binding affinity of the different StrepII tagged constructs to a Strep-Tactin column to determine which construct would

be most appropriate to look for protein co-purification. We found that the C-S-β_2 has both higher expression and better affinity for the Strep-Tactin column compared with the N-S-β_2 (**#1-3, Table 4-6 and Figure 4-10**). The I-S-β_2 did not bind to the Strep-Tactin column (**#4, Table 4-6**).

Our choice of tagged E115A-β_2 to look for chaperone protein co-elution was based on studies which have demonstrated that Fe loading status effects protein-protein affinity. Because the binding of proteins we are interested in is likely to be weak, we therefore also run a control with wt-β_2. We then compared the protein elution profiles monitored by SDS-PAGE and looked for differences between the two experiments. However, a comparison of the elution profiles on SDS-PAGE from wt and E115A mutant gave no obvious difference with either C- or N-terminal Strep-tagged β_2 (**#1-3, Figure 4-10**). To test whether overexpression of β_2 could lead to protein co-purification, 5 mM arabinose was used to induce the expression of C-S-β_2. The results demonstrate similar co-purification patterns compared to studies observed with low arabinose induction (**#7, Table 4-6, Figure 4-10**).

C. Elution with lower [NaCl]: Because the wash buffer for the Strep-Tactin columns contained 150 mM NaCl, which could potentially facilitate dissociation of weakly bound proteins, the experiments were repeated in the absence of NaCl. The results indicate no difference in the elution patterns between wt and E115A of C-S-β_2 induced by 0.01 mM arabinose (**#5, Table 4-6, Figure 4-10**).

D. Crude cell lysate prepared under anaerobic conditions: To examine whether the oxidation of Fe^{2+} to Fe^{3+} in crude cell lysate is the cause for the lack of co-purified proteins with β_2 E115A,

cells were cracked open under anaerobic conditions using a Bugbuster solution. The Bradford assay of the crude cell lysate indicates that the Bugbuster solution has comparable cell-lysis efficiency as the French Press. Despite these efforts, the co-purification patterns between wt and E115A β_2 are very similar (**#6, Table 4-6, Figure 4-10**), indicating oxidation was not the cause.

E. Protein co-purification with 6×His tagged β_2: To examine the possibility that a Strep tag at the N- or C-terminus of β_2 interfered with the binding of a chaperone protein(s) to wt and E115A β_2, internal 6×His tagged β_2 was expressed and purified by Ni-affinity chromatography. The results show no obvious additional protein(s) co-purified with the tagged E115A β_2 (**#8, Table 4-6, Figure 4-10**).

*F. Protein co-purification with **N-S-β_2** after non-specific cross-linking by formaldehyde:* The results described above may imply that the binding of iron loaded chaperones to E115A mutant is too weak or too transient to be detected by co-purification under the conditions examined. To overcome the challenge of co-purifying proteins that are weakly bound, non-specific cross-linking by formaldehyde (FA) on the whole cells was tested (*7, 13, 42*). We first examined the cross-linking using the N-S-β_2. The cross-linking conditions, % of FA, incubation time and temperature, are protein dependent and needs to be optimized (*13*). We first selected 3% FA for 20 min at 4 ºC as our initial condition as these conditions have been successfully used to cross-link proteins in *E. coli* (*11, 42*). The protein expression was induced with 0.01 mM arabinose for 2 h and then treated with FA. The crude cell lysate from the cells disrupted by the French Press looked paler than the normal brownish crude cell lysate. After loading the samples and washing the Strep-Tactin column, no protein eluted from the column (**#10, Table 4-6**).

The failed protocol might be associated with the choice of concentration of FA for our system and the potential cross-linking of Strep tag to proteins inside the cell, preventing access to the Strep-Tactin column. Therefore, the concentrations of arabinose (5 mM) and FA (1%) were varied. In no case was β_2 bound to the affinity column (**#11, 12, Table 4-6**).

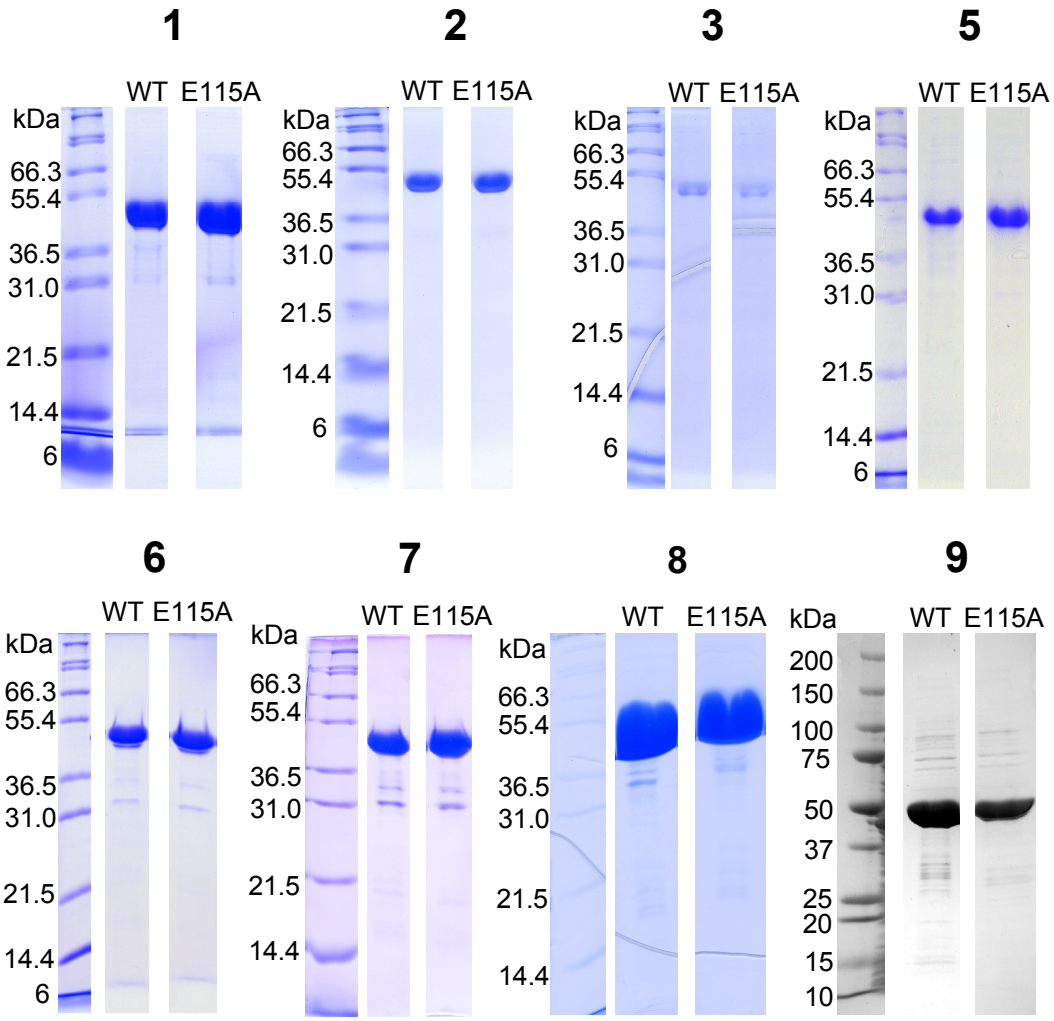

Figure 4-10. Comparisons of protein co-purification profiles between wt and E115A β_2 on SDS-PAGE. The growth and purification conditions of affinity-tagged wt or E115A β_2 are listed in **Table 4-6**. The numbers of the corresponding experiments in T**able 4-6** are shown. Experiment #9 was analyzed on 4-20% gradient SDS-PAGE, whereas all the others were analyzed on 15% gradient SDS-PAGE.

Table 4-6. Conditions tested for tagged β_2 expression and protein co-purification.

#	Constructs[a]	Induction conditions. [arabinose], time	Formaldehyde cross-linking conditions[b]	Wash conditions[c]	Elute conditions[d]	Notes[e]
1	CS-β_2	0.01 mM, 2 h	-	A	F	
2	NS-β_2	1 mM, 2 h	-	A	F	
3	NS-β_2	0.01 mM, 2 h	-	A	F	
4	IS-β_2	0.01 mM, 1.5 h	-	A	F	I
5	CS-β_2	0.01 mM, 3 h	-	B	F	
6	CS-β_2	0.01 mM, 3 h	-	B	F	II
7	CS-β_2	5 mM, 3 h	-	B	F	
8	IH-β_2	0.5 mM, 3.5 h	-	D	G	
9	IH-β_2	0.05 mM, 2 h	-	E	H	
10	NS-β_2	0.01 mM, 2 h	3% FA, 20 min, 4 ºC	A	F	I
11	NS-β_2	5 mM, 2.5 h	1% FA, 20 min	B	F	I
12	NS-β_2	5 mM, 2.5 h	1% FA, 40 min	B	F	I
13	CS-β_2	5 mM, 3 h	1% FA, 20 min	B	F	
14	CS-β_2	5 mM, 3 h	1% FA, 40 min	B	F	
15	CS-β_2	0.01 mM, 3 h	3% FA, 20 min, RT	C	F	III, I
16	IH-β_2	0.05 mM, 2 h	0.4% FA; 15 min	E	H	
17	IH-β_2	0.05 mM, 2 h	0.4% FA; 30 min	E	H	
18	IH-β_2	0.05 mM, 2 h	0.4% FA; 50 min	E	H	
19	IH-β_2	0.05 mM, 2 h	1% FA; 15, 30, 50 min	E	H	I
20	IH-β_2	0.05 mM, 2 h	3% FA; 15, 30, 50 min	E	H	I

a: abbreviations for the constructs: NS-β_2, N-terminal StrepII-tagged β_2; CS-β_2, C-terminal StrepII-tagged β_2; IS-β_2, Internal StrepII-tagged β_2; IH-β_2, Internal 6xHis-tagged β_2.

b: Formaldehyde (FA). All the cross-linking experiments were carried out at 37 ºC.

c: **A:** 100 mM Tris, pH 8.0, 150 mM NaCl, 5% glycerol, **B:** 100 mM Tris-HCl, pH 8.0, 20% glycerol, **C:** PBS (50 mM K_2HPO_4, 150 mM NaCl, pH 7.4), **D:** 50 mM Na_2HPO_4, pH 7.0, 10 mM imidazole, **E:** 50 mM NaH_2PO_4, 300 mM NaCl, 20 mM imidazole, pH 8.0.

d: **F:** 100 mM Tris, pH 8.0, 150 mM NaCl, 5% glycerol, 2.5 mM desthiobiotin, **G:** 50 mM Na_2HPO_4, pH 7.0, 250 mM imidazole, **H:** 50 mM NaH_2PO_4, 300 mM NaCl, 250 mM imidazole, pH 8.0.

e: **I:** Protein did not bind to the column, **II:** Cells were lysed anaerobically by Bugbuster, **III:** Cells were lysed aerobically by Bugbuster (primary amine-free) followed by FA cross-linking.

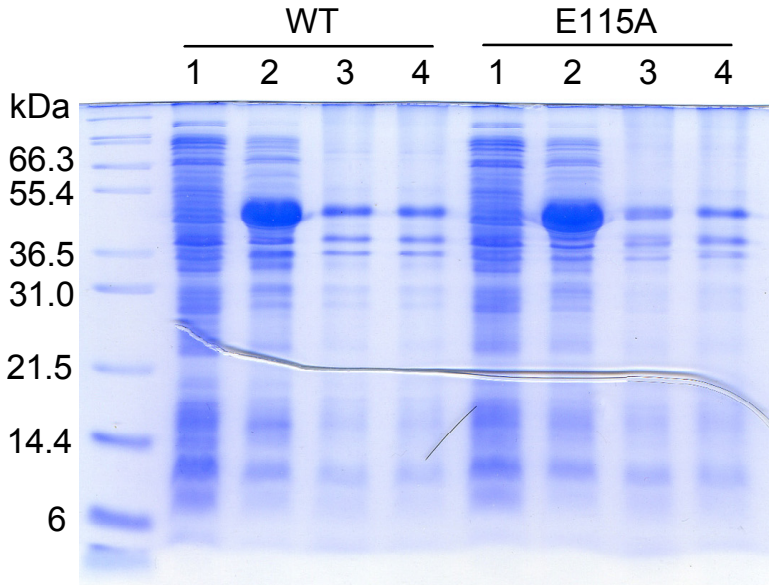

Figure 4-11. Effects of formaldehyde on the *E. coli* whole cells monitored by 15% SDS-PAGE. Expression of C-S-β_2 was induced by 5 mM arabinose for 3 h, after which 1% FA was added into the culture and the cells were grown for another 20 or 40 min at 37 ºC. The same amounts of the cells judged by A_{600nm} were suspended in 2x Laemmli buffer, boiled in 100 ºC sand bath and loaded onto a 15% SDS-PAGE. Lane 1: before arabinose induction, lane 2: after arabinose induction, lane 3: 20 min after addition of formaldehyde, lane 4: 40 min after addition of formaldehyde.

G. Protein co-purification with ***C-S-β_2*** *after non-specific cross-linking by formaldehyde:* Another explanation for the lack of protein elution from the Strep-Tactin columns could be due to weak affinity of the N-terminal StrepII tag. These cross-linking experiments were thus re-examined with the C-terminal StrepII-tagged β_2. Expression of C-S-β_2 was induced by 5 mM arabinose for 3 h, followed by incubation with 1% FA for 20 and 40 min. To examine the effect of FA on the proteins inside the cells, *E. coli* cells before and after arabinose induction and after

FA treatments were loaded directly onto 15% SDS-PAGE after being boiled in Laemmli buffer (**Figure 4-11; #13, 14, Table 4-6**). The result shows that C-S-β_2 is over-produced after arabinose induction, however, the total amount of protein decreases after FA treatment, probably due to low efficiency of cell lysis, which could explain the lack of protein eluted from the Strep-Tactin columns using N-S-β_2. Since there was a reasonable amount of C-S-β_2 after 1% FA treatment, the FA treated cells (20 min sample) were disrupted by the French Press and the crude cell lysate was loaded onto a Strep-Tactin column. Purified C-S-β_2 was obtained from the eluent, however, no difference in the co-elution pattern between wt and E115A β_2 was observed (**#13, Figure 4-12, Table 4-6**). To test whether a direct FA treatment in the crude cell lysate could increase cross-linking efficiency, the crude cell lysate from C-S-β_2 induced by 0.01 mM arabinose was purified and treated with 3% FA. However, C-S-β_2 loses its affinity toward the Strep-Tactin column (**#15, Table 4-6**), implying that the StrepII tag may be cross-linked to other proteins in the crude cell lysate, which would prohibit its binding to the column. In addition, dilution required to crack open the cells is likely to disrupt weak protein-protein interactions.

*H. Protein co-purification with **I-H-β_2** after non-specific cross-linking by formaldehyde:* To test the proposal that decreased affinities of binding tags is due to cross-linking of the tag by FA to other proteins, the internal 6×His-tagged β_2 was used. The I-H-β_2 was expressed by 0.05 mM arabinose induction for 2 h, followed by addition of 0.4. 1 and 3% FA and the cells were grown for 15, 30 and 50 min before the reaction was quenched by addition of glycine. Because of the number of conditions tested, Ni-NTA spin columns were used for rapid analyses. The result of the spin-column purification of the I-H-β_2 without FA treatment is shown in **Figure 4-10 (#9, Table 4-6**). Pure I-H-β_2 was obtained from the spin columns. No difference in the co-

purification pattern is observed between wt and E115A β_2. After 0.4% FA treatment for 30 or 50 min, the overall yields of the purified protein are less than those with only 15 min treatment (**#16-18, Table 4-6, Figure 4-12**). Furthermore, the co-purification patterns between wt and E115A β_2 on the 30 and 50 min samples appear to be the same (**#17, 18, Figure 4-12**). However, in the 15 min sample, there is a protein band of higher molecular mass in the E115A β_2, not present in the wt sample (**#16a, Figure 4-12**). After the sample was boiled to reverse the cross-linking, an extra band of lower molecular mass was observed (**#16b, Figure 4-12**).

This gel band was excised and submitted to the Proteomics Core Facility of MIT for in-gel trypsin digestion and LC-MS/MS analysis to determine the identity of the protein that cross-linked to I-H-β_2-E115A (**Table 4-7**). After examination of the proteins identified through peptide matching in a database search, the result seems to indicate that the "new" band is truncated β_2.

Despite the various approaches employed to increase our chances of finding an iron chaperone protein(s), no additional protein that co-purifies with E115A β_2 was found. The lack of protein co-purification could be due to low concentration and/or weak binding of chaperone proteins. In the former case, silver staining of the SDS-PAGE could reveal proteins not detected by the Coomassie blue staining. To overcome problems associated with a weak binding, examine of washes with increasing salt concentrations needs to be carried out; cross-linking reagents with different lengths of linkers between cross-linking functional groups may increase the chance of insolating proteins that co-purify with affinity tagged β_2. Future experiments are required to examine these proposals.

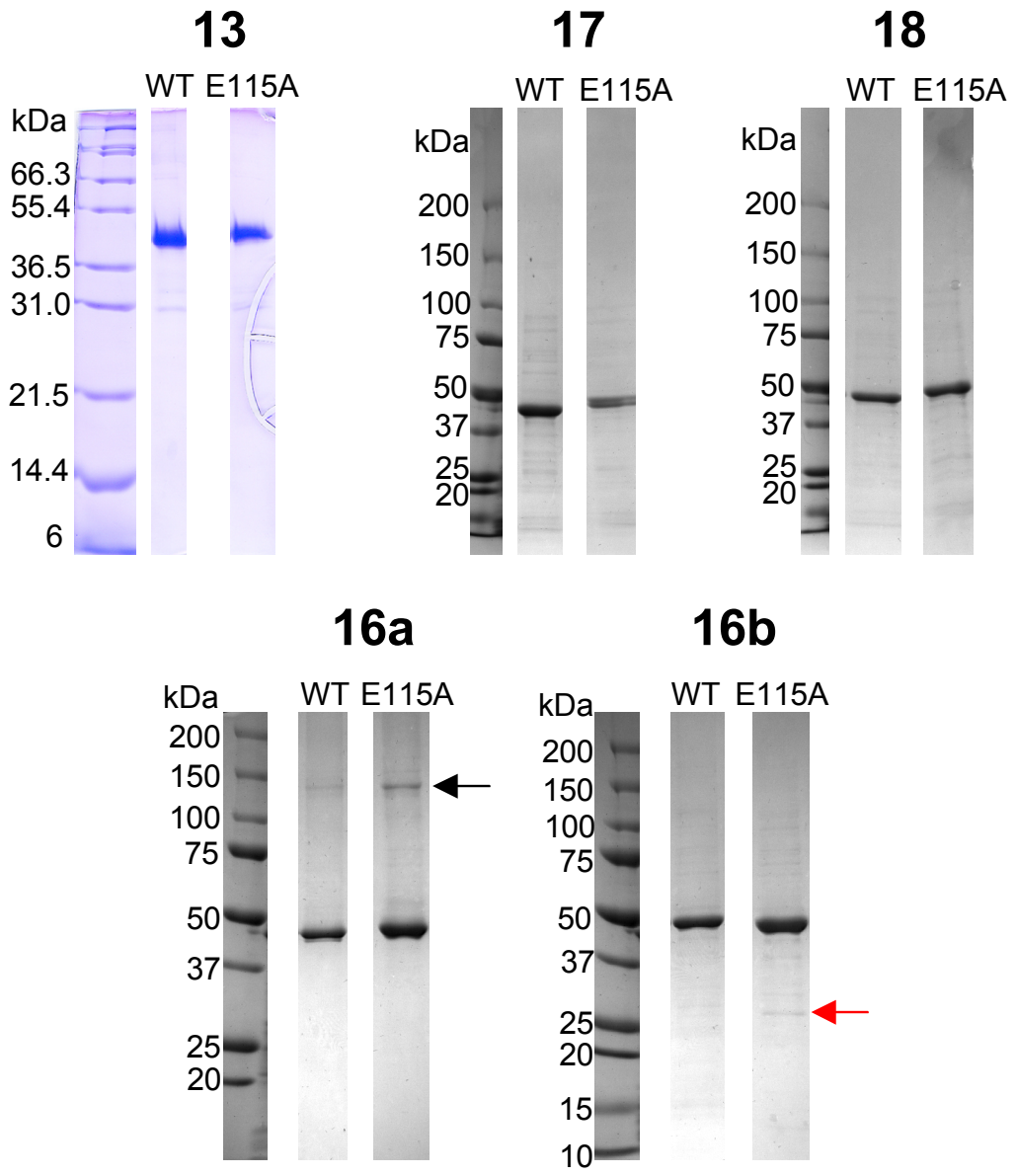

Figure 4-12. Comparisons of protein co-purification profiles between wt and E115A β_2 after non-specific cross-linking in vivo by FA. The growth, cross-linking and purification conditions of affinity-tagged wt or E115A β_2 are listed in **Table 4-6**. The numbers of the corresponding experiments in **Table 4-6** are shown. Experiment #13 was analyzed on 15% SDS-PAGE, whereas experiment #16-18 were analyzed on 4-20% gradient SDS-PAGE. (16a) The eluents were diluted in 2x Laemmli buffer without incubation at 100 ºC before being loaded onto the gel. The black arrow indicates a stronger band of higher molecular mass in E115A-β_2. (16b) Similar to 16a but the Laemmli samples were incubated in 100 ºC sand bath for 20 min before being loaded onto the gel. The boiling step reverses the cross-linkages and separates the cross-linked products. The red arrow indicates the new band formed in I-H-β_2-E115A that is absent in wild type after incubation at 100 ºC.

Table 4-7. List of the identification of proteins that cross-linked to internal His-tagged β_2-E115A by in-gel digestion with trypsin, LC-MS/MS analysis and database search.

Protein	Probability	Number of different peptides	MW
TPIS_ECOLI (P0A858) Triosephosphate isomerase	2.01E-11	8	26954.8
RS3_ECOLI (P0A7V3) 30S ribosomal protein S3	6.81E-10	4	25967.2
GRPE_ECOLI (P09372) Protein grpE (Heat shock protein B25.3, HSP-70 cofactor)	1.96E-09	1	21784.2
GPMA_ECOLI (P62707) 2,3-bisphosphoglycerate-dependent phosphoglycerate mutase	3.03E-09	3	28538.8
RIR2_ECOLI (P69924) Ribonucleoside-diphosphate reductase 1 subunit beta	5.63E-08	6	43489.8
RL1_ECOLI (P0A7L0) 50S ribosomal protein L1	7.05E-08	2	24714.3
GNTY_ECOLI (P63020) Protein gntY (predicted gluconate transport associated)	7.77E-08	2	20984.3
UDP_ECOLI (P12758) Uridine phosphorylase	1.35E-07	4	27141.9
EFTU_ECOLI (P0A6N1) Elongation factor Tu	1.78E-07	2	43286.4
NARL_ECOLI (P0AF28) Nitrate/nitrite response regulator protein narL	3.01E-07	1	23911.7
OMPR_ECOLI (P0AA16) Transcriptional regulatory protein ompR	3.39E-07	1	27336.2
TRMJ_ECOLI (P0AE01) tRNA	3.82E-07	2	27030.9
YDCF_ECOLI (P34209) Hypothetical protein ydcF	4.61E-07	1	29687.0
RS4_ECOLI (P0A7V8) 30S ribosomal protein S4	8.17E-07	2	23454.6

Note 1: Database search was carried out in a protein database of wt *E. coli* K-12. The probability means the odds of a random peptide sequence that happens to match the identified protein. The smaller the number, the better the fit. The number of different peptides identified that are matched to the target proteins is shown. The more peptides that match to the target protein, the more confident one is about the accuracy of the protein identification.

IV. Using whole cell EPR spectroscopy in an effort to identify iron delivery pathways for β_2

Our recent studies using whole cell EPR spectroscopy and quantitative Western analyses of *E. coli* TOP10 cells containing pBAD-*nrdB* showed that up to 4.4 mM Fe (76% of total iron) can be directed or redirected to load into β_2 after 0.5 mM arabinose induction for 2 h, which is ~3.2-fold of the total cellular iron (~1.4 mM) without arabinose induction (*18*). A robust and efficient iron delivery system is required to redirect such high amount of iron. Even though the iron delivery pathways for β_2 are likely growth dependent and redundant, there might only be a few of them that play a dominant role for the cluster biosynthesis of β_2. If this hypothesis is correct, it may be possible to observe a decrease in Y• signal in the whole cells when β_2 is overexpressed in mutant strains in which the genes encoding proteins involved in the key iron delivery pathways are deleted. To test this hypothesis, we first grew *E. coli* TOP10 cells in M9 minimal medium in order to control the growth conditions. However, cells grown in the minimal medium resulted in poor β_2 expression, and consequently resulted in weak Y• signals that could not be quantitatively assessed by whole cell EPR spectroscopy. Therefore, we decide to carry out experiments in LB medium.

We first focused our efforts on iron transporter deletion strains (**Table 4-1**). From our previous studies (*18*), induction of β_2 expression by 0.5 mM arabinose in LB medium generated ~33% of β_2 in the apo-form, suggesting that the rate of production of β_2 exceeds the iron-delivering capacity inside the cells. Under these growth conditions, if a major iron transporter associated with the iron delivery pathway for apo-β_2 is deleted, a decrease in the whole cell EPR signal of Y• might be observed, assuming that the Y• signal is proportional to the Fe-loading in β_2 in the different deletion strains.

Whole cell EPR spectroscopy of single transporter deletion strains: Single gene deletion strains of seven membrane transporters that are known to involve iron transport were obtained from Japan Keio collection (**Table 4-1**) (*24*). The accuracies of these gene-deletion strains were confirmed by PCR and DNA sequencing.

Initially the growth of the different deletion strains subsequent to β_2 induction was examined to evaluate whether there is any observable growth defect due to the deletion of each iron transporter. The growth curves from three independent cultures started from a single colony are shown in **Figure 4-13**. All strains have similar growth rates, except for *ΔfepA*, which grew slower than the others. This observation could be due to the importance of the ferric-enterobactin transporter, causing a shortage in iron supply. In addition to examining the growth curves, production of β_2 after induction with 0.5 mM arabinose was monitored by SDS-PAGE. The induction gels are shown in **Figure 4-14**. The results indicate that β_2 is overexpressed in the wt cells and in all the mutant strains, suggesting that the arabinose induction system is not affected by defects in iron transports and implying that variations of the whole cell EPR signal, if observed, may not be associated with different expression levels of β_2 between different strains.

The growth curves and the ability to overexpress β_2 in each strain, set the stage for monitor Y• by whole cell EPR. The Y• is assumed to be correlated with the extent of iron loading of apo-β_2.

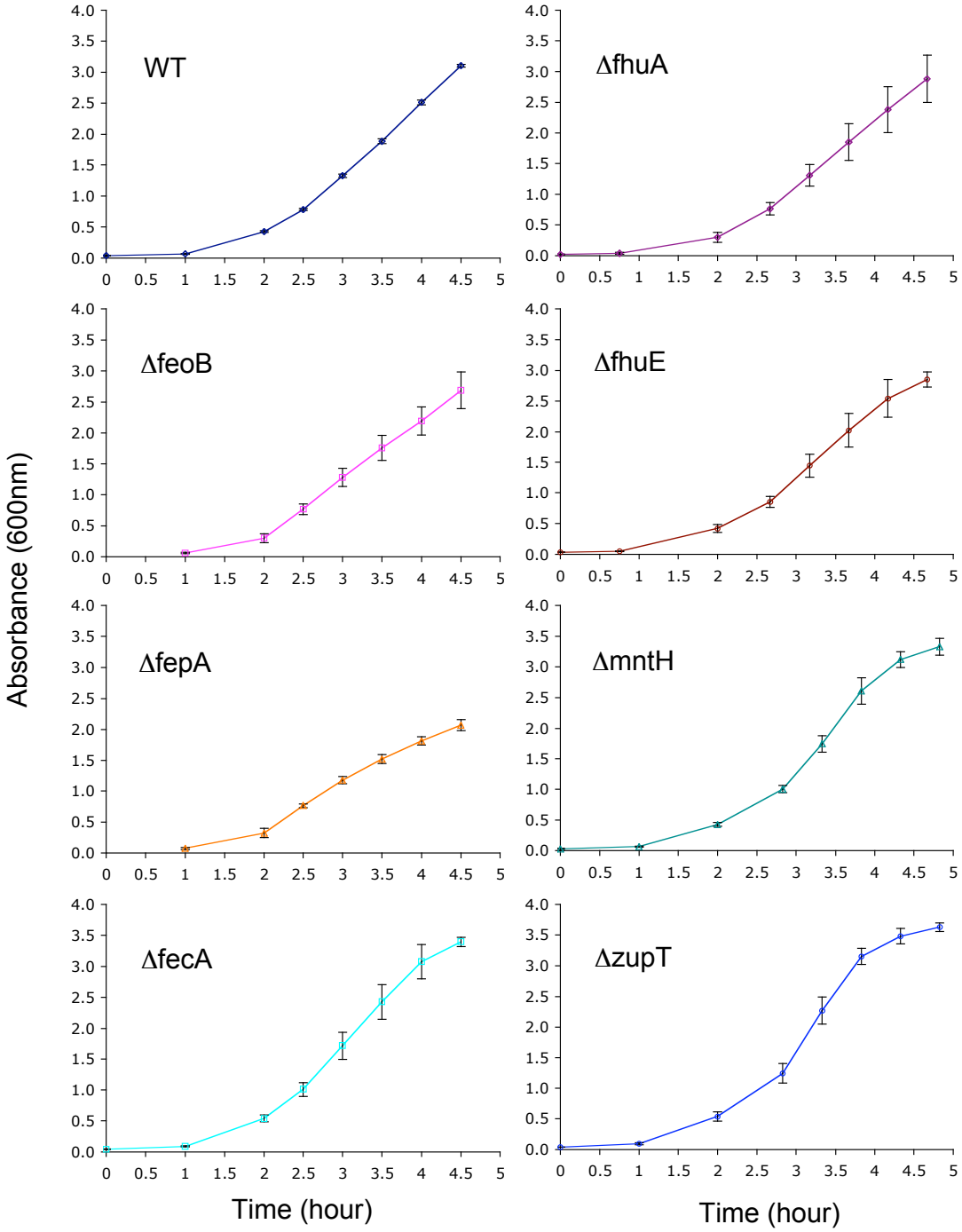

Figure 4-13. Growth curves of wt *E. coli* and iron transporter deletion strains overexpressed with β_2. An overnight culture (2.5 mL) of wt *E. coli* or iron transporter deletion strains containing pBAD-*nrdB* was inoculated into 500 mL LB-ampicillin and grown at 37 ºC, 200 rpm until A_{600nm} reached ~0.8-0.9, at which time 0.5 mM arabinose was added into the culture and the cells grown for another 2 h before being harvested. A_{600nm} of each culture was monitored at different time points during the course of growth.

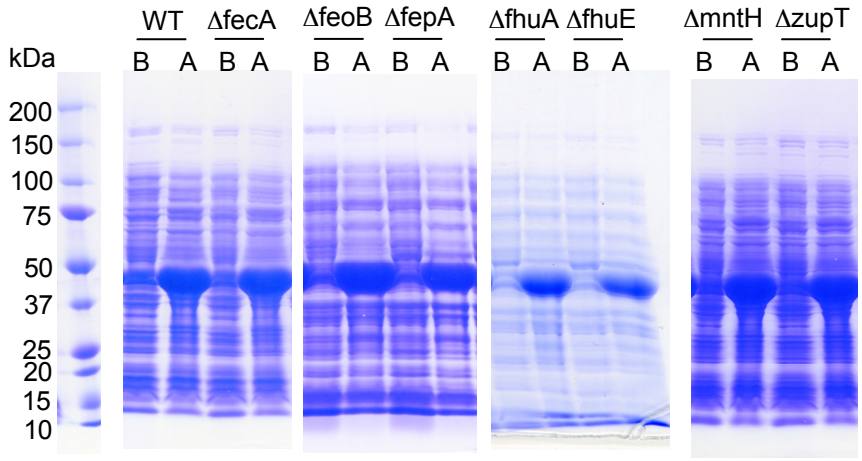

Figure 4-14. Induction gel of β_2 overexpressed in different host cell lines. Whole cells from experiments in **Figure 4-13** were loaded onto 4-20% gradient SDS-PAGE (A: 2 h after induction, B: before induction). In all cases β_2 was overexpressed after arabinose induction.

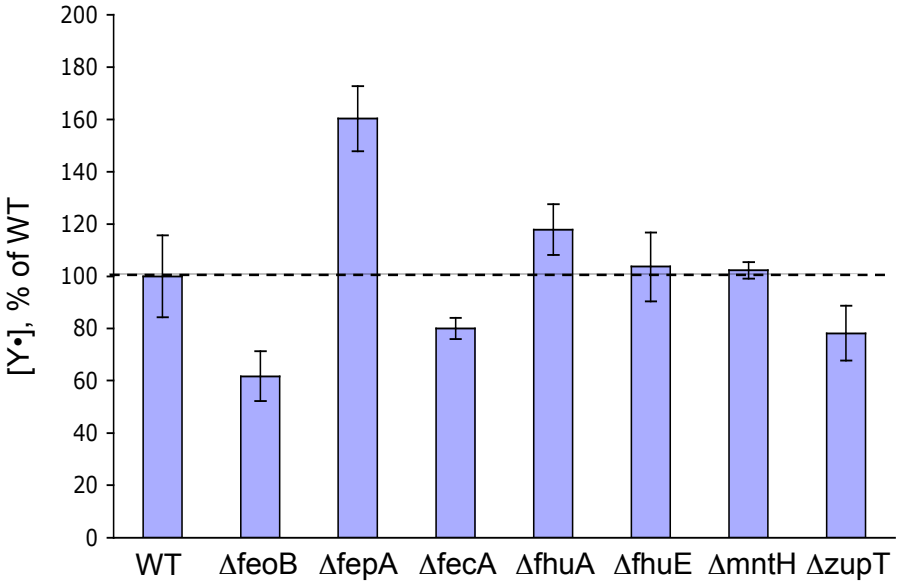

Figure 4-15. EPR signals of Y• in whole cells with β_2 overexpressed. Cells harvested from the experiments in **Figure 4-13** were suspended in 1 mL buffer C/g cell paste (buffer A: 100 mM Tris-HC, 150 mM NaCl, 5% glycerol, pH 7.6) and packed into EPR tubes. The EPR spectrum from 4 to 6 independent cell growths was recorded at 77 K, microwave power = 0.05 mW, receiver gain = 2.5×10^3, modulation amplitude = 1.5 G. The relative signals of the Y• in the whole cell samples compared to wt are shown.

Figure 4-15 shows the results from 4 to 6 independent cell growths of the whole cell Y• signals relative to wt β_2. A factor that could result in variations of the whole cell EPR signals is cell loading in the EPR tubes. To examine whether the same numbers of cells were loaded into the EPR tubes, the whole cell EPR samples (1 mL buffer C/g cell paste) were serial diluted (2000×) and A_{600nm} were recorded. The results show a very consistent A_{600nm} (A_{600nm} = 0.38 ± 0.01, six independent EPR samples) with a standard deviation of ~1.6%, suggesting the consistency of the cell loading in the EPR tubes.

The Y• signal from the ferrous transporter deletion strain, *ΔfeoB*, shows the most dramatic decrease (~40%) compared to wt. The ferric-citrate transporter (FecA) and the non-specific divalent cation transporter (ZupT) deletion also show ~20% decrease of the Y• signals compared to wt. The ferric-hydroxamate transporter (FhuE) and the other non-specific divalent cation transporter (MntH) deletion show no change in the intensity of Y• signals from the whole cells. The other ferric-hydroxamate transporter (FhuA) knockout has a slight increase of the EPR signal. Interestingly, the ferric-enterobactin transporter (FepA) knockout shows a dramatic increase (~60%) of the whole cell Y• signal compared to wt.

These results imply that the ferrous iron transporter FeoB could play a major role for the iron delivery into apo-β_2 and the ferric-citrate transporter FecA and the ZupT-transporter could function as backup systems for the cluster assembly of β_2. An increase of the whole cell Y• signal in *ΔfepA* is rather puzzling, which might be associated with its slower growth rate and/or defects in iron-uptake which in turn triggers alternative pathways that can generate the Y• more effectively. Future experiments using atomic absorption spectroscopy and Western blots to quantitate the iron-uptake and β_2 expression levels inside the cell, respectively, may help us to gain some insight into the mechanisms that cause variations in the Y• signal.

Whole cell EPR spectroscopy on multiple iron transporter deletion strains: In addition to single iron transporter deletion strains, we also investigated multiple iron transporter deletion strains in an effort to gain insight about iron delivery pathways for apo-β_2. This strategy requires construction of a multiple deletion of every known iron transport system, and comparisons of the Y• of strains with only one functional iron transport system. If this specific iron transport system is required for iron delivery for β_2, the addition of this system could result in an increase of the whole cell Y• signal.

To test this strategy, multiple transporter deletion strains were obtained from Prof. Rensing (**Table 4-1)** (*23*). The strain, GR536, contains deletions of two non-specific divalent cation transporters (ZupT and MntH), the major ferrous transport system (FeoABC), a protein essential for enterobactin biosynthesis (EntC), and the ferric-citrate uptake system (FecABCDE). The strains GR499, GR537 and GR538 contain deletions of these five transport systems but an intact ferric-citrate uptake system, ZupT and MntH, respectively (**Table 4-1**). Experiments to monitor Y• by whole cell EPR spectroscopy were carried out using methods described above for the single deletion strains (0.5 mM arabinose induction for 2 h in LB medium).

Figure 4-16 shows the level of the Y• signals relative to W3110 wt. Deletions of the five iron transport systems (GR536) causes about 80% decrease of the Y• signal compared to wt strain. The addition of either ZupT or MntH back to this strain does not show a recovery of Y• signal. The addition of the ferric-citrate transport system results in a 40% recovery of Y• signal compared to GR536, suggesting the ferric-citrate transport system is one of the pathways for iron delivery into apo-β_2. This result is consistent with the observations in the single ferric-citrate transporter deletion strain ΔfecA which also shows a decrease in the Y• signal compared to the

wt strain (**Figure 4-15**). These results suggest the potential of using multiple deletion strains to gain insight about iron delivery pathways for β_2.

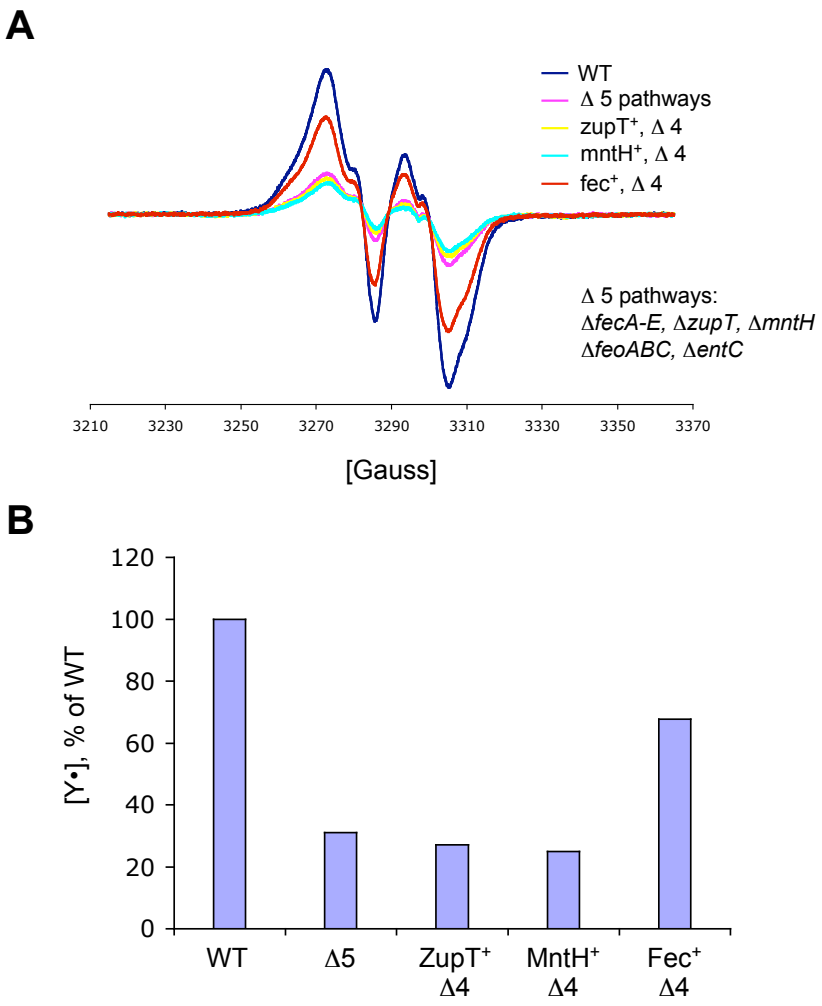

Figure 4-16. EPR signals of Y• in whole cells with β_2 overexpressed in multiple iron transporter deletion strains. The EPR spectra (A) and the relative [Y•] (B) compared to wt are shown. WT: *E. coli* W3110, Δ5 (GR536, table 4-2): deletion of five iron transporters, ZupT$^+$-Δ4 (GR537, table 4-2): deletion of four iron transporters with only ZupT functioning, MntH$^+$-Δ4 (GR538, table 4-2): deletion of four iron transporters with only MntH functioning, Fec$^+$-Δ4 (GR499, table 4-2): deletion of four iron transporters with only ferric-citrate transporter functioning. The same growth conditions and EPR parameters in **Figure 4-15** were followed. See **Table 4-2** for the genetic backgrounds of the deletion strains.

V. Whole cell Mössbauer spectroscopy after arabinose induction

Our previous studies using whole cell EPR spectroscopy and quantitative Western blots of cells grown subsequent to induction of β_2 with 0.01, 0.02, 0.05 or 0.5 mM arabinose indicate substoichiometric amount of Y• (0.26-0.5 Y•/β_2) inside the cell (*18*). To gain some insight to the iron loading of β_2 and the population of β_2 species (active β_2, met-β_2 and apo-β_2) in vivo, the crude cell lysate from cells grown under these different conditions (induction with 0.01, 0.02, 0.05 mM arabinose) were titrated with $[2Fe2S]^{1+}$-YfaE followed by exposure to O_2. Strikingly, the quantitation of [β_2] and [Y•] after the titration showed a stoichiometry of 2 Y•/β_2, indicating that β_2 is fully loaded with iron (4 Fe/β_2). This also suggests that active β_2 and met-β_2 are the only two β_2 species inside the cell when the [β_2] in vivo is <122 μM. In the case of β_2 induction with 0.5 mM arabinose, up to ~1.7 mM of β_2 was expressed inside the cell but the Y•/β_2 drops to 1.3, suggesting that the cell had reached its limit to deliver Fe to β_2 and a population of apo-β_2 was generated. In this experiment, quantitation of β_2 and iron revealed that up to 4.4 mM Fe^{2+} is directed (redirected) to load β_2 (*18*), which is ~3-fold of total iron inside the cell without β_2 overexpression (~1.4 mM). These results imply an up-regulation of the Fe uptake into the cells for the cofactor assembly of β_2. To establish that the loading with iron occurred in vivo and not from exogenous Fe in growth media, buffers or glassware, etc, Mössbauer spectroscopy was used to monitor the diferric-β_2 in the whole cell samples supplemented with ^{57}Fe.

Whole cell Mössbauer spectroscopy: detection of diferric-β_2 at 0.5 mM arabinose. The spectrum of whole cells packed into a Mössbauer cup after 0.5 mM arabinose induction for 2 h is shown in **Figure 4-17 (A)** and is dominated by two quadupole doublets, which are assigned to the diferric cluster of β_2. In addition, there is a small peak at +2.8 mm/s, which is typical of the high-energy

line of high-spin Fe(II), and a shoulder at +0.9 mm/s (indicated by an arrow). These features are also observed in the spectrum of the control sample (**B, Figure 4-17**) in which cells were grown under the same conditions except that no arabinose was added. The observed signals are the superposition of the spectral features of all Fe-species present in the cell, according to their relative concentrations. Approximately 40% of the iron is high-spin Fe(II) ($\delta \approx 1.3$ mm/s, $\Delta E_Q \approx 2.9$ mm/s) and the remainder represents several overlapping quadrupole doublets, which may include FeS cluster-containing proteins (primarily $[4Fe\text{-}4S]^{2+}$ and $[2Fe\text{-}2S]^{2+}$), low-spin Fe(II) hemes, and possibly fast-relaxing high-spin Fe(III) species. These features can be approximated as a broad quadrupole doublet with δ_{app} of 0.46 mm/s and ΔE_{Qapp} of 0.94 mm/s which accounts for ~60% of the total iron. Subtraction of the features observed in the control spectrum (**B, Figure 4-17**) (15% of Fe(II) and 9% of the broad quadrupole doublet) from the spectrum resulting from arabinose induction (**A, Figure 4-17**) yields the spectrum of diferric species assumed to be associated with β_2, which accounts for 76 ± 4% of total iron (**C, Figure 4-17**). The spectrum can be simulated with parameters ($\delta(1) = 0.46$ mm/s, $\Delta E_Q(1) = 2.40$ mm/s, $\delta(2) = 0.54$ mm/s, $\Delta E_Q(2) = 1.65$ mm/s) that are similar to those reported for diferric cluster of β_2 (*27, 43*). These experiments demonstrate high iron loading of β_2 and suggest that subsequent to arabinose induction that iron uptake is enhanced. They also suggest that whole cell Mössbauer spectroscopy may be a useful tool to monitor iron movement in vivo.

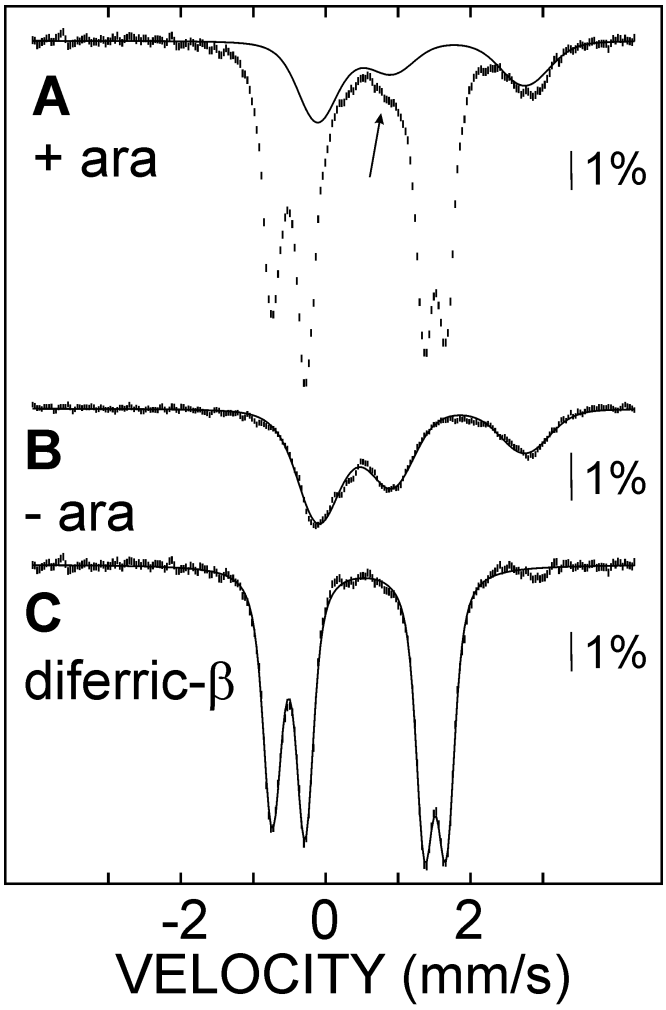

Figure 4-17: Mössbauer spectra of a sample of whole cells grown in a ^{57}Fe-supplemented medium. The production of β_2 was induced with 0.5 mM arabinose (A) and the cells grown for an additional 2 h. The control sample (B) is identical to A except that arabinose was omitted. The solid lines in (B) represent two quadrupole doublets, one associated with high-spin Fe(II) species and the second with all other Fe species in the cell (see text for parameters). Removal of the spectral component of these Fe species from the experimental spectrum (A) yields a spectrum of the diferric cluster of β (C), which can be simulated with two quadrupole doublets (solid line) using the parameters given in the text.

Monitoring iron migration in vivo by whole cell Mössbauer spectroscopy: optimization of induction conditions: Growth conditions were optimized in which β_2 is expressed under minimal cell growth so that iron loading of induced β_2 occurred from an iron pool within the cell, not from iron uptake. To find these conditions cells were induced by 0.5 mM arabinose at different growth phases (A_{600nm} ~ 0.5, 1.0 or 1.5) and grown for an additional 10 or 20 min (**Table 4-8**). Cell growth was monitored by A_{600nm} and the results indicates that under the same induction time (10 or 20 min) the cell culture induced at A_{600nm} = 1.5 has the least cell growth compared to cultures induced at A_{600nm} ~0.5 or 1.0. Furthermore, under the same induction time, the cell culture induced at A_{600nm} = 1.5 has the strongest Y• signal, suggesting the highest β_2 expression. Therefore, the best growth condition for monitoring the iron migration inside the cell is to induce the β_2 expression by 0.5 mM arabinose at A_{600nm} ~ 1.5 for at least 10 or 20 min.

Sample preparation for time course study to be acquired by whole cell Mössbauer spectroscopy: After the growth conditions were chosen, the cells were grown in LB containing 50 μM ^{57}Fe (~80% enrichment of the total iron in the culture medium) and β_2 expression was induced by 0.5 mM arabinose at A_{600nm} ~ 1.5. The cells were grown for 10, 20 and 40 min and harvested by centrifugation. Some of the cell paste was packed directly into Mössbauer cups and some was suspended in 1 mL buffer C/g cell paste and loaded into EPR tubes for analysis.

Figure 4-18 shows the induction gel (**A)** and the whole cell EPR spectra of the Y• (**B**). No Y• signal was observed before addition of arabinose. The gel monitoring β_2 induction and the whole cell EPR spectra indicate a gradual increase with time of the expression of β_2 and the intensity of the Y• signal, respectively. The spin quantitation shows a ratio of 1:2.2:4.2 of the Y• signal after 10, 20 and 40 min induction, respectively.

Table 4-8. Cell growth and Y• signal of *E. coli* TOP10-pBAD-*nrdB* induced with 0.5 mM arabinose at different A_{600nm}.

Induction condition	Induction time (min)	A_{600nm}	% cell growth	[Y•], μM [a]
A_{600nm} ~0.5	0	0.52	-	-
	10	0.58	12	11
	20	0.64	23	28
A_{600nm} ~1.0	0	1.02	-	-
	10	1.15	13	13
	20	1.30	27	30
A_{600nm} ~1.5	0	1.52	-	-
	10	1.63	7	17
	20	1.78	17	41

[a] concentrations of Y• in the EPR sample was determined by spin quantitation using a Cu-standard.

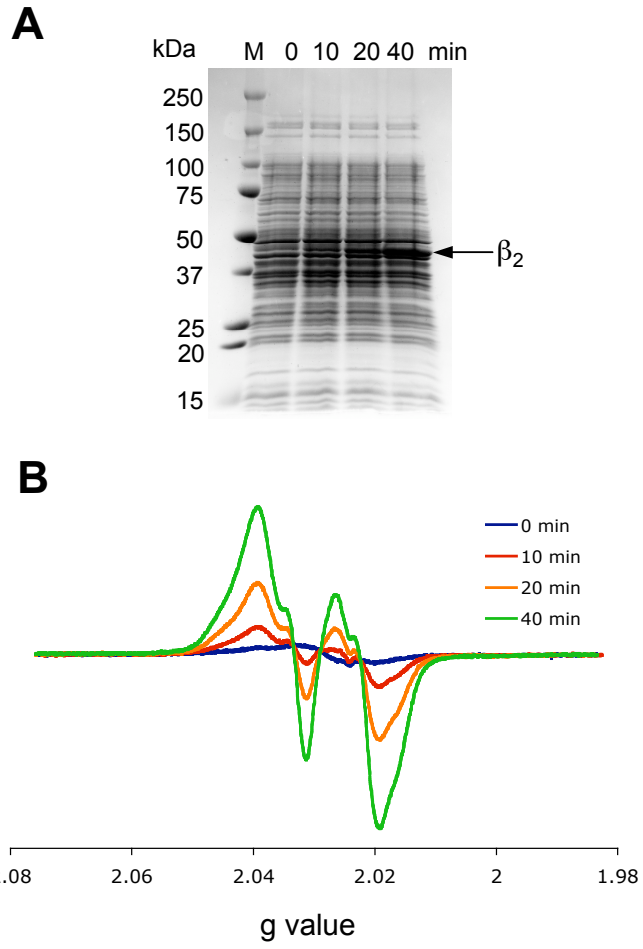

Figure 4-18. β_2 expression and Y• formation measured subsequent to arabinose induction. *E. coli* TOP10 cells containing pBAD-*nrdB* were grown at 37 ºC, 200 rpm until A_{600nm} reached ~1.5. Expression of β_2 was then induced by 0.5 mM arabinose. Aliquots of the culture were taken before induction or 10, 20, and 40 min after induction and the cells were spun down by centrifugation at 8,000*g* for 10 min at 4 ºC. The cell paste was suspended in 1 mL buffer C per gram of cell paste for analysis by EPR spectroscopy. (A) Expression of the β_2 was examined by 4-20% gradient SDS-PAGE. The arrow indicates the expression of β_2. (B) EPR signals of Y• from the whole cell samples.

Figure 4-19 shows the corresponding Mössbauer spectra at different time points after arabinose induction. Before arabinose induction, the whole cell sample shows features associated with high spin ferrous and ferric iron, similar to the observations in **Figure 4-17**. The spectrum at 10 min after arabinose induction looks very similar to the one before arabinose induction despite a small increase in the Y• signal. Features from diferric-β_2 begin to appear at 20 min and are more prominent at 40 min. As analyzed below, the decrease of signals from the original Fe^{2+} and Fe^{3+} species accompany the increase of the diferric-β_2 signals.

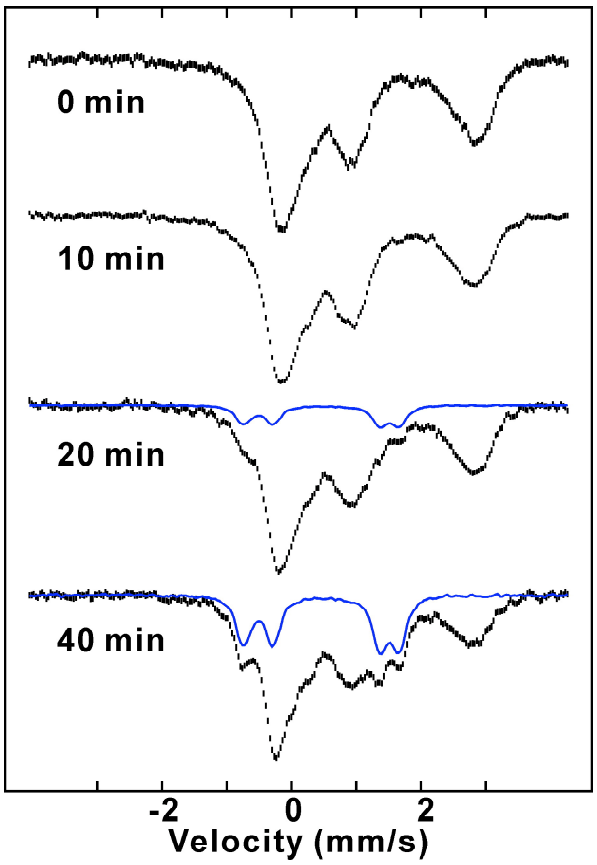

Figure 4-19. Mössbauer spectra of TOP10-pBAD-nrdB induced with arabinose for indicated periods of time. Cell paste from the experiment described in **Figure 4-18** was packed into Mössbauer cups and frozen in liquid N_2 for analysis. Mössbauer spectra of the whole cells with 0.5 mM arabinose induction for 0, 10, 20 and 40 min (black) and simulations of diferric cluster from β_2 (blue) are shown.

The analysis of the Mössbauer spectra is shown in **Figure 4-20** and the parameters are summarized in **Table 4-9**. The green, red and blue lines indicate the simulations of Fe^{2+}, Fe^{3+} and diferric-β_2, respectively. Before arabinose induction, 50% of the total iron inside the cells is Fe^{3+} and 46% of the total iron is Fe^{2+}. The remaining 4% of the total iron could be in the forms of FeS clusters, which are present in insufficient amounts to simulate with good accuracy. The spectrum of 20 min sample after arabinose induction shows the appearance of diferric-β_2 signal, which represents 10% of the total cellular iron. Of this 10% iron, 8% comes from ferrous iron pools and 2% comes from ferric iron pools. Forty minutes after arabinose induction, the diferric-β_2 represents 26% of the total cellular iron, and 18% comes ferrous iron pools and 7% comes ferric iron pools.

These results show that in the early stage (20 min) of expression of β_2, higher ratio of Fe^{2+} (Fe^{2+}:Fe^{3+} ~ 4:1) is delivered into β_2 than in the later stage (40 min) (Fe^{2+}:Fe^{3+} ~ 2.6:1). One possible explanation is that ferrous iron pools are more direct iron sources for the assembly of differic cluster in β_2 in vivo. The over-production of apo-β_2 depletes specific ferrous iron pools associated with supplying the iron to β_2 and the ferric iron species inside the cells are converted to ferrous iron for the biosynthesis of the diferric cluster of β_2. This hypothesis is also in line with the observations in the whole cell EPR spectroscopic experiments on iron transporter deletion strains, which imply a ferrous iron transporter, FeoB that may play a role in the iron delivery pathways for the cofactor biosynthesis of β_2.

In addition, the results also show the first evidence that both Fe^{2+} and Fe^{3+} inside the cell can be delivered to apo-β_2 and suggest that one or more reductants are present that make Fe^{3+} delivery possible. By applying whole cell Mössbauer spectroscopy on deletion of potential ferric

reductases could reveal pathways for the reduction of Fe^{3+} pools to supply the Fe^{2+} required for β_2 diferric-Y• cofactor assembly.

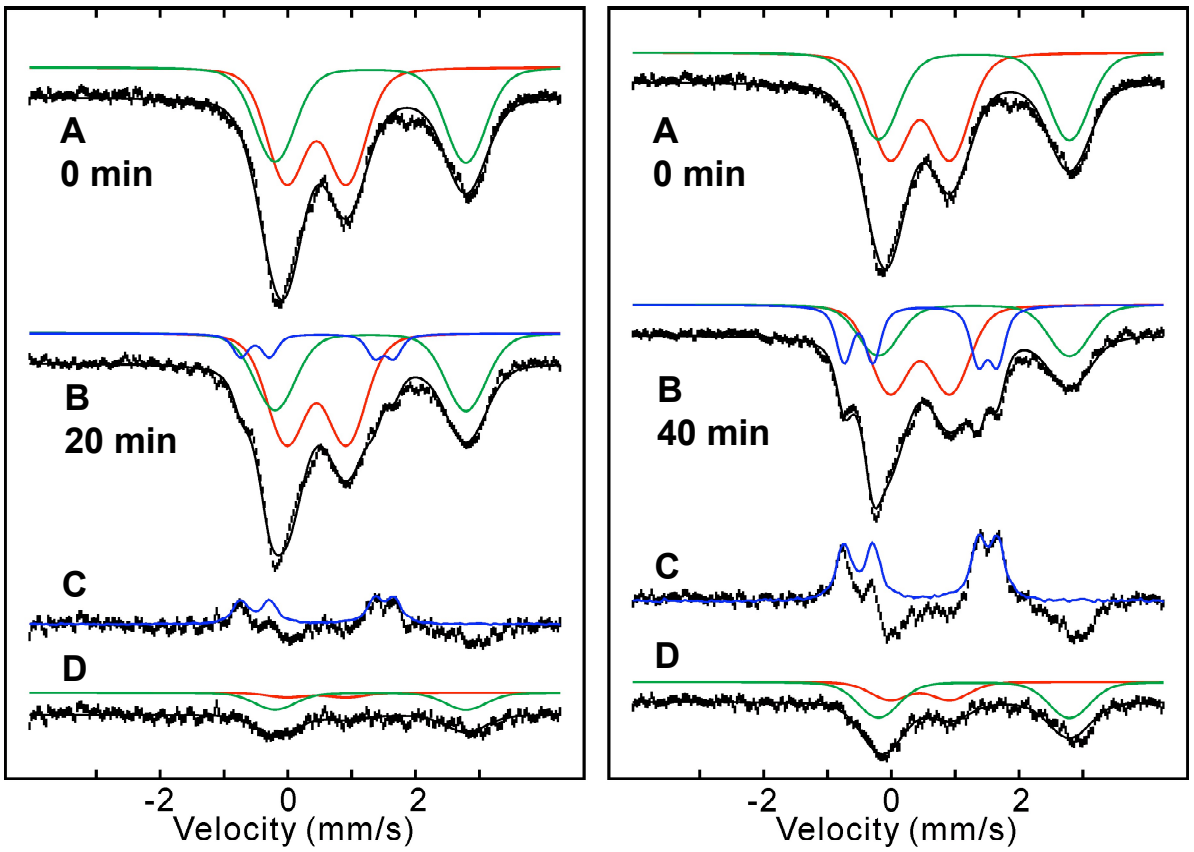

Figure 4-20. Analysis of Mössbauer spectra of TOP10-pBAD-nrdB induced with arabinose for different periods of time. The Mössbauer spectra (black) and simulations of Fe^{2+} (green), Fe^{3+} (red) and diferric-β_2 (blue) are shown. (A) Before arabinose induction. (B) 20 min (left) or 40 min (right) after induction. (C) Difference spectra between after and before arabinose induction. (D) Difference spectra after the diferric-β_2 feature in C is subtracted.

Table 4-9. Mössbauer simulation parameters of Fe^{3+}, Fe^{2+} and diferric cluster of β_2 in the whole cells induced with arabinose for different periods of time.

Sample	Specie	Relative amount (%)	δ (mm/s)	ΔE_Q (mm/s)
0 min	Fe^{3+}	50	0.50	0.85
	Fe^{2+}	46	1.27	3.03
20 min	Fe^{3+}	48	0.50	0.85
	Fe^{2+}	39	1.27	3.03
	diferric-β_2	10	0.46	2.40
			0.54	1.65
Δ-20 min	Fe^{3+}	2	0.50	0.85
	Fe^{2+}	8	1.27	3.03
40 min	Fe^{3+}	44	0.50	0.89
	Fe^{2+}	28	1.23	2.97
	diferric-β_2	26	0.46	2.40
			0.54	1.65
Δ-40 min	Fe^{3+}	7	0.50	0.76
	Fe^{2+}	18	1.34	3.07

Note: "Δ-20 min" and "Δ-40 min" indicate the changes of iron species after arabinose induction.

DISCUSSION

In order to elucidate how iron is delivered to β_2, several strategies have been employed, including investigating the function of CyaY, looking for iron chaperones by developing assays to monitor iron incorporation in apo-β_2 and by protein co-purification. Unfortunately these strategies were unsuccessful. On the other hand, results from whole cell EPR and Mössbauer spectroscopies indicate the potential of these tools in revealing pathways for iron delivery to β_2.

Comparisons of the whole cell Y• signal between single deletion strains of iron transporters reveal that the ferrous transporter FeoB plays a significant role in iron delivery to β_2. This Fe^{2+} system is encoded by the *feoABC* operon in *E. coli* (*44, 45*). FeoA (8 kDa) and FeoC (9 kDa) are small proteins with elusive function, and FeoB is an 85-kDa plasma membrane protein with a tight binding to Fe^{2+} (K_d ~0.5 μM) (*46*). Deletion of FeoA decreases the Fe^{2+} uptake by FeoB, whereas FeoC is not essential for the function of FeoB (*47, 48*). FeoB has been shown to have a GTPase activity and the binding of GTP is required for efficient Fe^{2+} uptake; however, the mechanism of how GTPase activity controls the Fe^{2+} transport remains to be established (*49*). Studies on *ΔfeoB* showed a 10-fold decrease compared to the wt of the iron uptake using $^{55}FeCl_2$ or ^{55}Fe-citrate as the only iron source in minimal media (*46*). The fact that Fe^{3+}-citrate uptake is affected by *ΔfeoB* suggests that the Fe^{2+} that is transported by FeoB could also come from the reduction of ferric-citrate or other ferric-siderophore complexes in the periplasm.

To prevent toxic Fenton chemistry by free Fe^{2+}, it is likely that there exist specific Fe^{2+} chelators or protein chaperones that interact with FeoB and transfer Fe^{2+} to specific targets (*50*). This model is supported by the observation that Fe^{2+} transported through a magnesium transporter (CorA) under low [Mg^{2+}] is toxic to the cell under aerobic conditions, implying a lack

of an appropriate Fe^{2+} chelation mechanism to prevent its reaction with O_2 species (*51*). It should be noted that it has been reported that Fe^{2+} cannot be transported by CorA when the cell is in the stationary phase, indicating the Fe^{2+} uptake system is sensitive to growth conditions (*52*).

The identity of the Fe^{2+} and Fe^{3+} pools inside the cell has been of great interest. Studies by Matzanke et al on the whole cell Mössbauer spectroscopy of wt *E. coli* K-12 indicates that the majority of the iron inside the cells are composed of ~1:1 ratio of Fe^{2+} and Fe^{3+} species that have parameters (isomer shift and ΔE_Q) distinct from haem iron, FeS clusters, bacterioferritin or ferritin (*21*). The ratio of the Fe^{2+} to Fe^{3+} pools decreases under glucose starvation but is restored after the addition of glucose, indicating a dynamic, interconvertible relationship between these pools. Of these Fe^{2+} pools, the existence of a "labile" or "chelatable" Fe^{2+} pool has been postulated and is estimated to be ~0.2-10 μM (*53-55*), which is only ~1% of the total Fe^{2+} pools in vivo (*18*). It has been proposed that a phosphorylated sugar derivative (*56, 57*) or glutathione (*58*) could be related to the maintenance of the labile Fe^{2+} pool, but no strong, direct experimental evidence has been provided to support either hypothesis.

Our whole cell Mössbauer experiments also show Fe^{2+} and Fe^{3+} pools inside the cell, which comprises over 96% of total cellular iron. Both pools are able to provide the iron for β_2 diferric cluster assembly. The observation that a higher percentage of the iron delivered to β_2 comes from the Fe^{2+} pool and the requirement that iron needs to be in the ferrous form for cluster assembly suggest that maybe the Fe^{2+} pool is a more direct iron supplier for β_2 and when the Fe^{2+} is depleted, the intracellular Fe^{3+} is reduced to furnish more Fe^{2+} and reestablish equilibrium. Our results show that the reduction of Fe^{3+} occurs even when only part of the total Fe^{2+} pool is consumed, implying that there might be a subset of Fe^{2+} pool specific for cluster assembly of β_2

and that a specific ferric redutase in the cytosol is responsible for maintaining the equilibrium between Fe^{2+} and Fe^{3+} subpools.

The existence of Fe^{2+} and Fe^{3+} subpools specific for β_2 cofactor biosynthesis could be examined by the whole cell Mössbauer spectroscopy. *E. coli* cells can be grown in ^{57}Fe enriched media until A_{600nm} ~1.5 and then switched to Fe-limiting media subsequent to β_2 overexpression. If these specific Fe^{2+} and Fe^{3+} subpools exist, only a certain ratio of Fe^{2+} and Fe^{3+} is expected to be depleted after overexpression of β_2. Similarly, the existence of specific ferric reductases responsible for balancing the Fe^{2+} and Fe^{3+} pools can be examined by whole cell Mössbauer spectroscopy using deletion strains of potential candidates such as Fre, sulfite reductase, ferrisiderophore reductase, or ferredoxin reductase (*59-62*). If the β_2-specific reduction of a Fe^{3+} subpool is carried out by a specific ferric reductase, the deletion of this gene could abolish the consumption of the Fe^{3+} pool after β_2 expression.

The tools we developed can also be applied to verify the proposed identity of the Fe^{2+} pool. For example, to examine the relationship between the labile iron pool and cellular glutathione, β_2 can be overexpressed in the deletion strains in which the glutathione pool is diminished (*58*). The Y• signal and the iron migration of these deletion strains can then be monitored by whole cell EPR and Mössbauer spectroscopies. If the labile iron pool is related to a pool of cellular glutathione, a decrease of the whole cell Y• signal and diferric-β_2 signal in EPR and Mössbauer spectra, respectively, could be observed in those deletion strains.

Based on the results in this chapter, another piece of the puzzle for the iron source for the biosynthesis of the diferric-Y• cofactor can be fit to the model (**Figure 4-21**).

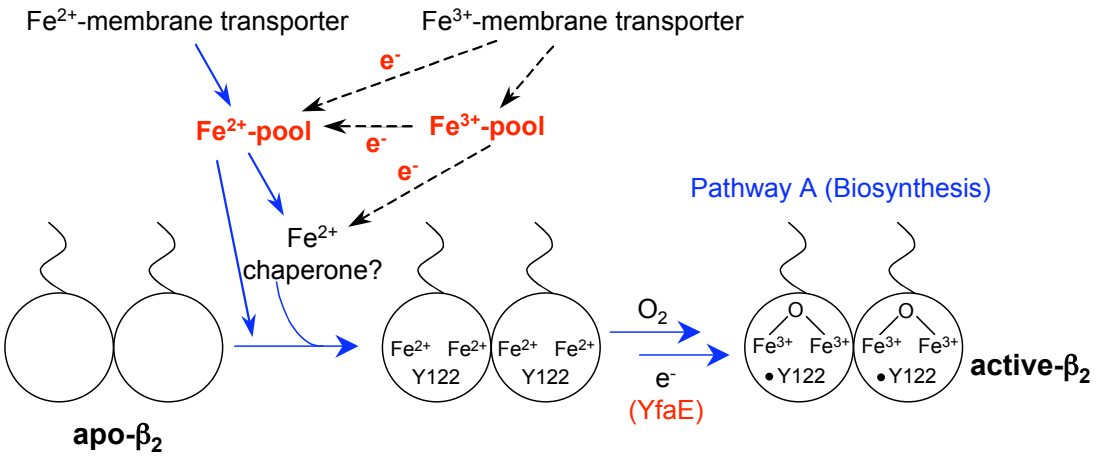

Figure 4-21. Model of the iron delivery pathways for the assembly of diferric-Y• cluster in β_2. Fe^{2+} plasma membrane transporters such as FeoB and Fe^{3+} outer membrane transporters such as FecA are involved in the iron delivery pathways for apo-β_2. Both Fe^{2+} and Fe^{3+} pools inside the cell can provide Fe^{2+} for apo-β_2. Mechanisms of reduction of the Fe^{3+} must exist to enable the Fe^{3+} pools function in this capacity. The iron pools could directly or mediated by iron chaperones to supply the ferrous iron for apo-β_2.

REFERENCES

(1) Kasrayan, A., Birgander, P. L., Pappalardo, L., Regnstrom, K., Westman, M., Slaby, A., Gordon, E., and Sjöberg, B. M. (2004) Enhancement by effectors and substrate nucleotides of R1-R2 interactions in *Escherichia coli* class Ia ribonucleotide reductase. *J Biol Chem 279*, 31050-7.

(2) Ormo, M., deMare, F., Regnstrom, K., Aberg, A., Sahlin, M., Ling, J., Loehr, T. M., Sanders-Loehr, J., and Sjöberg, B. M. (1992) Engineering of the iron site in ribonucleotide reductase to a self-hydroxylating monooxygenase. *J Biol Chem 267*, 8711-4.

(3) Aberg, A., Ormo, M., Nordlund, P., and Sjoberg, B. M. (1993) Autocatalytic generation of dopa in the engineered protein R2 F208Y from *Escherichia coli* ribonucleotide reductase and crystal structure of the dopa-208 protein. *Biochemistry 32*, 9845-50.

(4) Parkin, S. E., Chen, S., Ley, B. A., Mangravite, L., Edmondson, D. E., Huynh, B. H., and Bollinger, J. M., Jr. (1998) Electron injection through a specific pathway determines the outcome of oxygen activation at the diiron cluster in the F208Y mutant of *Escherichia coli* ribonucleotide reductase protein R2. *Biochemistry 37*, 1124-30.

(5) Houry, W. A., Frishman, D., Eckerskorn, C., Lottspeich, F., and Hartl, F. U. (1999) Identification of in vivo substrates of the chaperonin GroEL. *Nature 402*, 147-54.

(6) Puig, O., Caspary, F., Rigaut, G., Rutz, B., Bouveret, E., Bragado-Nilsson, E., Wilm, M., and Seraphin, B. (2001) The tandem affinity purification (TAP) method: a general procedure of protein complex purification. *Methods 24*, 218-29.

(7) Ethier, M., Lambert, J. P., Vasilescu, J., and Figeys, D. (2006) Analysis of protein interaction networks using mass spectrometry compatible techniques. *Anal Chim Acta 564*, 10-8.

(8) Morgan-Kiss, R. M., Wadler, C., and Cronan, J. E., Jr. (2002) Long-term and homogeneous regulation of the *Escherichia coli* araBAD promoter by use of a lactose transporter of relaxed specificity. *Proc Natl Acad Sci U S A 99*, 7373-7.

(9) Voss, S., and Skerra, A. (1997) Mutagenesis of a flexible loop in streptavidin leads to higher affinity for the Strep-tag II peptide and improved performance in recombinant protein purification. *Protein Eng 10*, 975-82.

(10) Terpe, K. (2003) Overview of tag protein fusions: from molecular and biochemical fundamentals to commercial systems. *Appl Microbiol Biotechnol 60*, 523-33.

(11) Manting, E. H., van der Does, C., and Driessen, A. J. (1997) In vivo cross-linking of the SecA and SecY subunits of the *Escherichia coli* preprotein translocase. *J Bacteriol 179*, 5699-704.

(12) Hall, D. B., and Struhl, K. (2002) The VP16 activation domain interacts with multiple transcriptional components as determined by protein-protein cross-linking in vivo. *J Biol Chem 277*, 46043-50.

(13) Vasilescu, J., Guo, X., and Kast, J. (2004) Identification of protein-protein interactions using in vivo cross-linking and mass spectrometry. *Proteomics 4*, 3845-54.

(14) Metz, B., Kersten, G. F., Baart, G. J., de Jong, A., Meiring, H., ten Hove, J., van Steenbergen, M. J., Hennink, W. E., Crommelin, D. J., and Jiskoot, W. (2006) Identification of formaldehyde-induced modifications in proteins: reactions with insulin. *Bioconjug Chem 17*, 815-22.

(15) Metz, B., Kersten, G. F., Hoogerhout, P., Brugghe, H. F., Timmermans, H. A., de Jong, A., Meiring, H., ten Hove, J., Hennink, W. E., Crommelin, D. J., and Jiskoot, W. (2004) Identification of formaldehyde-induced modifications in proteins: reactions with model peptides. *J Biol Chem 279*, 6235-43.

(16) Ortigosa, A. D., Hristova, D., Perlstein, D. L., Zhang, Z., Huang, M., and Stubbe, J. (2006) Determination of the in vivo stoichiometry of tyrosyl radical per betabeta' in *Saccharomyces cerevisiae* ribonucleotide reductase. *Biochemistry 45*, 12282-94.

(17) Eriksson, S., Sjöberg, B. M., and Hahne, S. (1977) Ribonucleoside diphosphate reductase from *Escherichia coli*. An immunological assay and a novel purification from an overproducing strain lysogenic for phage lambdadnrd. *J Biol Chem 252*, 6132-8.

(18) Hristova, D., Wu, C. H., Jiang, W., Krebs, C., and Stubbe, J. (2008) Importance of the maintenance pathway in the regulation of the activity of *Escherichia coli* ribonucleotide reductase. *Biochemistry 47*, 3989-99.

(19) Popescu, C. V., Bates, D. M., Beinert, H., Munck, E., and Kiley, P. J. (1998) Mössbauer spectroscopy as a tool for the study of activation/inactivation of the transcription regulator FNR in whole cells of *Escherichia coli*. *Proc Natl Acad Sci U S A 95*, 13431-5.

(20) Benda, R., Tse Sum Bui, B., Schunemann, V., Florentin, D., Marquet, A., and Trautwein, A. X. (2002) Iron-sulfur clusters of biotin synthase in vivo: a Mossbauer study. *Biochemistry 41*, 15000-6.

(21) Matzanke, B. F., Muller, G. I., Bill, E., and Trautwein, A. X. (1989) Iron metabolism of *Escherichia coli* studied by Mössbauer spectroscopy and biochemical methods. *Eur J Biochem 183*, 371-9.

(22) Adinolfi, S., Trifuoggi, M., Politou, A. S., Martin, S., and Pastore, A. (2002) A structural approach to understanding the iron-binding properties of phylogenetically different frataxins. *Hum Mol Genet 11*, 1865-77.

(23) Grass, G., Franke, S., Taudte, N., Nies, D. H., Kucharski, L. M., Maguire, M. E., and Rensing, C. (2005) The metal permease ZupT from *Escherichia coli* is a transporter with a broad substrate spectrum. *J Bacteriol 187*, 1604-11.

(24) Baba, T., Ara, T., Hasegawa, M., Takai, Y., Okumura, Y., Baba, M., Datsenko, K. A., Tomita, M., Wanner, B. L., and Mori, H. (2006) Construction of *Escherichia coli* K-12 in-frame, single-gene knockout mutants: the Keio collection. *Mol. Syst. Biol. 2*, 2006 0008.

(25) Fish, W. W. (1988) Rapid colorimetric micromethod for the quantitation of complexed iron in biological samples. *Methods Enzymol 158*, 357-64.

(26) Bou-Abdallah, F., Adinolfi, S., Pastore, A., Laue, T. M., and Dennis Chasteen, N. (2004) Iron binding and oxidation kinetics in frataxin CyaY of *Escherichia coli*. *J Mol Biol 341*, 605-15.

(27) Atkin, C. L., Thelander, L., Reichard, P., and Lang, G. (1973) Iron and free radical in ribonucleotide reductase. Exchange of iron and Mössbauer spectroscopy of the protein B2 subunit of the *Escherichia coli* enzyme. *J Biol Chem 248*, 7464-72.

(28) Bollinger, J. M., Tong, W. H., Ravi, N., Huynh, B. H., Edmondson, D. E., and Stubbe, J. (1994) Mechanism of assembly of the tyrosyl radical-diiron(III) cofactor of *Escherichia coli* ribonucleotide reductase. 2. Kinetics of the excess Fe^{2+} reaction by optical, EPR, and Mössbauer spectroscopies. *J. Am. Chem. Soc. 116*, 8015-8023.

(29) Salowe, S. P., and Stubbe, J. (1986) Cloning, overproduction, and purification of the B2 subunit of ribonucleoside-diphosphate reductase. *J Bacteriol 165*, 363-6.

(30) Broman, L., Malmström, B. G., Aasa, R., and Vanngard, T. (1962) Quantitative electron spin resonance studies on native and denatured ceruloplasmin and laccase. *J. Mol. Biol. 5*, 301-10.

(31) Hayashi, K., Morooka, N., Yamamoto, Y., Fujita, K., Isono, K., Choi, S., Ohtsubo, E., Baba, T., Wanner, B. L., Mori, H., and Horiuchi, T. (2006) Highly accurate genome sequences of *Escherichia coli* K-12 strains MG1655 and W3110. *Mol Syst Biol 2*, 2006 0007.

(32) Datsenko, K. A., and Wanner, B. L. (2000) One-step inactivation of chromosomal genes in *Escherichia coli* K-12 using PCR products. *Proc Natl Acad Sci U S A 97*, 6640-5.

(33) Casadaban, M. J., and Cohen, S. N. (1980) Analysis of gene control signals by DNA fusion and cloning in *Escherichia coli*. *J Mol Biol 138*, 179-207.

(34) Grant, S. G., Jessee, J., Bloom, F. R., and Hanahan, D. (1990) Differential plasmid rescue from transgenic mouse DNAs into *Escherichia coli* methylation-restriction mutants. *Proc Natl Acad Sci U S A 87*, 4645-9.

(35) Studier, F. W., and Moffatt, B. A. (1986) Use of bacteriophage T7 RNA polymerase to direct selective high-level expression of cloned genes. *J Mol Biol 189*, 113-30.

(36) Bulteau, A. L., O'Neill, H. A., Kennedy, M. C., Ikeda-Saito, M., Isaya, G., and Szweda, L. I. (2004) Frataxin acts as an iron chaperone protein to modulate mitochondrial aconitase activity. *Science 305*, 242-5.

(37) Zhang, Y., Lyver, E. R., Knight, S. A., Lesuisse, E., and Dancis, A. (2005) Frataxin and mitochondrial carrier proteins, Mrs3p and Mrs4p, cooperate in providing iron for heme synthesis. *J Biol Chem.*

(38) Layer, G., Ollagnier-de Choudens, S., Sanakis, Y., and Fontecave, M. (2006) Iron-sulfur cluster biosynthesis: characterization of *Escherichia coli* CyaY as an iron donor for the assembly of [2Fe-2S] clusters in the scaffold IscU. *J Biol Chem 281*, 16256-63.

(39) Kondapalli, K. C., Kok, N. M., Dancis, A., and Stemmler, T. L. (2008) *Drosophila* frataxin: an iron chaperone during cellular Fe-S cluster bioassembly. *Biochemistry 47*, 6917-27.

(40) Bonomi, F., Iametti, S., Ta, D., and Vickery, L. E. (2005) Multiple turnover transfer of [2Fe2S] clusters by the iron-sulfur cluster assembly scaffold proteins IscU and IscA. *J Biol Chem 280*, 29513-8.

(41) Guzman, L. M., Belin, D., Carson, M. J., and Beckwith, J. (1995) Tight regulation, modulation, and high-level expression by vectors containing the arabinose pBAD promoter. *J Bacteriol 177*, 4121-30.

(42) Prossnitz, E., Nikaido, K., Ulbrich, S. J., and Ames, G. F. (1988) Formaldehyde and photoactivatable cross-linking of the periplasmic binding protein to a membrane component of the histidine transport system of *Salmonella typhimurium*. *J Biol Chem 263*, 17917-20.

(43) Lynch, J. B., Juarez-Garcia, C., Münck, E., and Que, L., Jr. (1989) Mössbauer and EPR studies of the binuclear iron center in ribonucleotide reductase from *Escherichia coli*. A new iron-to-protein stoichiometry. *J Biol Chem 264*, 8091-6.

(44) Hantke, K. (1987) Ferrous iron transport mutants in *Escherichia coli* K12. *FEMS Microbiology Letters 44*, 53-57.

(45) Cartron, M. L., Maddocks, S., Gillingham, P., Craven, C. J., and Andrews, S. C. (2006) Feo--transport of ferrous iron into bacteria. *Biometals 19*, 143-57.

(46) Velayudhan, J., Hughes, N. J., McColm, A. A., Bagshaw, J., Clayton, C. L., Andrews, S. C., and Kelly, D. J. (2000) Iron acquisition and virulence in *Helicobacter pylori*: a major role for FeoB, a high-affinity ferrous iron transporter. *Mol Microbiol 37*, 274-86.

(47) Kammler, M., Schon, C., and Hantke, K. (1993) Characterization of the ferrous iron uptake system of *Escherichia coli*. *J Bacteriol 175*, 6212-9.

(48) Perry, R. D., Mier, I., Jr., and Fetherston, J. D. (2007) Roles of the Yfe and Feo transporters of *Yersinia pestis* in iron uptake and intracellular growth. *Biometals 20*, 699-703.

(49) Marlovits, T. C., Haase, W., Herrmann, C., Aller, S. G., and Unger, V. M. (2002) The membrane protein FeoB contains an intramolecular G protein essential for Fe(II) uptake in bacteria. *Proc Natl Acad Sci U S A 99*, 16243-8.

(50) Rong, C., Huang, Y., Zhang, W., Jiang, W., Li, Y., and Li, J. (2008) Ferrous iron transport protein B gene (feoB1) plays an accessory role in magnetosome formation in *Magnetospirillum gryphiswaldense* strain MSR-1. *Res Microbiol 159*, 530-6.

(51) Hantke, K. (1997) Ferrous iron uptake by a magnesium transport system is toxic for *Escherichia coli* and *Salmonella typhimurium*. *J Bacteriol 179*, 6201-4.

(52) Papp, K. M., and Maguire, M. E. (2004) The CorA Mg^{2+} transporter does not transport Fe^{2+}. *J Bacteriol 186*, 7653-8.

(53) Epsztejn, S., Kakhlon, O., Glickstein, H., Breuer, W., and Cabantchik, I. (1997) Fluorescence analysis of the labile iron pool of mammalian cells. *Anal Biochem 248*, 31-40.

(54) Keyer, K., and Imlay, J. A. (1996) Superoxide accelerates DNA damage by elevating free-iron levels. *Proc Natl Acad Sci U S A 93*, 13635-40.

(55) Petrat, F., de Groot, H., Sustmann, R., and Rauen, U. (2002) The chelatable iron pool in living cells: a methodically defined quantity. *Biol Chem 383*, 489-502.

(56) Bohnke, R., and Matzanke, B. F. (1995) The mobile ferrous iron pool in *Escherichia coli* is bound to a phosphorylated sugar derivative. *Biometals 8*, 223-30.

(57) Veiga, N., Torres, J., Mansell, D., Freeman, S., Dominguez, S., Barker, C. J., Diaz, A., and Kremer, C. (2009) "Chelatable iron pool": inositol 1,2,3-trisphosphate fulfils the conditions required to be a safe cellular iron ligand. *J Biol Inorg Chem 14*, 51-9.

(58) Thorgersen, M. P., and Downs, D. M. (2008) Analysis of *yggX* and *gshA* mutants provides insights into the labile iron pool in Salmonella enterica. *J Bacteriol 190*, 7608-13.

(59) Covès, J., and Fontecave, M. (1993) Reduction and mobilization of iron by a NAD(P)H:flavin oxidoreductase from *Escherichia coli*. *Eur J Biochem 211*, 635-41.

(60) Fontecave, M., Coves, J., and Pierre, J. L. (1994) Ferric reductases or flavin reductases? *Biometals 7*, 3-8.

(61) Andrews, S. C., Shipley, D., Keen, J. N., Findlay, J. B., Harrison, P. M., and Guest, J. R. (1992) The haemoglobin-like protein (HMP) of *Escherichia coli* has ferrisiderophore reductase activity and its C-terminal domain shares homology with ferredoxin NADP+ reductases. *FEBS Lett 302*, 247-52.

(62) Yeom, J., Jeon, C. O., Madsen, E. L., and Park, W. (2008) Ferredoxin-NADP+ reductase from *Pseudomonas putida* functions as a ferric reductase. *J Bacteriol*. in press

Chapter 5:

Investigation on the Role of YfaE as an Iron Chaperone for β_2

INTRODUCTION

In Nature FeS clusters can exist in multiple forms in the same proteins in response to different growth environments. It has also been established both in vitro and in vivo that these multiple forms modulates the function of the FeS-containing protein. In both cases clusters are known to undergo interconversion between [2Fe2S] and [4Fe4S] units. This work provides a potential mode for how YfaE can not only serve as a reductant, but perhaps as an Fe chaperone.

In the studies in vitro of the FeS cluster assembly scaffold protein IscU, the isolated IscU contains one $[2Fe2S]^{2+}$ or two $[2Fe2S]^{2+}$ clusters per dimer. The two $[2Fe2S]^{2+}$ clusters can then convert to one $[4Fe4S]^{2+}$ cluster per dimer (*1*). This process can be facilitated by dithionite or reduced ferredoxin (*2*). The $[4Fe4S]^{2+}$ cluster in IscU is labile and degraded upon exposure to oxygen. Interestingly, only the $[4Fe4S]^{2+}$-IscU, but not the $[2Fe2S]^{2+}$-IscU, is able to transfer the FeS cluster into apo-aconitase which requires a [4Fe4S] cluster for its functions (*3*). In vivo, the process of transferring [2Fe2S] or [4Fe4S] clusters from scaffold proteins into recipient apo-proteins is facilitated by the presence of DTT, ferredoxins and/or molecular chaperones (see Chapter 1).

This interconversion between [2Fe2S] and [4Fe4S] clusters have been observed in other FeS proteins. For example, in the transcription regulator FNR (fumurate nitrate reduction), the $[4Fe4S]^{2+}$ clusters in FNR is rapidly degraded after being exposure to air and forms a $[2Fe2S]^{2+}$-FNR in which the DNA binding activity is diminished (*4*). However, the active $[4Fe4S]^{2+}$-FNR can be restored from $[2Fe2S]^{2+}$-FNR in the presence of Fe, DTT, cysteine and cysteine desulfurase, NifS. This interconversion process has also been observed in whole cells by Mössbauer spectroscopy. When *E. coli* cells with overexpressed-FNR were grown aerobically in ^{57}Fe-enriched media, the Mössbauer spectra of the whole cells showed a dominant $[2Fe2S]^{2+}$-

FNR species. When the cells were shifted to an anaerobic environment, the $[4Fe4S]^{2+}$-FNR was regenerated (*5*).

Studies on the synthetic analogues of FeS clusters also demonstrate the chemical feasiblility of this conversion (*6*). In the binuclear 2Fe2S analogues, the $[2Fe2S]^{1+}$ cluster undergoes spontaneous conversion to a structurally more stable, cubane-type $[4Fe4S]^{2+}$ cluster (**Eq 5-1**). Since both clusters have the same oxidation state, no redox reaction occurs at the Fe sites. For the oxidized $[2Fe2S]^{2+}$ cluster, it can also proceed slowly by internal redox reaction to form a $[4Fe4S]^{2+}$ cluster (**Eq 5-2**). In this case, the reducing equivalent for reduction of two ferric irons is provided by formation of a disulfide bond (*7*).

Eq 5-1 $2\ [Fe_2S_2(SR)_4]^{3-} \rightarrow [Fe_4S_4(SR)_4]^{2-} + 4\ RS^-$

Eq 5-2 $2\ [Fe_2S_2(SR)_4]^{2-} \rightarrow [Fe_4S_4(SR)_4]^{2-} + 2\ RS^- + RSSR$

(R = alkyl or aryl ligand)

The unusually labile [2Fe2S] cluster of YfaE (*8*) and the serendipitous observation that diferric-Y• cofactor was formed after incubation of apo-β_2 with $[2Fe2S]^{1+}$-YfaE followed by oxidation led us to speculate if YfaE could function as an iron chaperone for β_2. Mössbauer studies on ^{57}Fe-reconstituted YfaE mixed with apo-β_2 demonstrated the transfer of ^{57}Fe into apo-β_2, possibly from $[4Fe4S]^{2+}$ clusters in YfaE. This formation of the diferric-Y• cluster from apo-β_2 incubated with $[2Fe2S]^{2+}$-YfaE is facilitated by the presence of DTT. SDS-PAGE and size-exclusion chromatography analyses show the presence of YfaE dimer and aggregates that may be produced though disulfide bond and/or $[4Fe4S]^{2+}$ cluster formations. A working hypothesis for the mechanism by which YfaE could deliver the iron into apo-β_2 is proposed.

MATERIALS AND METHODS

Materials

Tris(hydroxymethyl)aminomethane hydrochloride (Tris-HCl) was from J.T. Baker. Dithiothreitol (DTT) was from Promega. ^{57}Fe was kindly provided by Prof. Carsten Krebs at Pennsylvania State University. Acrylamide/Bis, N,N,N,N-tetramethyl-ethylenediamine (TEMED), beta-mercaptoethanol (β-ME), and low molecular weight gel filtration standards were from Bio-Rad.

Preparation of YfaE and apo-β_2

Procedures described in Chapter 2 were followed for the purification and reconstitution of YfaE and [^{57}Fe]-YfaE (*8*). Procedures in Chapter 4 were followed for the purification of apo-β_2. The concentrations of YfaE and apo-β_2 were determined by ε_{420nm} = 11 $mM^{-1}cm^{-1}$ and ε_{280nm} = 117 $mM^{-1}cm^{-1}$, respectively. The amount of iron in the proteins was determined by the ferrozine assay (*9*).

Y• formation from apo-β_2 in the presence of YfaE and O_2 monitored by UV-visible spectroscopy

In a custom-designed glove box (M. Braun, Newburyport, MA) located in a cold room at 4 ºC, a 300 μL sample containing apo-β_2 (10 μM) and $[2Fe2S]^{1+}$-YfaE (40 μM) in 100 mM Tris-HCl, pH 7.8 with or without 10 mM DTT was brought out of the glove box in a 0.7 mL cuvette fitted with a gastight screw cap. The sample was then oxidized by blowing O_2 over the surface of the sample for ~5 sec followed by mixing the sample by inverting the cuvette. UV-visible spectra of the sample were recorded at room temperature in a Varian Cary 3 spectrophotometer

(Walnut Creek, CA). For UV-visible spectra recorded at 37 ºC, the cuvette holder of the spectrophotometer was connected to a 37 ºC water bath and the sample was allowed to equilibrate for ~10 min before being oxidized, after which the spectra were recorded every 10 min for 360 min. The sample was then taken out of the cuvette and frozen in an EPR tube (Wilmad) in liquid N_2 for analysis by EPR spectroscopy.

EPR spectroscopy

EPR spectra were recorded on a Bruker ESP-300 X-band (9.4 GHz) spectrometer at 77 K using a liquid N_2 finger dewar. The parameters: 0.05 mW microwave power, 2.5×10^3 receiver gain, 1.5 G modulation amplitude, 10-20 scans were used for recording the Y• signal, and 1.0 mW microwave power, 3.17×10^4 receiver gain, 10 G modulation amplitude, 10 scans were used for recording the $[2Fe2S]^{1+}$-YfaE signal. A $CuSO_4$ standard and the Win-EPR program (Bruker) were used for spin quantitation (*10*).

Monitoring diferric cluster formation in apo-β_2 in the presence of YfaE and O_2 by Mössbauer spectroscopy

A sample of 550 μL of 307 μM apo-β_2 with 1.23 mM $[2^{57}Fe2S]^{1+}$-YfaE in 100 mM Tris-HCl, pH 7.8 was taken out of a glove box in a 4 ºC cold room and O_2 was blown over the surface of the sample for ~30 sec followed by mild vortexing for ~10 sec. This oxidation procedure was repeated 4 times to ensure complete oxidation of the sample. Part of the oxidized sample (450 μL) was transferred to a custom-designed Mössbauer cup and frozen in liquid N_2 for Mössbauer analysis. The other 50 μL of the oxidized sample was diluted into 200 μL of 100 mM Tris-HCl, pH 7.8, packed into an EPR tube and frozen in liquid N_2 for analysis by EPR spectroscopy. One

control with the same sample composition, but without exposure to O_2, and a second control with only $[2^{57}Fe2S]^{1+}$-YfaE (1.9 mM) were prepared and frozen anaerobically in liquid N_2 for analysis by Mössbauer and spectroscopies.

Mössbauer spectroscopy

Mössbauer spectra were recorded at 4.2 K with a magnetic field of 53 mT applied parallel to the γ-radiation source. Details of instrument setup and data analysis are described in Chapter 2.

Size exclusion chromatography of oxidized YfaE incubated with DTT

In a final volume of 200 μL, oxidized YfaE (125 μM) was mixed 10 mM DTT in 100 mM Tris-HCl, pH 7.8 centrifuged at 21000 *g* for 10 min at 4 ºC. The supernatant (50 μL) was injected into a Superose 12 gel filtration column (10/300 GL, 25 mL, 10 x 300 mm, GE Healthcare, Little Chalfont, U.K.) pre-equilibrated with 120 mL of 50 mM K_2HPO_4, 150 mM NaCl, pH 7.0, which had been filtered with a 0.2 μm, 47 mm Nylon membrane, followed by degassing with Ar over 20 min. The flow rate was maintained at 0.5 mL/min by Waters 2480 HPLC system (Waters) and A_{280nm} and A_{340nm} were monitored. Molecular mass standards (thyroglobulin: 670 kDa, gamma globulin: 158 kDa, ovalbumin: 44 kDa, myoglobin: 17 kDa, vitamin B-12: 1.35 kDa) were run prior to each experiment.

RESULTS

Formation of Y• from apo-β_2 in the presence of YfaE and O_2

Our previous studies on reconstituted $[2Fe2S]^{1+}$-YfaE have shown that about 20% of the total iron is in a $[4Fe4S]^{2+}$ form, which represents ~11% of the total FeS clusters in YfaE (*8*). Furthermore, the quantitation of sulfide showed 3.2 ± 0.2 S/YfaE (8 determinations from 3 different batches of purified YfaE), which is higher than 1.9 ± 0.2 Fe/YfaE by the ferrozine assays (7 determinations from 3 different batches of purified YfaE). The higher sulfide content may be due to formation of persulfides with cysteines at the C-terminus of YfaE. Could the $[4Fe4S]^{2+}$ cluster and the unusual higher sulfide content come from artifacts of in vitro reconstitution or could YfaE play a role other than providing electrons for cluster biosynthesis and maintenance? To investigate the this possibility, the reconstituted $[2Fe2S]^{1+}$-YfaE (40 μM) was mixed with apo-β_2 (10 μM) anaerobically. The UV-visible spectrum of the sample shows normal features of $[2Fe2S]^{1+}$-YfaE. However, when the sample was exposed to O_2, a small peak that resembles diferric-Y• cofactor appeared (**Figure 5-1**). The EPR spectrum confirmed the formation of the Y• and the quantitation of the signal gave ~0.3 Y•/β_2. The iron content of apo-β_2 (determined by ferrozine assay) was less than 0.1 Fe/β_2, which could maximally generate 0.05 Y•/β_2 if the Y• was formed from YfaE reduction of met-β_2. Therefore, the remaining iron in apo-β_2 cannot account for the amount of the Y• formed. The only possible iron source for cluster assembly is YfaE. Since the $[2Fe2S]^{1+}$ cluster in YfaE is relatively stable, the iron may be coming from decomposition of the $[4Fe4S]^{2+}$ cluster in YfaE. If 10% of YfaE contains a $[4Fe4S]^{2+}$ cluster, then 40 μM of YfaE would contain ~4 μM of $[4Fe4S]^{2+}$ (~8 μM of ferrous iron). If this ferrous iron was used to form diferric-Y• cofactor of β_2, ~4 μM Y•, equivalent to

~0.4 Y•/β_2 could be generated, which is in fair agreement with the observed EPR results (~0.3 Y•/β_2).

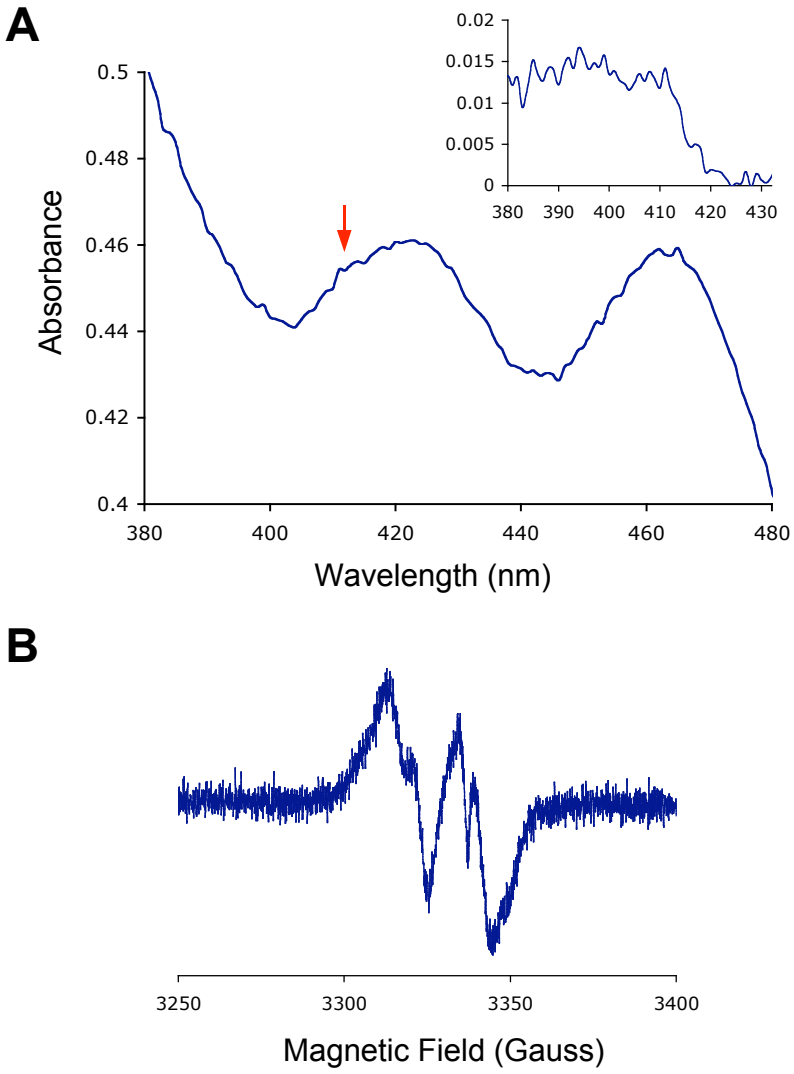

Figure 5-1. Formation of diferric-Y• cofactor in apo-β_2 (10 μM) after mixing with $[2Fe2S]^{1+}$-YfaE (40 μM) followed by exposure to oxygen. (A) UV-visible spectrum of the apo-β_2/YfaE mixture right after exposure to oxygen. The red arrow indicates the small bulge at ~410 nm on top of the absorption peaks of oxidized YfaE. (Inset) difference spectrum after subtracting the spectrum of 40 μM oxidized YfaE from the oxygen-exposed apo-β_2/YfaE mixture. The feature in the difference spectrum is similar to that of the diferric-Y• in β_2. (B) EPR spectrum (9.4 GHz) of the apo-β_2/YfaE mixture right after exposure to oxygen. The spectrum is recorded at 77 K, microwave power = 0.05 mW, receiver gain = 2.5 × 10^3, modulation amplitude = 1.5 G. The feature of the spectrum is identical to that of the diferric-Y• in β_2.

Therefore, the amount of $[4Fe4S]^{2+}$ could account for the observed Y• in this experiment. The same experiments were repeated several times and the formation of the Y• was reproducible. In order to confirm that the iron in the diferric-Y• cofactor is coming from YfaE and verify the role of $[4Fe4S]^{2+}$ in the cluster formation, Mössbauer spectroscopy was applied to monitor the changes of FeS species in YfaE in the presence of apo-β_2.

Assembly of diferric-Y• cluster from apo-β_2 in the presence of YfaE and O_2 monitored by Mössbauer spectroscopy

To verify the role of YfaE in the cluster assembly of apo-β_2, YfaE was reconstituted in the presence of $^{57}Fe^{2+}$, $^{57}Fe^{3+}$ and S^{2-} following our published procedures (*8*). Samples of $[2^{57}Fe2S]^{1+}$-YfaE (1.23 mM) with apo-β_2 (307 μM) with or without exposure to oxygen were prepared. The reproducibility of Y• formation using ^{57}Fe-reconstituted YfaE was confirmed by EPR spectroscopy. The EPR spectrum from the sample containing YfaE and apo-β_2 without exposure to oxygen shows features associated with reduced YfaE and the lack of features from the Y•, indicating the sample was oxygen free (**A, Figure 5-2**). On the other hand, after the YfaE/apo-β_2 mixture was exposed to O_2, the Y• was observed in the EPR spectrum (**B, Figure 5-2**). The Y• quantitation indicates formation of ~60 μM Y• (~0.5 Y•/β_2) which would require at least 120 μM of iron be delivered into apo-β_2. Assuming 10% of YfaE contains a $[4Fe4S]^{2+}$ cluster (~123 μM), ~246 μM Fe^{2+} is available for cluster assembly. The amount of Y• generated suggests only ~50% of the Fe^{2+} in the $[4Fe4S]^{2+}$ is transferred to apo-β_2.

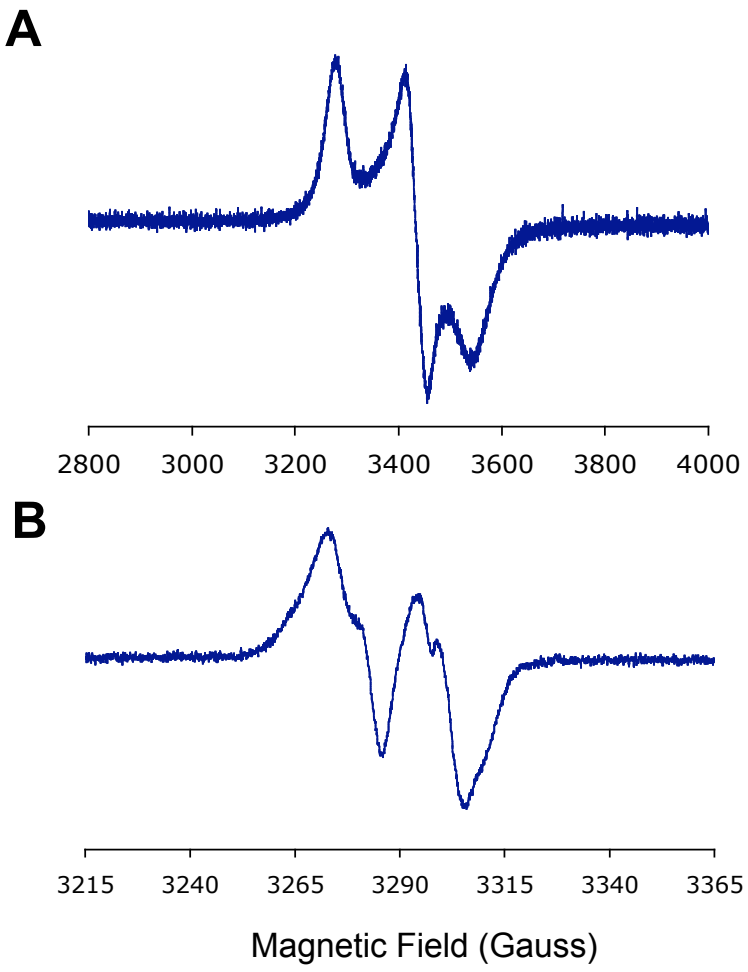

Figure 5-2. EPR spectra of apo-β_2 mixed with ^{57}Fe-reconstituted $[2Fe2S]^{1+}$-YfaE without (A) or with (B) exposure to O_2. Apo-β_2 (307 μM) was mixed with ^{57}Fe-reconstituted $[2Fe2S]^{1+}$-YfaE (1.23 mM) (apo-β_2 : YfaE = 1: 4) anaerobically followed by loading the sample into EPR tubes with or without oxidation. Features of the reduced YfaE and the Y• were observed in (A) and (B), respectively.

The results from the Mössbauer experiments are shown in **Figure 5-3** and the parameters of simulations are summarized in **Table 5-1**. The reconstituted YfaE contains ~11% $[4Fe4S]^{2+}$ (20% of total Fe) which is consistent with our previous studies (*8*), suggesting the reproducibility between reconstitutions. Furthermore, ~6% $[2Fe2S]^{2+}$ can be simulated in the spectrum (**Table 5-1**), in line with an upper limit of 7% $[2Fe2S]^{2+}$ in the reconstituted $[2^{57}Fe2S]^{1+}$-YfaE reported in our previous reconstitution of YfaE (*8*).

Compared to the spectrum of the $[2^{57}Fe2S]^{1+}$-YfaE only, the addition of apo-β_2 causes the decomposition of ~50% of $[4Fe4S]^{2+}$ cluster into $[2Fe2S]^{1+}$ and $[2Fe2S]^{2+}$ clusters (**B, Figure 5-3**), in line with the prediction from Y• quantitation. Because the YfaE : apo-β_2 is 4:1, assuming one YfaE binds to one subunit of apo-β_2, ~50% of the YfaE can be in direct contact with apo-β_2. Therefore, one possible explanation for only 50% of the $[4Fe4S]^{2+}$ was decomposed upon addition of apo-β_2 is that the decomposition of $[4Fe4S]^{2+}$ is triggered by direct interaction with apo-β_2.

Upon exposure to O_2, an upper limit of 5% diferric-β_2 can be simulated (~125 μM iron), which is in excellent agreement with the EPR quantitation of the Y• (~60 μM) (**C, Figure 5-3**). These results suggest that the YfaE-mediated diferric-Y• cluster formation has a stoichiometry of one Y• formed per two irons delivered. Interestingly, the quadruple splitting of the oxidized YfaE (ΔE_Q = 0.67 mm/s) is significantly different from the oxidized YfaE in the absence of β_2 (ΔE_Q = 0.58 mm/s) (*8*), suggesting a conformational change of the $[2Fe2S]^{2+}$ cluster in YfaE triggered by the presence of β_2.

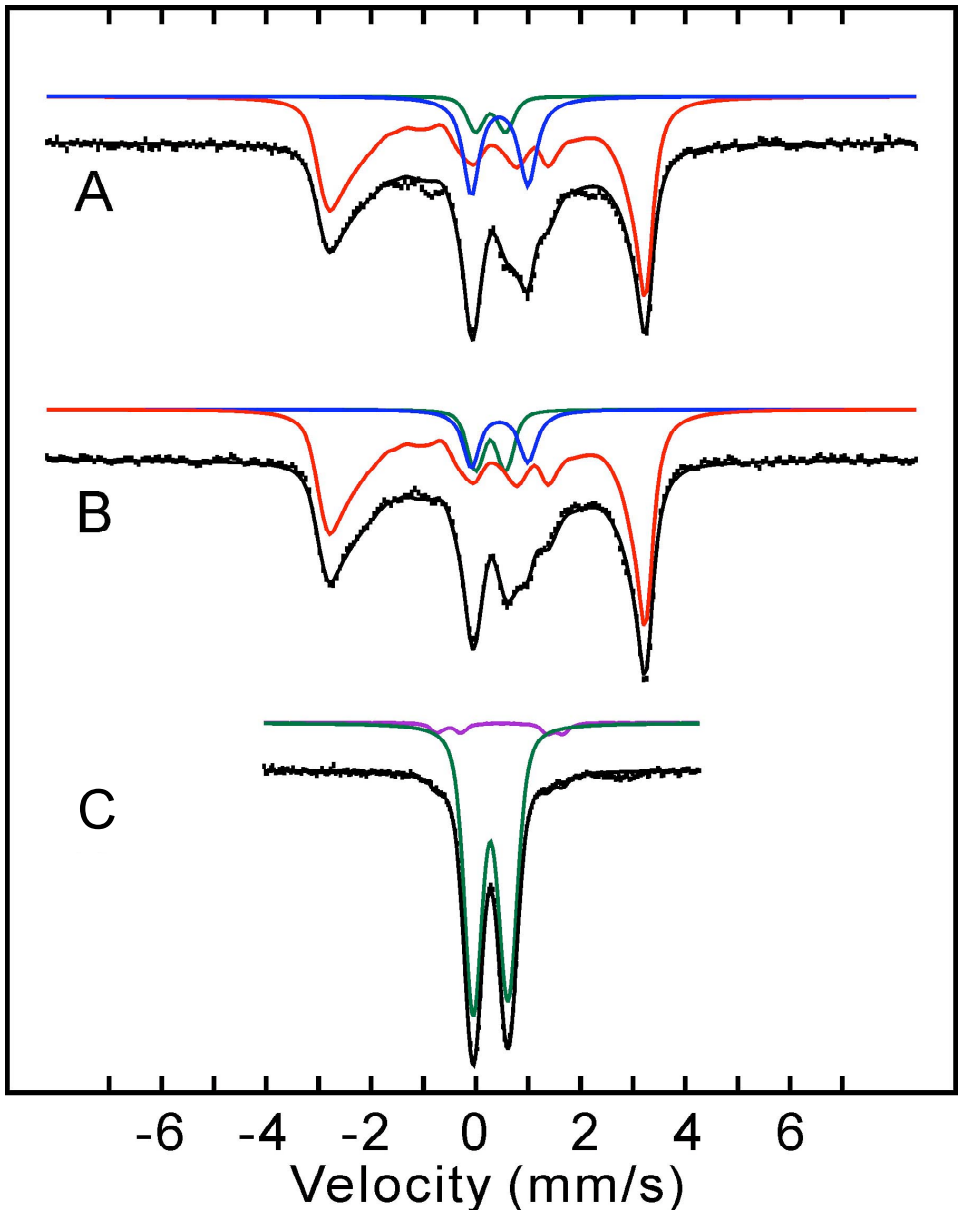

Figure 5-3. 4.2-K Mössbauer spectra of apo-β_2 mixed with ^{57}Fe-reconstituted $[2Fe2S]^{1+}$-YfaE with or without exposure to O_2. Mixtures of apo-β_2 (307 μM) and ^{57}Fe-reconstituted $[2Fe2S]^{1+}$-YfaE (1.23 mM) (total 450 μL, apo-β_2 : YfaE = 1: 4) were loaded anaerobically into Mössbauer cups and frozen in liquid N_2 with or without exposure to O_2. (A) $[2Fe2S]^{1+}$-YfaE only (1.9 mM). (B) $[2Fe2S]^{1+}$-YfaE mixed with apo-β_2 prior to exposure to O_2. (C) $[2Fe2S]^{1+}$-YfaE mixed with apo-β_2 followed by exposure to O_2. Red: $[2Fe2S]^{1+}$, green: $[2Fe2S]^{2+}$, blue: $[4FeS]^{2+}$, purple: diferric-β_2. Simulation parameters are listed in **Table 5-1**.

Table 5-1. Mössbauer simulation parameters of apo-β_2 mixed with ^{57}Fe-reconstituted $[2Fe2S]^{1+}$-YfaE with or without exposure to O_2.

Sample	Cluster	Relative amount (%)	Site	δ (mm/s)	ΔE_Q (mm/s)
YfaE	$[2Fe2S]^{1+}$	74	Fe^{3+}	0.33	0.78
			Fe^{2+}	0.60	-3.13
	$[2Fe2S]^{2+}$	6	Fe^{3+}	0.28	0.58
	$[4Fe4S]^{2+}$	20	$Fe^{2.5}$	0.44	1.07
YfaE + apo-β_2	$[2Fe2S]^{1+}$	80	Fe^{3+}	0.33	0.78
			Fe^{2+}	0.60	-3.13
	$[2Fe2S]^{2+}$	10	Fe^{3+}	0.28	0.58
	$[4Fe4S]^{2+}$	10	$Fe^{2.5}$	0.44	1.07
YfaE + apo-β_2 + O_2	$[2Fe2S]^{2+}$	95	Fe^{3+}	0.28	0.67
	diferric-β_2	5	Fe^{3+}	0.46	2.40
				0.54	1.65

Monitoring YfaE-mediated Y• formation at 37 ºC in the absence of DTT

Although the Mössbauer experiment confirmed the iron source is supplied by YfaE and could potentially come from the $[4Fe4S]^{2+}$ cluster, sub-stoichiometric amounts of Y•/β_2 were obtained, which could result from the "slow" and incompletely understood oxidation process of the reduced cluster. Our earlier studies have demonstrated that $[2Fe2S]^{2+}$-YfaE is "very" unstable and that the FeS clusters in YfaE decomposes within a few hours at room temperature (**Figure 2-5,** Chapter 2). Because the same lability of a $[2Fe2S]^{2+}$ cluster has been observed in the endogenously purified scaffold protein $[2Fe2S]^{2+}$-IscU (*11*), we thought that this lability could be associated with the iron delivery to apo-β_2. To address this question, the same experiment described in **Figure 5-1** was conducted except that the oxidized sample was incubated at 37 ºC and the UV-visible spectrum of the sample was monitored every 30 min for 4 h (**Figure 5-4**). Surprisingly, formation of the Y• concomitant with the decay of the FeS cluster in oxidized YfaE was observed. Quantitation by EPR spectroscopy showed ~0.8 Y•/β_2 was formed, which is higher than 0.3-0.5 Y•/β_2 in our earlier experiments.

Because the iron needs to be in the ferrous state to be delivered to apo-β_2, a reduction mechanism must exist to reduce ferric iron of the oxidized YfaE. One special feature of YfaE compared to other ferredoxins is the additional cysteines at the C-terminus of YfaE (C72 and C73, see **Figure 3-8** in Chapter 3). One might postulate that the intermolecular disulfide bond formation between these cysteines might provide the electrons for reduction of Fe^{3+}. To look for evidence of disulfide bond formation, SDS-PAGE of the sample from the experiment described in **Figure 5-4** with or without incubation with β-mercaptoethanol (β-ME) was carried out (**Figure 5-5**). The results show that in the absence of β-ME, a high molecular mass aggregate of YfaE was observed which disappeared in the presence of 2-ME. This disappearance was

concomitant with the appearance of YfaE, suggesting the aggregation occurred through disulfide bond formation.

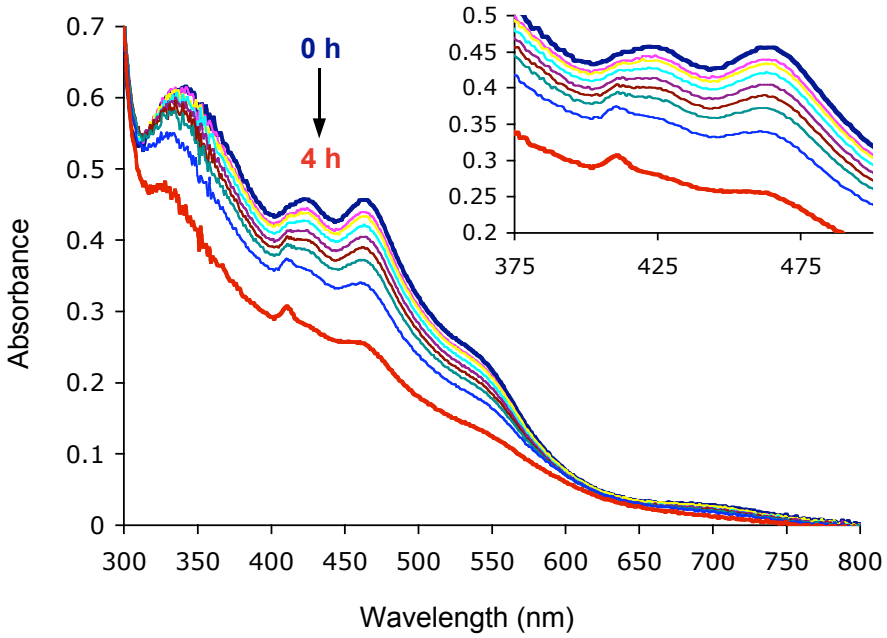

Figure 5-4. UV-vis spectra of apo-β_2 (10 μM) incubated with $[2Fe2S]^{1+}$-YfaE (40 μM) at 37 ºC after exposure to O_2 and monitored over time. Apo-β_2 was mixed with $[2Fe2S]^{1+}$-YfaE anaerobically, then O_2 was blown over the sample. Spectra were recorded every 30 min (thin lines) at 37 ºC subsequent to O_2 exposure (thick blue line). The last spectrum was recorded 4 h after the oxidation began (thick red line). The spectra show concomitant decay of the $[2Fe2S]^{2+}$-YfaE with the formation of the Y•. Inset: blow-ups of the spectra.

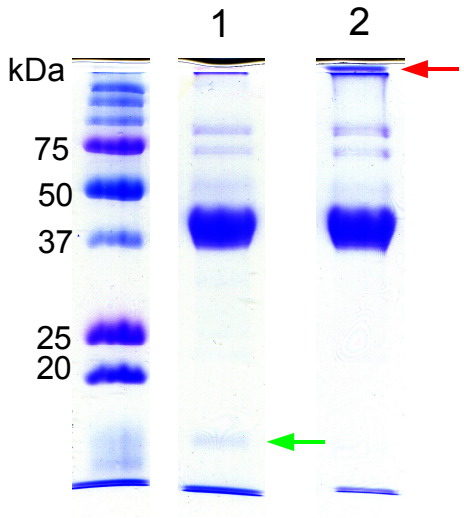

Figure 5-5. SDS-PAGE of apo-β_2 (10 μM) mixed with $[2Fe2S]^{1+}$-YfaE (40 μM) after exposure to O_2 for 6 h at 37 ºC. Oxidized apo-β_2/YfaE mixture (10 μL) was loaded into a 15% SDS-PAGE gel with Laemmli buffer in the presence β-ME (lane 1) or with β-ME omitted (lane 2). The gel shows a dominant band from β_2 monomer (43.5 kDa). The green arrow indicates the YfaE monomer (9.4 kDa), which is absent in the samples without β-ME (lane 2). The sample without incubation with β-ME shows high molecular mass species on top of the gel (red arrow).

Monitoring YfaE-mediated Y• formation at 37 ºC in the presence of DTT

If the disulfide bond formation between YfaE monomers really is associated with its ability to deliver iron apo-β_2, the presence of DTT could potentiate the iron transfer process. An experiment similar to that described in **Figure 5-4** was carried out except that 10 mM DTT was added to the apo-β_2/YfaE mixture. Excitingly, the formation of the Y• is much faster than that without DTT, further supports a correlation between disulfide bond formation and the Y• formation (**Figure 5-6**). Spin quantitation of the Y• by EPR spectroscopy also gave 0.8 Y•/β_2, the same observed in the absence of DTT (**Figure 5-4**), suggesting that DTT facilitates the formation of Y• instead of changing the stoichiometry of the reaction. A control experiment without addition of apo-β_2 shows that oxidized YfaE is stable in the presence of DTT, indicating the presence of apo-β_2 triggers the dissociation of the FeS cluster in YfaE.

Both disulfide formation between YfaE monomer or DTT oxidation could provide the reducing equivalent for ferric iron reduction. However, the product of reduction still remains to be determined. One possibility is that $[2Fe2S]^{2+}$ cluster is reduced to $[2Fe2S]^{1+}$ cluster and the $[2Fe2S]^{1+}$ provides the Fe^{2+} for apo-β_2. However, longer incubation of apo-β_2 with $[2Fe2S]^{1+}$-YfaE does not result in higher Y• formation, suggesting $[2Fe2S]^{1+}$ cluster is not the iron donor. Furthermore, there is only one ferrous iron in each $[2Fe2S]^{1+}$ cluster, which implies the formation of one diferric-Y• cluster would require dissociation and association of YfaE to furnish two ferrous iron in one subunit of β_2. This is highly unlikely given the weak binding of ferrous iron to apo-β_2 and the reactivity of ferrous iron with O_2 in the solution. The possibility of that $[2Fe2S]^{2+}$ is reduced to $[2Fe2S]^{0}$ seems unlikely as the reduction potential for $[2Fe2S]^{1+/0}$ is too low (-410 to -840 mV) (*12, 13*) to be carried out by DTT oxidation or disulfide bond formation (-200 to -300 mV) (*14, 15*).

Based on the studies on synthetic analogues of FeS complex and FeS proteins that contain interconvertable $[2Fe2S]^{2+}$ and $[4Fe4S]^{2+}$ clusters, one possibility is that the electrons provided by disulfide formation are used to reductively couple two $[2Fe2S]^{2+}$ clusters to form one $[4Fe4S]^{2+}$ cluster (*2*, *4*, *6*). The $[4Fe4S]^{2+}$ cluster then contains two ferrous irons that can be delivered into apo-β_2 from a single YfaE. The [4Fe4S]-mediated iron delivery would also be consistent with the observations in the Mössbauer experiment (**Figure 5-3**) in which $[4Fe4S]^{2+}$ clusters in YfaE decompose after addition of apo-β_2.

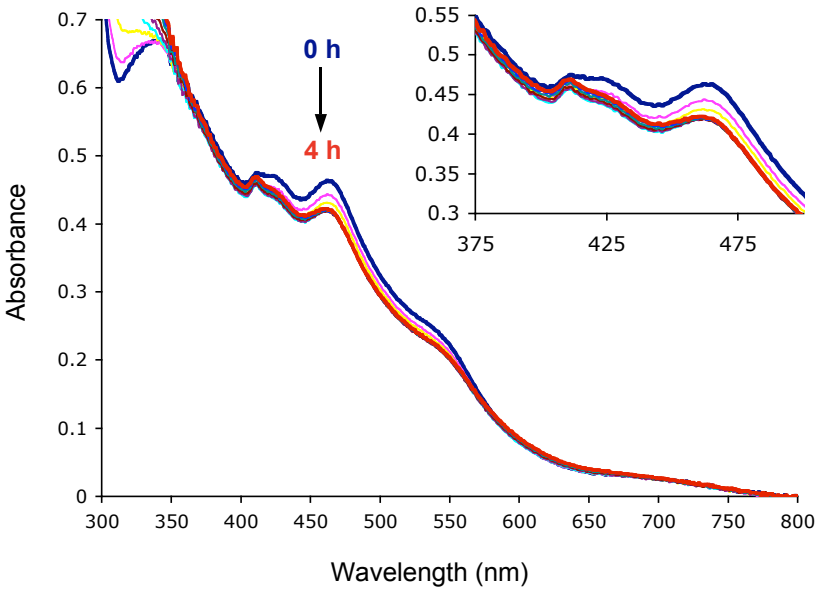

Figure 5-6. Changes in UV-vis spectra of apo-β_2 (10 μM), $[2Fe2S]^{1+}$-YfaE (40 μM) and DTT (10 mM) mixture at 37 ºC after exposed to O_2. Apo-β_2 was mixed with $[2Fe2S]^{1+}$-YfaE and DTT anaerobically and then O_2 was blown over the reaction mixture. Spectra were recorded every 30 min (thin lines) at 37 ºC after O_2 oxidation (thick blue line). The last spectrum was recorded 4 h after the oxidation of the sample (thick red line). Inset: blow-ups of the spectra.

Size-exclusion chromatography revealed formation of YfaE dimer in the presence of DTT

The proposed reductive coupling between two $[2Fe2S]^{2+}$ to form one $[4Fe4S]^{2+}$ implies that two YfaE monomers would associate to form a dimer. Because in the absence of DTT, oxidized YfaE forms high molecular mass aggregates (**Figure 5-5**), investigation to confirm the existence of YfaE dimers was carried out in the presence of DTT. Size-exclusion chromatography (SEC) was employed to look for presence of a YfaE dimer (**Figure 5-7**). $[2Fe2S]^{2+}$-YfaE incubated in an O_2 atmosphere for ~1 h was mixed with 10 mM DTT and immediately injected onto a SEC column. The SEC trace showed a peak corresponding to oxidized YfaE aggregate, eluted in the void volume, and a peak that corresponds to the YfaE monomer (**A, Figure 5-7**). Excitingly, after the same sample was incubated with 10 mM DTT for ~1 h, the SEC trace showed a small decrease of the YfaE monomer peak concomitant with the appearance of a new peak in which the calculated molecular mass is equivalent to a YfaE dimer (red arrow, **B, Figure 5-7**). Furthermore, because the A_{340nm}/A_{280nm} ratio can be used to evaluate the integrity of FeS clusters, a A_{340nm}/A_{280nm} of 0.84 in the monomer YfaE suggests the presence of intact $[2Fe2S]^{2+}$ clusters and a A_{340nm}/A_{280nm} of 0.66 in the aggregation peak indicates some decomposition of the cluster. Interestingly, the A_{340nm}/A_{280nm} of the YfaE dimer peak was 0.67, which could be due to a YfaE dimer that contains substoichiometric amounts of $[2Fe2S]^{2+}$ clusters and/or a $[4Fe4S]^{2+}$ cluster. In summary, these results support a model in which DTT facilitates the reductive coupling between two $[2Fe2S]^{2+}$ clusters to form a $[4Fe4S]^{2+}$ cluster and the dimerization of YfaE. This $[4Fe4S]^{2+}$ cluster at the interface of the two YfaE monomers could potentially be the species which delivers iron into apo-β_2.

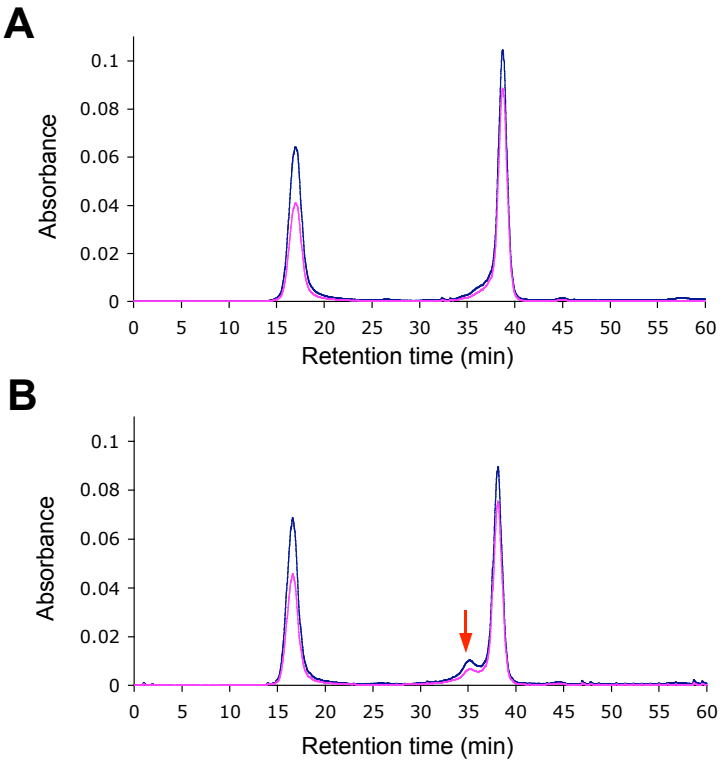

Figure 5-7. SEC of oxidized YfaE in the presence of DTT. Oxidized YfaE (~16 μM) was mixed with 10 mM DTT and injected onto Superose-12 size-exclusion column immediately after mixing (A) or 1 h after the mixing (B). A_{280nm} (blue) and A_{340nm} (pink) were monitored. The oxidized YfaE aggregates eluted in the void volume (~16 min), whereas the YfaE monomers eluted at ~38 min. The red arrow in (B) indicates the peak corresponding to a molecular mass of a YfaE dimer (~35 min). The Superose-12 column was equilibrated in 50 mM K_2HPO_4, 150 mM NaCl, pH 7.0 at a flow rate of 0.5 mL/min.

Homology model of YfaE

Because it was suspected that the two cysteines (C72, C73) in YfaE might play a role in the formation of a $[4Fe4S]^{2+}$ cluster and/or in the assembly of the diferric-Y•, a homology model of YfaE was generated. When generating a homology model, the sequence identity between the target protein and the template protein determines the accuracy of the model. A BLAST search on the available structures in the Protein Data Bank using *E. coli* YfaE as the search vehicle indicates that a ferredoxin (pdb: 1IUE) (*16*) from the human malaria parasite (*Plasmodium falciparum*) has the highest sequence identity (34%). Based on the sequence alignment between YfaE and *P. falciparum* Fdx, a homology model was generated.

Figure 5-8 shows the resulting homology model of YfaE. There are seven cysteines in YfaE. The four conserved cysteinyl ligands (C36, C41, C44, C71) for the 2Fe2S cluster are located in loops, similar to the cysteine ligands in all 2Fe2S-ferreodxins (*17, 18*). The two additional cysteines (C72, C73) are located in a flexible loop right next to the FeS cluster binding motif. The seventh cysteine (C14) is not conserved among other YfaE-like ferredoxins (**Figure 3-8**, Chapter 3). From the sequence alignment (**C**, **Figure 5-8**) the malaria Fdx has cysteines that are equivalent to C14 and C73 in YfaE. Interestingly, the malaria Fdx was purified by anion-exchange and size-exclusion chromatographies under aerobic conditions, suggesting that the oxidized Fdx is relatively stable (*16, 19*). Furthermore, from the homology model, C72 has sufficient surface exposure to be able to form intermolecular disulfide bonds. Therefore, it appears that C72 could be involved in the reductive coupling or aggregation of YfaE, and may also play a role in transferring ferrous iron into apo-β_2 given its proximity to the 2Fe2S cluster. This model suggests that a cysteine-mediated ligand exchange may provide a mechanism for delivering the ferrous iron to apo-β_2 without exposing the metal to solvent or O_2.

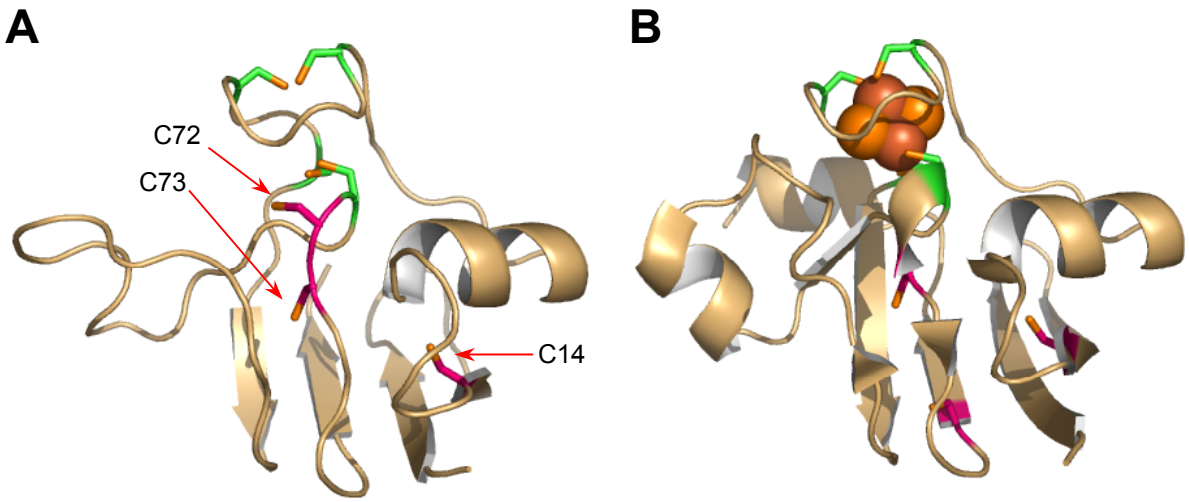

C

```
YfaE -MARVTLRITG--TQLLCQDEHPSLLAALESHNVAVEYQCREGYCGSCRTRLVAGQVD-- 55
Pf-Fdx AFYNITLRTNDGEKKIECNEDE-YILDASERQNVELPYSCRGGSCSTCAAKLVEGEVDND 59
       : .:*** ..  .:: *::::.  :* * * :** : *.** * *.:* ::** *:**

YfaE ---WIAEPLAFIQPGEILPCCCRAKGDIEIEM--------- 84
Pf-Fdx DQSYLDE--EQIKKKYILLCTCYPKSDCVIETHKEDELHDM 98
         :: *    *:   ** * * .*.*  **
```

Figure 5-8. Homology model of YfaE (A) generated using software Swiss-Model (http://swissmodel.expasy.org) and the crystal structure of the malaria ferredoxin (B, pdb: 1IUE) as a template for modeling. Green, four conserved cysteines (C36, C41, C44 and C71 in YfaE) in the 2Fe2S cluster; pink, additional cysteines; B: orange spheres, ions of the 2Fe2S cluster. (C) ClustalW2 (http://www.ebi.ac.uk/Tools/clustalw2) sequence alignment between YfaE and *P. falciparum* Fdx.

This model suggests that a cysteine within β_2 might also be involved in iron delivery. Recent studies of Yee in our lab on C268S-β_2 have demonstrated unexpectedly that a high Y• content (~1.6 Y•/β_2) in this mutant upon its reconstitution with Fe^{2+} and O_2 (*20*). Thus the position of C268 relative to the proposed docking surface for YfaE and C72 was examined structurally. The relative position of C268 to the conserved lysines (K38, K42, K229) thought to provides the interaction surface with YfaE, suggests C268 does not play a role in cysteine-mediated metal transfer (**Figure 5-9**). Furthermore, results from a ferrozine analysis showed the iron content of C268S-β_2 was similar to wt-β_2 (~3.3 Fe/β_2), suggesting the higher Y• content is not due to higher iron loading (*20*). Therefore the C268 may not be involved the process of iron delivery. No other cysteine within β_2 is near the conserved lysines, indicating a cysteine-mediated ligand exchange for the iron delivery from YfaE to apo-β_2 is unlikely.

Another possibility for iron delivery from YfaE would involve two cysteines in ligating an extra FeS cluster. Recent studies on mono- or di-thiol glutaredoxins have revealed a labile $[2Fe2S]^{2+}$ cluster formed between two gluraredoxin monomers through active site cysteines and reduced glutathiones (GSH) (*21, 22*). This labile $[2Fe2S]^{2+}$ cluster decomposes when the GSH ligands are oxidized to GSSG under oxidative stress conditions. Thus, it has been proposed that this [2Fe2S] cluster acts as a redox sensor (*23*). Recently it was also discovered that the [2Fe2S] cluster in a plant monothiol glutaredoxin (Grx4) can be transferred to apo-ferredoxin anaerobically in vitro in the presence of DTT at a rate (20,000 $M^{-1}min^{-1}$) that is 25-fold faster than the cluster transfer in vitro from scaffold protein IscU (800 $M^{-1}min^{-1}$) (*22, 24*). It is however unlikely that the same mechanism occurs during the process of iron delivery from YfaE. The 2Fe2S-ferredoxins are structurally distinct from glutaredoxins and the cysteine ligands for the FeS clusters have different geometrical patterns between ferredoxins and glutaredoxins (*25, 26*).

Furthermore, the 2Fe2S clusters in glutaredoxins show a single broad absorption feature at ~415 nm in the UV-visible spectrum, which has not been observed in YfaE. Thus, these results suggest that the diferric-Y• cofactor is not assembled through a glutaredoxin-like 2Fe2S intermediate in YfaE (*22, 23*). Interestingly, the conserved protein, NrdH in the operons of class Ib RNRs shares the same CXXC motif as glutaredoxins (*27*). Whether a 2Fe2S cluster can be assembled between NrdH monomers and be delivered into NrdF (the small subunit of RNR) remains to be elucidated.

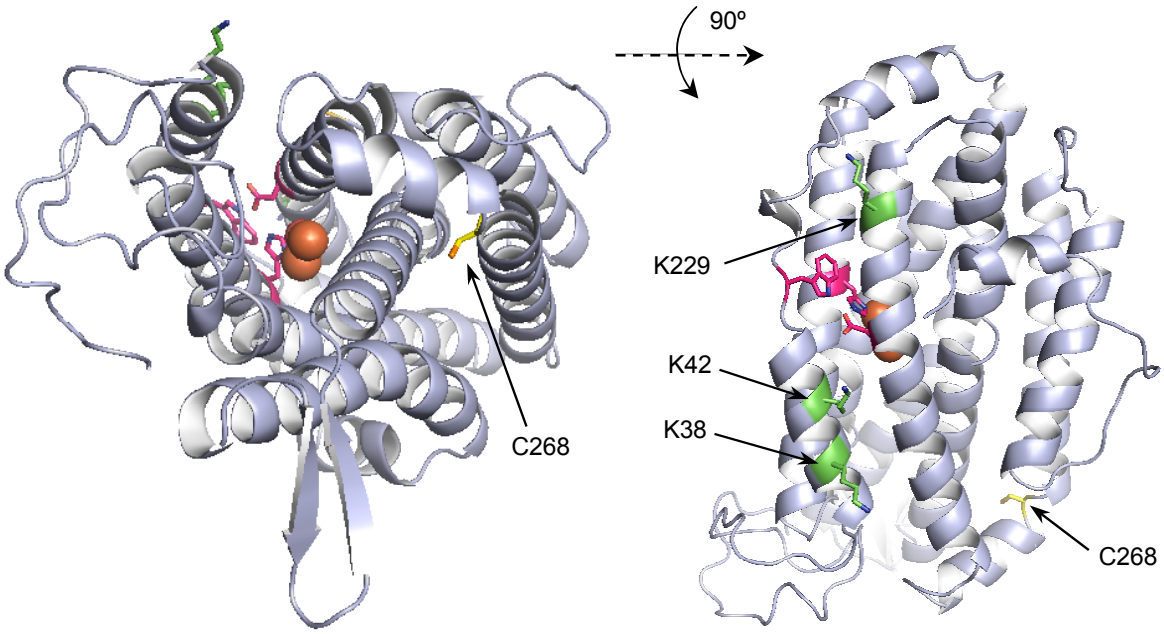

Figure 5-9. The position of C268 of *E. coli* β_2 (pdb: 1AV8) relative to the proposed binding site for YfaE. Orange spheres, iron of diferric cluster; green, conserved lysine residues proposed to interact with YfaE (K38, K42, K229), yellow, C268; pink, conserved amino acids for the electron transfer pathway (W48, H118, D237).

DISCUSSION

Based on the model and experimental support for the FeS cluster assembly onto scaffold proteins, a working hypothesis for a mechanism by which YfaE could deliver the ferrous iron into apo-β_2 is proposed (**Figure 5-10**). The model starts with two monomers of $[2Fe2S]^{2+}$-YfaE coming together and forming a $[4Fe4S]^{2+}$ cluster at the interface between the two monomers (**Step 1, Figure 5-10**). The two electrons required for the formation of a $[4Fe4S]^{2+}$ cluster could come from DTT. In the absence of DTT the electrons could be supplied through the formation of a disulfide bond between YfaE monomers or between two of the cysteine ligands released from the $[2Fe2S]^{2+}$ binding. Studies in model systems have shown that a thiol-ligated $[4Fe4S]^{2+}$ complex can be self-assembled from two thiol-ligated $[2Fe2S]^{2+}$ complexes with the formation of the disulfides (*6, 7*). A similar reductive coupling without exogenous reducing agents has been observed between two $[2Fe2S]^{2+}$-IscU monomers even though the rate of formation was very slow (several hours) and the source of the electrons was unclear (*1*). However, when using dithionite or reduced ferredoxin as reductants, the formation of $[4Fe4S]^{2+}$-IscU was accelerated, similar to our observations in the experiments with DTT (*2*).

After the $[4Fe4S]^{2+}$ cluster is formed in YfaE, the decomposition of the cluster could be triggered by the presence of apo-β_2 and the dissociated ferrous iron could incorporate into apo-β_2 to form diferrous-β_2 which in the presence of O_2 forms active-β_2 with the diferric-Y• cofactor (**Step 2, Figure 5-10**). The dissociation of the ferrous iron from $[4Fe4S]^{2+}$ cluster and its delivery into apo-β_2 could be mediated by the cysteines (C72, C73) at the C-terminus of YfaE. Finally, DTT helps the oxidized YfaE remain soluble and in the absence of DTT aggregates of YfaE are formed through intermolecular disulfide bonds (**Step 3, Figure 5-10**).

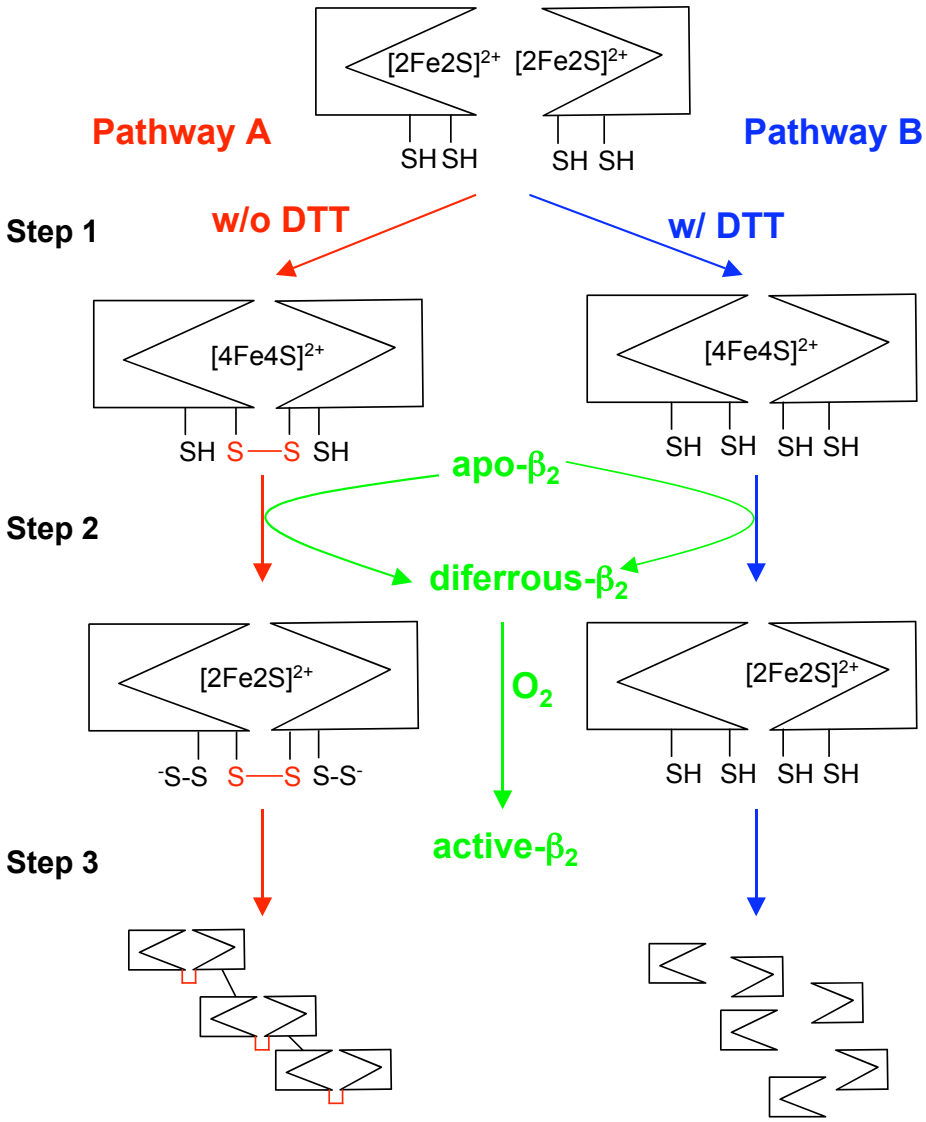

Figure 5-10. Working hypothesis for a mechanism by which YfaE could deliver ferrous iron to apo-β_2. The model is based on experimental observations in this chapter and our knowledge of [2Fe2S] and [4Fe4S] cluster assembly in IscU. The first step of this mechanism is reductive coupling of two $[2Fe2S]^{2+}$ clusters to form a $[4Fe4S]^{2+}$ cluster. DTT could provide the electrons for this reductive coupling (Pathway B). In the absence of DTT (Pathway A), the electrons could come from formation of a disulfide bond between cysteine residues (C72, C73) at the C-terminus tail of YfaE. In the second step, two ferrous irons from the $[4Fe4S]^{2+}$ cluster are transferred to apo-β_2 which forms active β_2 in the presence of O_2 (green). The two sulfides from the $[4Fe4S]^{2+}$ cluster could dissociate from the protein or form persulfides or polysulfides with the cysteines (C72, C73) which could lead to aggregation of YfaE through disulfide formation (Step 3). The presence of DTT could prevent this aggregation and maintain the solubility of YfaE.

In this model, the key steps are the formation of a $[4Fe4S]^{2+}$ between two YfaE monomers for the iron delivery to apo-β_2 and the formation of YfaE aggregates through disulfide bonds. Mutational studies on C72 and C73 could test the function of these cysteines and their relationship to the formation of YfaE aggregates. The creation of a YfaE mutant that is stable in an oxidized state will be very helpful for binding studies using isothermal titration calorimetry. The Mössbauer studies have shown that the iron in the diferric-Y• cluster are coming from YfaE. Quantitative analysis of the amount of the Y• formed and the amount of the $[2Fe2S]^{2+}$ destroyed could help us understand the stoichiometry of the reaction. The real challenge will be to "enrich" the amount of [4Fe4S]-YfaE. This might be achieved by a combination of the right YfaE cysteine mutants and the choice of reducing conditions (*28*). Even though DTT seems to be able to facilitate the Y• formation, presumably through faster $[4Fe4S]^{2+}$ formation by reductive coupling, other reductants such as dithionite and photoreduced deazaflavin could be useful for $[4Fe4S]^{2+}$ formation (*2, 29*). Reducing equivalents in vivo such as thioredoxin, glutathione or ferredoxin could also be used to reductively couple the clusters.

Once a $[4Fe4S]^{2+}$-YfaE can be reconstituted in vitro, studies by UV-vis, EPR and Mössbauer spectroscopies could help us reveal the mechanisms of the iron delivery. The next question would be whether the $[4Fe4S]^{2+}$-YfaE is physiologically relevant. The controls on the formation of $[4Fe4S]^{2+}$-YfaE in vivo could be made by carrying out a gene replacement experiment with a mutant YfaE in vivo that is stable in oxidized state and by modulating the growth conditions (*11*). Similar studies have been done to study the interconversion between [2Fe2S] and [4Fe4S] clusters in FNR (fumurate nitrate reduction) in vivo under different growth condition (*5*).

It should be noted, however, that our results from quantitative Western blot analysis on the whole cells indicate low [YfaE] in vivo (< 0.3 μM) compared to β_2 (~3 μM). Therefore, the efficiency of iron delivery by YfaE has to be greatly enhanced in vivo or the expression of YfaE needs to be up-regulated under certain growth conditions to meet the rate of cluster biosynthesis of β_2. Furthermore, a ClustalW2 sequence alignment of YfaE-like ferredoxins from a BLAST search shows that only the four cysteines in the 2Fe2S cluster are absolutely conserved. Thus, the proposed role of the "additional" cysteines in the C-terminus of YfaE may not be general among all YfaEs.

If YfaE really can function as an iron chaperone, the results in our previously published paper in which YfaE was titrated into crude cell lysate to generate 2 Y•/β_2 needs to be re-interpreted (*30*). The Y• could be formed from apo-β_2 by iron loading from YfaE instead of from met-β_2 by YfaE reduction. In either case the ability to generate 2 Y•/β_2 with excess YfaE is unquestionable. Whether the 2 Y•/β_2 is physiologically relevant and whether there are other components inside the cells that assist in the loading of 4 Fe/β_2 remain to be established.

Why would the class Ia RNR use an FeS protein as an iron chaperone? It is believed that FeS proteins appeared at the early stages of evolution under anaerobic conditions before the oxygen catastrophe caused by photosynthesis. The presence of oxygen facilitates the degradation of the FeS clusters (*31*). It is tempting to speculate that during the evolution of an oxygen and iron dependent RNR, the RNR took advantage of the lability of FeS clusters and "hijacked" the already existing iron homeostasis pathways dependent on FeS chemistry instead of evolving its own iron delivery system (*32*). Why not?

REFERENCES

(1) Agar, J. N., Krebs, C., Frazzon, J., Huynh, B. H., Dean, D. R., and Johnson, M. K. (2000) IscU as a scaffold for iron-sulfur cluster biosynthesis: sequential assembly of [2Fe-2S] and [4Fe-4S] clusters in IscU. *Biochemistry 39*, 7856-62.

(2) Chandramouli, K., Unciuleac, M. C., Naik, S., Dean, D. R., Huynh, B. H., and Johnson, M. K. (2007) Formation and properties of [4Fe-4S] clusters on the IscU scaffold protein. *Biochemistry 46*, 6804-11.

(3) Unciuleac, M. C., Chandramouli, K., Naik, S., Mayer, S., Huynh, B. H., Johnson, M. K., and Dean, D. R. (2007) In vitro activation of apo-aconitase using a [4Fe-4S] cluster-loaded form of the IscU [Fe-S] cluster scaffolding protein. *Biochemistry 46*, 6812-21.

(4) Khoroshilova, N., Popescu, C., Munck, E., Beinert, H., and Kiley, P. J. (1997) Iron-sulfur cluster disassembly in the FNR protein of *Escherichia coli* by O_2: [4Fe-4S] to [2Fe-2S] conversion with loss of biological activity. *Proc Natl Acad Sci U S A 94*, 6087-92.

(5) Popescu, C. V., Bates, D. M., Beinert, H., Munck, E., and Kiley, P. J. (1998) Mössbauer spectroscopy as a tool for the study of activation/inactivation of the transcription regulator FNR in whole cells of *Escherichia coli*. *Proc Natl Acad Sci U S A 95*, 13431-5.

(6) Venkateswara Rao, P., and Holm, R. H. (2004) Synthetic analogues of the active sites of iron-sulfur proteins. *Chem Rev 104*, 527-59.

(7) Hagen, K. S., Reynolds, J. G., and Holm, R. H. (1981) Definition of reaction sequences resulting in self-assembly of $[Fe_4S_4(SR)_4]^{2-}$ clusters from simple reactants. *J. Am. Chem. Soc. 1013*, 4054-63.

(8) Wu, C. H., Jiang, W., Krebs, C., and Stubbe, J. (2007) YfaE, a ferredoxin involved in diferric-tyrosyl radical maintenance in *Escherichia coli* ribonucleotide reductase. *Biochemistry 46*, 11577-88.

(9) Fish, W. W. (1988) Rapid colorimetric micromethod for the quantitation of complexed iron in biological samples. *Methods Enzymol 158*, 357-64.

(10) Malmström, B. G., Reinhammar, B., and Vänngard, T. (1970) The state of copper in stellacyanin and laccase from the lacquer tree *Rhus vernicifera*. *Biochim Biophys Acta 205*, 48-57.

(11) Raulfs, E. C., O'Carroll, I. P., Dos Santos, P. C., Unciuleac, M. C., and Dean, D. R. (2008) In vivo iron-sulfur cluster formation. *Proc Natl Acad Sci U S A 105*, 8591-6.

(12) Verhagen, M. F., Link, T. A., and Hagen, W. R. (1995) Electrochemical study of the redox properties of [2Fe-2S] ferredoxins. Evidence for superreduction of the Rieske [2Fe-2S] cluster. *FEBS Lett 361*, 75-8.

(13) Im, S. C., Kohzuma, T., McFarlane, W., Gaillard, J., and Sykes, A. G. (1997) Formation, properties, and characterization of a fully reduced Fe(II)Fe(II) form of spinach (and parsley) [2Fe-2S] ferredoxin with the macrocyclic complex [Cr(15-aneN(4))(H(2)O)(2)](2+) as reductant. *Inorg Chem 36*, 1388-1396.

(14) Cleland, W. W. (1964) Dithiothreitol, a new protective reagent for Sh groups. *Biochemistry 3*, 480-2.

(15) Kadokura, H., Katzen, F., and Beckwith, J. (2003) Protein disulfide bond formation in prokaryotes. *Annu Rev Biochem 72*, 111-35.

(16) Kimata-Ariga, Y., Kurisu, G., Kusunoki, M., Aoki, S., Sato, D., Kobayashi, T., Kita, K., Horii, T., and Hase, T. (2007) Cloning and characterization of ferredoxin and ferredoxin-NADP+ reductase from human malaria parasite. *J Biochem 141*, 421-8.

(17) Kakuta, Y., Horio, T., Takahashi, Y., and Fukuyama, K. (2001) Crystal structure of *Escherichia coli* Fdx, an adrenodoxin-type ferredoxin involved in the assembly of iron-sulfur clusters. *Biochemistry 40*, 11007-12.

(18) Muller, J., Lugovskoy, A. A., Wagner, G., and Lippard, S. J. (2002) NMR structure of the [2Fe-2S] ferredoxin domain from soluble methane monooxygenase reductase and interaction with its hydroxylase. *Biochemistry 41*, 42-51.

(19) Matsumura, T., Kimata-Ariga, Y., Sakakibara, H., Sugiyama, T., Murata, H., Takao, T., Shimonishi, Y., and Hase, T. (1999) Complementary DNA cloning and characterization of ferredoxin localized in bundle-sheath cells of maize leaves. *Plant Physiol 119*, 481-8.

(20) Yee, C. S. (2004) Mechanistic investigations of the radical initiation pathways of class I ribonucleotide reductase from *Escherichia coli*. Thesis Ph. D. Massachusetts Institute of Technology, Department of Chemistry. pp 297

(21) Johansson, C., Kavanagh, K. L., Gileadi, O., and Oppermann, U. (2007) Reversible sequestration of active site cysteines in a 2Fe-2S-bridged dimer provides a mechanism for glutaredoxin 2 regulation in human mitochondria. *J Biol Chem 282*, 3077-82.

(22) Bandyopadhyay, S., Gama, F., Molina-Navarro, M. M., Gualberto, J. M., Claxton, R., Naik, S. G., Huynh, B. H., Herrero, E., Jacquot, J. P., Johnson, M. K., and Rouhier, N.

(2008) Chloroplast monothiol glutaredoxins as scaffold proteins for the assembly and delivery of [2Fe-2S] clusters. *EMBO J 27*, 1122-33.

(23) Lillig, C. H., Berndt, C., Vergnolle, O., Lonn, M. E., Hudemann, C., Bill, E., and Holmgren, A. (2005) Characterization of human glutaredoxin 2 as iron-sulfur protein: a possible role as redox sensor. *Proc Natl Acad Sci U S A 102*, 8168-73.

(24) Chandramouli, K., and Johnson, M. K. (2006) HscA and HscB stimulate [2Fe-2S] cluster transfer from IscU to apoferredoxin in an ATP-dependent reaction. *Biochemistry 45*, 11087-95.

(25) Rouhier, N., Unno, H., Bandyopadhyay, S., Masip, L., Kim, S. K., Hirasawa, M., Gualberto, J. M., Lattard, V., Kusunoki, M., Knaff, D. B., Georgiou, G., Hase, T., Johnson, M. K., and Jacquot, J. P. (2007) Functional, structural, and spectroscopic characterization of a glutathione-ligated [2Fe-2S] cluster in poplar glutaredoxin C1. *Proc Natl Acad Sci U S A 104*, 7379-84.

(26) Gibson, L. M., Dingra, N. N., Outten, C. E., and Lebioda, L. (2008) Structure of the thioredoxin-like domain of yeast glutaredoxin 3. *Acta Crystallogr D Biol Crystallogr 64*, 927-32.

(27) Stehr, M., Schneider, G., Aslund, F., Holmgren, A., and Lindqvist, Y. (2001) Structural basis for the thioredoxin-like activity profile of the glutaredoxin-like NrdH-redoxin from *Escherichia coli*. *J Biol Chem 276*, 35836-41.

(28) Ugulava, N. B., Gibney, B. R., and Jarrett, J. T. (2000) Iron-sulfur cluster interconversions in biotin synthase: dissociation and reassociation of iron during conversion of [2Fe-2S] to [4Fe-4S] clusters. *Biochemistry 39*, 5206-14.

(29) Ollagnier-De Choudens, S., Sanakis, Y., Hewitson, K. S., Roach, P., Baldwin, J. E., Munck, E., and Fontecave, M. (2000) Iron-sulfur center of biotin synthase and lipoate synthase. *Biochemistry 39*, 4165-73.

(30) Hristova, D., Wu, C. H., Jiang, W., Krebs, C., and Stubbe, J. (2008) Importance of the maintenance pathway in the regulation of the activity of *Escherichia coli* ribonucleotide reductase. *Biochemistry 47*, 3989-99.

(31) Imlay, J. A. (2006) Iron-sulphur clusters and the problem with oxygen. *Mol Microbiol 59*, 1073-82.

(32) Reichard, P. (1997) The evolution of ribonucleotide reduction. *Trends Biochem Sci 22*, 81-5.

CHIA-HUNG WU

77 MASSACHUSETTS AVE, BLDG 18-523 Tel: 617-253-0084
CAMBRIDGE, MA 02139 Fax: 617-258-4247
Email: CHIAHWU@MIT.EDU

EDUCATION

2003 - 2009	**Massachusetts Institute of Technology** Ph.D. Candidate, Department of Chemistry	**Cambridge, MA**
1995 - 1999	**National Taiwan University** Bachelor of Science in Chemistry	**Taipei, Taiwan**

HONORS AND AWARDS

1995 - 1998	**Presidential Award (National Taiwan University)** **Gifted Student Scholarship (National Taiwan University)**
1995	**Silver Medal, 27th International Chemistry Olympiad**

PUBLICATIONS AND PRESENTATIONS

Hristova, D., **Wu, C. -H.**, Jiang, W., Krebs, C. and Stubbe, J. Importance of the Maintenance Pathway in the Regulation of the Activity of *Escherichia coli* Ribonucleotide Reductase. *Biochemistry* 47, 3989-99 (2008).

Wu, C. -H., Jiang, W., Krebs, C. and Stubbe, J. YfaE, a Ferredoxin Involved in Diferric-Tyrosyl Radical Maintenance in *Escherichia coli* Ribonucleotide Reductase. *Biochemistry* 46, 11577-78 (2007)

Wu, C. -H. Jiang, W., Krebs, C. and Stubbe, J. Role of YfaE in the Cofactor Assembly and Maintenance of *E. coli* Ribonucleotide Reductase. *ACS Meeting* Boston, MA (2007)

Wu, C. -H. and Stubbe, J. Efforts to Understand Biosynthesis of Diferric Tyrosyl Radical Cofactor of *E. coli* Ribonucleotide Reductase Small Subunit. *Frontiers in Metallobiochemistry,* Pennsylvania State University, State College, PA (2006).

Chen, K. -C.*, **Wu, C. -H.***, Chang, C. -Y., Lu, W. -C., Tseng, Q., Prijovich, Z. M., Schechinger, W., Leu, Y. -L. and Roffler, S. R. Directed Evolution of a Lysosomal Enzyme by Mammalian Cell Surface Display for Improved Anti-Cancer Prodrug Activation. *Chem. Biol.* 15, 1277-86 (2008)

Wu, C. -H., Balasubramanian W. R., Ko, Y. -P., Hsu, G., Chang, S. E., Prijovich, Z. M., Chen, K. -C., Roffler, S. R. A Simple Method for the Production of Recombinant Proteins from Mammalian Cells. *Biotechnol. Appl. Biochem.* 40, 167-72 (2004)

RESEARCH EXPERIENCE

2003 – 2009 **Massachusetts Institute of Technology** **Cambridge, MA**
Graduate Student, Department of Chemistry
Advisor: JoAnne Stubbe, Ph.D.

- Investigated the biosynthesis of the diferric tyrosyl radical cofactor in *E. coli* ribonucleotide reductase small subunit (R2) by applying various strategies such as homologous recombinations, two hybrid systems, protein co-purification and cross-linkings, activity and colorimetric assays, genomic analyses and whole cell Electron Paramagnetic Resonance (EPR) and Mössbauer spectroscopies on different knockout strains of iron transporter/iron storage proteins.
- Identified a new [2Fe-2S]-ferredoxin, YfaE, and established its role in the cofactor maintenance of R2 by quantitative analyses by titration, EPR and stopped-flow UV-vis spectroscopies. Studied the binding sites between YfaE and R2 and investigated the role of Fre (NAD(P)H-flavin reductase) as a redox partner for YfaE.

2001 - 2003 **Academia Sinica** **Taipei, Taiwan**
Research Assistant, Institute of Biomedical Sciences
Advisor: Steve R. Roffler, Ph.D.

- Engineered human β-glucuronidase to increase its activity in neutral pH for pro-drug anti-cancer therapy. Constructed mutation libraries using DNA shuffling, error-prone PCR and site-directed mutagenesis and developed ELF 97-glucuronide staining method for screening by cell flow cytometry.
- Worked on mammalian cell culture and retrovirus transduction, conducted pharmacokinetics of immunoenzyme in BALB/c mice.

1999 - 2001 Mandatory military service. Fixed and maintained Hummers and telephones.

1998 - 1999 **Academia Sinica** **Taipei, Taiwan**
Student Researcher, Institute of Atomic and Molecular Sciences
Advisor: Ta-Chau Chang, Ph.D.

- Investigated the guanine-quartet structure in DNA-BODIPY conjugates using homemade dye laser systems for absorption, emission, and low temperature hole-burning spectroscopies.

1996 - 1997 **National Taiwan Normal University** **Taipei, Taiwan**
Summer Student, Department of Chemistry
Advisor: I-Jy Chang, Ph.D.

- Developed chemical equilibrium methods to measure the redox potentials of cytochrome c, hemoglobin, and myoglobin.

TEACHING EXPERIENCE

2005 – 2009 **Massachusetts Institute of Technology**
Cambridge, MA

- Trained and mentored junior graduate students and postdocs to start new projects, advised labmates on experimental designs and taught labmates to fix various lab equipment.

2004 **Massachusetts Institute of Technology** **Cambridge, MA**
5.32: Intermediate Chemical Experimentation, Teaching Assistant

- Taught undergraduates basic laboratory techniques in biological chemistry experiments. Wrote exams and graded reports.

2003 **Massachusetts Institute of Technology** **Cambridge, MA**
5.310: Laboratory Chemistry, Teaching Assistant

- Taught undergraduates basic laboratory techniques in general chemistry experiments. Wrote exams and graded reports.

Appendix I

Plasmid Maps

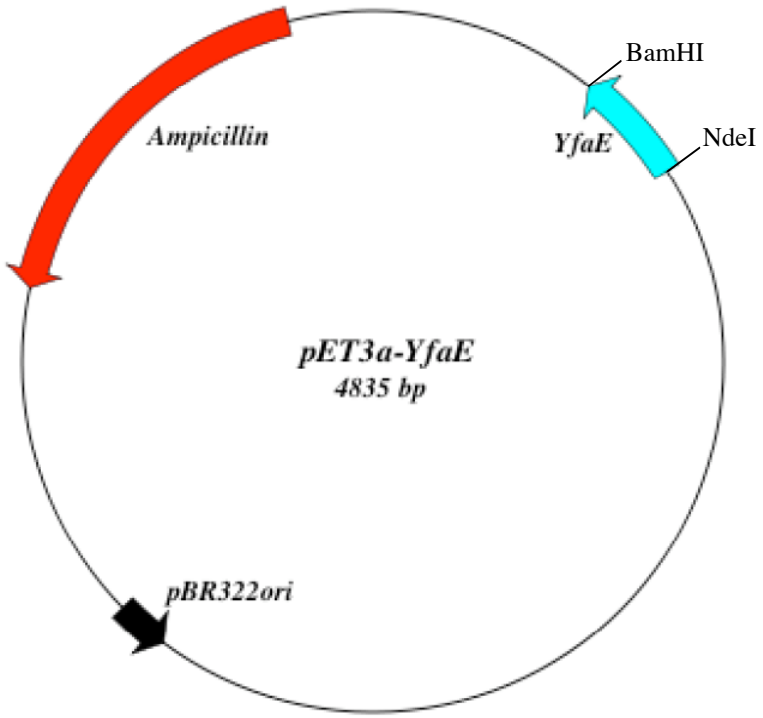
BamHI
Ampicillin
YfaE
NdeI
pET3a-YfaE
4835 bp
pBR322ori

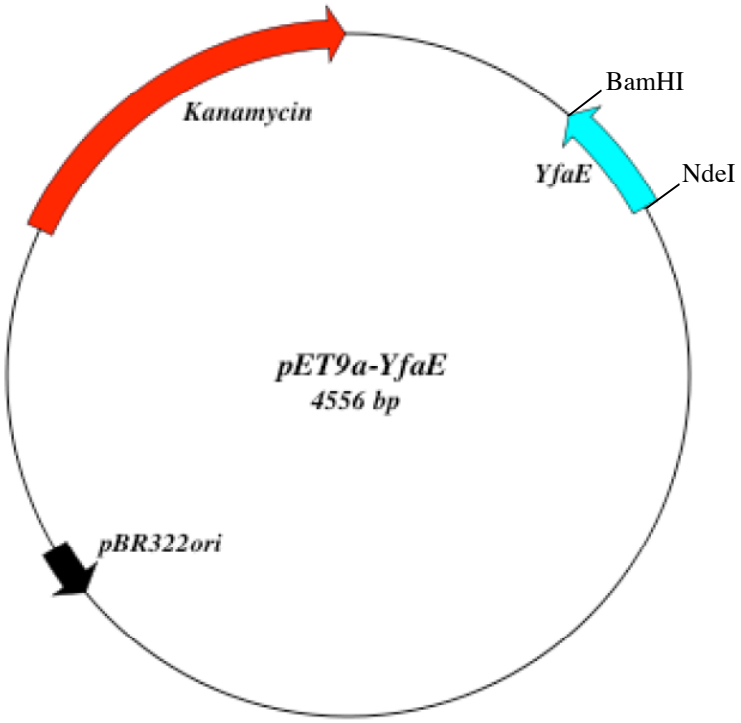
Kanamycin
BamHI
YfaE
NdeI
pET9a-YfaE
4556 bp
pBR322ori

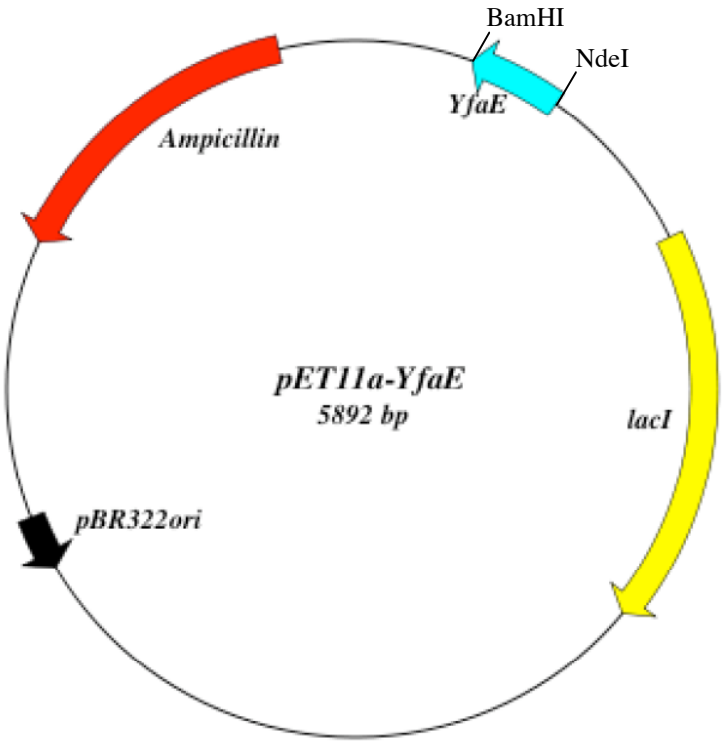

Available mutants: E26A, E26K, E33A, C71A, C72A, C73A, C72A/C73A, C72S/C73S

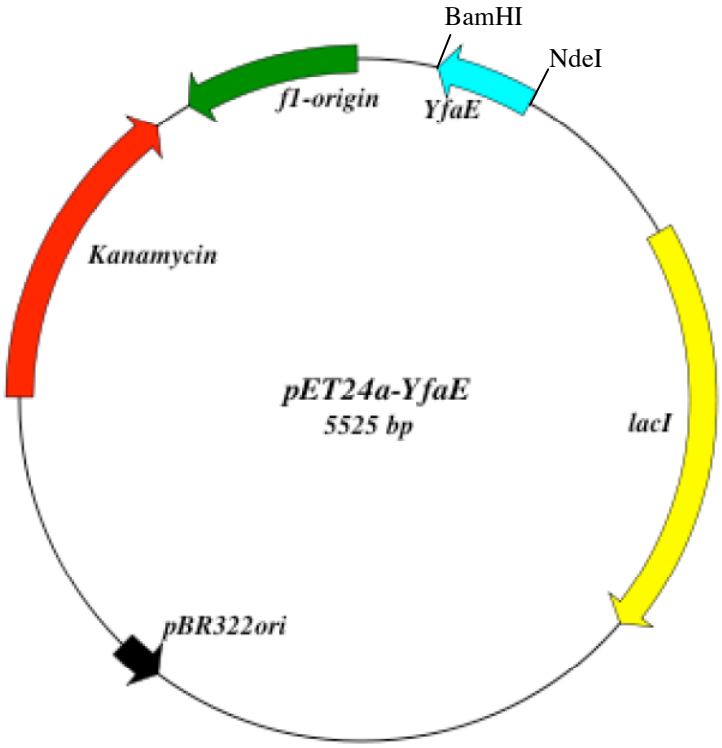
BamHI
NdeI
f1-origin
YfaE
Kanamycin
pET24a-YfaE
5525 bp
lacI
pBR322ori

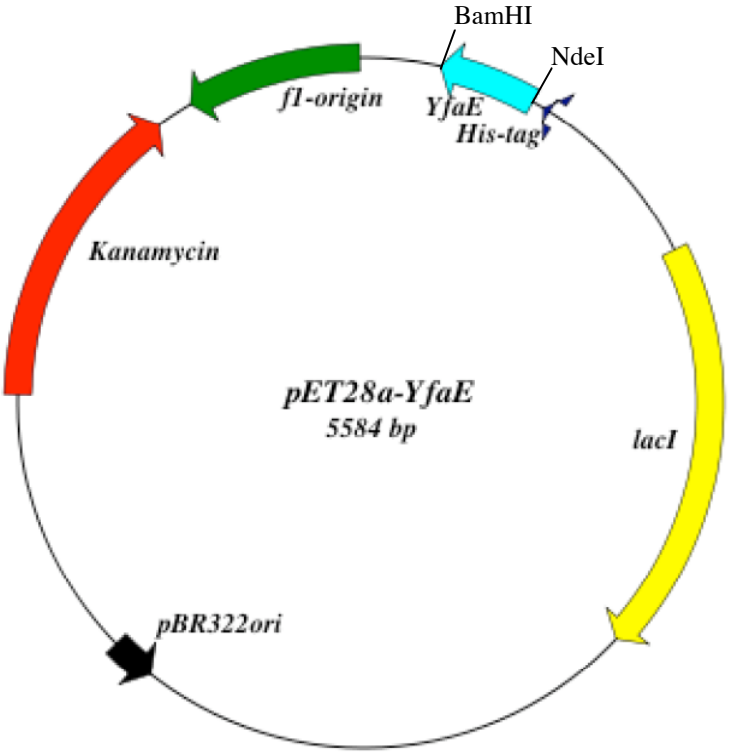
BamHI
NdeI
f1-origin
YfaE
His-tag
Kanamycin
pET28a-YfaE
5584 bp
lacI
pBR322ori

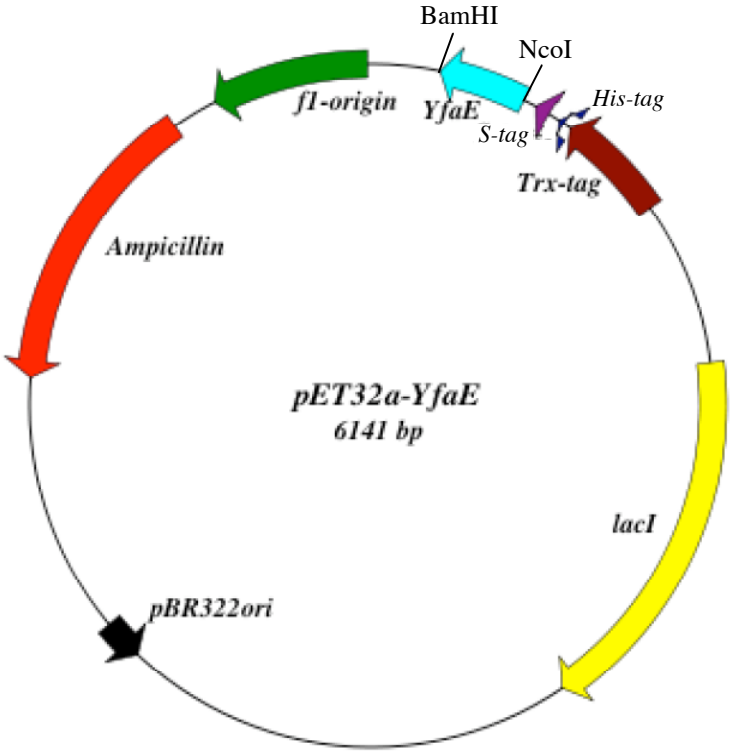
BamHI
NcoI
f1-origin
YfaE
His-tag
S-tag
Trx-tag
Ampicillin
pET32a-YfaE
6141 bp
lacI
pBR322ori

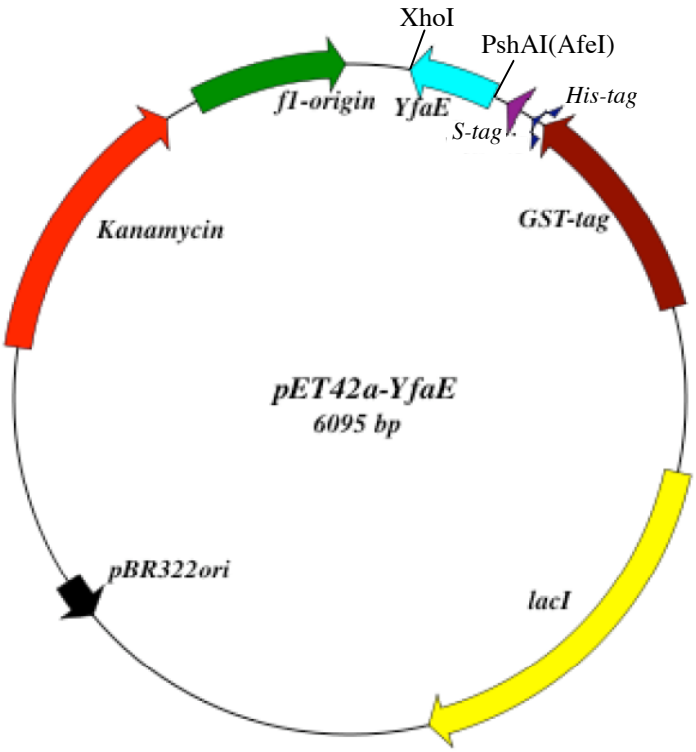
XhoI
PshAI(AfeI)
f1-origin
YfaE
His-tag
S-tag
Kanamycin
GST-tag
pET42a-YfaE
6095 bp
pBR322ori
lacI

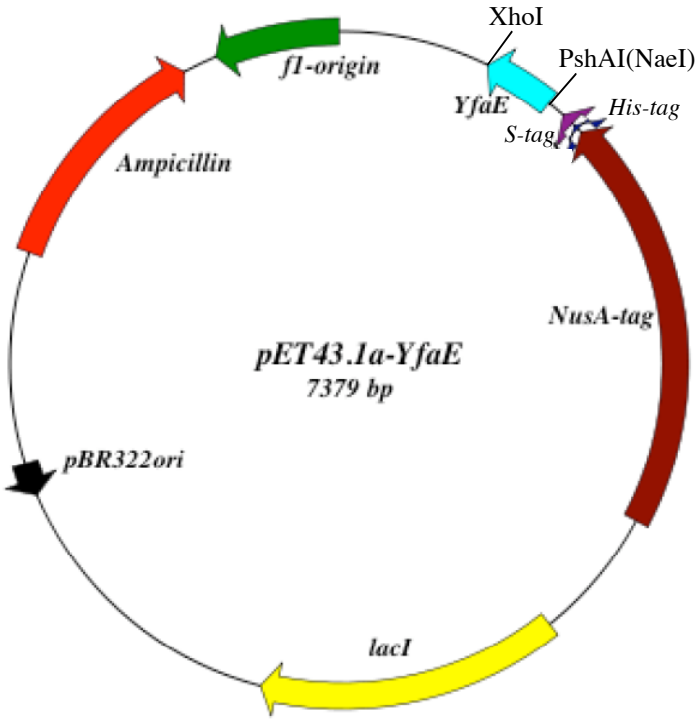
XhoI
PshAI(NaeI)
f1-origin
YfaE
His-tag
S-tag
Ampicillin
NusA-tag
pET43.1a-YfaE
7379 bp
pBR322ori
lacI

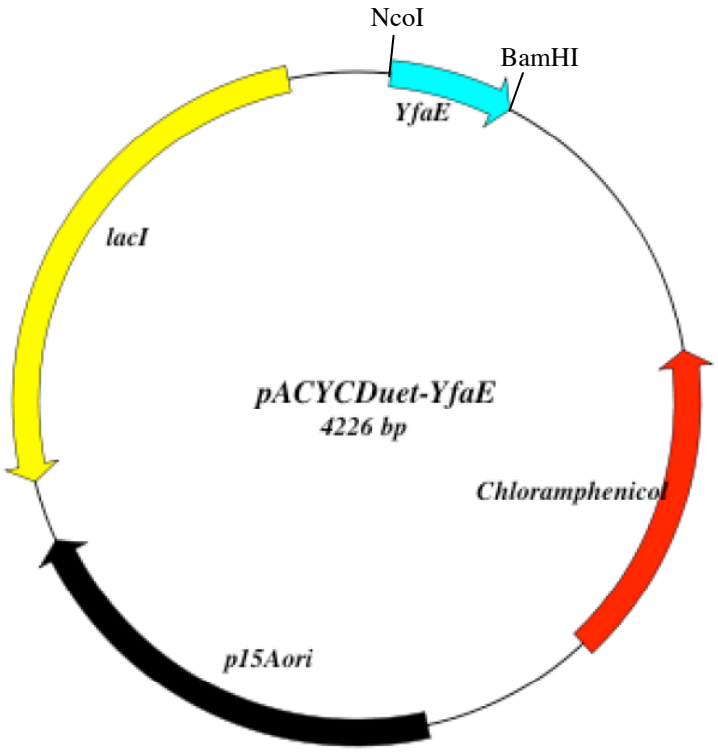

Note: Compatible with pBR322 plasmids

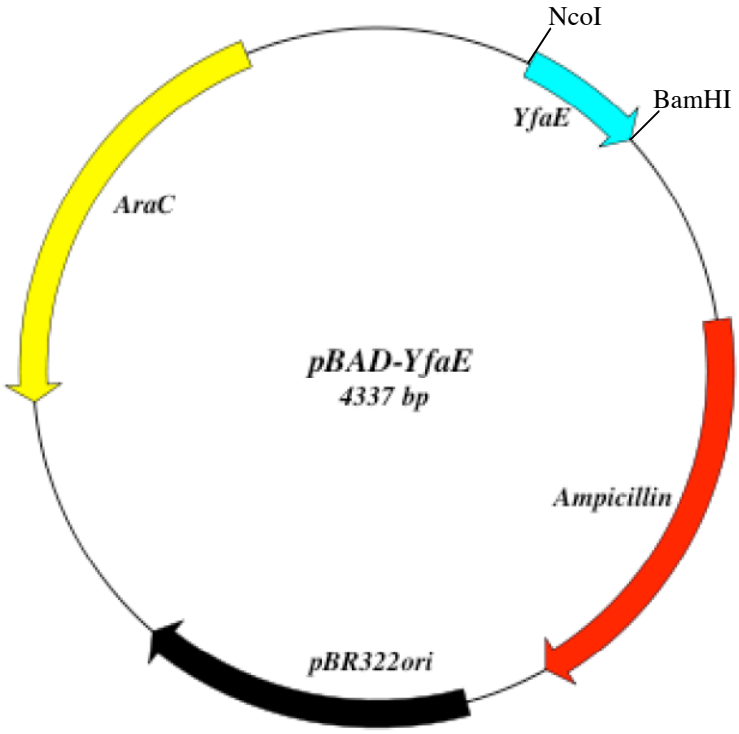
NcoI
BamHI
YfaE
AraC
pBAD-YfaE
4337 bp
Ampicillin
pBR322ori

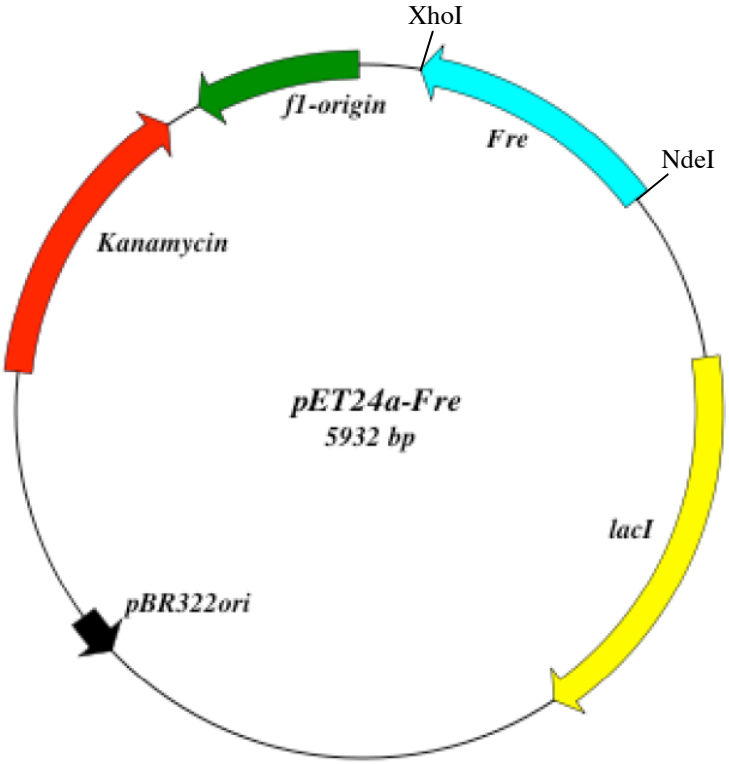
XhoI
f1-origin
Fre
NdeI
Kanamycin
pET24a-Fre
5932 bp
lacI
pBR322ori

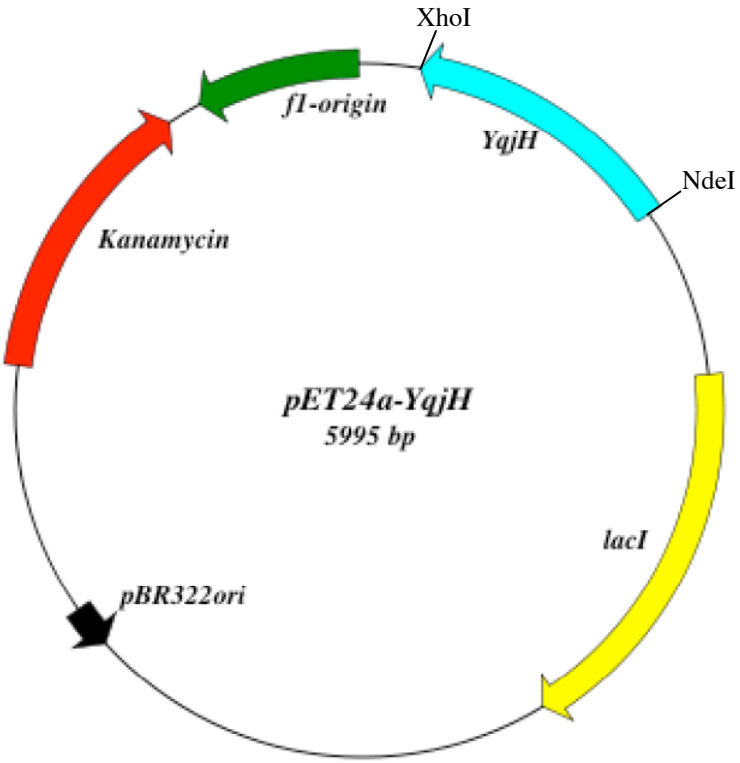
XhoI
f1-origin
YqjH
NdeI
Kanamycin
pET24a-YqjH
5995 bp
lacI
pBR322ori

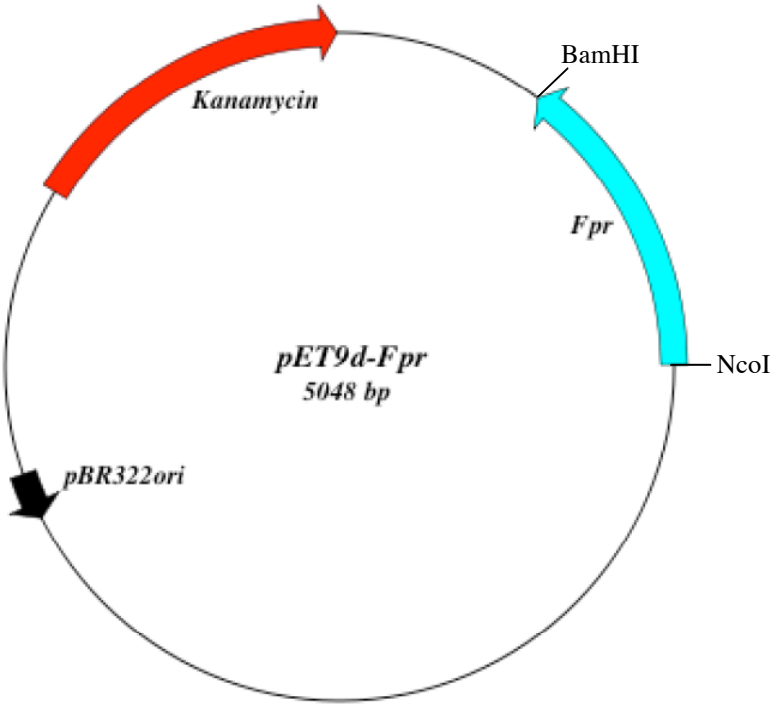
BamHI
Kanamycin
Fpr
pET9d-Fpr
5048 bp
NcoI
pBR322ori

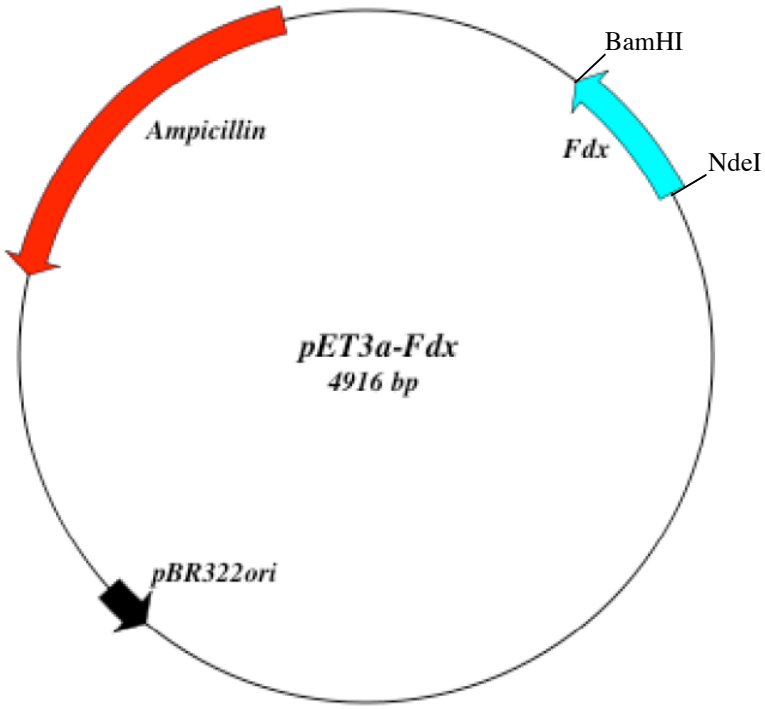
BamHI
Ampicillin
Fdx
NdeI
pET3a-Fdx
4916 bp
pBR322ori

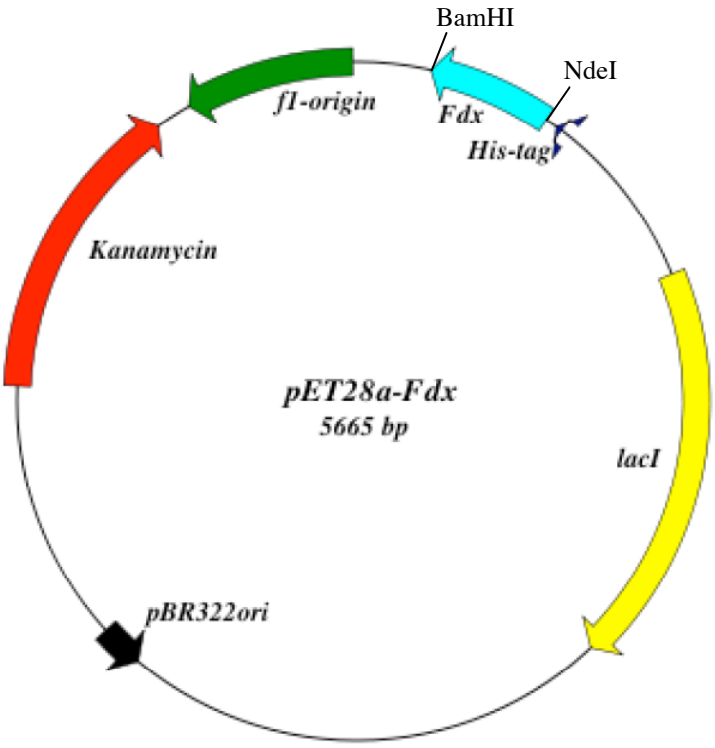
BamHI
NdeI
f1-origin
Fdx
His-tag
Kanamycin
pET28a-Fdx
5665 bp
lacI
pBR322ori

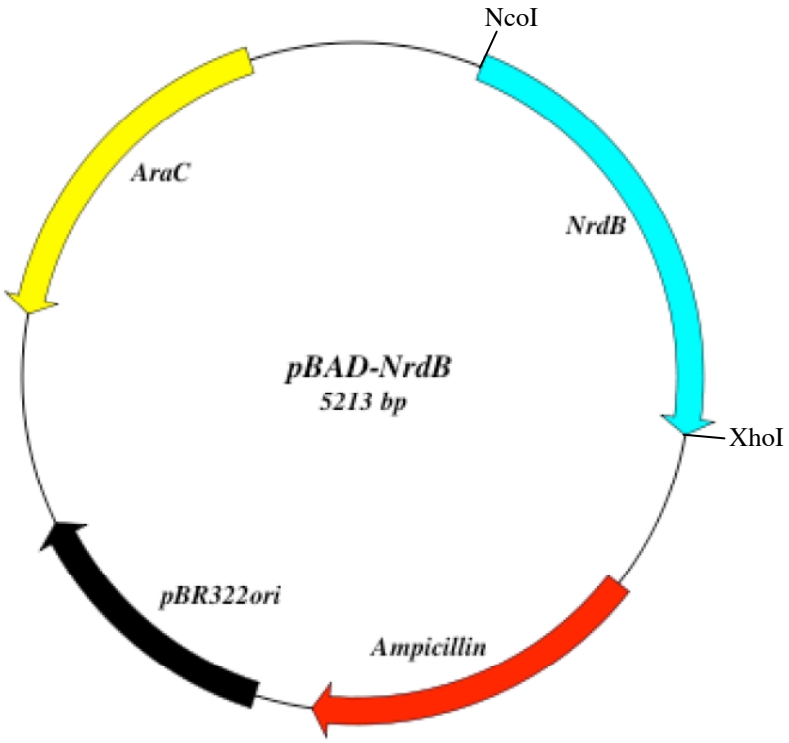

Available mutant: E115A

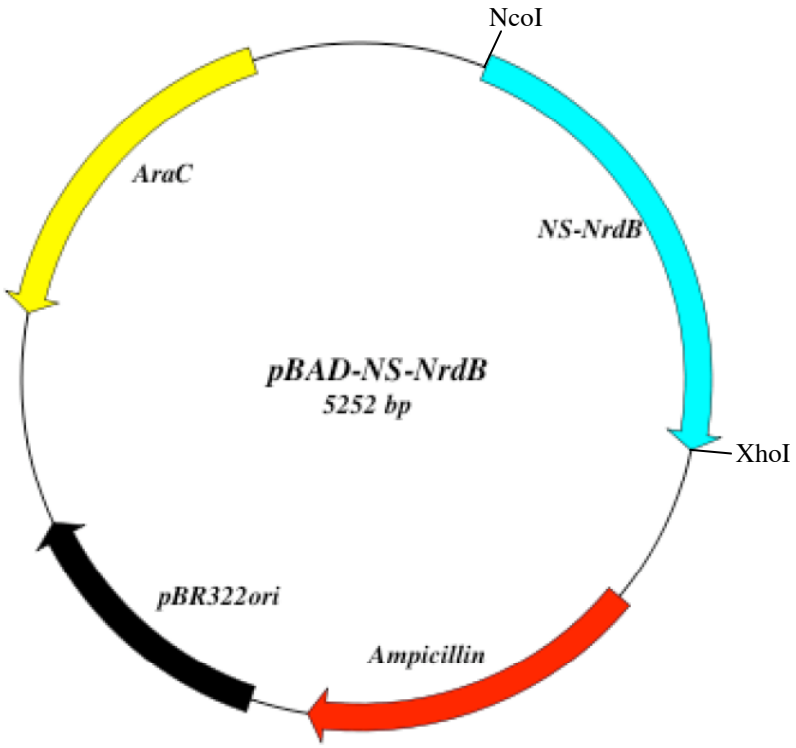

Available mutant: E115A

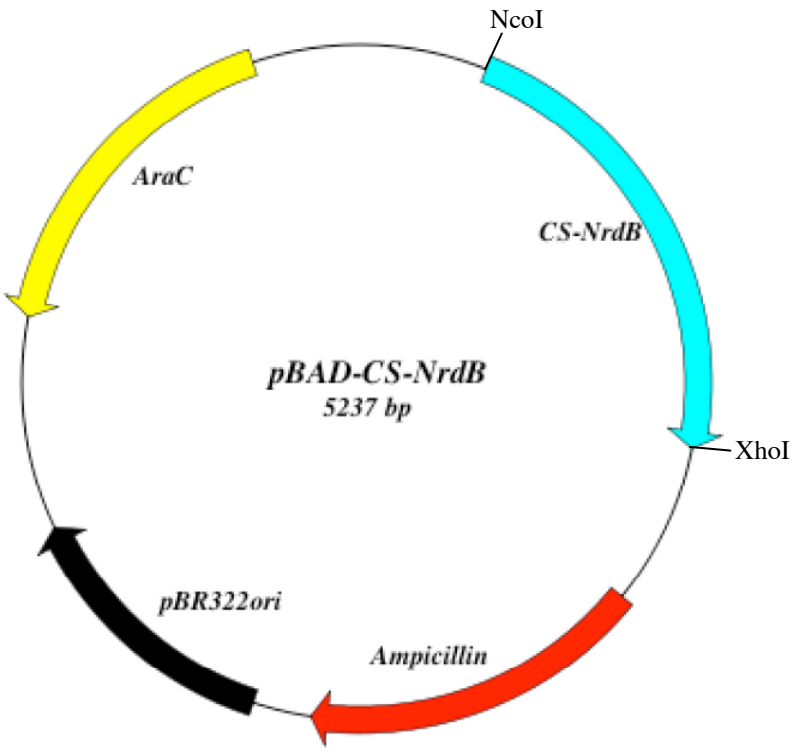

Available mutants: E115A, K38A, K42A, K229A, Y122F, Y356F, K38A/K42A, K38A/K42A/K229A

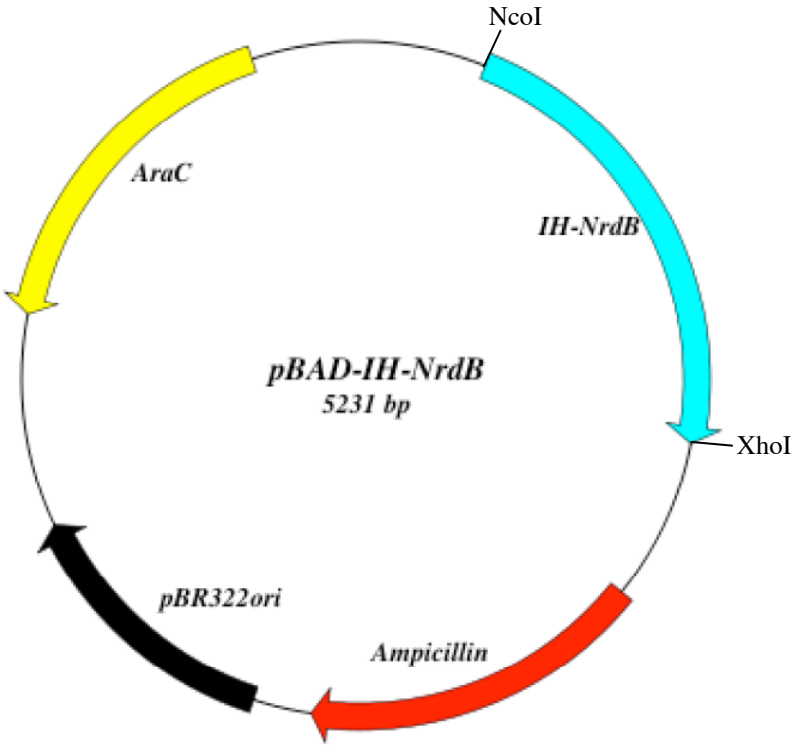

Available mutant: E115A

Appendix II

Genome Analysis

Five hundred bacterial genomes in the RNR database (http://rnrdb.molbio.su.se/, last update on January 23, 2009) which contain both *nrdA* and *nrdB* (encoding class Ia RNR) were used for BLAST search of YfaE-like proteins. Summary of the analysis is shown below.

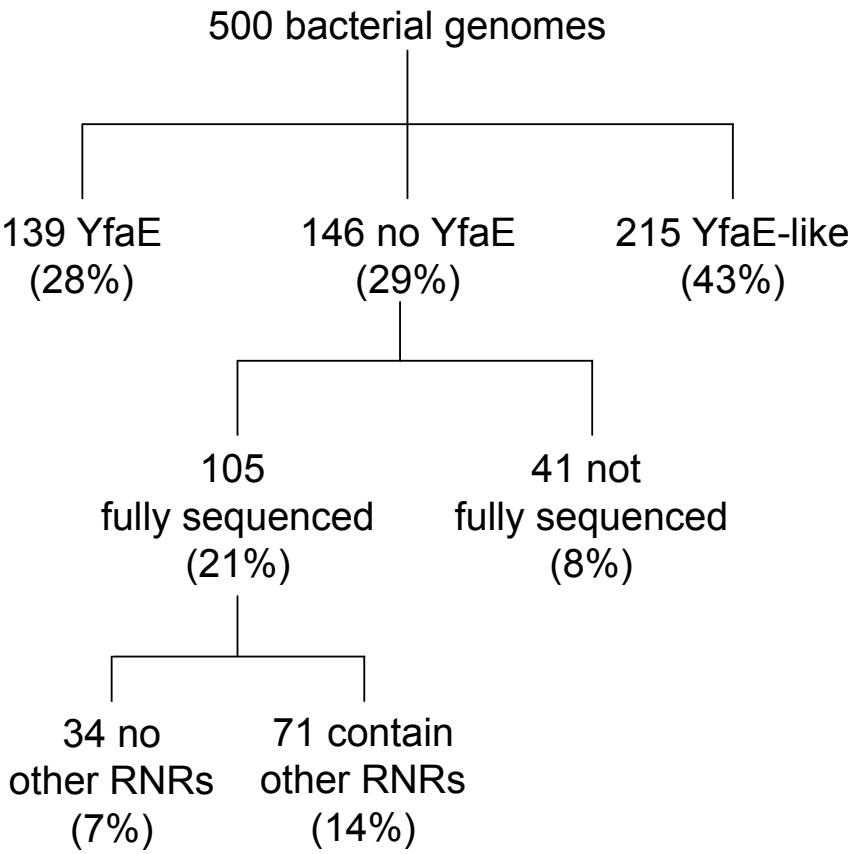

Organism	Fully sequenced	Class Ib	Class II	Class III	YfaE-like	Note
Acaryochloris marina MBIC11017	Y			Y	Y	ferredoxin (99)
Acidiphilium cryptum JF-5	Y		Y	Y	Y	ferredoxin (356)
Acidithiobacillus ferrooxidans ATCC 53993	Y			Y	Y	ferredoxin (114)
Acidothermus cellulolyticus 11B	Y		Y		Y	ferredoxin (161)
Acidovorax avenae subsp. citrulli AAC00-1	Y		Y		Y	ferredoxin (99)
Acidovorax sp. JS42	Y		Y	Y	Y	ferredoxin (97)
Acinetobacter baumannii ACICU	Y				Y	flavodoxin reductase (318)
Acinetobacter baumannii ATCC 17978	Y				Y	oxidoreductase (271)
Acinetobacter baumannii AYE	Y				Y	ferredoxin (317)
Acinetobacter baumannii SDF	Y				Y	oxidoreductase (318)
Acinetobacter sp. ADP1	Y				Y	oxidoreductase (353)
Actinobacillus pleuropneumoniae L20	Y			Y	Y	oxidoreductase (339)
Actinobacillus pleuropneumoniae serovar 1 str. 4074				Y	Y	flavodoxin reductase (339)
Actinobacillus pleuropneumoniae serovar 3 str. JL03	Y			Y	Y	oxidoreductase (339)
Actinobacillus pleuropneumoniae serovar 7 str. AP76	Y			Y	Y	oxidoreductase (339)
Actinobacillus succinogenes 130Z	Y			Y	Y	YfaE (85)
Aeromonas hydrophila subsp. hydrophila ATCC 7966	Y		Y	Y	Y	YfaE (81)
Aeromonas salmonicida subsp. salmonicida A449	Y		Y	Y	Y	YfaE (106)
Alcanivorax borkumensis SK2	Y				Y	oxidoreductase (344)
Alcanivorax sp. DG881					Y	oxidoreductase (372)
Algoriphagus sp. PR1					Y	ferredoxin (151)
Aliivibrio salmonicida LFI1238	Y				Y	YfaE (91)
Alpha proteobacterium HTCC2255			Y		Y	YfaE (88)
Alteromonadales bacterium TW-7					Y	YfaE (90)
Alteromonas macleodii 'Deep ecotype'	Y			Y	Y	YfaE (90)
Anaerostipes caccae DSM 14662				Y		
Anaplasma marginale str. St. Maries	Y					succinate dehydrogenase (262)
Anaplasma phagocytophilum HZ	Y					succinate dehydrogenase (262)
Aquifex aeolicus VF5	Y				Y	ferredoxin (96)
Arcobacter butzleri RM4018	Y			Y		fumarate reductase (243)
Azotobacter vinelandii AvOP			Y		Y	oxidoreductase (353)
Bacillus coagulans 36D1			Y	Y		FeS protein (441)
Bacillus halodurans C-125	Y		Y			
Bacillus selenitireducens MLS10			Y	Y		
Bacillus sp. NRRL B-14911			Y		Y	hypothetical protein (79)
Bacillus sp. SG-1			Y		Y	hypothetical protein (78)
Bacteroides fragilis NCTC 9343	Y		Y	Y	Y	quinone reductase (423)

Organism	Fully sequenced	Class Ib	Class II	Class III	YfaE-like	Note
Bacteroides fragilis YCH46	Y		Y	Y	Y	quinone reductase (423)
Bacteroides vulgatus ATCC 8482	Y		Y	Y	Y	quinone reductase (424)
Baumannia cicadellinicola str. Hc	Y				Y	YfaE (88)
Bdellovibrio bacteriovorus HD100	Y		Y	Y	Y	hypothetical protein (95)
Bordetella avium 197N	Y				Y	ferredoxin (113)
Bordetella bronchiseptica RB50	Y				Y	ferredoxin (113)
Bordetella parapertussis	Y				Y	ferredoxin (113)
Bordetella pertussis Tohama I	Y				Y	ferredoxin (113)
Bordetella petrii DSM 12804	Y			Y	Y	ferredoxin-reductase (341)
Bradyrhizobium japonicum USDA 110	Y		Y		Y	ferredoxin-reductase (336)
Brevundimonas sp. BAL3			Y	Y		succinate dehydrogenase (265)
Buchnera aphidicola str. APS (Acyrthosiphon pisum)	Y				Y	YfaE (87)
Buchnera aphidicola str. Bp (Baizongia pistaciae)	Y				Y	YfaE (87)
Buchnera aphidicola str. Sg (Schizaphis graminum)	Y					
Burkholderia ambifaria IOP40-10					Y	oxidoreductase (343)
Burkholderia ambifaria MC40-6	Y		Y		Y	ferredoxin (321)
Burkholderia ambifaria MEX-5					Y	ferredoxin (100)
Burkholderia cenocepacia AU 1054	Y				Y	ferredoxin (100)
Burkholderia cenocepacia HI2424	Y				Y	ferredoxin (100)
Burkholderia cenocepacia J2315	Y		Y		Y	ferredoxin (100)
Burkholderia cenocepacia MC0-3	Y				Y	ferredoxin (100)
Burkholderia cenocepacia PC184	Y				Y	ferredoxin (100)
Burkholderia cepacia AMMD	Y				Y	ferredoxin (100)
Burkholderia cepacia R1808			Y		Y	ferredoxin (117)
Burkholderia cepacia R18194					Y	ferredoxin (100)
Burkholderia dolosa AUO158	Y		Y	Y	Y	ferredoxin (343)
Burkholderia fungorum LB400	Y		Y		Y	ferredoxin (120)
Burkholderia graminis C4D1M					Y	ferredoxin (105)
Burkholderia mallei ATCC 10399	Y		Y	Y	Y	ferredoxin (381)
Burkholderia mallei ATCC 23344	Y		Y	Y	Y	ferredoxin (381)
Burkholderia mallei NCTC 10229	Y		Y	Y	Y	ferredoxin (380)
Burkholderia mallei SAVP1	Y		Y	Y	Y	ferredoxin (380)
Burkholderia multivorans ATCC 17616	Y		Y		Y	ferredoxin (105)
Burkholderia oklahomensis C6786			Y	Y	Y	ferredoxin (329)
Burkholderia oklahomensis EO147			Y	Y	Y	ferredoxin (98)
Burkholderia phymatum STM815	Y		Y		Y	ferredoxin (129)
Burkholderia phytofirmans PsJN	Y		Y		Y	ferredoxin (103)
Burkholderia pseudomallei 1106b			Y	Y	Y	ferredoxin (96)

Organism	Fully sequenced	Class Ib	Class II	Class III	YfaE-like	Note
Burkholderia pseudomallei 112				Y	Y	ferredoxin (96)
Burkholderia pseudomallei 14				Y	Y	ferredoxin (96)
Burkholderia pseudomallei 1710b	Y		Y	Y	Y	ferredoxin (96)
Burkholderia pseudomallei 7894			Y	Y	Y	ferredoxin (96)
Burkholderia pseudomallei DM98			Y	Y	Y	ferredoxin (96)
Burkholderia pseudomallei K96243	Y		Y	Y	Y	ferredoxin (96)
Burkholderia pseudomallei NCTC 13177			Y	Y	Y	ferredoxin (96)
Burkholderia pseudomallei S13	Y		Y	Y	Y	ferredoxin (88)
Burkholderia sp. 383	Y				Y	ferredoxin (100)
Burkholderia sp. H160			Y		Y	ferredoxin (126)
Burkholderia thailandensis Bt4			Y	Y	Y	ferredoxin (96)
Burkholderia thailandensis E264	Y		Y	Y	Y	ferredoxin (96)
Burkholderia thailandensis MSMB43			Y	Y	Y	ferredoxin (96)
Burkholderia thailandensis TXDOH			Y	Y	Y	ferredoxin (96)
Burkholderia ubonensis Bu			Y		Y	ferredoxin (83)
Burkholderia vietnamiensis G4	Y		Y		Y	ferredoxin (117)
Burkholderia xenovorans LB400	Y		Y		Y	ferredoxin (120)
Caminibacter mediatlanticus TB-2				Y		fumarate reductase (322)
Campylobacter coli RM2228						fumarate reductase (241)
Campylobacter concisus 13826	Y			Y		fumarate reductase (239)
Campylobacter curvus 525.92	Y			Y		fumarate reductase (239)
Campylobacter fetus subsp. fetus 82-40	Y			Y		fumarate reductase (246)
Campylobacter jejuni RM1221						fumarate reductase (241)
Campylobacter jejuni subsp. doylei 269.97	Y					fumarate reductase (241)
Campylobacter jejuni subsp. jejuni 260.94						fumarate reductase (241)
Campylobacter jejuni subsp. jejuni 81-176	Y					fumarate reductase (241)
Campylobacter jejuni subsp. jejuni CF93-6						fumarate reductase (241)
Campylobacter jejuni subsp. jejuni CG8421						fumarate reductase (241)
Campylobacter jejuni subsp. jejuni NCTC 11168	Y					fumarate reductase (241)
Campylobacter lari RM2100				Y		fumarate reductase (241)
Campylobacter upsaliensis RM3195						fumarate reductase (241)
Campylobacterales bacterium GD 1				Y		fumarate reductase (247)
Candidatus Amoebophilus asiaticus 5a2	Y					
Candidatus Blochmannia floridanus	Y				Y	YfaE (95)
Candidatus Blochmannia	Y				Y	YfaE (96)

pennsylvanicus

Organism	Fully sequenced	Class Ib	Class II	Class III	YfaE-like	Note
Candidatus Blochmannia pennsylvanicus str. BPEN	Y				Y	YfaE (96)
Candidatus Pelagibacter sp. HTCC7211					Y	ferredoxin (120)
Candidatus Pelagibacter ubique HTCC1002						succinate dehydrogenase (257)
Candidatus Pelagibacter ubique HTCC1062	Y		Y			succinate dehydrogenase (257)
Candidatus Vesicomyosocius okutanii HA	Y				Y	ferredoxin (87)
Caulobacter crescentus CB15	Y		Y			succinate dehydrogenase (260)
Caulobacter sp. K31	Y		Y		Y	oxidoreductase (669)
Cellulophaga sp. MED134						succinate dehydrogenase (248)
Cellvibrio japonicus Ueda107	Y					succinate dehydrogenase (234)
Chromobacterium violaceum ATCC 12472	Y		Y	Y	Y	oxidoreductase (342)
Chromohalobacter salexigens DSM 3043	Y	Y			Y	ferredoxin (322)
Citrobacter koseri ATCC BAA-895	Y	Y		Y	Y	YfaE (84)
Clostridium acetobutylicum ATCC 824	Y		Y	Y		
Clostridium beijerinckii NCIMB 8052	Y		Y	Y		
Clostridium bolteae ATCC BAA-613				Y	Y	hypothetical protein (166)
Clostridium botulinum A str. ATCC 3502	Y			Y	Y	FeS protein (576)
Clostridium botulinum A3 str. Loch Maree	Y			Y	Y	FeS protein (576)
Clostridium botulinum B str. Eklund 17B	Y			Y	Y	oxidoreductase (384)
Clostridium botulinum B1 str. Okra	Y			Y	Y	FeS protein (576)
Clostridium botulinum Bf				Y	Y	FeS protein (576)
Clostridium botulinum C str. Eklund				Y	Y	ferredoxin ? (277)
Clostridium botulinum E3 str. Alaska E43	Y			Y	Y	oxidoreductase (384)
Clostridium botulinum F str. Langeland	Y			Y	Y	FeS protein (576)
Clostridium botulinum NCTC 2916				Y	Y	FeS protein (576)
Clostridium butyricum 5521				Y		
Clostridium nexile DSM 1787				Y		
Clostridium novyi NT	Y			Y		sulfite reductase (263)
Clostridium perfringens ATCC 13124	Y			Y		oxidoreductase (326)
Clostridium perfringens E str. JGS1987				Y		oxidoreductase (326)
Clostridium perfringens SM101	Y			Y		oxidoreductase (326)
Clostridium perfringens str. 13	Y			Y		oxidoreductase (326)

Organism	Fully sequenced	Class Ib	Class II	Class III	YfaE-like	Note
Clostridium phytofermentans ISDg	Y			Y		dihydroxy-acid dehydratase (573)
Clostridium ramosum DSM 1402				Y		hypothetical protein (572)
Clostridium scindens ATCC 35704				Y	Y	hypothetical protein (533)
Clostridium sporogenes ATCC 15579				Y	Y	hypothetical protein (576)
Collinsella intestinalis DSM 13280				Y		
Collinsella stercoris DSM 13279				Y		
Colwellia psychrerythraea 34H	Y			Y	Y	YfaE (106)
Comamonas testosteroni KF-1			Y		Y	ferredoxin (100)
Congregibacter litoralis KT71			Y			fumarate reductase (258)
Coxiella burnetii 'MSU Goat Q177'						
Coxiella burnetii CbuG_Q212	Y					
Coxiella burnetii Dugway	Y					
Coxiella burnetii RSA 493	Y					
Crocosphaera watsonii WH 8501					Y	ferredoxin (99)
Cupriavidus taiwanensis	Y		Y		Y	ferredoxin (99)
Cyanothece sp. ATCC 51142	Y				Y	ferredoxin (99)
Cyanothece sp. CCY 0110					Y	ferredoxin (99)
Cyanothece sp. PCC 7424					Y	ferredoxin (111)
Cyanothece sp. PCC 8801					Y	ferredoxin (99)
Cyanothece sp. PCC 8802					Y	ferredoxin (99)
Cytophaga hutchinsonii ATCC 33406	Y					fumarate reductase (250)
Dehalococcoides sp. VS			Y			ferredoxin (640)
Delftia acidovorans SPH-1	Y		Y		Y	ferredoxin (117)
Dichelobacter nodosus VCS1703A	Y			Y		
Ehrlichia canis str. Jake	Y					succinate dehydrogenase (258)
Ehrlichia chaffeensis str. Arkansas						succinate dehydrogenase (258)
Ehrlichia chaffeensis str. Sapulpa						succinate dehydrogenase (158)
Ehrlichia ruminantium str. Gardel	Y					succinate dehydrogenase (264)
Ehrlichia ruminantium str. Welgevonden	Y					succinate dehydrogenase (258)
Enterobacter cancerogenus ATCC 35316		Y		Y	Y	YfaE (81)
Enterobacter sakazakii ATCC BAA-894	Y	Y		Y	Y	YfaE (84)
Enterobacter sp. 638	Y	Y		Y	Y	YfaE (84)
Erwinia carotovora subsp. atroseptica SCRI1043	Y	Y		Y	Y	YfaE (86)
Erwinia tasmaniensis Et1/99	Y				Y	YfaE (86)
Erythrobacter sp. NAP1						succinate dehydrogenase (260)
Erythrobacter sp. SD-21					Y	oxidoreductase (185)
Escherichia albertii TW07627		Y		Y	Y	YfaE (84)
Escherichia coli 101-1		Y		Y	Y	YfaE (84)
Escherichia coli 536	Y	Y		Y	Y	YfaE (84)
Escherichia coli 53638		Y		Y	Y	YfaE (84)
Escherichia coli APEC O1	Y	Y			Y	YfaE (84)

Organism	Fully sequenced	Class Ib	Class II	Class III	YfaE-like	Note
Escherichia coli ATCC 8739	Y	Y		Y	Y	YfaE (84)
Escherichia coli B171		Y		Y	Y	YfaE (84)
Escherichia coli B7A		Y		Y	Y	YfaE (84)
Escherichia coli CFT073	Y	Y		Y	Y	YfaE (84)
Escherichia coli E110019		Y		Y	Y	YfaE (84)
Escherichia coli E22		Y		Y	Y	YfaE (84)
Escherichia coli F11		Y		Y	Y	YfaE (84)
Escherichia coli HS	Y	Y			Y	YfaE (84)
Escherichia coli K12, MG1655	Y	Y		Y	Y	YfaE (84)
Escherichia coli O157:H7	Y	Y		Y	Y	YfaE (84)
Escherichia coli O157:H7 EDL933	Y	Y		Y	Y	YfaE (84)
Escherichia coli O157:H7 str. EC4024		Y		Y	Y	YfaE (84)
Escherichia coli O157:H7 str. EC4045		Y		Y	Y	YfaE (84)
Escherichia coli O157:H7 str. EC4206		Y		Y	Y	YfaE (84)
Escherichia coli O157:H7 str. EC4501		Y		Y	Y	YfaE (84)
Escherichia coli SMS-3-5	Y	Y		Y	Y	YfaE (84)
Escherichia coli W3110		Y		Y	Y	YfaE (84)
Eubacterium dolichum DSM 3991				Y		
Exiguobacterium sibiricum 255-15	Y			Y		
Exiguobacterium sp. AT1b				Y		
Faecalibacterium prausnitzii M21/2				Y		
Fervidobacterium nodosum Rt17-B1			Y	Y	Y	oxidoreductase (369)
Finegoldia magna ATCC 29328	Y			Y	Y	hypothetical protein (525)
Flavobacteria bacterium BAL38						succinate dehydrogenase (253)
Flavobacteria bacterium BBFL7					Y	flavodoxin reductase (347)
Flavobacteriales bacterium ALC-1					Y	FeS protein (357)
Flavobacteriales bacterium HTCC2170			Y			succinate dehydrogenase (249)
Flavobacterium johnsoniae UW101	Y			Y	Y	ferredoxin (350)
Flavobacterium psychrophilum JIP02/86	Y					fumarate reductase (254)
Flavobacterium sp. MED217			Y		Y	ferredoxin (154)
Francisella novicida GA99-3548						
Francisella philomiragia subsp. philomiragia ATCC 25017	Y					succinate dehydrogenase (233)
Francisella tularensis subsp. holarctica FSC022	Y					succinate dehydrogenase (233)
Francisella tularensis subsp. novicida GA99-3548						
Francisella tularensis subsp. novicida U112	Y					succinate dehydrogenase (233)
Francisella tularensis subsp. tularensis SCHU S4	Y					succinate dehydrogenase (233)

Organism	Fully sequenced	Class Ib	Class II	Class III	YfaE-like	Note
Francisella tularensis subsp. tularensis WY96-3418	Y					succinate dehydrogenase (233)
Fusobacterium nucleatum subsp. nucleatum ATCC 25586	Y			Y		
Fusobacterium nucleatum subsp. polymorphum ATCC 10953	Y			Y		
Fusobacterium nucleatum subsp. vincentii ATCC 49256				Y		
Gemmata obscuriglobus UQM 2246			Y			ferredoxin (250)
Geobacillus kaustophilus HTA426	Y		Y		Y	hypothetical protein (117)
Geobacillus sp. WCH70			Y			
Geobacillus sp. Y412MC10			Y	Y	Y	ferredoxin (129)
Geobacillus thermodenitrificans NG80-2	Y					
Gluconacetobacter diazotrophicus PAl 5	Y					succinate dehydrogenase (260)
Gluconobacter oxydans 621H	Y		Y			xanthine dehydrogenase (486)
Gramella forsetii KT0803	Y		Y		Y	oxidoreductase (349)
Granulibacter bethesdensis CGDNIH1	Y				Y	flavodoxin reductase (249)
Haemophilus ducreyi 35000HP	Y			Y		
Haemophilus influenzae 22.4-21				Y	Y	YfaE (82)
Haemophilus influenzae 3655				Y	Y	YfaE (82)
Haemophilus influenzae 86-028NP	Y			Y	Y	YfaE (82)
Haemophilus influenzae PittAA					Y	YfaE (82)
Haemophilus influenzae PittEE	Y			Y	Y	YfaE (82)
Haemophilus influenzae R2846				Y	Y	YfaE (82)
Haemophilus influenzae R2866				Y	Y	YfaE (82)
Haemophilus influenzae R3021				Y	Y	YfaE (82)
Haemophilus influenzae Rd KW20	Y			Y	Y	YfaE (82)
Haemophilus parasuis 29755				Y		fumarate reductase (256)
Haemophilus somnus 129PT	Y			Y	Y	YfaE (85)
Haemophilus somnus 2336	Y			Y	Y	YfaE (85)
Hahella chejuensis KCTC 2396	Y		Y		Y	flavodoxin reductase (384)
Helicobacter acinonychis str. Sheeba	Y					fumarate reductase (245)
Helicobacter hepaticus ATCC 51449	Y					fumarate reductase (247)
Helicobacter pylori 26695	Y					fumarate reductase (245)
Helicobacter pylori G27	Y					fumarate reductase (234)
Helicobacter pylori HPAG1	Y					fumarate reductase (245)
Helicobacter pylori HPKX_438_AG0C1						fumarate reductase (66)
Helicobacter pylori J99	Y					fumarate reductase (245)
Helicobacter pylori P12	Y					fumarate reductase (245)
Helicobacter pylori Shi470	Y					fumarate reductase (245)
Herminiimonas arsenicoxydans	Y			Y	Y	oxidoreductase (342)

Organism	Fully sequenced	Class Ib	Class II	Class III	YfaE-like	Note
Hydrogenivirga sp. 128-5-R1-1				Y	Y	ferredoxin (96)
Hyphomonas neptunium ATCC 15444	Y		Y		Y	xanthine dehydrogenase (216)
Idiomarina baltica OS145					Y	YfaE (87)
Idiomarina loihiensis L2TR	Y			Y	Y	YfaE (86)
Janthinobacterium sp. Marseille	Y				Y	YfaE (86)
Klebsiella pneumoniae subsp. pneumoniae MGH 78578	Y	Y		Y	Y	YfaE (84)
Kordia algicida OT-1					Y	hypothetical protein (357)
Lawsonia intracellularis PHE/MN1-00	Y					FeS protein ? (437)
Legionella pneumophila str. Corby	Y				Y	oxidoreductase (627)
Legionella pneumophila str. Lens	Y				Y	hypothetical protein (318)
Legionella pneumophila str. Paris	Y				Y	hypothetical protein (627)
Legionella pneumophila subsp. pneumophila str. Philadelphia 1	Y				Y	hypothetical protein (657)
Lentisphaera araneosa HTCC2155					Y	ferredoxin (97)
Leptothrix cholodnii SP-6	Y		Y		Y	ferredoxin (111)
Limnobacter sp. MED105					Y	ferredoxin (381)
Listeria innocua Clip11262	Y			Y		
Listeria monocytogenes EGD-e	Y			Y		
Listeria monocytogenes str. 1/2a F6854				Y		
Listeria monocytogenes str. 4b F2365	Y			Y		
Listeria monocytogenes str. 4b H7858				Y		
Listeria welshimeri serovar 6b str. SLCC5334	Y			Y		
Lyngbya sp. PCC 8106					Y	ferredoxin (112)
Mannheimia haemolytica PHL213	Y			Y		
Mannheimia succiniciproducens MBEL55E	Y			Y	Y	YfaE (87)
Maricaulis maris MCS10	Y		Y	Y		succinate dehydrogenase (259)
Marine gamma proteobacterium HTCC2080						succinate dehydrogenase (235)
Marine gamma proteobacterium HTCC2143						succinate dehydrogenase (235)
Marinobacter algicola DG893			Y		Y	oxidoreductase (353)
Marinobacter aquaeolei VT8	Y		Y		Y	oxidoreductase (330)
Marinobacter sp. ELB17			Y		Y	ferredoxin (364)
Marinomonas sp. MED121					Y	ferredoxin (110)
Marinomonas sp. MWYL1	Y				Y	YfaE (98)
Methylibium petroleiphilum PM1	Y		Y	Y	Y	ferredoxin (108)
Methylobacillus flagellatus KT	Y		Y		Y	YfaE (139)
Methylococcus capsulatus str. Bath	Y		Y		Y	ferredoxin (122)
Microcystis aeruginosa NIES-843	Y				Y	ferredoxin (122)
Microcystis aeruginosa PCC 7806					Y	ferredoxin (122)

Organism	Fully sequenced	Class Ib	Class II	Class III	YfaE-like	Note
Microscilla marina ATCC 23134					Y	oxidoreductase (354)
Moritella sp. PE36				Y	Y	YfaE (87)
Myxococcus xanthus DK 1622	Y		Y		Y	ferredoxin reductase (322)
Neisseria gonorrhoeae FA 1090	Y				Y	YfaE (96)
Neisseria meningitidis 053442	Y				Y	YfaE (96)
Neisseria meningitidis FAM18	Y				Y	YfaE (96)
Neisseria meningitidis MC58	Y				Y	YfaE (96)
Neisseria meningitidis Z2491	Y				Y	YfaE (96)
Neorickettsia sennetsu str. Miyayama	Y					succinate dehydrogenase (254)
Nitratiruptor sp. SB155-2	Y		Y	Y		succinate dehydrogenase (254)
Nitrococcus mobilis Nb-231			Y		Y	oxidoreductase (345)
Nitrosococcus oceani ATCC 19707	Y					
Nitrosomonas europaea ATCC 19718	Y				Y	oxidoreductase (348)
Nitrosomonas eutropha C71	Y				Y	oxidoreductase (348)
Nitrosospira multiformis ATCC 25196	Y				Y	oxidoreductase (349)
Novosphingobium aromaticivorans DSM 12444	Y				Y	FeS protein (169)
Oceanicaulis alexandrii HTCC2633			Y			succinate dehydrogenase (261)
Oceanobacillus iheyensis HTE831	Y					
Oceanobacter sp. RED65	Y				Y	YfaE (159)
Oceanospirillum sp. MED92					Y	YfaE (88)
Orientia tsutsugamushi Boryong	Y					succinate dehydrogenase (263)
Orientia tsutsugamushi str. Ikeda	Y					succinate dehydrogenase (261)
Paenibacillus larvae subsp. larvae BRL-230010			Y	Y		dihydroxy-acid dehydratase (556)
Parachlamydia sp. UWE25			Y		Y	YfaE (88)
Parvibaculum lavamentivorans DS-1	Y		Y			fumarate reductase (259)
Pasteurella multocida subsp. multocida str. Pm70	Y			Y	Y	YfaE (82)
Pedobacter sp. BAL39		Y		Y	Y	oxidoreductase (356)
Peptostreptococcus micros ATCC 33270				Y		
Phenylobacterium zucineum HLK1	Y		Y			succinate dehydrogenase (260)
Photobacterium profundum 3TCK			Y	Y	Y	ferredoxin (95)
Photobacterium profundum SS9	Y		Y	Y	Y	ferredoxin (95)
Photobacterium sp. SKA34				Y	Y	ferredoxin (98)
Photorhabdus asymbiotica subsp. asymbiotica ATCC 43949				Y	Y	YfaE (88)
Photorhabdus luminescens subsp. laumondii TTO1	Y	Y		Y	Y	YfaE (88)
Plesiocystis pacifica SIR-1			Y		Y	ferredoxin (98)
Polaribacter irgensii 23-P					Y	oxidoreductase (348)
Polaromonas naphthalenivorans CJ2	Y		Y		Y	ferredoxin (103)

Organism	Fully sequenced	Class Ib	Class II	Class III	YfaE-like	Note
Polaromonas sp. JS666	Y		Y		Y	ferredoxin (110)
Polynucleobacter necessarius STIR1	Y				Y	oxidoreductase (348)
Polynucleobacter sp. QLW-P1DMWA-1	Y				Y	oxidoreductase (348)
Proteus mirabilis HI4320	Y	Y		Y	Y	YfaE (92)
Providencia stuartii ATCC 25827		Y		Y	Y	YfaE (74)
Pseudoalteromonas atlantica T6c	Y				Y	YfaE (90)
Pseudoalteromonas haloplanktis TAC125	Y				Y	YfaE (90)
Pseudoalteromonas tunicata D2					Y	YfaE (87)
Pseudomonas aeruginosa C3719	Y		Y	Y	Y	hypothetical protein (366)
Pseudomonas aeruginosa PA7	Y		Y	Y	Y	oxidoreductase (355)
Pseudomonas aeruginosa PACS2			Y	Y	Y	oxidoreductase (321)
Pseudomonas aeruginosa PAO1	Y		Y	Y	Y	oxidoreductase (318)
Pseudomonas aeruginosa UCBPP-PA14	Y		Y	Y	Y	ferredoxin (366)
Pseudomonas entomophila L48	Y				Y	oxidoreductase (366)
Pseudomonas fluorescens Pf-5	Y				Y	oxidoreductase (366)
Pseudomonas fluorescens PfO-1	Y				Y	oxidoreductase (366)
Pseudomonas mendocina ymp	Y				Y	ferredoxin (309)
Pseudomonas putida F1	Y				Y	ferredoxin (316)
Pseudomonas putida W619	Y				Y	ferredoxin (316)
Pseudomonas stutzeri A1501	Y		Y	Y	Y	oxidoreductase (730)
Pseudomonas syringae pv. phaseolicola 1448A	Y				Y	oxidoreductase (312)
Pseudomonas syringae pv. syringae B728a	Y				Y	oxidoreductase (312)
Pseudomonas syringae pv. tomato str. DC3000	Y				Y	oxidoreductase (312)
Psychrobacter arcticus 273-4	Y				Y	YfaE (86)
Psychrobacter cryohalolentis K5	Y				Y	YfaE (88)
Psychrobacter sp. 273-4					Y	YfaE (86)
Psychrobacter sp. PRwf-1	Y				Y	YfaE (85)
Psychroflexus torquis ATCC 700755			Y		Y	oxidoreductase (347)
Psychromonas ingrahamii 37	Y			Y	Y	YfaE (83)
Psychromonas sp. CNPT3				Y	Y	YfaE (82)
Ralstonia eutropha H16	Y		Y	Y	Y	oxidoreductase (352)
Ralstonia eutropha JMP134	Y		Y		Y	oxidoreductase (354)
Ralstonia metallidurans CH34	Y		Y	Y	Y	oxidoreductase (351)
Ralstonia pickettii 12D			Y	Y	Y	ferredoxin (320)
Ralstonia pickettii 12J	Y		Y	Y	Y	ferredoxin (316)
Ralstonia solanacearum GMI1000	Y		Y	Y	Y	ferredoxin (328)
Ralstonia solanacearum UW551				Y	Y	ferredoxin (328)
Reinekea sp. MED297			Y	Y		succinate dehydrogenase (235)
Rhodoferax ferrireducens DSM 15236	Y		Y	Y	Y	ferredoxin (323)

Organism	Fully sequenced	Class Ib	Class II	Class III	YfaE-like	Note
Rhodospirillum centenum SW	Y		Y	Y		succinate dehydrogenase (260)
Rhodospirillum rubrum ATCC 11170	Y		Y	Y	Y	ferredoxin (127)
Rickettsia akari str. Hartford	Y					succinate dehydrogenase (261)
Rickettsia bellii OSU 85-389	Y					succinate dehydrogenase (261)
Rickettsia bellii RML369-C	Y					succinate dehydrogenase (261)
Rickettsia canadensis str. McKiel	Y					succinate dehydrogenase (261)
Rickettsia conorii str. Malish 7						succinate dehydrogenase (261)
Rickettsia felis URRWXCal2	Y					succinate dehydrogenase (261)
Rickettsia massiliae MTU5	Y					succinate dehydrogenase (261)
Rickettsia prowazekii str. Madrid E	Y					succinate dehydrogenase (261)
Rickettsia rickettsii	Y					succinate dehydrogenase (261)
Rickettsia rickettsii str. 'Sheila Smith'	Y					succinate dehydrogenase (261)
Rickettsia sibirica 246						succinate dehydrogenase (261)
Rickettsia typhi str. Wilmington	Y					succinate dehydrogenase (261)
Rickettsiella grylli						succinate dehydrogenase (261)
Robiginitalea biformata HTCC2501			Y		Y	oxidoreductase (349)
Rubrivivax gelatinosus PM1			Y	Y	Y	oxidoreductase (341)
Ruminococcus gnavus ATCC 29149				Y		
Ruminococcus torques ATCC 27756				Y		
Saccharophagus degradans 2-40	Y				Y	ferredoxin (366)
Salinibacter ruber DSM 13855	Y		Y		Y	ferredoxin (127)
Salinispora arenicola CNS-205	Y		Y		Y	oxidoreductase (384)
Salinispora tropica CNB-440	Y		Y		Y	ferredoxin (330)
Salmonella enterica subsp. arizonae serovar 62:z4,z23:--	Y	Y		Y	Y	YfaE (84)
Salmonella enterica subsp. enterica serovar Choleraesuis str. SC-B67	Y	Y		Y	Y	YfaE (84)
Salmonella enterica subsp. enterica serovar Gallinarum str. 287/91	Y	Y			Y	YfaE (84)
Salmonella enterica subsp. enterica serovar Kentucky str. CDC 191				Y	Y	YfaE (84)
Salmonella enterica subsp. enterica serovar Paratyphi A str. ATCC 9150	Y	Y		Y	Y	YfaE (84)
Salmonella enterica subsp. enterica serovar Typhi Ty2	Y	Y		Y	Y	YfaE (84)
Salmonella enterica subsp. enterica serovar Typhi str. CT18	Y	Y		Y	Y	YfaE (84)
Salmonella typhimurium LT2	Y	Y		Y	Y	YfaE (84)
Serratia proteamaculans 568	Y	Y		Y	Y	YfaE (86)
Shewanella amazonensis SB2B	Y			Y	Y	YfaE (117)
Shewanella baltica OS155	Y			Y	Y	YfaE (140)
Shewanella baltica OS195	Y			Y	Y	YfaE (163)
Shewanella baltica OS223				Y	Y	YfaE (140)

Organism	Fully sequenced	Class Ib	Class II	Class III	YfaE-like	Note
Shewanella benthica KT99				Y	Y	YfaE (124)
Shewanella denitrificans OS217	Y			Y	Y	YfaE (134)
Shewanella frigidimarina NCIMB 400	Y			Y	Y	YfaE (133)
Shewanella halifaxensis HAW-EB4	Y			Y	Y	YfaE (127)
Shewanella loihica PV-4	Y			Y	Y	YfaE (126)
Shewanella oneidensis MR-1	Y			Y	Y	YfaE (144)
Shewanella pealeana ATCC 700345	Y			Y	Y	YfaE (136)
Shewanella putrefaciens CN-32	Y			Y	Y	YfaE (151)
Shewanella sediminis HAW-EB3	Y			Y	Y	YfaE (116)
Shewanella sp. ANA-3	Y			Y	Y	YfaE (136)
Shewanella sp. MR-4	Y			Y	Y	YfaE (136)
Shewanella sp. MR-7	Y			Y	Y	YfaE (136)
Shewanella sp. W3-18-1	Y			Y	Y	YfaE (136)
Shewanella woodyi ATCC 51908	Y			Y	Y	YfaE (125)
Shigella boydii CDC 3083-94	Y	Y		Y	Y	YfaE (84)
Shigella boydii Sb227	Y	Y		Y	Y	YfaE (84)
Shigella dysenteriae Sd197	Y	Y		Y	Y	YfaE (84)
Shigella flexneri 2a str. 2457T	Y	Y		Y	Y	YfaE (84)
Shigella flexneri 2a str. 301	Y	Y		Y	Y	YfaE (84)
Shigella flexneri 5 str. 8401	Y	Y		Y	Y	YfaE (84)
Shigella sonnei Ss046	Y	Y		Y	Y	YfaE (84)
Sodalis glossinidius str. 'morsitans'	Y				Y	YfaE (86)
Sorangium cellulosum 'So ce 56'	Y				Y	ferredoxin (103)
Sphingomonas sp. SKA58					Y	hypothetical (636)
Sphingomonas wittichii RW1	Y				Y	ferredoxin (769)
Sphingopyxis alaskensis RB2256	Y				Y	ferredoxin (179)
Stenotrophomonas maltophilia K279a	Y				Y	oxidoreductase (369)
Stenotrophomonas maltophilia R551-3	Y				Y	ferredoxin (215)
Stigmatella aurantiaca DW4/3-1						
Streptomyces avermitilis MA-4680	Y		Y		Y	oxidoreductase (366)
Streptomyces clavuligerus ATCC 27064			Y		Y	ferredoxin (351)
Streptomyces coelicolor A3(2)			Y		Y	oxidoreductase (364)
Streptomyces griseus subsp. griseus NBRC 13350	Y		Y		Y	oxidoreductase (360)
Streptomyces jumonjinensis						
Streptomyces microflavus						
Streptomyces pristinaespiralis ATCC 25486	Y		Y		Y	ferredoxin (370)
Streptomyces sp. Mg1	Y		Y		Y	oxidoreductase (381)
Streptomyces sp. SPB74			Y		Y	ferredoxin (724)
Streptomyces sviceus ATCC 29083	Y		Y		Y	oxidoreductase (312)

Organism	Fully sequenced	Class Ib	Class II	Class III	YfaE-like	Note
Sulfurovum sp. NBC37-1	Y			Y		fumarate reductase
Symbiobacterium thermophilum IAM 14863	Y		Y		Y	ferredoxin (233)
Synechococcus sp. PCC 7002	Y				Y	ferredoxin (122)
Synechocystis sp. PCC 6803	Y				Y	ferredoxin (97)
Tenacibaculum sp. MED152					Y	ferredoxin reductase (348)
Thermus aquaticus Y51MC23			Y			
Thermus thermophilus HB27	Y		Y			
Thermus thermophilus HB8	Y		Y			
Thioalkalivibrio sp. HL-EbGR7			Y		Y	oxidoreductase (340)
Thiobacillus denitrificans ATCC 25259	Y		Y	Y	Y	flavin-reductase (345)
Thiomicrospira crunogena XCL-2	Y				Y	ferredoxin (83)
Thiomicrospira denitrificans ATCC 33889	Y			Y	Y	ferredoxin (378)
Treponema denticola ATCC 35405	Y			Y		
Treponema pallidum subsp. pallidum str. Nichols	Y					
Verminephrobacter eiseniae EF01-2	Y		Y		Y	ferredoxin (323)
Vibrio alginolyticus 12G01				Y	Y	ferredoxin (93)
Vibrio angustum S14				Y	Y	ferredoxin (98)
Vibrio campbellii AND4				Y	Y	YfaE (92)
Vibrio cholerae MO10				Y	Y	ferredoxin (89)
Vibrio cholerae O1 biovar El Tor str. N16961	Y			Y	Y	YfaE (92)
Vibrio fischeri ES114	Y			Y	Y	YfaE (92)
Vibrio harveyi ATCC BAA-1116	Y			Y	Y	YfaE (92)
Vibrio parahaemolyticus RIMD 2210633	Y			Y	Y	YfaE (92)
Vibrio shilonii AK1				Y	Y	YfaE (91)
Vibrio sp. Ex25	Y			Y	Y	flavodoxin reductase (605)
Vibrio sp. MED222		Y		Y	Y	YfaE (92)
Vibrio splendidus 12B01				Y	Y	YfaE (92)
Vibrio vulnificus CMCP6	Y			Y	Y	YfaE (92)
Vibrio vulnificus YJ016	Y			Y	Y	YfaE (92)
Vibrionales bacterium SWAT-3				Y	Y	YfaE (92)
Wolbachia endosymbiont of Drosophila ananassae	Y					succinate dehydrogenase (270)
Wolbachia endosymbiont of Drosophila melanogaster	Y					succinate dehydrogenase (270)
Wolbachia endosymbiont strain TRS of Brugia malayi	Y					succinate dehydrogenase (262)
Wolbachia pipientis	Y					
Wolinella succinogenes DSM 1740	Y			Y	Y	hypothetical protein (99)
Xanthomonas axonopodis pv. citri str. 306	Y				Y	oxidoreductase (306)
Xanthomonas campestris pv.	Y				Y	oxidoreductase (326)

campestris str. ATCC 33913

Organism	Fully sequenced	Class Ib	Class II	Class III	YfaE-like	Note
Xanthomonas campestris pv. vesicatoria str. 85-10	Y				Y	oxidoreductase (319)
Xanthomonas oryzae pv. oryzae KACC10331	Y				Y	oxidoreductase (364)
Xanthomonas oryzae pv. oryzae MAFF 311018	Y				Y	oxidoreductase (358)
Xanthomonas oryzae pv. oryzae PXO99A	Y				Y	oxidoreductase (358)
Xanthomonas oryzae pv. oryzicola BLS256					Y	oxidoreductase (358)
Xylella fastidiosa 9a5c	Y					succinate dehydrogenase
Xylella fastidiosa Ann-1						succinate dehydrogenase
Xylella fastidiosa Dixon						succinate dehydrogenase
Xylella fastidiosa Temecula1	Y					succinate dehydrogenase
Yersinia bercovieri ATCC 43970		Y		Y	Y	YfaE (85)
Yersinia enterocolitica subsp. enterocolitica 8081	Y	Y		Y	Y	YfaE (81)
Yersinia frederiksenii ATCC 33641		Y		Y	Y	YfaE (85)
Yersinia intermedia ATCC 29909		Y		Y	Y	YfaE (85)
Yersinia mollaretii ATCC 43969		Y		Y	Y	YfaE (88)
Yersinia pestis Angola	Y			Y	Y	YfaE (85)
Yersinia pestis CO92	Y	Y		Y	Y	YfaE (85)
Yersinia pestis KIM	Y	Y		Y	Y	YfaE (85)
Yersinia pestis biovar Medievalis str. 91001	Y	Y		Y	Y	YfaE (85)
Yersinia pseudotuberculosis IP 32953	Y	Y		Y	Y	YfaE (85)
Zymomonas mobilis subsp. mobilis ZM4	Y			Y	Y	oxidoreductase (105)